INFORMATION TO USERS

This manuscript has been reproduced from the microfilm master. UMI films the text directly from the original or copy submitted. Thus, some thesis and dissertation copies are in typewriter face, while others may be from any type of computer printer.

The quality of this reproduction is dependent upon the quality of the copy submitted. Broken or indistinct print, colored or poor quality illustrations and photographs, print bleedthrough, substandard margins, and improper alignment can adversely affect reproduction.

In the unlikely event that the author did not send UMI a complete manuscript and there are missing pages, these will be noted. Also, if unauthorized copyright material had to be removed, a note will indicate the deletion.

Oversize materials (e.g., maps, drawings, charts) are reproduced by sectioning the original, beginning at the upper left-hand corner and continuing from left to right in equal sections with small overlaps.

UMI®

IF WE KNEW WHAT WE WERE DOING, IT WOULD NOT BE CALLED RESEARCH, WOULD IT?
- ALBERT EINSTEIN

RULE #1, NO WHINING.
- GENE ROBERTSON

University of Alberta

Accuracy of On-Board Vehicle Emission Measurements

BY

Travis Benjamin Manchur ©

A Thesis Submitted to the Faculty of Graduate Studies and Research in

Partial Fulfilment of the Requirements for the Degree of Master of Science

Department of Mechanical Engineering

Edmonton, Alberta

Fall 2005

Abstract

Advanced development of a portable vehicle exhaust emissions measurement system was completed to answer unsolved issues from preceding research, as well as to further knowledge of real-time in-use emission studies. Addition of a fast responding nitric oxide sensor and OBDII scanner provided the sensor capabilities needed to accomplish these goals, while the development of repeatable certification cycles ensured relevance of results. An analysis of transients between slow and fast responding NOx sensors has shown fast response sensors measure 20% to seven times greater emission rates than conventional on-board sensors. Utilizing mathematical algorithms to correct for slow response has resulted in negligible to 250% increases in emission rates with limitation outweighing its useful benefits. The effects of acceleration and loading have shown expected trends for all species. Transient severity decreased NOx rates 48% for urban routes but were unchanged for highway cycles. Loaded operation did not significantly effect urban driving whereas a 19% increase in NOx rates occurred during highway testing. Engine operation transients were found to exhibit a time constant less than 1 s, which indicated that both fast and slow response sensors with 2 s and 7 s response times vary from too slow to much-too-slow to accurately resolve concentration and hence mass emission rates. Although limits to the on-board system were found, conclusive results on the significance of sensor time response, the effects of loading and acceleration, and the accuracy of vehicle ECM data, have proven the system's credibility.

Acknowledgments

The graduate studies and research I completed at the University of Alberta, have been the best years of my educational experience. Edmonton has become a second home to me and thanks to an enjoyable work environment and good friends, my Master's degree experience has been everything I could have asked for.

I would like to first recognize and thank Dr. David Checkel for providing me with the opportunity, funding, and resources required to complete my M.Sc. Degree while teaching me valuable life lessons and work experiences through his supervision. I would also like to thank Mr. Terry Nord for his assistance in the development and troubleshooting of this second generation emissions measurement system.

My graduate student life was well rounded thanks to the numerous friendships I made within our Combustion and Environment research group. I would like to thank Lindsay, Andrew (honorable member), Matt, Ryan, and Pat for their friendship, email breaks, project support, and their tales of grad school experiences shared over morning coffees and afternoon beer breaks. I thank Panfeng for his good humor and friendship, and for providing me with numerous unforgettable grad school stories which I will recite for years to come. I thank my first cubical partner Pascal for making work an enjoyable place to come to everyday, for our Bomber parties, and for the memories of our all you can eat pirogi dinners.

My extended stay at the University of Alberta would not have been possible without the contributions of my friends but nor would I have changed a thing looking back. Special thanks have to go out to two of my best friends. To Dave Arthur, I thank you for your support during my project, for our debates which knew no end, and for reinforcing my political views and my love of meat. I thank Senthil Ponnusamy for making each day enjoyable in and especially out of the lab, for opening my mind up to new a new style of music, and for allowing me to refine my squash game in an ultra-competitive "leave friendship at the door" environment.

The most important acknowledgment I can make is to my parents and my sister. I would like to thank my parents for the support, encouragement, and guidance they have given me prior to, and throughout my time in graduate studies. I cannot imagine where I would be without them. My thanks to my sister are for the laughter we shared and the encouragement she has given me on countless occasions. I also thank her for being an unwavering role model for hard work, perseverance, and the ability to balance life's work with leisure.

The acknowledgments and recognition which I have listed here do not end after this thesis is printed. The contributions my friends and family have made to my life will be remembered and cherished forever.

Table of Contents

List of Tables

List of Figures

Abbreviations

a	Instantaneous Vehicle Acceleration [m/s^2] - a(I) or a(t)
accel	Acceleration
A/F	Air to Fuel Ratio (Mass Based) [unitless]
avg	Average
C	Actual "Well Mixed" Concentration in the Cell [kg/m^3]
$\dfrac{dC}{dt}$	Concentration Gradient
CARB	California Air Resources Board
C_d	Drag Coefficient [unitless]
C_{in}	Corrected Input Concentration
C_r	Rolling Resistance Coefficient [unitless]
CDT	Coast Down Test
CO	Carbon Monoxide
CO_2	Carbon Dioxide
COV	Coefficient of Variation
CVS	Constant Volume Sample
D	Diameter of Tire [m]
DAQ	Data Acquisition
dist	Distance
ECM	Engine Control Module
EGR	Exhaust Gas Recirculation
EPA	Environmental Protection Agency
$ER_{time,i}$	Instantaneous Mass Emission Rate [g i / s]
$ER_{dist,i}$	Instantaneous Mass Emission Rate [g i / km]
$ER_{pow,i}$	Instantaneous Mass Emission Rate [g i / kWh]
$ER_{fuel,i}$	Instantaneous Mass Emission Rate [g i / g fuel]
$E_{time,i}$	Mass Emission Rate - Cumulative total [g i / s]

$E_{dist,i}$	Mass Emission Rate - Cumulative total [g i / km]
$E_{pow,i}$	Emissions Flow Rate - Cumulative total [g i / kWh]
$E_{fuel,i}$	Emissions Flow Rate - Cumulative total [g i / g fuel]
	where: i - (HC, CO, CO_2, O2, NOx - Horiba & Vetronix)
F_{aero}	Aerodynamic Resistence [N]
$F_{inertial}$	Inertial Resistence [N]
$F_{rolling}$	Rolling Resistence [N]
$\dot{F}_{mass}$	Fuel Consumption (mass basis) [kg fuel / min]
$\dot{F}_{vol}$	Fuel Consumption per stroke (volume basis) [m^3 / stroke]
FA	Frontal Area [m^2]
FE	Fuel Economy
FID	Flame Ionization Detector
FTP	Federal Test Program
g	Gravitational Acceleration Constant [m/s^2]
GUI	Graphical User Interface
GVWR	Gross Vehicle Weight Rating
H	Vehicle Height [m]
HC	Hydrocarbons
H/C	Hydrogen to Carbon Ratio
I_{eq}	Equivalent Moment of Inertia of Rotating Parts
I/M	Inspection and Maintenance
IR	Infrared
LDT	Light-Duty Truck
LDV	Light-Duty Vehicle
m	Vehicle Mass [kg]
m_r	Equivalent Rotating Mass [kg]
$\dot{m}$	Mass Flow Rate [kg/s]

$\dot{m}_{exh}$	Mass Flow Rate of Vehicle Exhaust [kg/s]
$\dot{m}_{air+fuel}$	Mass Flow Rate of Air and Fuel [kg/s]
$\dot{m}_{air}$	Mass Flow Rate of Air [kg/s]
$\dot{m}_{exh}$	Mass Flow Rate of Exhaust [kg/s]
$\dot{m}_{fuel}$	Mass Flow Rate of Fuel [kg/s]
M	Mass in Well-Mixed Flow Cell [kg]
MAF	Mass Air Flow
MAP	Manifold Absolute Pressure
max.	Maximum
MW_{air}	Molecular Weight of Ambient Air [kg/kmol]
MW_i	Molecular Weight of the ith Emission Species [kg i/kmol i]
MW_{exh}	Molecular Weight of the Exhaust Components [kg/kmol]
N_t	Transmission Ratio [unitless]
N_f	Final Drive Ratio [unitless]
N_{tf}	Combine Drive Ratio [unitless] (combination of transmission and final drive ratios)
n	Engine Speed [rpm] -or- Number of Points in Data File
NDIR	Non-Dispersive Infrared
NI	National Instruments
NO_x	Oxides of Nitrogen
O_2	Oxygen
OBDII	On-Board Diagnostics (Generation) 2
OEM	Original Equipment Manufacturer
P	Total Vehicle Tractive Power [kW]
PM	Particulate Matter
Q	Cell Volume [m³]

$\dot{Q}$	Volume Flow Rate [m³/s]
$\dot{Q}_{in}$	Flow Rate - Into Control Volume [m³/s]
$\dot{Q}_{out}$	Flow Rate - Out of Control Volume [m³/s]
r_{tire}	Tire Rolling Radius [m]
RPM	Revolutions per Minute
Resp.	Response
Ru	Universal Gas Constant [kJ/(kmol-K)] = 8.3143
Re_D	Reynolds Number (flow in a circular tube) [unitless]
SAE	Society of Automotive Engineers
SFTP	Supplemental Federal Test Program
SG_{fuel}	Specific Gravity of Fuel (0.740)
SSSF	Steady State Steady Flow
t	Time [s]
T_{amb}	Ambient Air Temperature [K]
$T_{i,air}$	Intake Air Temperature [K]
T_{aero}	Torque Required to Overcome Aerodynamic Drag [N-m]
$T_{inertial}$	Torque Required for a Given Acceleration [N-m]
$T_{rolling}$	Torque Required to Overcome Rolling Resistance [N-m]
T_{wheels}	Total Torque Required at Wheels to Drive Vehicle [N-m]
T_{engine}	Total Torque Required at the Engine to Drive Vehicle [N-m]
UEGO	Universal Exhaust Gas Oxygen (sensor)
ULEV	Ultra-Low Emissions Vehicle
US06	U.S. EPA Supplemental Federal Test Procedure Driving Cycle
UV	Ultraviolet
V	Vehicle Velocity [m/s]
w	Work Done by the Vehicle [kWh]
W	Vehicle Width [m]

$X_{independent,i}$	Independently installed vehicle operation measurement sensor
X_{OBD}	Vehicle operation measured by vehicle's sensor
Y_{NOx}	Mass Fraction of NOx [kg NOx / kg exh]
$Y_{NOx,in}$	Mass Fraction of NOx entering Well Mixed Cell [kg NOx / kg exh]
$Y_{NOx,out}$	Mass Fraction of NOx leaving Well Mixed Cell [kg NOx / kg exh]
ε_A	Error in Air Calculation
ε_B	Error in HC concentration [mol HC / mol]
ε_D	Error in CO concentration [mol CO / mol]
ε_E	Error in CO_2 concentration [mol CO_2 / mol]
ε_F	Error in O_2 concentration [mol O_2 / mol]
ε_G	Error in NOx concentration [mol NOx / mol]
ε_I	Error in N_2 concentration [mol N_2 / mol]
ε_J	Error in H_2O concentration [mol H_2O / mol]
$\varepsilon_{A/F}$	Error in A/F Ratio Calculation [unitless]
ε_{MWexh}	Error in Exhaust Molecular Weight [g/mol]
ε_{MFF}	Error in Mass Fuel Flow Rate [g fuel / s]
ε_{Ei}	Error in Mass Emission Rate of Species i [g i/ s]
$\varepsilon_{Epow,i}$	Error in Mass Emission Rate of Species i [g i / kWh]
$\varepsilon_{Efuel,i}$	Error in Mass Emission Rate of Species i [g i / g fuel]
ε_{FA}	Error in Frontal Area [m]
τ	Residence Time in the Well Mixed Cell
η_t	Transmission Efficiency [percent/100%]
ρ_{air}	Density of Air [kg/m^3]
$\rho_{air}{}^{o}$	Density of Air [=1.205 kg/m^3], at T = 293.15 [K], P = 101.3 [kPa]
ρ_{fuel}	Density of Fuel [kg/m^3]

ρ_{water}	Density of Water [= 1000 kg/m³]
χ_i	Mole Fraction of the ith species (i.e. coefficients B,D,E,F,G,I,J)
χ_{NOx}	Mole Fraction of NOx [kmol NOx / kmol exh]
$\chi_{NOx,in}$	Mole Fraction of NOx entering Well Mixed Cell [kmol NOx / kmol exh]
$\chi_{NOx,out}$	Mole Fraction of NOx leaving Well Mixed Cell [kmol NOx / kmol exh]
θ	Road Grade (defined as positive uphill) [rad]

CHAPTER 1

Introduction to On-Board & Real-Time Emission Measurement Systems

Chapter 1 details the benefits of on-board real-time emission measurement systems to supplement laboratory based systems. This chapter highlights the main goals of the research project and gives an outline of the contents of the following chapters.

1.0   Introduction

The introduction of new on-road vehicle emissions legislation in Canada and the United States as of January 1, 2004, is a testament to the increasing importance society is placing on controlling air pollution. These stricter standards for newly produced vehicles, are an attempt at minimizing the future health and environmental problems created by emissions from an ever expanding automotive fleet. Knowing that the automobile comprises a significant portion of the overall emission inventory, it is essential that studies are conducted to improve researchers' understanding of vehicle emissions over a wide range of operating conditions.

The recent development of on-board emissions measurement systems has led to a number of interesting findings linking vehicle operation with pollution production. One of the more prominent findings discovered through on-road testing revealed the existence of emissions defeating devices on heavy-duty diesel trucks.[1,2] In addition to validating the need for on-road testing, these results also confirmed the benefits of testing emissions outside of known driving cycles and laboratory conditions.

The current method for approving a new vehicle for sale under emissions certification standards requires measurement of mass emission rates in controlled laboratory testing conditions, while operating under simulated driving cycles. Although this is the most accurate and repeatable method for confirming emission compliance, significant benefits of on-board emission measurement studies can compliment laboratory testing. The production of commercially available, portable gas measurement sensors and systems which are smaller and more affordable, is a major reason for the growth in on-board emissions testing research. This cost advantage is a significant benefit over the complexity and expense associated with lab-based CVS systems.

Emission measurement systems which record data while on-road, have numerous advantages which cannot be produced using standard lab-based systems. The most critical of these benefits is the ability of an on-board system to measure and record vehicle and emissions data on a second-by-second basis (real-time). Gathering data in real-time allows researchers to examine the causes of emission events or the effects of vehicle events on emissions. The use of a constant volume sampler (CVS) lab-based systems does not facilitate this flexibility, instead producing single value final results which are based on long duration portions of a complete cycle.

On-board systems may be used to measure emissions due to traffic congestion and assist in the design and management of traffic facilities.[3] Additionally, they may also be used in evaluating emissions system conversion efficiency. A vehicle mounted emissions system can also be utilized in remote locations which is not possible with lab-based systems. This enables the testing of vehicles under a variety of ambient temperatures, road conditions, grades, accelerations, loading,

2

and wind conditions. Producing actual on-road data to determine the effects of these variables on pollution production is the most realistic way to simulate how vehicles are performing on the road, but leads to limitations due to a lack of control. Controlling all of these variables except an identified parameter is difficult when testing on-road and leads to results with larger uncertainties when compared to lab-based systems.

A literature review of vehicle emission measurement systems currently employed indicated three sparsely covered areas that appear to require investigation. First, the influence of sensor response time on mass emission rate calculations has been sparsely discussed. Few researchers are accounting for transient sensor behavior impacts, which introduces error to experimental calculations.

Secondly, the effects of load and acceleration on mass emission rates have only briefly been discussed with noticeably more vehicles requiring testing under a wider range of conditions.[4,5] The examination of emission rates under various driving modes is also supported by results from research done by the EPA which concluded that the driving mode generating the most emissions varies widely between vehicles.[6] A third area necessitates evaluation of on-board diagnostics generation two (OBDII) port accuracy. Although used by previous researchers [1,7], the lack of discussion coupled with the predicted usage increase in OBDII port data utilization, suggest an evaluation of the OBD data accuracy should be completed.

The main objective of this study was to advance the knowledge and capabilities of on-board emissions measurement systems to provide an improved tool for testing vehicle emissions. The effects of load, acceleration, and drive cycle type on vehicle mass emission rates were also studied to identify the contributions of these parameters. To facilitate these objectives, the following questions were set out to ensure this would be achieved in a quantitative way:
1. What difference in emission rate results over short and long temporal mass air flow step changes when comparing a fast response NOx sensor to a slow response NOx sensor? What impact will this difference have on overall emission rates?
2. How much NOx signal response improvement can be obtained when utilizing mathematical algorithms to correct first order simple lag response functions? Is this sufficient to allow the continued use of slow response NOx sensors in on-board real-time emissions studies?
3. What effect does transient severity have on overall emission levels of HC, CO, CO_2, and NOx over simulated FTP driving cycles?
4. What effect does vehicle load have on overall emission levels of HC, CO, CO_2, and NOx over simulated FTP driving cycles?
5. Will OBDII port information provide accurate enough information on vehicle operation to eliminate the installation of separate sensors?

A literature search was undertaken to become familiar with the issues surrounding emissions measurement of vehicles. The results of the literature review are presented in Chapter 2. The literature review describes the current emissions

3

regulations in place for North America and how dynamometer testing is done to certify vehicles to emission standards. An overview of the major issues facing on-board emissions systems is provided which highlights data synchronization, time response correction, and on-board diagnostics generation two (OBDII) port data accuracy issues as current concerns. Chapter 2 also discusses the systems being used by researchers, along with their results and limitations to illustrate work required in this area.

The first and second questions highlighted above are answered in Chapter 3 as a paper format chapter. SAE paper 2005-01-0674 illustrates the improvement in accuracy which can be achieved through the use of a fast response NOx sensor and also illustrates the effect of response correction algorithms on slow and fast NOx sensor data.

The fourth chapter (presented as a stand-alone paper similar to Chapter 3) addresses the third and fourth questions described above by analyzing the effect of acceleration, load, and driving route type on emission rates. The design of the driving routes and the methods used to ensure repeatability is also discussed to provide confidence in the experimental procedure.

The issue of OBDII port accuracy is addressed in Chapter 5 through a quantitative comparison of the data gathered from the OBDII port with independently calibrated and installed sensors. This chapter is intended to answer the fifth question of this research to validate or disprove the use of OBDII data as a useful means for gathering real-time vehicle operation measurements.

The last chapter of this thesis summarizes the conclusions presented in the previous three chapters to provide an overview of the findings produced from this project. The answer to each of the presented questions will be illustrated to indicate the precise results generated for each goal set.

Seven appendices provide information which supports the previous chapters. Appendix A illustrates the experiments, results, and conclusions of vehicle and gas analyzer data alignment as well as results of sensor response experiments. Appendix B describes the response correction algorithm used in this research to recreate step change profiles from first order simple lag response data. The accuracy of this response correction algorithm is evaluated and discussed in Appendix C to confirm the selected programming code and choice of algorithm. The equations used to calculate emissions and vehicle operation results are presented in Appendix D and E respectively with the inclusion of the associated error analysis for each equation. Appendix F describes the sensor calibrations performed on temperature, mass air flow, and gas analyzer sensors. Appendix G documents the Matlab code written to process the data. A description of what each program does and which ".m" files it uses or is used in, is also given to improve the transfer of knowledge for future work.

4

REFERENCES

[1]   U.S. Department of Justice, "Notice of Filing of Consent Decree Under the Clean Air Act," Federal Register, Vol.63, No.212, Nov.3 1998, p.59333 - 59334. http://frwebgate.access.gpo.gov/cgi-bin/multidb.cgi

[2]   Jimenez J.L., McRae G.J., Nelson D.D., Zahniser M.S., Kolb C.E., "Remote Sensing of NO and NO_2 Emissions from Heavy Duty Diesel Trucks Using Tunable Diode Lasers," Environmental Science and Technology, Vol.34, No.12, pp.2380-2387, 2000.

[3]   Frey H.C., Rouphail N.M., Unal A., Colyar J.D., "Measurement of On-Road Tailpipe CO, NO, and Hydrocarbon Emissions Using a Portable Instrument," in Proceedings - Annual Meeting of the Air and Waste Management Association, June 24-28, 2001.

[4]   Cicero-Fernandez, P., Long, L.R., "Grades and Other Loads Effects on On-Road Emissions: An On-Board Analyzer Study," California Air Resources Board, Mobile Source Division, Fifth CRC On-Road Vehicle Emissions Workshop, Apr.3-5, 1995.

[5]   Cicero-Fernandez, P., Long, J.R., and Winer, A.M., "Effects of Grades and Other Loads on On-Road Emissions of Hydrocarbons and Carbon Monoxide," Journal of Air & Waste Management, ISSN 1047-3289, 47:898-904, 1997.

[6]   U.S. Environmental Protection Agency, Office of Air and Radiation, Office of Mobile Sources, Certification Division, "Final Technical Report on Aggressive Driving Behavior for the Revised Federal Test Procedure Notice of Proposed Rulemaking," Jan.31, 1995. http://www.epa.gov/oms/regs/ld-hwy/ftp-rev/ftp-us06.pdf

[7]   Vojtisek-Lom M., Lambert D.C., Wilson P.J., "Real-world Emissions From 40 Heavy-Duty Diesel Trucks Recruited at Tulare, CA Rest Area," SAE Technical Paper 2002-01-2901, Society of Automotive Engineers, 2002.

5

CHAPTER 2

Review of Current Emissions Regulations,
Testing Procedures and On-Board Emission Measurement Studies

A literature review of the issues surrounding vehicle emission certification and current research on emissions measurement systems is presented in Chapter 2. The aim of this chapter is to present justification for the rationale behind the goal selection presented in Chapter 1. The background to emissions certification is presented to highlight the regulations, certification procedures, and testing methods used to approve vehicles for sale in North America. Challenges to on-board emission systems are then discussed to highlight important issues effecting the study of vehicle emissions. Finally, a discussion on OBDII port accuracy and current on-board emission measurement system studies highlights the results, limitations, and future work required in these areas.

2.0 Introduction

The impact of air pollution due to exhaust emissions from vehicles was first noticed in the California Basin in 1946.[1] Initially, limits on evaporative emissions, crankcase ventilation, the use of EGR, and eventually the development of catalytic converters and fuel injection, enabled automakers to produce vehicles with a dramatically lower environmental footprint. These changes in vehicle design came about due to the formation of government departments and later legislation which mandated the measurement and reduction of vehicle pollutants.

In addition to the evolution of automotive exhaust emission legislation, the measurement techniques and driving cycles used to quantify the improvements in exhaust production have also been changing. The following literature review will illustrate the challenges of measuring exhaust emissions in real-world conditions and highlight the benefits and deficiencies of previous on-road emissions systems. A brief discussion on driving cycle simulations used during emissions certification procedures will also be given.

The first section of the literature review briefly discusses current emissions regulations governing the sale of vehicles in Canada and the United States. The aim of this section is to illustrate the continuous tightening and importance of emissions standards imposed on automotive manufacturers.

The second section will briefly discuss the current laboratory methods used for measurement and certification of vehicles, with attention given to the evolution of FTP drive cycles used to conduct repeatable dynamometer testing.

The last topic of this literature review discusses measurement accuracy challenges researchers are facing with on-board emissions systems. On-Board Diagnostics (OBD) theory and background are subsequently discussed. Following this background, a discussion of in-use emissions measurement systems focuses on what researchers have accomplished and where they have been limited.

2.1 Current Emissions Regulations

The U.S. Environmental Protection Agency (EPA) develops emissions regulations governing the sale of automobiles in the United States. Since 1988, Environment Canada has followed this legislation to harmonize the manufacturing of vehicles between the two very integrated countries.[2] The harmonization allows Canada to have the lowest emission vehicles on the road at the lowest possible cost. As of Jan.1, 2004, new Tier 2 emissions standards for on-road vehicles were implemented in the form of the Canadian Environmental Protection Act (CEPA), 1999, which illustrate the commitment of both governments to continued emissions reductions from on road vehicle sources.[3]

7

The standards set for vehicles vary according to vehicle weight class and specify acceptable mass emission rates for intermediate and full useful life vehicle ages. The current method used to certify vehicles for compliance is the Constant Volume Sampler system which has been used extensively by the EPA. Future emissions standards will likely continue to impose more stringent control on toxic emissions to limit the impact that increasing numbers of on road vehicles have on the environment.

2.2. Dynamometer Testing
2.2.1 Description of FTP Certification Testing

The emissions testing equipment used to pass environmental legislation certification is known as the Constant Volume Sampler (CVS) system. An illustration of the setup of this system is shown in Figure 2-1. The main premise behind the operation of the CVS system is to maintain a constant total volume of dilution air and exhaust gas in the system.

Once the test vehicle has been secured on the chassis dynamometer and connected to the CVS system, the vehicle will be driven according to a specific certification drive cycle in simulation of on-road conditions. As vehicle exhaust is brought into the system it is mixed together into a homogeneous stream with filtered ambient dilution air which has been filtered to stabilize the hydrocarbon concentration. The principle component of the CVS system is the flow measurement unit which has been changed from the older positive displacement pump systems to newer critical flow venturi models.[4]

Once the flow has been mixed and adjusted for constant flow, a non-reactive stainless steel (and Teflon) surfaced sampling system transfers part of the CVS sample through fiberglass filters and into an exhaust sample bag. Proper switching between bags during various test sections can be done either automatically or manually depending on the CVS system setup.

The final step in the determination of vehicle emissions is analysis of the bag samples. The pollutant species tested are carbon monoxide (CO), hydrocarbons (HC), nitrogen oxides (NOx), carbon dioxide (CO_2), and oxygen (O_2). An NDIR analyzer is used to measure CO and CO_2, a chemiluminescent analyzer is used to measure NOx, and an FID analyzer is used to measure HC.

CVS Limitations (still uncertainties exist in this method) [4]:
> - the design of the CVS system has a large impact on tailpipe depression or pressurization which can effect vehicle performance. CVS systems can exert positive pressure on the vehicle during acceleration or cruise modes or produce "tailpipe depression" during idle modes
> - must ensure condensation does not form inside of the system since some species of emissions are soluable to water e.g. NOx

8

- deposits can slowly build up inside the CVS, most often in the heat exchanger, therefore frequent use of a CVS should also be followed with frequent cleaning
- analysis system cannot measure real-time second-by-second emissions rates

The introduction of new emissions certification driving cycles, specifically US06 (discussed later), has resulted in a requirement to increase CVS system capacities due to the higher mass air flow rates experienced during testing.[5]

2.2.2 Driving Cycles

Standardized driving cycles which represent real world driving behavior have been developed to certify vehicles according to each country's emissions standards. The three drive cycle certification tests of interest for Canadian and U.S. vehicle emission standards are the FTP75, SC03, and US06 driving cycles.

The FTP driving schedule was intended to represent typical urban driving patterns of commuters between home and work.[6] The speed time trace for the vehicle was developed through trial and error in the 1960s using a variety of drivers and routes with the same test vehicle. The FTP75 cycle (also known as FTP78) consists of three phases; the cold start phase, a stabilized phase, and a warm start phase (following an idle period) as shown in Figure 2-2. Originally, FTP75 was the only developed driving schedule required to verify emissions compliance against.

In 1990, the amended Clean Air Act prompted the investigation of current driving cycles to determine if current cycles were adequately representing current vehicle driving patterns. Results of the investigation by EPA's FTP Review project team found several shortcomings and proposed new test cycles to address these untested operating conditions. Full details regarding the final regulations of the FTP procedures revisions can be found in 40 CFR Part 86 of the EPA Federal Register [5]. Table 2-1 illustrates the shortcomings of the FTP75 cycle which led to the development of SFTP cycles.

These new cycles termed Supplemental Federal Test Procedure (SFTP) cycles, came in the form of the US06 and SC03 driving cycles and address limitations 1 through 4 of Table 2-1 with road grade remaining the only omission. An illustration of the speed-time traces which make up the US06 and SC03 cycles are shown in Figures 2-3 and 2-4 respectively. The intention was to produce a corrected test procedure to bring control stringency to areas previously unregulated.[5] It should be noted that these revisions to the FTP cycle apply to all gasoline LDVs and LDTs and diesel LDVs and LDT1s.

9

Table 2-1 FTP75 Cycle Limitations [5] [6]

1	Speed	Max Speed of 57 mph misses a significant portion of in-use operation, specifically high speed highway driving
2	Acceleration	Rates were artificially lowered to accommodate dynamometer testing capabilities of the times, which fails to represent aggressive driving
3	Air Conditioning	Actual air conditioner operation during driving
4	Driving Behavior	FTP75 driving patterns were smooth and did not represent microtransient behavior (rapid speed fluctuations)
5	Road Grade	Not accounted for in FTP75

The development of the SC03 Supplemental FTP test was designed to address emission effects of three factors; vehicle air conditioning operation, microtransient driving conditions, and warm start conditions. The US06 SFTP cycle addresses the FTP limitations on speed, acceleration (aggressive microtransients), and driving behavior. Table 2-2 illustrates the various dynamic parameters which comprise the certification cycles. It is evident that the much higher average and maximum test speed experienced during the US06 cycle will provide a more thorough exploration of a vehicles emission characteristics when used in conjunction with FTP and SC03 cycles.

Table 2-2 FTP Certification Driving Cycles [7]

Cycle	Dist.	Time	Avg. Speed	Max. Speed
	[km]	[s]	[km/h]	[km/h]
FTP75 Urban	17.77	1874	34.1	91.2
US06	12.89	600	77.8	129.2
SC03	5.76	600	34.7	88.2

The effect of driver aggressiveness was studied thoroughly in this research because of the significantly large relative impact transients have on overall emissions and the relatively small amount of data and knowledge available. In the U.S. EPA's final report which analyzed driving behavior before revising the FTP test route (described above), it was found that non FTP driving operation can result in high emissions and vary greatly between vehicles.[6] The California Air Resources Board (CARB) which conducted the aggressive driving tests quickly realized that little was known about aggressive driving emissions significance under real world conditions. During the US06 testing program, the EPA also discovered that catalyst conversion efficiency was very sensitive to air/fuel ratio which is significant during rapid transients due to the large range with which A/F can vary.[5]

10

The development of driving routes and cycles has focused on reproducing similar speed-time traces, transient levels, speeds, and energy usage. The intent of this premeditated route planning was to examine similar vehicle operation modes in approximately similar proportions to certification cycles. The duplication of a similar driving cycle on-road would ensure on-board emissions testing was encompassing a representative cycle of what actual vehicle experience on the road.

A study completed by Battelle of Columbus, Ohio for the EPA's Environmental Technology Verification (ETV) program suggested these two routes (US06 Highway and FTP75 Urban) as necessary to verify the accuracy of on-road emissions monitoring systems.[8] The data collect therefore allows for future comparison to dynamometer tests, and also duplicate emissions systems, which will enable system comparison criteria to be analyzed for accuracy and repeatability under accepted driving cycles.

Use of the US06 Highway driving cycle in on-road testing is intended to test higher rates of vehicle speed transients, vehicle power severity, and vehicle operation at higher velocities. Knowing that limited work has been done in this area of on-board emissions testing, suggests examination of these parameters is necessary. To accurately evaluate whether an on-board emissions system is capable of measuring these conditions, in addition to typical moderate transient urban driving, a knowledge of engine operation transient rates is required.

Manifold absolute pressure (MAP) is a measurement of engine demand for air/fuel ratio in response to an increased demand in engine load. Mass air flow (MAF) rates closely indicate the power demand required of the engine in response to a load. Since vehicle emissions production varies in relation to both of these variables, it is important to understand the transient rates of these parameters resulting from certification cycle driving.

Table 2-3 shows the average and standard deviation of the time constants for MAP and MAF for a series of urban and highway simulation certification cycles. Examination of the rate of change of MAP (from vehicle ECM data) indicates that engine operation changes with a first-order time constant less than 0.4 s. Similar results for MAF were noticed with the FTP Urban cycle simulation tests showing a 0.7 s time constant, indicating emission production rates would be less than 1 s. MAF results for Highway testing showed a longer time constant result in response to significant speed changes during tests from idle to highway speeds which were characteristic of the US06 cycle.

This quantified examination of vehicle transient operation illustrates that it is necessary for any emissions sensor to respond at the same rate as engine operation transients, to produce an accurately resolved mass emission rate.

11

Table 2-3 Engine Operation - Rate of Transients

	MAP Time Constant	MAF Time Constant
	[s]	[s]
FTP75 Urban - Normal Accel	0.35 +/- 0.01	0.71 +/- 0.28
US06 Highway - Rapid Accel	0.36 +/- 0.02	3.15 +/- 0.42

Modal analysis of FTP75 Urban and US06 Highway simulation driving routes supports the importance of accurately measuring vehicle and emission data during engine operation transients. Table 2-4 shows the percent amount of time spent in each driving mode as an average and standard deviation of 4 tests per mode. These results indicate that between 15 and 27% of the time, the vehicle was found to be in the acceleration mode which requires varying engine loads and vehicle speeds. Although rapid acceleration testing has shown less time in the acceleration mode, the magnitude of its effects on emissions would be more significant due to the higher power demand in a shorter period of time.

Table 2-4 Modal Analysis of FTP Certification Cycles

	FTP75 Urban		US06 Highway	
	Normal Accel	Rapid Accel	Normal Accel	Rapid Accel
Idle	19.0 +/- 0.4%	18.6 +/- 0.3%	9.3 +/- 0.4%	9.5 +/- 0.3%
Acceleration	26.8 +/- 1.2%	15.5 +/- 0.4%	26.0 +/- 1.3%	17.6 +/- 1.1%
Deceleration	27.4 +/- 1.5%	30.9 +/- 1.6%	27.7 +/- 0.9%	29.8 +/- 2.5%
Cruise	26.9 +/- 1.8%	35.0 +/- 2.0%	37.0 +/- 1.8%	43.1 +/- 3.2%

2.3 Current On-Road Real-Time Emissions Studies

The study of vehicle emissions while in operation on the road has been examined for more than 10 years. However, recent improvements in emissions equipment size, portability, and affordability, coupled with the increased importance legislators are putting on air pollution from vehicles has lead to an increasing amount of research on portable on-road emissions measurement systems.

2.3.1 Challenges to Time Alignment of Emissions Data

Analyzing real-time emissions data gathered from on-board sensors is of significant value if the emissions values collected can be confidently known to have been recorded at the exact time the vehicle parameters were recorded. This is one of the

12

three main challenges to accurately determining mass emission rate data from on-board emissions systems. The remaining two challenges are sensor response time and sample line smearing which will be discussed later.

Previous work completed by Hawirko [9] used a constant time shifting algorithm to align emissions data to vehicle operation parameters. Although this method properly aligns the initial mass air flow rate spike to the start of NOx transients, variable flow rates created by the engine will theoretically vary the time with which exhaust exits the tailpipe. The importance of time alignment is further supported by numerous other researchers working with on-board emissions measurement systems.

Work completed by BMW, DaimlerChrysler, and Porsche has shown that time alignment of data is a difficult task to do properly when trying to resolve mass emission rates from modal raw concentration data. It was found that a misalignment of only +/- 2 seconds in the parameters used to calculate emission rates, can dramatically effect the mass emission rate of various species.[10]

Similarly, research conducted by Ford Motor Company and the University of Bath has shown that aligning emissions data to one signal point, as done during constant value time shifting, is an indeterminate way of accurately aligning data. This research suggested that varying gas speeds due to varying engine operation conditions will result in shorter/longer transport delays through a vehicles exhaust system.[11] In further research studies it was shown that a +/- 1 second mismatch between NOx sampling points would cause NOx catalytic conversion efficiency to range from 4.3 - 15.2 %.[12]

Work done by Vojtisek-Lom and Cobb confirmed the existence of a variable time delay in the exhaust pipe with varying engine operating conditions.[13] Research results presented used a constant average time shifting algorithm, which was likely due to simplicity. This method was also used by Frey et al. in aligning separate emissions and vehicle data files.[14]
The experiences of numerous researchers illustrate the significance of properly aligning emissions data and vehicle data, with agreement that variable shifting of data to account for variable transit delay times is preferential to constant value shifting. Therefore, research into the development and analysis of variable time shifting algorithms is justified and appears ready to be integrated into on-road data.

2.3.2 Time Response Correction

Another significant factor in producing accurate mass emission rate results is the consideration of sensor time response. Knowing that emission sensors using chemical cell, NDIR, and ZrO_2 principles [15] respond in a first order response, simple lag manner, the presence of a significantly long time constant can have adverse effects on mass emission rates.

13

Work completed by Honda R&D Americas and the University of California used a 1998 Honda Accord in ULEV configuration to show the effect a response correction algorithm can have on an emissions sensor with a 20 second time constant [16]. The results of this study indicated that the use of the well mixed flow model for correcting slow response sensors is appropriate and beneficial to overall results. The effect of using the algorithm on simple lag response data was that signal noise was created in the new corrected signal; however, this is relatively minor compared to the ability of the corrected signal to follow the step change concentration.[16] It is also acknowledged that the algorithm could not create data where no data was present so the benefits of utilizing response correction algorithms are still inferior to fast response sensors.

Similar work completed by Horiba and the Japan Automobile Research Institute has examined the effect of sensor time response on accuracy of mass emission rates.[17] In this research, an inverse filter function, similar to the well mixed flow model above, was used to correct the T_{90}-T_{10} sensor response time from 0.9 to 0.7 seconds. The research also performed algorithm optimization and filtering to prevent overshoot of the signal. The algorithm was verified by showing agreement in results when comparing the slower response inverse filter corrected mass emission data with faster response non-corrected mass emission data.

The work completed by these researchers is promising and supports the use of time response correction algorithms used in this thesis. Although limitations in the form of noise amplification, possible response overshoot, and the inability to create data where no data was present, are a hindrance, the use of these algorithms is seen as an improvement.

2.3.3 OBDII Port Data Accuracy / Discussion

On Board Diagnostics generation two (OBDII) is a collection of sensors and signal protocol designed to ensure all vehicles produced on and after 1996 maintain properly functioning emissions control systems and other engine related components. The Clean Air Act of 1970 which resulted in the formation of the EPA, began the evolutionary process of reducing automotive air pollution. In response to the first emissions control standards, manufacturers began to develop sensors to monitor engine performance and in turn adjust the engine to minimize emissions species concentration. In 1988, the Society of Automotive Engineers (SAE) set a standard connector plug and diagnostic test signal set which was adopted by the EPA and eventually expanded into OBDII form in Jan.1, 1996.[18]

The On-Board Diagnostics system of a vehicle controls most engine functions, monitors parts of the chassis, body & accessory devices, and diagnostic control network of the car. This system can be used to pinpoint malfunctioning components from over 300 measured readings (depending on manufacturer and model) of a vehicle which cause vehicular or emissions performance reductions.

14
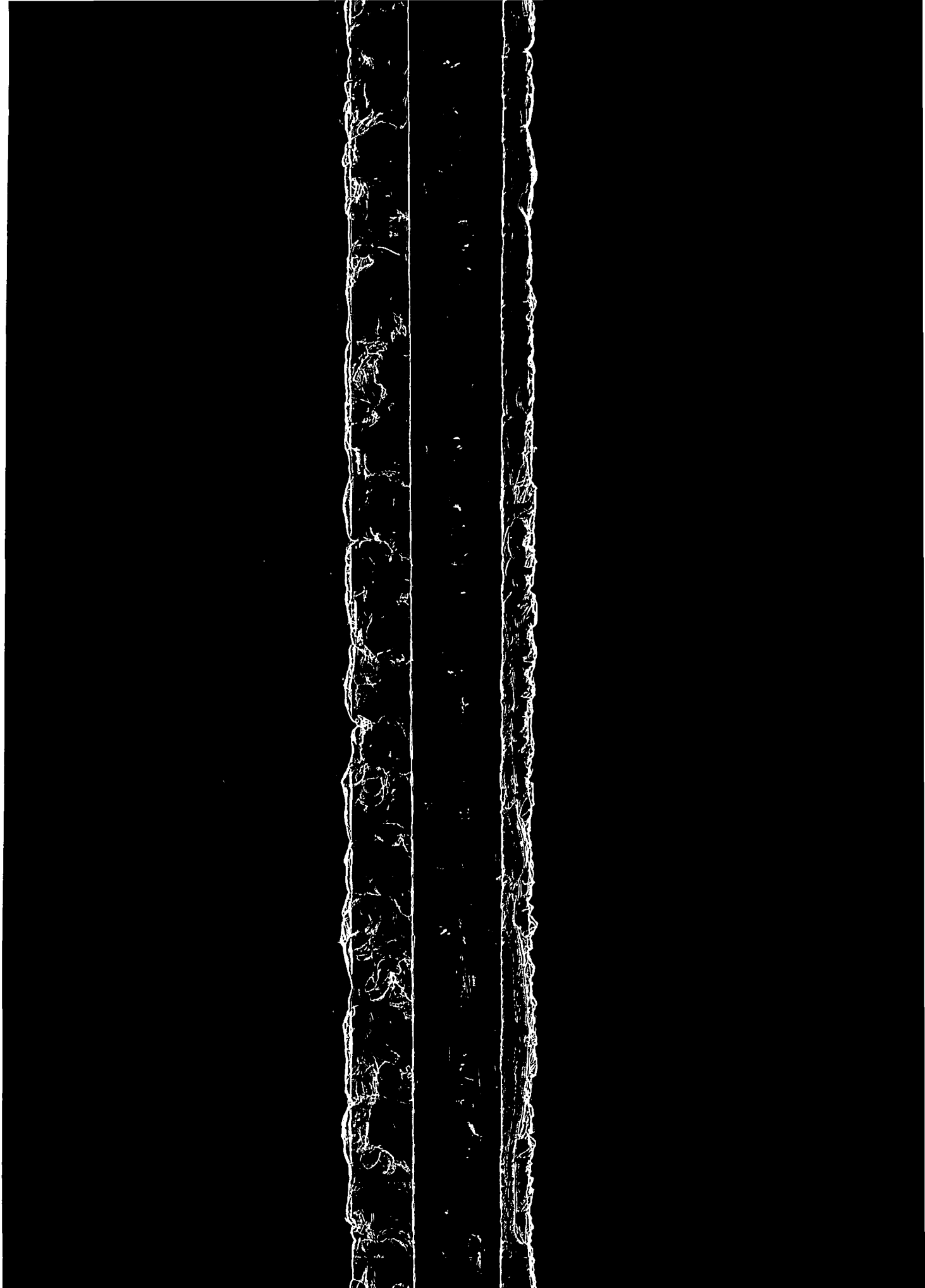
Environmental regulations require that vehicles meet and maintain emissions controlled levels throughout the useful life of the vehicle. New Tier 2 emission standards for vehicles are pushing the definition of a vehicle's useful life from 160,000 km to 192,000 km which requires even more robust emission system design. Using OBDII ensures universal inspection and diagnosis of these system components which helps to enable all vehicle to perform to regulated standards.

Numerous on-board emissions measurement studies have utilized OBD information for years to produce emission rate results without any consideration for the accuracy of the information gathered. Studies completed by North Carolina State University on a 1999 Ford Taurus read eight OBD parameters through the OEM-2100™ emissions unit manufactured by Clean Air Technologies International.[14] These parameters included manifold absolute pressure, vehicle speed, engine speed, intake air temperature, coolant temperature, intake mass air flow, percent wide open throttle, and open/closed loop flag. The study did not indicate that the accuracy of the vehicle's OBD sensors was tested or verified but rather used the data gathered as though it was correct.

Early on-board emissions research conducted by Vojtisek-Lom and Cobb on a fleet of university compressed natural gas vans utilized a pre-OBDII data port to measure a variety of sensors including mass air flow rate and vehicle speed.[13] Independent verification of these parameters was not completed due to the cost and desire to avoid tampering with vehicle operation. More recent work by Vojtisek-Lom et al. with an OEM-2100 "Montana" System gathered emissions and vehicle data from 21 heavy-duty diesel trucks without the discussion of vehicle sensor accuracy.[19] This research used ECM data via a diagnostics link to measure vehicle mass air flow data.

Similar work completed by CARB's mobile source division used pre-OBDII ECM data from a 1991 GM Lumina to gather key vehicle parameters.[20] The calculation of mass air flow rate was determined using engine speed, manifold absolute pressure, and intake temperature which all may be in error since independent verification of the sensors was not mentioned. In all of these cases discussed, no mention of verifying the data gathered from the vehicle sensors against independent sensor data was mentioned, which therefore leads to questions about data quality and accuracy.

The benefits of using OBDII port data however are numerous and include; minimizing tampering with vehicle operation, decreased system install time, access to numerous vehicle fault detection sensors, and commonality in sensor use if comparing various on-board emissions systems. In addition to these benefits, a study conducted by Jim Lindner of the EPA has shown that OBD is more effective at identifying high-emitting vehicles than I/M240 testing.[21]

To be effective on a real-time basis as an accurate measurement of engine operation during transient events, OBDII information needs to be gathered at a

15

frequency greater than 2 Hz. Table 2-3 has shown that engine operation events are changing with a time constant less than 0.4 s which therefore requires a similar scale of data collection for accurate parameter measurement.

The future of OBD systems (OBDIII) appears to be heading towards incorporating wireless equipment into vehicles with the expectation that vehicles could relay changes in emissions system operation to ground based roadside sensors. DiGenova of Sierra Research has shown this system to be technically feasible using a fleet of five vehicles.[21] It is expected that although costly initially, the financial trade off would be better than the more expensive current I/M programs being used.

2.3.4 On-Road Emissions Measurement Methods

In determining how to advance the development of a previously developed emissions system, to improve system accuracy and account for numerous challenges to NOx measurement, a review of current on-board systems was completed. The following section will describe what equipment other researchers are using to perform on-board emissions testing and what capabilities, limitations, and results are being achieved.

Research presented to the Coordinating Research Council in 1995 by the California Air Resources Board (CARB) Mobile Source Division used a Sierra Research instrumented vehicle to determine the effect of grades and A/C loads on HC and CO emissions.[21] The paper discusses results of the testing done on grades of 0 to 7%, loads of 1 - 4 passengers, and air conditioning in maximum and off settings. The results of this paper illustrated the exacerbation of emission levels when fully loading a vehicle and when running the A/C at maximum. The results also showed that driving on grades above 3% produced emissions which deviated from flat terrain corrected values 86% of the time. The equipment used by CARB to conduct these tests was not discussed in much detail nor was a discussion regarding the accuracy of the OBD data given. The paper does however, illustrate the importance of loads on vehicles and indicates the significant variance with which off FTP cycle modes can effect overall cycle results.

The next significant step in the field of on-board emissions testing resulted when Vojtisek-Lom and Cobb of the University of Pittsburgh developed a system to test a fleet of university compressed natural gas vans in 1997.[13] The equipment consisted of a 5 gas analyzer (OTC SPX RG240) and an ECM scanner, and tested vehicle emissions on FTP and I/M240 test cycles. The results of this project produced much scatter between vehicles and tests, and the system produced many malfunctions but as a starting point to on-road emissions testing, this research proved valuable. As with this research, after initial development of the emission measurement system (Hawirko), the goal of the second phase of this project was to produce a more accurate system.

16

At the turn of the century, the research into on-road emissions measurement systems greatly accelerated as industry and academics began pushing the capabilities and knowledge of on-board testing further. In 2000, a collaborative effort by Horiba and NGK Insulators began the work of developing an on-road emissions testing system which used a variety of independently installed and calibrated sensors to measure vehicle and emissions operation.[16] The experiments performed over a period of one year on a diesel powered vehicle showed the system was capable of measuring NOx mass emissions within 4%, fuel consumption within 3%, and running distance within 1% of CVS systems. The research was a step forward in emissions system technology but it was incapable of measuring HC, CO, or CO_2 emissions, it failed to use OBDII data or address time alignment of data, and it did not test gasoline vehicles which consists a significant portion of the driving population.

Early use of OBDII port data was done by North Carolina State University in 2001 when researchers used Clean Air Technologies International emissions testing unit OEM-2100™ on a 1999 Ford Taurus.[14] This instrumentation package gathered eight vehicle operation OBD parameters in a data file plus emission concentration measurements. The emissions were sampled through a long sample line which routed tailpipe emissions into the vehicle where the remote gas analyzer was located. The conclusions of this research were that emissions occurring during accelerations were much higher than during idle conditions, emissions are heavily influenced by short trips, and a significant number of vehicles can be tested when utilizing a system that is capable reading OBDII port data. The research failed to address the accuracy of OBDII port data, time alignment of data, or emission sensor response time on the accuracy of short transient and full cycle emissions results.

The desire to expand the capabilities of the OEM-2100™ "Montana" emissions testing system by illustrating it's ability to measure numerous diesel vehicles and possibly replace chassis dynamometer I/M programs with stationary programs was done in 2002.[19] The results of this second set of experiments illustrated large NOx emissions were caused by improperly tuned engines or emissions defeating devices which was a significant finding. It also disproved the ability of this system to fully replace chassis dynamometer I/M testing with stationary testing. It should be cautioned that the system utilized the diesel vehicle's batteries to power the unit and thus may have increased the load placed on the engine.

The development of an on-board emissions system by the University of Alberta, which was the basis for the emissions system in this thesis, utilized a network of installed sensors and a five gas analyzer located in the vehicle to study driver behavior and emissions characteristics.[23] Experimentation with the system over a range of temperatures later allowed for the quantification of vehicle emission factors for a typical gasoline powered truck representative of the local fleet.[24] These two research experiments where able to develop temperature and driver behavior insight into on-road vehicle emissions. The limitation to this system was that no OBD port data was utilized and the use of a slow response NOx sensor led

17

to questions of NOx emissions calculation accuracy.

The significance of accuracy determination of on-board emissions measurement systems has been shown to be of increasing importance. Initially, portable emissions systems attempted to be accurate with respect to CVS full cycle emission readings. In 2003, research completed by Horiba Instruments developed an exhaust gas simulator, the Horiba VEES-100, to study real-time emissions system accuracy (which is accurate to CVS systems within 0.5%).[25] The new exhaust gas simulator was capable of controlling concentrations of CO_2, CO, propane, and NO, in addition to mass air flow rate to produce emissions and flow rates representative of vehicles. The results of these tests showed that the on-board emissions system OBS-1100 developed by Horiba, could accurately reproduce ULEV emission levels, including the Horiba Mexa-720NOx (used in this thesis apparatus) to within 30ppm of NOx. However, the system showed a noticeable decrease in accuracy when SULEV emission levels were used. The two limitations of this research were uncertainties in determining what FTP emissions concentration profiles should look like, as well as portability issues of a system weighing 80 kg plus batteries.

The most recent on-board emissions testing research reported has been completed by Weaver and Petty with the development of the Ride-Along Vehicle Emissions Measurement (RAVEM™) System in 2004.[26] The development of this system has taken place over the past four years with numerous improvements made with the testing of vehicles. The system has been tested on natural gas garbage trucks in Mexico, diesel ferryboats in San Francisco Bay, and others. RAVEM™ differs from other emission systems mentioned in that it is a partial flow CVS system which gives pollutant concentration proportional to mass flow rate. The results of using this system have indicated that there is good correlation for CO_2, NOx, and PM but less accuracy in measuring CO emissions. This system weighs 120 kg however, and requires 600 Watts of power to operate which imparts a significant load on the vehicle at all times. The principal error noted was determining the proportion of sample exhaust to admit to the dilution tunnel of the partial flow system.

2.4 Sensor Response Characteristics

Industry, government, and academic demand for small, accurate, and unobtrusive on-board vehicle emission sensors has driven down cost and increased options available. The use of a new "fast response" NOx sensor from Horiba instruments has been shown to be one of the fastest sensors available with tests confirming a first-order time constant of 2.0 s. Knowing engine operation transient behavior exhibits a time constant less than 0.4 s, which directly relates to emissions production, its clear that current sensors available are unable to fully measure real-time emissions behavior. The use of the term "fast response" should therefore be utilized in relative terms to sensors with longer time constants, with the realization that a truly fast sensor would achieve less than 0.5 s first order response.

18

2.5 Conclusions

The importance of reducing on-road vehicle emissions is clear when looking at the stringency of regulations, the vastness of government environmental departments, and the sheer number of researchers and industry partners working toward the goal of reducing emissions. Significant work in evaluating specific on-road emissions behavior remains however, and was illustrated by discussing the changing FTP driving cycles, challenges to accurate emissions measurement, and the limitations and problems of current on-road emissions studies.

Understanding the issues of time alignment, sensor time response, and design of on-road emissions systems while performing tests under representative driving conditions was the aim of conducting this literature review. It was hoped that by learning from other researchers results and limitations, greater progress could be made in the development of the current emissions measurement system.

19
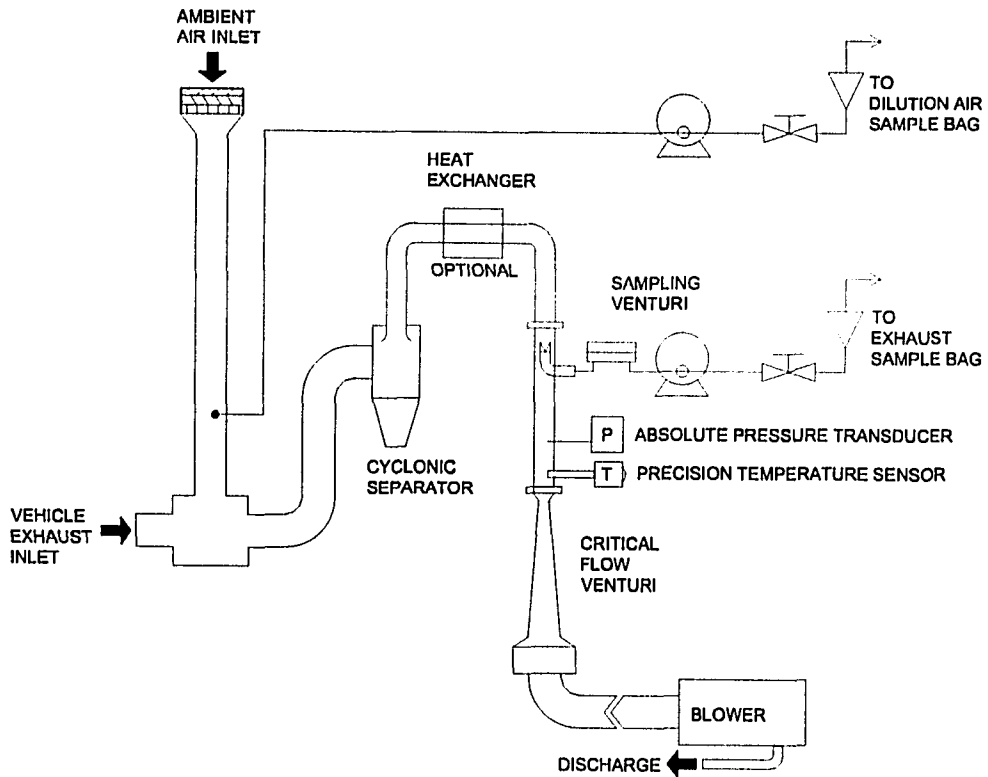
Figure 2-1 CFV - CVS Sampler Unit
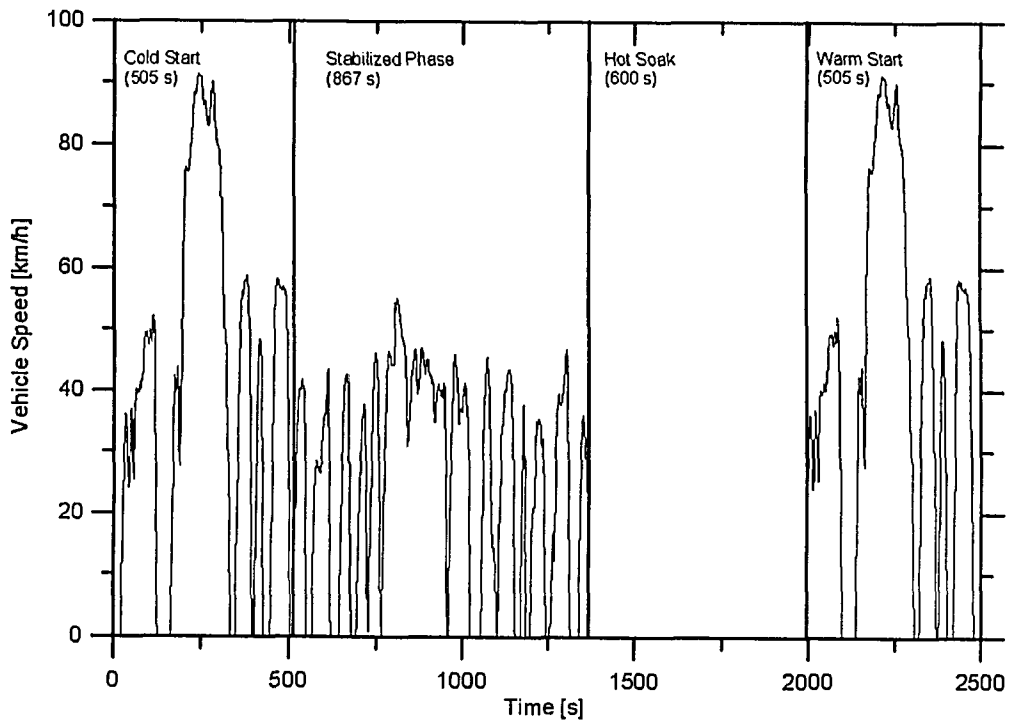
Figure 2-2 FTP-75 Urban Driving Cycle

20
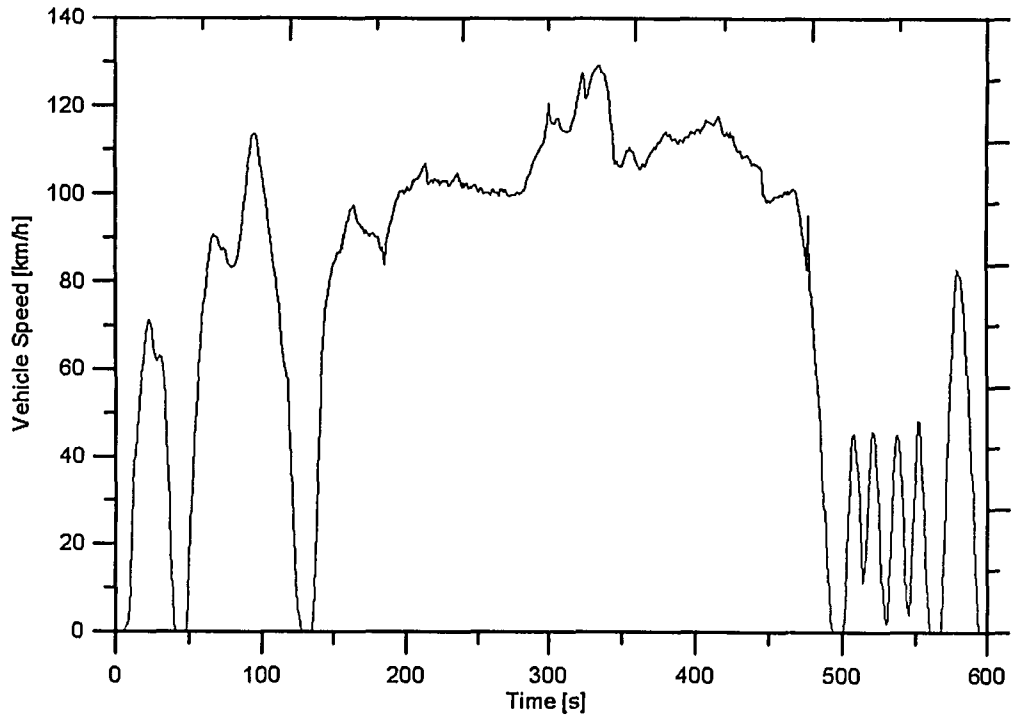
Figure 2-3 US06 Supplemental FTP Driving Cycle
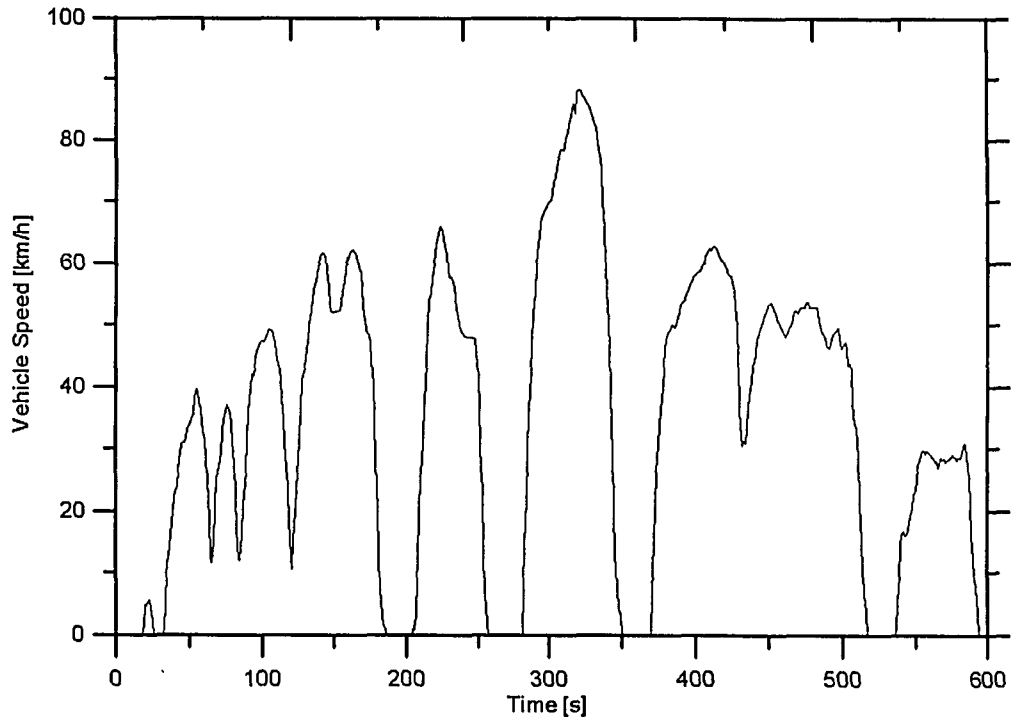
Figure 2-4 SC03 Supplemental FTP Driving Cycle

21

REFERENCES

[1]   Mondt, J.R., "Cleaner Cars," Society of Automotive Engineers, Warrendale, PA., 2000.

[2]   "Canadian Environmental Protection Act, 1999", Canada Gazette, Part II, SOR/2003-1 to 20 and SI/2003-1 to 6, Statutory Instruments 2003, Pg.2 - 499. http://canadagazette.gc.ca/partII/2003/20030101/html/sor2-e.html

[3]   U.S. EPA Office of Mobile Sources, Regulatory Announcement, "EPA's Program for Cleaner Vehicles and Cleaner Gasoline," EPA420-F-99-051, Dec. 1999.

[4]   2000 SAE Handbook, Vol.1, "Constant Volume Sampler System For Exhaust Emissions Measurement," SAE J1094 JUN92, p.13.140.

[5]   Federal Register, U.S. Environmental Protection Agency, "Motor Vehicle Emissions Federal Test Procedure Revisions; Final Regulations, Part II," 40 CFR Part 86, Oct.22, 1996. www.epa.gov/otaq/url-fr/fr22oc96.pdf

[6]   U.S. Environmental Protection Agency, Office of Air and Radiation, Office of Mobile Sources, Certification Division, "Final Technical Report on Aggressive Driving Behavior for the Revised Federal Test Procedure Notice of Proposed Rulemaking," Jan.31, 1995. http://www.epa.gov/oms/reg/ld-hwy/ftp-rev/ftp-us06.pdf

[7]   U.S. Environmental Protection Agency Certification Drive Cycle Information: http://www.epa.gov/otaq/sftp.htm#cycles http://www.epa.gov/otaq/labda.htm

[8]   Battelle, "Generic Verification Protocol for On-Board Vehicle Emission Monitors," U.S. Environmental Protection Agency, Environmental Technology Verification Program, Aug.2002.

[9]   Hawirko, J.D., "Modeling Vehicle Emission Factors Determined with an In-Use & Real-Time Emissions Measurement System," Master of Science Thesis, Department of Mechanical Engineering, University of Alberta, 2003.

[10]   Thiel, W., Hornreich C., Morsch O., Seifert G.E., "Problems of Partial Sample Systems for Modal Raw Exhaust Mass Emission Measurement," SAE Technical Paper 2003-01-0779, Society of Automotive Engineers, 2003.

[11]   Hawley J.G., Brace C.J., Cox A., Ketcher D., Stark R., "Influence of Time-Alignment on the Calculation of Mass Emissions on a Chassis Rolls Dynamometer," SAE Technical Paper 2003-01-0395, Society of Automotive Engineers, 2003.

[12] Bannister C.D. "Further Investigation on Time-Alignment," SAE Technical Paper 2004-01-1441, Society of Automotive Engineers, 2004.

[13] Vojtisek-Lom M., Cobb J.T., "Vehicle mass emissions measurements using a portable 5-gas analyzer and engine computer data," in Proceedings - Emissions Inventory, Planning for the Future, Air & Waste Management Association; Pittsburgh, PA, 1997.

[14] Frey H.C., Rouphail N.M., Unal A., Colyar J.D., "Measurement of On-Road Tailpipe CO, NO, and Hydrocarbon Emissions Using a Portable Instrument," in Proceedings - Annual Meeting of the Air and Waste Management Association, June 24-28, 2001.

[15] Kato, N., Kurachi, H., and Hamada, Y. "Thick Film ZrO2 NOx Sensor for the Measurement of Low NOx Concentration," SAE Technical Paper 980170, Society of Automotive Engineers, 1998.

[16] Truex T.J., Collins J.F., Jetter J.J., Knight B., Hayashi T., Noriyuki K., Suzuki N., "Measurement of Ambient Roadway and Vehicle Exhaust Emissions - An Assessment of Instrument Capability and Initial On-Road Test Results with an Advanced Low Emission Vehicle," SAE Technical Paper, Society of Automotive Engineers, 2000.

[17] Asano I, Nakamura H, Miyai M., Adachi M., Hosoi K., "Improvement of Modal Mass Analysis with Analyzer Hardware Optimizations and Mathematically Enhanced Response Time," SAE Technical Paper 2004-01-0970, Society of Automotive Engineers, 2004.

[18] The OBDII Home Page, Sponsored by AutoTap, "OBD-II Background," Oct.20, 2004. www.obdii.com

[19] Vojtisek-Lom M., Lambert D.C., Wilson P.J., "Real-world Emissions From 40 Heavy-Duty Diesel Trucks Recruited at Tulare, CA Rest Area," SAE Technical Paper 2002-01-2901, Society of Automotive Engineers, 2002.

[20] Cicero-Fernandez, P., Long, J.R., and Winer, A.M. "Effects of Grades and Other Loads on On-Road Emissions of Hydrocarbons and Carbon Monoxide," Journal of Air & Waste Management, ISSN 1047-3289, 47:898-904, 1997.

[21] Cadle S.H., et al. "Real-World Vehicle Emissions: A Summary of the Tenth Coordinating Research Council," On-Road Vehicle Emissions Workshop, March 2000.

[22] Cicero-Fernandez, P., Long, J.R., "Grades and Other Loads Effects on On-Road Emissions: An On-Board Analyzer Study," California Air Resources

23

Board, Mobile Source Division, Fifth CRC On-Road Vehicle Emissions Workshop, Apr.3-5, 1995.

[23]   Hawirko J.D., Checkel M.D., "Real-Time, On-Road Measurement of Driving Behavior, Engine Parameters and Exhaust Emissions" SAE Technical Paper 2002-01-1714, Society of Automotive Engineers, 2002.

[24]   Hawirko J.D., Checkel M.D., "Quantifying Vehicle Emission Factors for Various Ambient Conditions using an On-Road, Real-Time Emissions System," SAE Technical Paper 2003-01-0301, Society of Automotive Engineers, 2003.

[25]   Oestergaard K., Porter S., and Nevius T., "Investigation into the Performance of an On-Board Emissions Measurement System Using a Vehicle Exhaust Emissions Simulator," SAE Technical Paper 2003-01-3746E, Society of Automotive Engineers, 2003.

[26]   Weaver C.S., Petty L.E., "Reproducibility and Accuracy of On-Board Emissions Measurements Using the RAVEM™ System," SAE Technical Paper 2004-01-0965, Society of Automotive Engineers, 2004.

24

CHAPTER 3

Time Resolution Effects on Accuracy of
Real-Time NOx Emissions Measurements

The effects of sensor time resolution on short transient and full cycle emission results was a contentious issue in previous on-board emissions reporting. The initial two goals of the research project were therefore set to enable the solution of this problem and to provide confidence for future emissions studies. Chapter 3 provides a comprehensive evaluation of the differences between a slow response multi-gas analyzer and a fast response in-line dedicated NOx sensor on a qualitative and quantitative basis. The challenges in measuring real-time and full cycle emission rates are identified and the sensors are compared in short and long duration time frames. The use of an analytical response correction algorithm is also presented with discussion of its benefits and limitations for use clearly described.

This chapter is based on a technical paper accepted for presentation at SAE International Congress 2005, (SAE 2005-01-0674).

3.0 Introduction

On-going urban air quality problems and the demand for improvements have prompted legislatures to develop continually more stringent environmental requirements for an ever increasing number of motorized machinery. January 1, 2004 marks another milestone in the U.S. EPA's time line of regulating increasingly lower on-road vehicle emissions as national Tier 2 emission standards take effect.[1,2] Modern automotive technologies have proven capable of meeting the required certification levels under specified test conditions. A standardized lab-based emissions testing system known as the Constant Volume Sampling (CVS) system provides the basis for individual vehicle certification while remote-sensing and tunnel studies are used to quantify fleet performance under certain operating conditions. The recent development of fast, accurate, and portable emissions testing equipment has also expanded researchers' focus on measuring real-time on-road emissions to quantify performance over a wide range of conditions.[3-18]

The advantages of real-time emission measurements include the ability to examine emissions generated from specific vehicle events, the capability to test in remote locations and environmental conditions, and an increased accuracy in measuring emission system durability. The previous existence of emissions defeating devices [19,20], which produce lower NOx emissions during FTP certification tests, also gives rise to the importance of on-board emissions testing. Previous defeat devices have used engine electronic control system strategies to lean out engine operation during extended steady cruise conditions thus achieving greater fuel savings at the expense of NOx emissions. On-road emissions measurement systems also allow for the improvement in roadway design based on minimizing vehicle operation in high emitting modes.[21]

This chapter will specifically examine NOx emissions from on-road vehicles, due to the significant effects NOx has on the environment and public health. NOx negatively impacts the environment through diminishing regional air quality by increasing ground level ozone and hence smog concentrations. Elevated levels of NOx, ozone, and smog are associated with measurable public health impacts such as an increased number of hospital admissions, emergency room visits, and restricted activity days. Directly attributable ill effects can come in the form of cumulative lung damage, nose and eye irritations, coughing, acute respiratory infections and a number of other respiratory illnesses.[22,23] NOx produced by on-road vehicles is a significant contributor to national emissions inventories, accounting for 49% of U.S. national NO_2 in 2002.[22] This combination of known environmental and health impacts with volumetric production makes it important to study vehicular NOx emissions, particularly in urban areas where human contact is highest.

The focus of this chapter will be on illustrating the challenges in accurately measuring real-time mass emissions of NOx with specific attention given to the issue of sensor time resolution. Challenges in accurately measuring mass emission

26

rates of real-time data include time alignment of vehicle and emissions data, sensor time response to transient emission levels, and sample line concentration smearing. The benefits and limitations of applying data alignment and response correction algorithms to improve emission results accuracy will also be shown. Laboratory test data as well as real-time emissions measurement data serve as a means of illustrating the qualitative and quantitative effects on accuracy.

3.1 Experimental Set-up / Configuration

The experimental setup used for this research was developed based on earlier research which measured on-road real-time emissions using a network of vehicle mounted sensors, an air/fuel ratio sensor, and a 5-gas emissions analyzer. The base system facilitated the measurement of vehicle operation parameters including mass air flow rate, ambient temperature, intake temperature, coolant temperature, air/fuel ratio, vehicle speed, acceleration, engine speed, and vehicle emissions. This measurement system was improved upon through the addition of two new measurement devices. These new instruments consisted of an OBDII port scanner and a fast response NOx sensor. Figure 3-1 emphasizes the physical locations of the NOx and vehicle (OBDII) sensors, sample handling equipment, and data gathering hardware.

Mass air flow rate was measured using a Siemens HFM 62B mass air flow rate sensor which was calibrated against an ASME standard nozzle. Temperature measurements were made using AD590 temperature probes [24]. The ambient temperature probe was mounted to the vehicle antenna located on the front quarter panel of the passenger side. Intake temperature measurements were taken by mounting the probe in the vehicle's intake system prior to the Siemens's installed and vehicle mass air flow sensors. Coolant temperature was measured as a relative value by fixing the probe to the coolant hose exiting the engine block. Barometric pressure was measured at one end of the trip using a lab barometer. Air fuel ratio was measured using an ECM AFRecorder 2400E fast response lambda sensor which facilitated the calculation of fuel consumption knowing the mass air flow rate. The AFRecorder also measured engine speed using an inductive spark pickup. The vehicle speed pickup unit and the accelerometer were removed from the original system and replaced with vehicle speed data (from an OBDII port scanner) and calculated values of acceleration (from vehicle speed data).

The addition of the AutoTap OBDII port scanner allowed for the viewing and recording of all vehicle sensor data in real-time. Standardized OBDII data ports are present on 1996 and newer vehicles as is a basic set of emissions related readings which was mandated by the U.S. EPA. SAE specification J1979 defines the legislated parameters. Vehicle parameters that were gathered include engine speed, vehicle speed, coolant temperature, intake air temperature, mass air flow rate, barometric pressure, current gear, calculated engine load (%), and numerous

27

others.

NOx emission measurements were obtained through two sources, the first was a Vetronix PXA-1100 portable five gas analyzer which measured Carbon Monoxide (CO), Carbon Dioxide (CO_2), unburnt Hydrocarbons (HC), Oxides of Nitrogen (NOx), and Oxygen (O_2). Infrared absorption was used to measure CO, CO_2, and HC, while chemical cells were used to measure NOx and O_2. The sample was obtained by drawing a continuous flow of exhaust gas through a sample line from the end of the vehicle tailpipe. The sample line was insulated to prevent condensation in the sample line and sample line freezing in extreme cold temperature testing. A standard tailpipe probe was used with the sample line to minimize instrument pressurization effects. The five-gas analyzer also included a coalescing filter in its internal sample system.

The second NOx sensor was a Horiba MEXA-720NOx zirconia ceramic type ("fast response") sensor which was mounted in the tailpipe immediately downstream of the catalytic converter. The addition of this fast response NOx sensor provided the benefit of improved resolution of transient NOx data as well as a reduction in the variability in emissions/vehicle data synchronization. An inherent benefit of the Horiba fast response NOx sensor, is its ability to measure the NOx concentration directly at the source without having to transfer sample gases through a sampling system which creates increased uncertainty in aligning emissions and vehicle data. Sensor calibration and maintenance procedures can be found in Appendix F.

Monitoring and recording of all data was conducted through the use of a Dell Inspiron laptop computer running Labview 6i and AutoTap proprietary software. Analog signals were collected and logged using a National Instruments (NI) DAQCard-AI-16E-4 PCMCIA data acquisition card which was capable of monitoring eight differential analog signal inputs with twelve bit resolution and selectable gains of 1, 2, 5, 10, 20, 50, or 100. Gas analyzer and OBDII port data were transmitted via serial connections (through a dual nine pin serial to USB converter) into the laptop.

Labview software was written to communicate with the analog signal inputs from the data acquisition card, as well as the Vetronix gas analyzer which communicated via an RS 232 serial connection. Simultaneous operation of the AutoTap software allowed for viewing and recording of vehicle ECM sensor data. The two data files were synchronized by matching initial engine speed readings as the vehicle was started, and eliminating all data up to engine startup. Sampling frequency of the Labview software varied between 1.5 and 2.0 Hz while OBDII port data varied between 1.3 and 1.7 Hz, depending on the number of parameters being recorded. Increasing the number of recorded parameters decreased the frequency of individual sensor readings. Figure 3-2 illustrates the parameters measured and the configuration of the on-board emissions measurement system.

28

3.2 Experimental Vehicle

A 1999 Chevrolet Silverado C1500, extended cab, four-wheel drive truck was used as the test vehicle for these experiments. The vehicle was equipped with a 5.4 L V8 Vortec gasoline fueled engine, automatic transmission, short-box bed, which operated in two-wheel drive mode for all tests. The dry weight of the vehicle with all sensors and emissions measurement equipment installed measured 2360 kg (~5200 lbs). Vehicle mileage ranged from 105,500 km at the start of testing in October 2003 to the current 108,500 km as of the last emissions experiment. Currently the C1500 is being used as an emissions research test vehicle, as well as a utility vehicle for student vehicle projects at the University of Alberta. The truck was originally obtained as an experimental vehicle for competition in the 2000 Ethanol Vehicle Challenge sponsored by General Motors and the U.S. and Canadian governments. At the completion of the competition, the vehicle was converted back to the stock gasoline power configuration.

3.3 On-Road NOx Measurement Tests

Vehicle emission measurements were taken with the goal of reproducing FTP type driving cycles. Driving patterns attempted to generate similar time, distance, and energy consumption values as the FTP-78 urban and highway cycles. The results presented below examine short time periods within full cycle tests in which vehicle operation conditions were rapidly changing (transients).

3.4 NOx Measurement Challenges

The calculation of mass NOx emission rates ideally requires the matching up of mass air flow data with NOx emission data, which responds at the same (ideally instant) rate. The presence of a delay time between NOx production in the engine and measurement at the sensor is due to exhaust pipe and sample line transit time. This challenge, coupled with the non-instantaneous response rates of the sensors, present the most significant challenges to instantaneous emission rate calculations.

NOx mass emission rate is calculated as:

$$E_{NOx} = \frac{\dot{m}_{exh} \times \chi_{NOx} \times MW_{NOx}}{MW_{exh}} \quad \text{[Equation 1]}$$

To generate accurate NOx mass emission rates, the four parameters which make up the mass emission rate calculation must be known accurately and on a timely basis. The molar mass of NOx is fixed so measuring an accurate emission rate required knowledge of the other three factors. Exhaust molar mass can be calculated accurately from known air and fuel flows, (by balancing a combustion equation) and confirmed by basic exhaust gas analysis. Exhaust mass flow rate is

29

the total of air and fuel input rates which are generally assumed to be well known, (provided leaks or additions from air pumps and gulp valves are minimal). However, engine mass flow rate changes rapidly with power demand, particularly for spark ignition engines, so there is some concern about the time response of air and fuel measurements. The final factor is molar concentration of NOx measured by some sort of exhaust gas sensor. Because of the transient nature of engine NOx output, any delay in obtaining and analyzing an exhaust sample for NOx is critical in accurately measuring the mass emission rate.

The three critical aspects of timely concentration analysis are: correct time alignment of NOx concentration and exhaust mass flow rate data, NOx sensor time response, and sample line mixing which "smears" sharp NOx concentration fronts and thus degrades response time. Figure 3-3 indicates the challenges associated with producing an accurate mass emission rate of NOx.

It is immediately evident when looking at the raw data (bottom graph of Figure 3-3), that using the raw time delayed (unaligned) concentration data with the instantaneous exhaust mass flow rate results in a mass emission rate that is greatly in error. Time alignment of the concentration and exhaust flow data (middle graph of Figure 3-3), results in a dramatically improved mass emission rate, although the effect of the sensors simple lag time response is still evident. The ideal case (top graph of Figure 3-3) illustrates the expected mass emission rate of NOx when sensor time response is no longer an issue, in other words, instantaneous response is achieved. The goal of on-road vehicle emission testing which attempts to produce real-time mass emission rates should therefore attempt to correct both time alignment and time response issues inherent in the raw data.

3.4.1 NOx Sensor Time Response

Figure 3-4 below indicates the typical response curves of the fast and slow responding NOx sensors to a step change NOx concentration and Table 3-1 presents the first order time constants drawn from analysis of Figure 3-4. The response rates were calculated by inputting the same NOx concentration step change to both sensors, to ensure consistency in procedure. Also, calibration of both sensors utilized similar NOx concentrations with a nominal calibration concentration of 2000 ppm for both sensors and additional intermediate values of 1000 ppm and 3000 ppm for the fast response sensor.

The comparison in Table 3-1 is between the faster in-line NOx sensor and the slower remote gas analyzer located in the vehicle cabin and drawing an exhaust sample through a sample line from the tailpipe. Laboratory experiments were conducted with both the Horiba ZrO_2 type NOx / O_2 sensor and the Vetronix PXA-1100 5-Gas Analyzer to quantify the time constant of each NOx sensor. Table 3-1 illustrates the noticeably faster response of the in-line sensor versus the remote analyzer, showing time constants of 2.0 s and 6.4 s. The test also confirmed a

30

further deterioration in remote-sensor response rate (to 7.0 s time constant) with the tailpipe-to-analyzer sample line installed. This extra time constant is attributed to axial diffusion in the sample line which operates as laminar flow due to its small diameter and low flow rate. Establishment of a fully developed laminar velocity profile "smears" sharp axial concentration steps since the velocity at the center of a laminar profile is approximately twice the bulk velocity. (It is noteworthy that, despite the low sample line Reynolds number <10^3, the laminar flow "smearing" was much less than predicted for a fully developed laminar flow.)

Table 3-1 First-Order Time Constants

	Effective Time Constant [s]	Std. Dev. [s]
In-Line Sensor	2.00	0.26
Remote w. Tailpipe Only	6.37	0.23
w. Tailpipe + Sample Line	6.97	0.11
Mass Air Flow Sensor	0.03	-

Figure 3-5 indicates that the "fast" in-line sensor exhibited first-order behavior when a step change concentration was introduced, whereas the remote analyzer showed less correlation to first-order behavior (Slow Resp. Sensor - [full resp.]). However, if the initial 2 seconds of response are omitted, it can be·seen that the remaining response curve (Slow Resp. Sensor [minus first 2 seconds]) quite appropriately defines a first-order curve. The time constant of the remaining response, which behaves as a first order curve, exhibited a significantly faster response of 4.30 seconds.

The impact of these noticeably different sensor response characteristics requires exploring on various small time scales to measure the impact response rate has on not only small section transient emission rates, but also on full cycle emissions analysis. An additional consideration of universal exhaust gas oxygen (UEGO) sensors (similar to the Horiba fast response NOx sensor) is their 1:1 response to ammonia emissions. Although the fast response sensor is known to be sensitive to ammonia, the ammonia emissions of this vehicle were thought to be negligible and were ignored.

3.4.2 Time Alignment of Emissions / Vehicle Data

The synchronization of pollutant concentration data with vehicle operation data is non-trivial due to a number of constant and variable delays present in the system, where variable time delays are functions of engine operation. The three time delays present in the emissions measurement system include transit delay times due to: the vehicle exhaust system, the analyzer sample line, and the internal plumbing of the analyzers. The schematic in Figure 3-6 indicates these time delays as well as

31

the sensor time constants of the comparative NOx sensors.

The difference in NOx sensor operation and sensor location drastically affects the time at which NOx emission events are recorded. The "fast" response NOx sensor is located in the exhaust pipe (in-line sensor) just downstream of the catalytic converter, requires no sample handling, and is exposed to exhaust within 1 second of the air and fuel being consumed by the engine. In contrast, the "slow" 5 gas analyzer waits for exhaust to pass through the entire exhaust pipe and then be drawn through its own sample line, processes which impose a 9 to 13 second transport delay time before the gas analyzer even "sees" a sample. The variability in transit delay time arises because exhaust mass flow rate and density vary with engine speed and load. Correctly accounting for this transit delay is crucial in ensuring that the NOx concentrations measured by a remote analyzer are multiplied by an appropriate exhaust mass flow rate since mass flow rate may vary by an order of magnitude within a time scale of seconds.

Although the sensitivity of emissions results has not been widely studied, it has been shown that a misalignment of even 1 second can have serious effects on short cycle results.[25] Similarly, a 1 second misalignment can drastically affect catalyst efficiency experiments.[26] Remote analyzer emission sensors have been shown to be the most affected by time alignment. Ignoring the roughly 10 second time constant shift of this emissions system, reduces remotely measured g/km numbers by 48% because the analyzer's highest NOx readings tend to fall after the high mass flow period. Many on-road emissions studies confirm the fact that continued work needs to be done to analyze the most appropriate way to align vehicle data with emissions data.[6,25,26]

In attempting to properly synchronize the emissions and vehicle data, three alignment algorithms were developed and analyzed with the goal of matching spikes in NOx concentration to spikes in mass air flow rate. This matching rational was chosen due to the fact that spikes in mass air flow rate result due to increases in engine load (engine cylinder pressure) and hence temperature, which are key factors in the production of NOx. Therefore, the goal was set to find an algorithm that most closely aligns these two parameters.

Constant time, variable time, and conservation of mass shifting algorithms composed the array of options for aligning vehicle and emissions data. Previous work by Hawirko [16,17] utilized the constant time shifting (CTS) algorithm, due to its simplicity and reasonable accuracy in matching concentration and mass flow rate data. Use of the new variable time shifting (VTS) algorithm, and conservation of mass shifting (COMS) algorithms, attempts to improve on the alignment of data by more accurately reflecting the real transit times occurring. The occurrence of varying engine speeds during the test cycle, undoubtedly results in changes in exhaust velocity and therefore transit delay times, which warrants examination of a variable time shifting algorithm.[25]

32

The CTS algorithm was arrived at by examining the value of time required to align the data based on results from a number of on-road tests. After trial and error visual inspection tests were completed, it was shown that a constant time shifting value of 12 and 0.75 seconds respectively, for the slow and fast NOx sensors, was required to properly align the data. Data processing then simply shifted all NOx data forward to match up with vehicle data. An example of the CTS algorithm applied to slow response NOx data is shown in Figure 3-7, similar results occur for the fast response sensor although shifting is done at 0.75 seconds.

The vehicle was initially cruising at a negligible load and an exhaust mass flow rate around 7 g/s. It then accelerates moderately for about 15 seconds with exhaust mass flow rate rising as high as 30 g/s. The remotely measured NOx concentration does not begin to respond to this event until the acceleration event is almost over and the mass flow is dropping back to 7 g/s. Proper adjustment for the sample transit delay time must account for the fixed sample line transit times and for the variable exhaust system transit time which is affected by exhaust system flow rate and density.

The VTS algorithm, which uses experimental data to predict the time shift, is used to account for the variable transit time which occurs in the exhaust with changes in engine operation. Plotting the transit time through the exhaust system versus exhaust mass flow rate resulted in a near linear fit from idle conditions of approximately 7 g/s up to 30 g/s. Exhaust mass flow rates greater than 30 g/s resulted in a fraction of a second exhaust transit time and therefore a constant overall system time delay due to sample line and internal delays, which are unchanged with engine operation. The VTS algorithm aligns the data by first finding the appropriate delay time, at each data point, from the calculated exhaust mass flow rate, then searching forward in time for the correct NOx data that matches up with current vehicle events.

The delay time was calculated by fitting a curve to the linear portion of the variable transit time curve up to 30 g/s exhaust flow rate. For exhaust flow rates above 30 g/s, a constant 8.9 s NOx delay time was used.

Figure 3-8 shows how the same emissions event depicted in Figure 3-7, is shifted using the variable time shifting algorithm. The VTS algorithm adjusts the time series by varying amounts to best reflect the time at which the emissions were produced by the engine. At periods of low mass flow rates, the transit time is longer (of the order of 12 seconds) and at higher mass flow rates, the transit time drops to less than 10 seconds.

Realizing that a sudden drop in mass exhaust flow rate may leave a "gap" in time in which recorded NOx data is not used in the new aligned data, a Matlab program was written and implemented directly following the time alignment code, which would test the number of points missed, their significance (magnitude), and average value. The results of this analysis are shown below in Table 3-2. From this table

33

it can be shown that the variable time shifting algorithm is using more than 99% of the original data points when re-aligning the data. The approximately 2 Hz data frequency, and relatively moderate mass flow rate increases are the likely reasons for this high degree of data utilization. An interpolation algorithm utilizing more than 2 points to fit a curve would therefore guarantee that no points are missed should the magnitude of the average value missed and number of points missed be an issue.

Table 3-2 VTS Algorithm - Missing Data Qualification

Test / Sensor	Pts Missed [No. of Pts. - % of Pts.]	Avg Value Missed [ppm]	Max Pt. Missed [ppm]
Case 1 Slow Resp. Fast Resp.	11 pts - 0.4% 0 pts - 0.0%	73.5 0.0	151.0 0.0
Case 2 Slow Resp. Fast Resp.	18 pts - 0.4% 2 pts - 0.0 %	67.6 19.4	279.0 30.0
Case 3 Slow Resp. Fast Resp.	22 pts - 0.7% 1 pts. - 0.0%	45.4 14.7	217.0 14.7
Case 4 Slow Resp. Fast Resp.	13 pts.- 0.5% 2 pts. - 0.1%	102.6 38.5	210.0 70.3

The third time shifting algorithm, COMS, utilizes the principle of conservation of mass in the exhaust system to theoretically evaluate the time shift. COMS assumes an average temperature and pressure in the exhaust pipe, as well as a molecular weight for exhaust components, to produce an estimated theoretical mass in the exhaust pipe. Referring to Heywood, the use of an average exhaust temperature of 500°C, ambient pressure, and a molecular weight of 33.2 kg/kmol results in a total emissions system mass of 18.6 g.

The transit time in the exhaust pipe is then calculated by integrating forward in time (from the current time) to find out how long it will take for the engine to fill the exhaust pipe with the theoretically calculated mass. Then the transit time delay value calculated is used to shift-back the delayed emission reading to align the emissions value to the vehicle event.

To calculate the most appropriate algorithm to match the data sets, a series of full cycle tests were examined to quantify the average misalignment. Initial use of 12.5 and 0.5 seconds as time shifting constants for the CTS algorithm, proved to require minor modifications as the average value over numerous tests showed a 0.55 seconds leading, and 0.25 second trailing response curve for the slow and fast sensors respectively. Therefore, CTS constants were altered to use the modified and now optimized 12.0 and 0.75 seconds for the slow and fast response sensors

34

respectively. The results of this analysis also indicate that the VTS algorithm seems to be accurately aligning the fast response sensor, however, the slow response sensor appears to be trailing the mass air flow data by nearly 1.4 seconds.

Table 3-3 Time Alignment Algorithm Evaluation / Optimization

Sensor	CTS Time [+/- s]	VTS Time [+/- s]	COMS Time [+/- s]
Slow Resp.	- 0.55	1.39	1.99
Fast Resp.	0.25	0.07	- 0.33

The misalignment in the VTS algorithm is likely the result of signal "smearing" which occurs due to the algorithm compression of data near the spike of a mass air flow rate curve. This compression of data is the result of shifting at smaller and smaller values due to increased exhaust flow rates, which results in an initial NOx plateau before the subsequent rise in concentration. When comparing the CTS and VTS shifted NOx data in Figure 3-9, it can be seen that the VTS signal is "smeared" with respect to the CTS shifted NOx data. The initial plateau in the VTS signal due to bunching is caused by shifting low initial concentration data which results from a sensor with a very large time constant. The signal generated from a fast response sensor would be represented much more accurately by the VTS algorithm.

Table 3-4 Alignment Algorithm Comparison

Test	Sensor (Resp.)	Unaligned [g/km]	CTS [g/km]	VTS [g/km]	COMS [g/km]
Case 1 (short trans)	Slow	0.027	0.251	0.125	0.113
	Fast	0.339	0.302	0.354	0.291
Case 2	Slow	0.037	0.230	0.217	0.211
	Fast	0.205	0.197	0.207	0.194
Case 3	Slow	0.033	0.280	0.239	0.237
	Fast	0.287	0.276	0.303	0.272
Case 4 (short trans)	Slow	0.126	0.188	0.190	0.132
	Fast	0.297	0.509	0.470	0.515
Case 5 long trans.	Slow	0.092	0.179	0.181	0.178
	Fast	0.164	0.154	0.170	0.149
Case 6 long trans.	Slow	0.099	0.173	0.154	0.155
	Fast	0.139	0.136	0.139	0.137

Therefore, due to the larger misalignment of both the VTS and COMS alignment algorithms, it has been concluded that using an optimized CTS algorithm would

35

provide the most accurate NOx mass emission results.

To understand the importance of the CTS algorithm constant to mass emission values, a sensitivity analysis was completed which varied the constants from +4 to -4 seconds from their current value. The results of this analysis are shown in Table 3-5 and indicate that the fast response sensor predicted maximum emission rates when shifted at the CTS constant value. This result is due to the alignment of MAF rates and NOx concentrations. The lone case in Table 3-5 where the mass emission rate increases, J28,3,A, is due to the re-alignment of a larger secondary NOx spike with the same mass flow rate which yields a larger mass emission rate. When looking at the slow response sensor results, it can be seen that the maximum mass emission value results at or near the CTS constant value. Larger values off center of the constant value are due to realignment of secondary spikes with mass flow rates.

Having acknowledged the challenges in measuring NOx mass emission rates resulting from time alignment and sensor time response, it has been shown that reasonable accuracy can be obtained in aligning emission and vehicle data. However, the issue of sensor time response on the overall accuracy of short and long transients, as well as full cycle results requires examination.

Table 3-5 Sensitivity Study of CTS Algorithm

Test		Overshift 1 + 4 s	Overshift 2 +1 s	CTS [g/km]	Undershift 1 -1 s	Undershift 2 - 4 s
Case 1 short trans.	Slow	0.246	0.276	0.251	0.204	0.069
	Fast	0.064	0.217	0.302	N/A	N/A
Case 2 long trans.	Slow	0.211	0.230	0.230	0.226	0.198
	Fast	0.154	0.179	0.197	N/A	N/A
Case 3 long trans.	Slow	0.278	0.289	0.280	0.268	0.228
	Fast	0.268	0.266	0.276	N/A	N/A
Case 4 short trans.	Slow	0.630	0.226	0.188	0.144	0.127
	Fast	0.859	0.465	0.509	N/A	N/A
Case 5 long trans.	Slow	0.129	0.167	0.179	0.182	0.177
	Fast	0.120	0.129	0.154	N/A	N/A
Case 6 long trans.	Slow	0.170	0.175	0.173	0.171	0.152
	Fast	0.125	0.134	0.136	N/A	N/A

3.4.2.1 Response Correcting Algorithms

Enhancing the temporal response of NOx sensors can be done using digital signal

36

processing. The use of the well-mixed flow model is one such algorithm that can accomplish this. The well-mixed flow model is outlined below with reference to Figure 3-10. Appendix B shows a more detailed derivation of this equation as well as how it may be written using mass flow rates instead of a volumetric flow rate basis.

$$M = CQ \quad \text{(Mass in the Well-Mixed Cell)}$$

Mass Balance:

$$\frac{dM}{dt} = \dot{Q}\left(C_{in} - C_{out}\right) \quad \text{which yields,} \quad \frac{d(CQ)}{dt} = \dot{Q}\left(C_{in} - C_{out}\right)$$

simplifying then yields,

$$\left(\frac{Q}{\dot{Q}}\right) * \frac{dC}{dt} = C_{in} - C_{out}$$

$$\tau * \frac{dC}{dt} = C_{in} - C_{out} \quad \text{where,} \quad \tau = \frac{Q}{\dot{Q}}$$

Therefore:

$$C_{in} = C_{out} + \tau * \frac{dC}{dt}$$

This algorithm uses conservation of mass to produce an algorithm which attempts to reproduce the step change input knowing the current cell concentration, cell residence time (time constant), and cell concentration gradient. Replacing the cell residence time with the first order time constant of the sensor generates similar results.

The use of response correcting signal processing is aimed at generating more accurate and representative real-time emissions results for sensors with significantly long time constants. However, the use of any digital signal processing algorithm is inherently going to magnify any noise present in the data signal.[6] Noise magnification results when the processing algorithm contains a gain term, which when multiplied by any signal noise results in amplification. Therefore, caution should be taken in choosing time constants and differentiating routines which will minimize overshoot so as not to introduce unnecessarily erroneous data. Appendix B details the time constant and differentiating routine options available for use with the well-mixed flow model.

It should also be noted that the use of post-processing to correct simple lag signals is not able to create data where no data is present. The omission of a concentration spike due to a slow response sensor, cannot be corrected through this technique, therefore the most accurate way to measure true transient emission values is

37

through the use of fast response sensors with equally sufficient sampling rates.

The use of the well-mixed flow algorithm was evaluated for both NOx sensors using a combination of time constant schemes and differentiating routines to produce 6 possible response correcting algorithm options. The three time constant alternatives chosen were the single time constant (exhibited by the sensor, shown in Table 3-1), and two variable value time constant options which were calculated by analyzing experimental data. The variable value time constant sets varied throughout the early first order response portion of the laboratory response curves to most accurately reproduce the step change input. Two different numerical differentiating routines were also applied which included a simple 2 point differential as well as a more accurate "enhanced" 5 point numerical differentiating algorithm.

An analysis of the accuracy of the response correction algorithms was completed on simulated signals representative of the actual response of the two sensors. From this analysis, it was decided that the most accurate method for correcting the sensor response was to use a single time constant value with simple differentiation in the well-mixed flow model. The results of this analysis are shown in Appendix C.

Figure 3-11 illustrates the application of the chosen correction algorithm to a simulated Horiba (fast response) NOx and Vetronix (slow response) NOx signal respectively.

Work completed by Truex, et al. [6] used the well mixed flow data to correct an FTIR emissions analyzer (which measured HC, CO, NO, and CO_2) with a 20 second cell fill time. It was found that for this slow response signal, although noise was magnified in the final signal, the impact was small relative to the overall improvement in accurately reproducing the input concentration. Similarly, signal processing by Asano, et al.[27] used de-convolution of the analyzer response to improve the response time of a 0.9 second time constant sensor to 0.7 seconds.

3.5 Results

To resolve the importance of sensor time resolution on mass emission rate results, it is important to focus in on relatively short specific high emitting events to obtain a clear understanding of how these events will contribute to overall full test cycle results. Vehicle transients which involve rapid accelerations or high power demand typically generate higher mass emissions rate events due to increased NOx concentration production coupled with higher exhaust flow rates.

During these transients, NOx production in the engine increases due to higher peak combustion temperatures and leaner mixtures. The higher peak temperatures are associated with increased throttle opening and advanced spark timing, events which are managed by the engine controller at time scales well under one second. Likewise, leaner mixtures may occur during air and fuel flow transients but the

engine control computer responds by adjusting air/fuel ratio at a rate of several Hertz. Some of this rapid variation in engine-out NOx emission rate is damped by the catalytic converter which is optimized for oxygen storage and NOx reduction with fluctuating air/fuel mixtures. However, it is still clear that tailpipe NOx emissions will vary rapidly with concentrations rising from low values to high peaks in less than a second.

The results shown below will focus on both short duration (0-7 s) transient events as well as long duration (7+ s) transient events with the goal of comparing the two NOx sensors on a mass emission rate basis. Before focusing on individual transient events which look at short and long duration vehicle events, a number of interesting results can be seen over longer time scales.

3.5.1 Resolution Differences

The difference in sensor resolution between the NOx sensors is the first notable observation which can be seen from Figure 3-12. Over a period of approximately one minute, three significant mass air flow spikes occur in addition to numerous small mass air flow changes. Although the slow response sensor is able to resolve three significant NOx concentration increases, the NOx created by short spiky mass air flow changes is not measured by the sensor. It is evident that the fast response sensor is able to resolve the NOx spikes as much higher in concentration, earlier in occurrence, shorter in duration, and more frequent in occurrence.

From Figure 3-12 it appears as though the exact matching of the major mass air flow spikes with slow response NOx concentration data, may result in greater mass emissions. However, the relative magnitude of the slow response concentration data compared with the fast response data, reduces the effect of this matching. Case 1 of Table 3-6 shows that the fast response sensor does in fact result in a 170% greater mass emission rate, which is also shown in the cumulative gram emission profile in Figure 3-12.

Table 3-6 Sensor Resolution Effect on NOx Emission Rate During Transients

Test	Slow Response Remote Analyzer (Vetronix 5-Gas)	Fast Response In-Line Sensor (Horiba NOx)
	[g/km]	[g/km]
Case 1 Fig 3-12	0.145 +/- 0.007	0.246 +/- 0.006
Case 2 Fig 3-14	0.128 +/- 0.084	0.270 +/- 0.079
Case 3 Fig 3-13	1.060 +/- 0.019	0.567 +/- 0.018

39

Sensor response time can also result in unmatched MAF and NOx data as evidenced in Figure 3-13. In this case, a rapid spike in MAF rate for approximately 5 seconds followed by a longer 10 second MAF spike produces two noticeably different NOx profiles. The fast response sensor shows an immediate and rapid rise in NOx emissions for each MAF spike, generating an emissions rate of 0.567 g/km (Case 3, Table 3-6). Conversely the slow response sensor illustrates the hindrance of slow response time on the sensors ability to produce reliable mass emissions data with the presence of a totally unmatched NOx spike with respect to MAF spikes. The effect of this slow responding profile is actually to produce an emission rate of 1.060 g/km, twice the value of the aligned, fast response sensor result. The result is clearly not producing an accurate value of vehicle emissions and therefore indicates the severity and significance of sensor response time.

Cases similar to case 3 in Table 3-6 which are the result of misalignment, are not the only conceivable cases which may result in higher than actual mass emission rates from a response time delayed sensor. In the event that a long duration mass air flow step change event occurs, it is possible that a large but brief actual NOx emission event would occur at the leading edge of the MAF then become relatively small in concentration for the remainder of the response. If a slower response sensor responded at a lower level during this same event but matched up with the MAF step change for a longer duration, it is possible that the mass emission rate may actually be greater. Therefore, increasing sensor response time does not always mean an increase in the overall mass emission rate, but rather a more accurate result of emissions produced will be achieved.

3.5.2 Missing Spikes

It is evident that differences in sensor response time result in dissimilar concentration profiles with the slow response sensor tending to smear out concentration results. Figure 3-14 shows that the slow response sensor also exhibits the possibility of missing NOx spikes if short and slight in magnitude. The result of this omission, coupled with the slow sensor response, is a factor of two reduction in calculated mass emission rates as shown in Table 3-6 (Case 2), but it also reduces accuracy in testing, which requires accurate knowledge of primarily the concentration profile. This difference would be critical if the objective was to measure concentration profiles for catalytic converter modeling for example.[25]

3.5.3 Long Duration Transients

Vehicle events occurring over a period of 10 seconds or longer, were classified as long duration transients in the analysis of these emissions results. To produce a representative sample of long duration transient events, eight separate events from varying days and tests were selected from the on-road data gathered. The results of processing the emission rates from both the slow and fast response sensors are

40

shown in Table 3-7. Also, corrected values generated from use of the response correction algorithm are included as is the associated percentage change in emission rate versus uncorrected values.

For the long duration transient cases studied, the fast response sensor measured emission rates that were approximately 50% or greater than the slow response sensor in half of the cases, with the other half resulting in similar mass emissions results (within error limits). In only one lone case did the slow response sensor calculate higher emissions values, shown in Figure 3-15. In this case, although the NOx concentration profile does not rise as high or as fast as the fast response sensor, the amount of time which the NOx profile is at an elevated level is greater, due to the slow response. This lengthy elevated NOx level, which matches up favorably with MAF rates, results in a larger mass emission rate.

When examining the effect of the response correction algorithm on NOx emission rates, the slow response sensor data can be seen to vary between an increase of 4% and 37%. These values show stable and predictable increases in the emission rates as a result of the attempts to recreate the step input NOx concentration. When examining the effect of response correction on the fast response sensor, the results appear greater in range. For this sensor, emission rates were found to increase between 10% and 103%. The reason for this large discrepancy is due to the possibility of large brief duration spikes being created by the response correcting algorithm in a minority of cases. As mentioned previously, this result is due to data sampling rates that at some points generate large gradients in NOx data during the initial rise of the fast response sensor. Increasing the sampling frequency of the data acquisition system would improve the effectiveness of the correction algorithm. Knowing that the emissions rate predicted by the fast response sensor is as great or greater than the slow responding sensor, indicates an initial concern for the accuracy of slow responding sensors to represent full cycle emissions results. These findings, coupled with the previous results showing misalignment of NOx data with MAF spikes and omission of other minor spikes, leads to these questions of accuracy for slow responding sensors. The next section will examine short duration vehicle events and is aimed at focusing even closer on short, but high emitting vehicle events on the order of 4 seconds.

3.5.4 Short Duration Transients

The evaluation of brief but high emitting events occurring during short, rapid transients is of interest because of the relative impact these events have on full cycle emission rates. Vehicle events of seven seconds duration and less were chosen to be examined, with the average test case on the order of 4 seconds. Eight cases were examined from various dates and tests to comprise the range of short duration tests.

In all short duration transient events analyzed, the fast response sensor predicted

41

higher g/km emission rates than the corresponding slow response sensor as shown in Table 3-8. Emission rates measured at least 20% and up to several times (+100%) greater for the fast response sensor which indicates the vast range with which slow response sensors can erroneously measure short transient events. When error is considered, the fast response sensor can still be confidently known to have equal to higher emissions rates in all cases. This is a clear indication that brief, but high emission contributing effects, are being under predicted by typical slow response multi-gas analyzers and therefore under predict full cycle emissions tests.

Figure 3-16 illustrates typical response characteristics of the NOx sensors and the effect of the response correction algorithm on those profiles. From examination of the fast response sensor data, it can been that the response correction algorithm is recreating the step change input predicted. However, the amplification of signal noise from small NOx gradients can also be seen as one of the algorithm limitations.

Examining the slow response sensor data shown in Figure 3-16 indicates what has been shown earlier. A response curve occurring after the short transient event (MAF spike), with smeared profile resolution. In this case the slow response NOx profile has been corrected to exhibit a faster time constant and better alignment with the MAF spike. Although improved, the corrected signal does not achieve the same concentration magnitudes as the corrected fast response sensor. The corrected slow response sensor does however, reasonably reflect a similar profile to the fast response sensor.

Analysis of numerous other graphs revealed similar representative results. In all response correction cases for short transients, the time constant of the NOx response was improved and shifted forward to better match the spikes of NOx with MAF rate. The result of this has been shown to be higher NOx mass emission rates ranging from negligible change to 250% of the original mass emission rate.

42

Table 3-7 Long Transient Results Summary

		Comparing Sensors			Result with Correction Algorithm			
	Time	Slow	Fast	Change	Slow	Change	Fast	Change
	[s]	[g/km]	[g/km]	[%]	[g/km]	[%]	[g/km]	[%]
Case 1 Fig 3-15	14.2	0.099 +/- 0.010	0.072 +/- 0.009	-27.3	0.109 +/- 0.100	10.1	0.082 +/- 0.008	13.9
Case 2	15.3	0.355 +/- 0.019	0.512 +/- 0.018	44.2	0.459 +/- 0.019	29.3	0.988 +/- 0.157	93.0
Case 3	19.2	0.231 +/- 0.022	0.198 +/- 0.020	-14.3	0.240 +/- 0.022	3.9	0.225 +/- 0.016	13.6
Case 4	11.2	0.284 +/- 0.026	1.702 +/- 0.025	499.3	0.353 +/- 0.026	24.3	1.871 +/- 0.036	9.9
Case 5	10.7	0.509 +/- 0.027	0.511 +/- 0.025	0.4	0.579 +/- 0.027	13.8	0.767 +/- 0.022	50.1
Case 6	13.1	0.228 +/- 0.024	0.354 +/- 0.022	55.3	0.271 +/- 0.024	18.9	0.624 +/- 0.018	76.3
Case 7	15.3	0.622 +/- 0.022	0.606 +/- 0.021	-2.6	0.666 +/- 0.022	7.1	1.229 +/- 0.025	102.8
Case 8	10.2	0.129 +/- 0.018	0.243 +/- 0.017	88.4	0.177 +/- 0.018	37.2	0.470 +/- 0.009	93.4

Table 3-8 Short Transient Results Summary

		Comparing Sensors			Result with Correction Algorithm			
	Time	Slow	Fast	Change	Slow	Change	Fast	Change
	[s]	[g/km]	[g/km]	[%]	[g/km]	[%]	[g/km]	[%]
Case 1	6.8	0.251 +/- 0.027	0.302 +/- 0.026	20.3	0.387 +/- 0.027	54.2	0.612 +/- 0.023	102.6
Case 2 Fig 3-16	4.5	0.145 +/- 0.025	0.189 +/- 0.023	30.3	0.323 +/- 0.025	122.8	0.300 +/- 0.020	58.7
Case 3	3.4	0.156 +/- 0.168	0.421 +/- 0.158	169.9	0.361 +/- 0.168	131.4	1.118 +/- 0.132	165.6
Case 4	2.3	0.056 +/- 0.028	0.135 +/- 0.026	141.1	0.084 +/- 0.028	50.0	0.174 +/- 0.025	28.9
Case 5	3.5	0.040 +/- 0.037	0.313 +/- 0.035	682.5	0.040 +/- 0.037	0	0.677 +/- 0.023	116.3
Case 6	4.5	0.689 +/- 0.057	1.896 +/- 0.059	175.2	2.006 +/- 0.059	191.1	5.097 +/- 0.212	168.8
Case 7	3.4	0.019 +/- 0.014	0.092 +/- 0.013	384.2	0.040 +/- 0.014	110.5	0.122 +/- 0.010	32.6
Case 8	3.9	0.046 +/- 0.072	0.247 +/- 0.068	437.0	0.168 +/- 0.073	265.2	0.325 +/- 0.066	31.6

43

3.5.5 Accuracy Limits of Emissions Sensors

Mass emission rate measurements are a direct function of species concentration and MAF rate as shown in Equation 1. To produce an accurate mass emission rate result, it is critical that the measurement sensor performs with a similar scale time response as the emissions production rate. Engine transient response rate was measured through analysis of the vehicle Manifold Absolute Pressure (MAP) and MAF data, gathered during EPA Urban and Highway driving cycles. Results indicated that the emission rate production exhibited a transient time constant less than 1 s in duration.

Transient concentration measurement analysis for fast and slow response NOx emissions sensors shows time constants of 2.0 and 7.0 s respectively. Knowing that the emissions production rate occurs at a faster rate than either of the NOx sensors suggests a possible limitation to the accuracy with even the fast response sensor. The use of the terms fast and slow response, should therefore be used in relation to each sensor and not in absolute terms. To produce accurate emissions results without error due to response time differences between production and measurement, a faster NOx sensor with a time constant less than 1 s should be utilized.

Data from emission analyzers and vehicle ECM data was gathered at a frequency less than 2Hz. Knowing that engine transient parameters such as MAP vary with a time constant less than 0.4 s indicates that measurement frequency is also a limitation in the abilities of the on-board emissions system. Improvement of the systems recording frequency for individual sensors (which are able to be configured) should be a priority in future emissions system modifications.

44

3.6 Conclusions

The advancement of a previous in-use emissions measurement system developed at the University of Alberta, has allowed for the ability to focus on illustrating the challenges in accurately measuring real-time mass emissions of NOx with specific attention given to the issue of sensor time resolution. Identified hindrances to accurately measuring emissions factors include; time alignment of vehicle and emissions data, sensor time response to transient emissions levels, and sample line concentration smearing. This chapter has focused on correcting these challenges to produce more accurate and trustworthy results.

The use of a constant time shifting algorithm has proven to be the most accurate method for aligning emissions data to vehicle data for slow responding remote emission analyzers. The inherent slow response nature of the remote sensor proved to be the limiting factor which prevented use of variable time shifting algorithms, due to the additional smearing of the shifted signal which occurs when shifting slow response data.

The examination of long duration transients has shown that in half of the cases, the fast response sensor measured 50% or greater emission rates, with the remaining half of the cases showing similar results. Similar results for long duration transients were likely the result of emission concentrations which remained elevated for a long period of time or due to misaligned air flow and concentration profiles.

In contrast, short transients, which generate a large proportion of the total emissions, clearly indicate the importance of sensor time resolution. Emission rates measured 20% to several times (100%+) greater values than slow response sensor measurements in repeated cases. NOx peak and MAF peak alignment differences between sensors combined with the possibility of missing small emissions spikes, contribute to the significance in utilizing fast response sensors.

The use of the well-mixed flow response correction algorithm has resulted in negligible to 250% higher mass emission rates for corrected versus uncorrected results. Other benefits have include improved data alignment of NOx concentration and MAF profiles, and increased peak emission level measurement, which is likely occurring in the exhaust. Limitations to the response correction algorithm include increased noise amplification, the creation of large emission spikes possibly not occurring, and the inability to generate data where no data is present as in case of the slow response sensor.

Although the current fast response NOx sensor is a significant improvement over previously used sensors, and is one of the fastest current production NOx sensors, limitations to its accuracy measurement still exist. Emission production rates exhibited a time constant less than 1 s, whereas the fastest responding NOx sensor used, could only achieve a 2.0 s time constant illustrating a lagging measurement response compared to the emissions production rate.

45
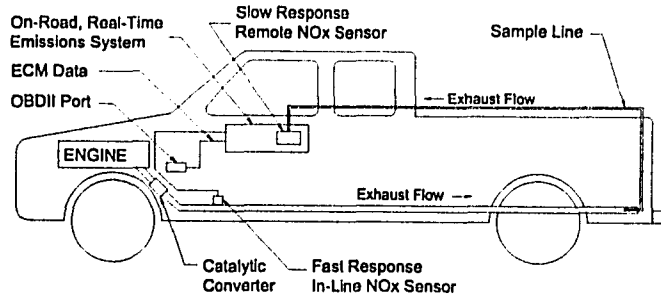
Figure 3-1 On-Board Emissions System Schematic
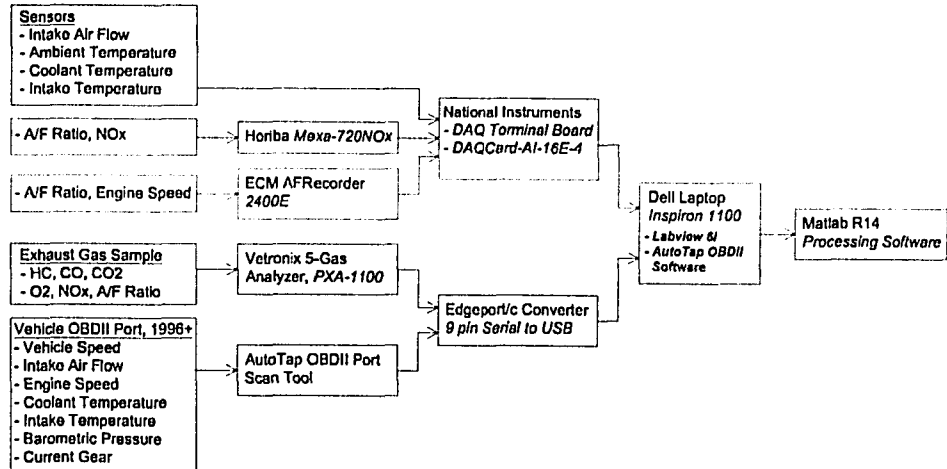
Figure 3-2 Hardware Configuration
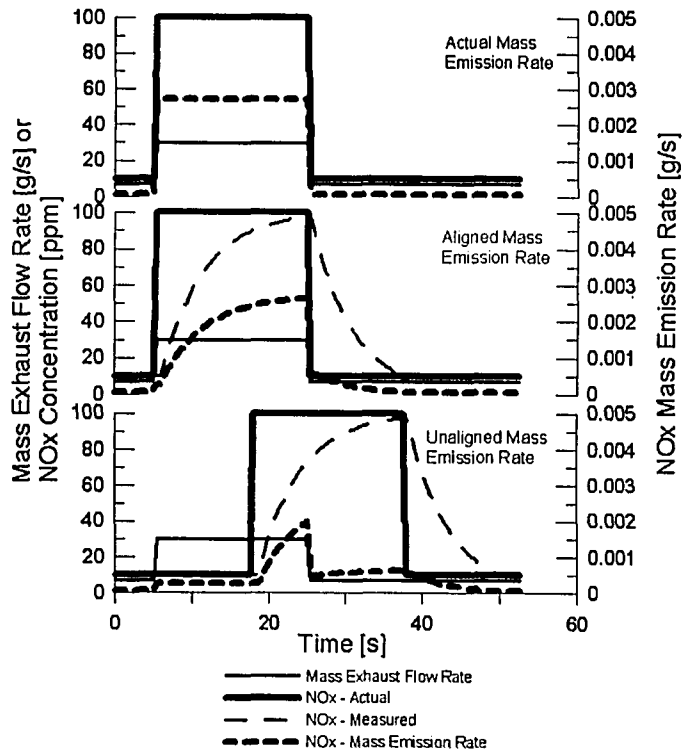
Figure 3-3 NOx Measurement Challenges

46
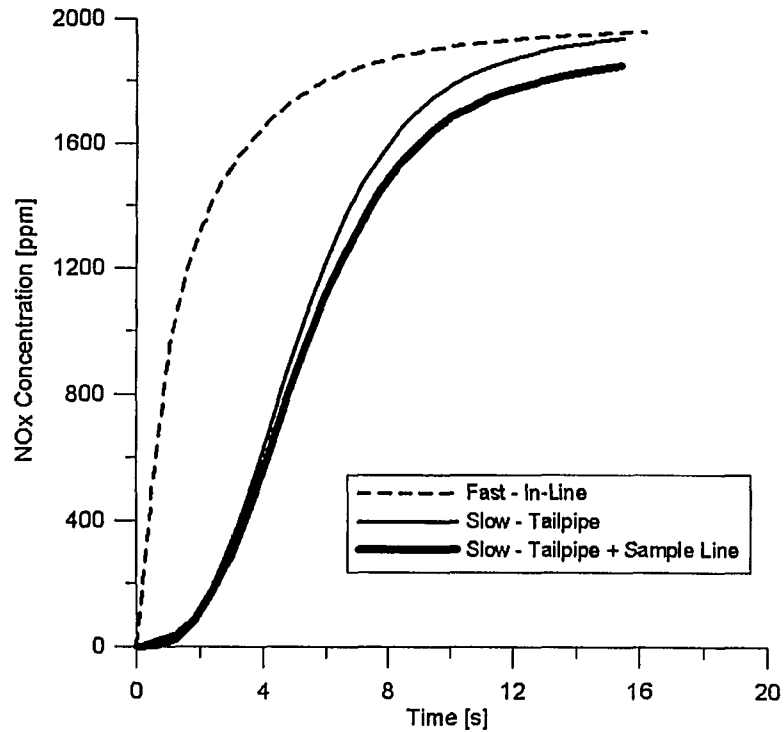
Figure 3-4 NOx Sensor Time Response Comparison
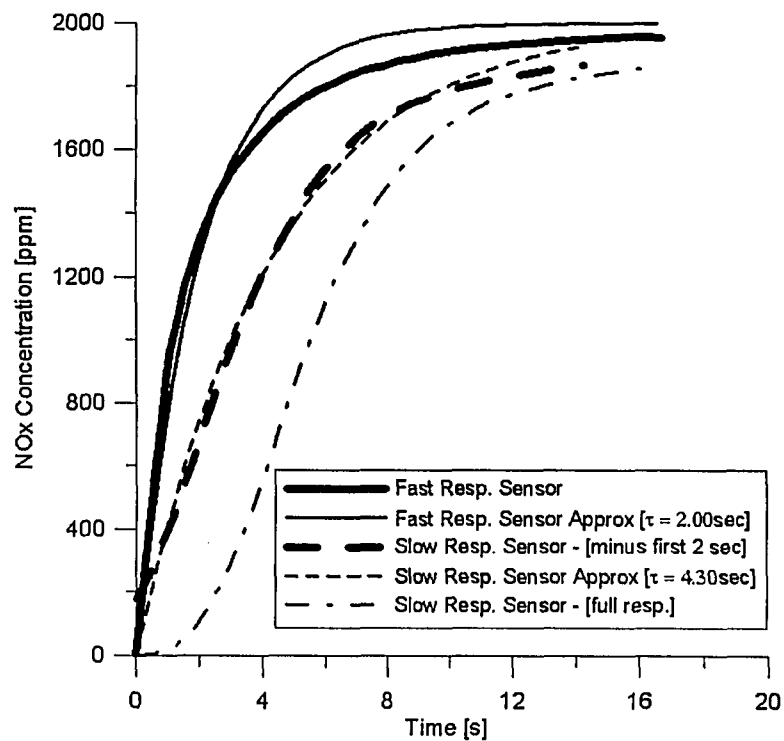
Figure 3-5 Approximate First Order Response Behavior of NOx Sensors

47
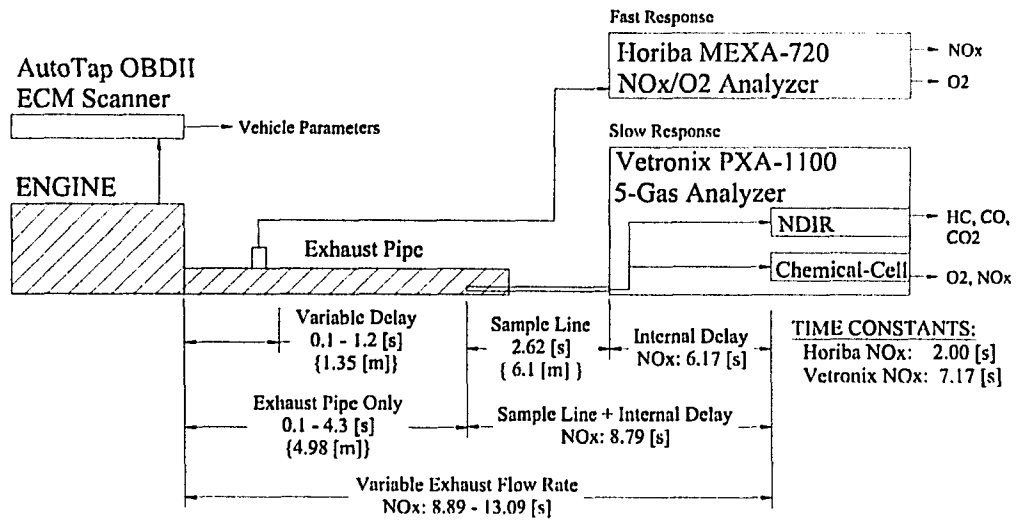
Figure 3-6 Emissions System Schematic
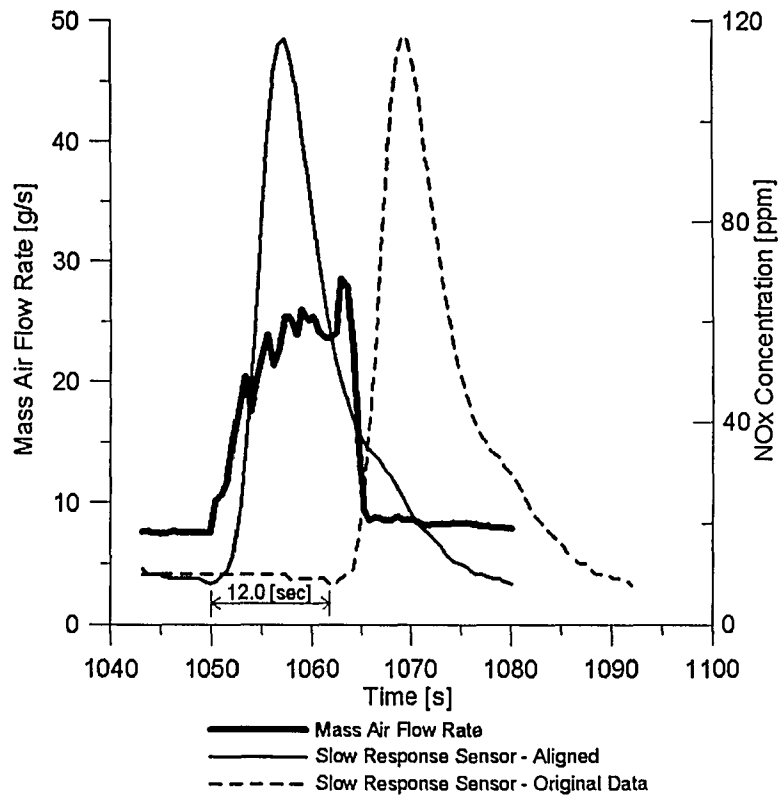
Figure 3-7 CTS Algorithm Applied to NOx Data

48
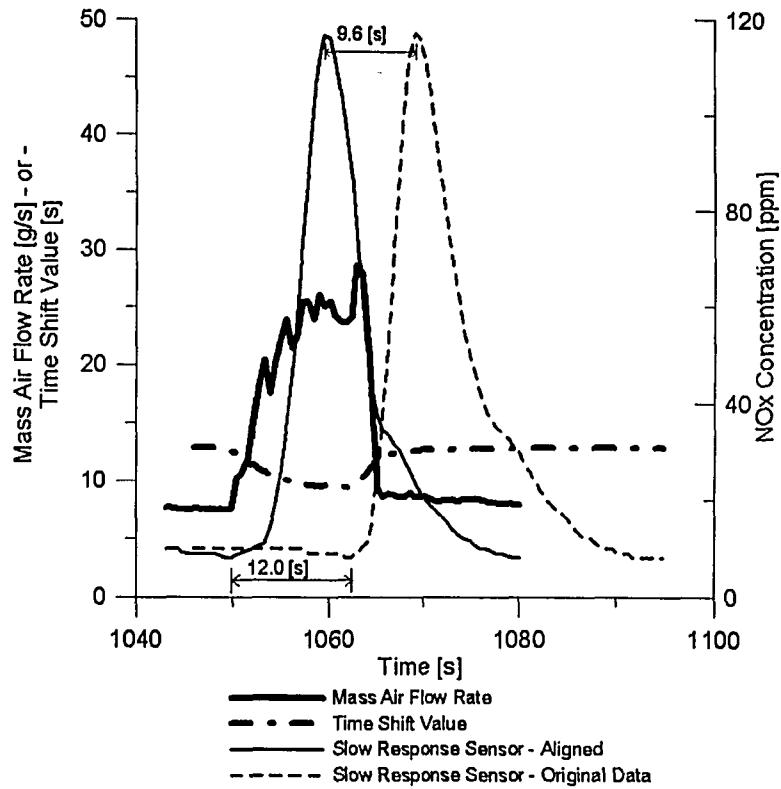
Figure 3-8 VTS Algorithm Applied to NOx Data
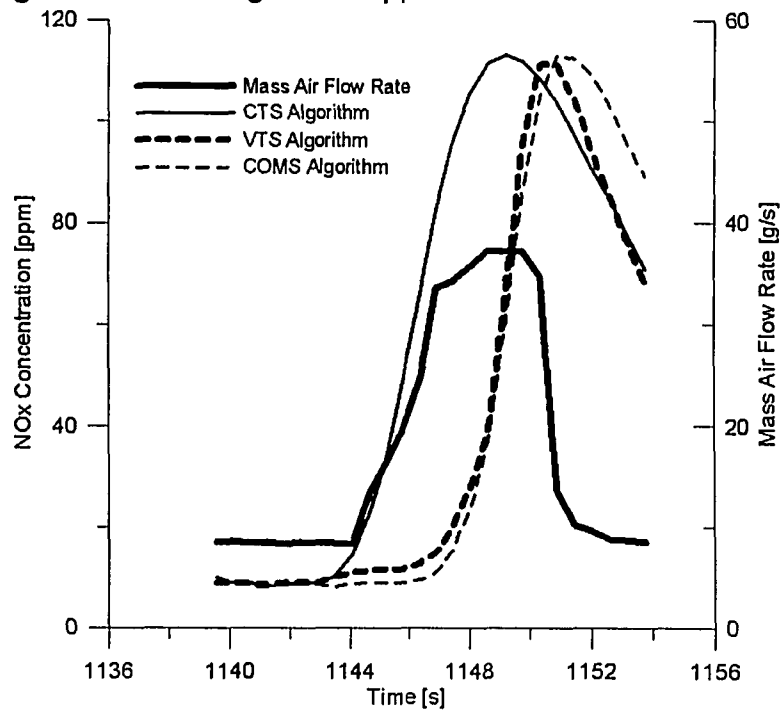
Figure 3-9 Alignment Algorithm Comparison

49

$$\dot{Q}_{in}C_{in} \implies \boxed{M = CQ} \implies \dot{Q}_{out}C_{out}$$
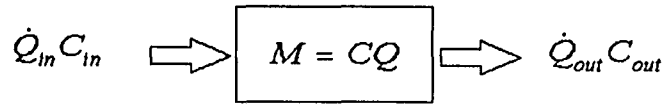
Figure 3-10 Well-Mixed Flow Model
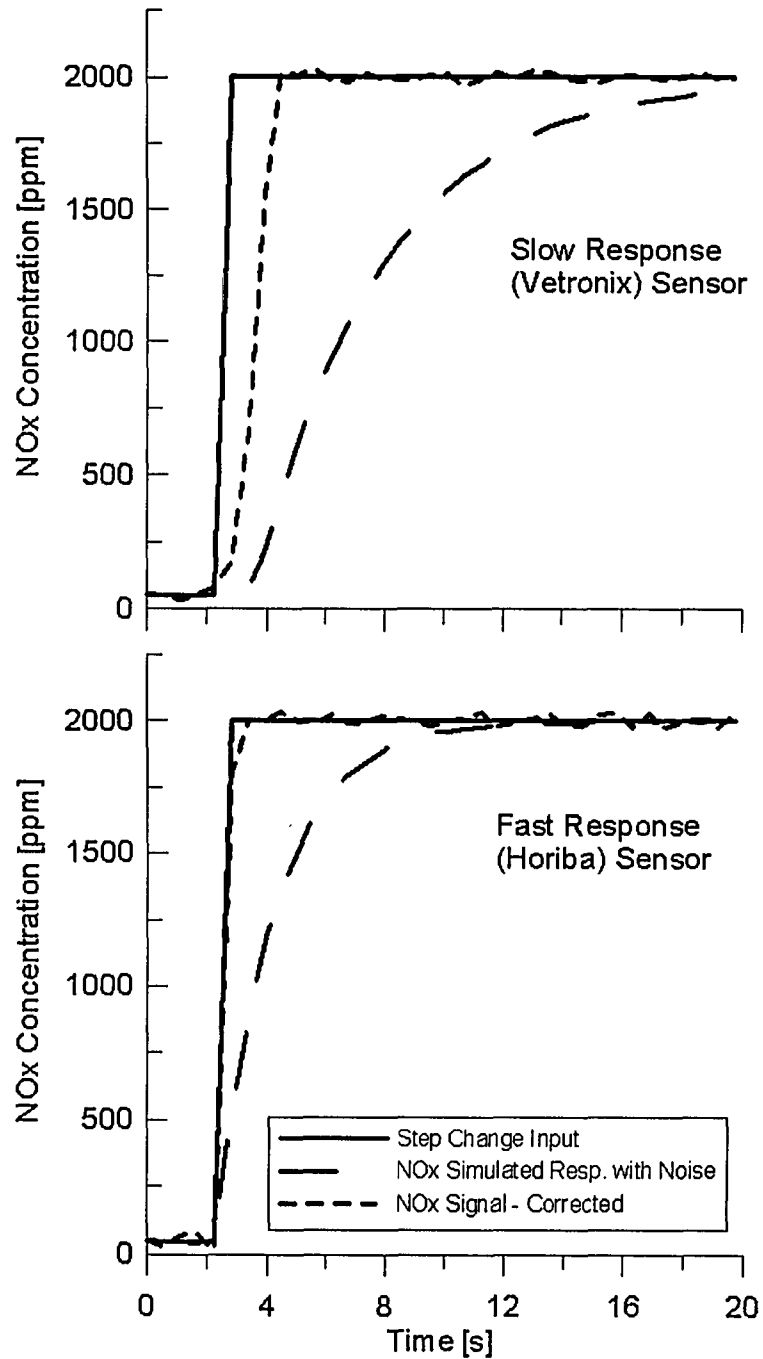
Figure 3-11 Response Correction of NOx Sensors

50
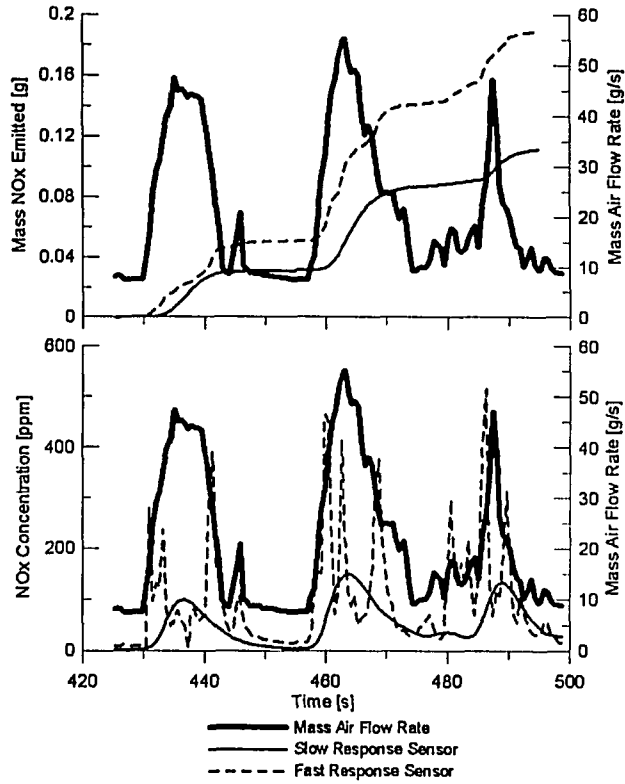
Figure 3-12 NOx Response to Multiple Transients
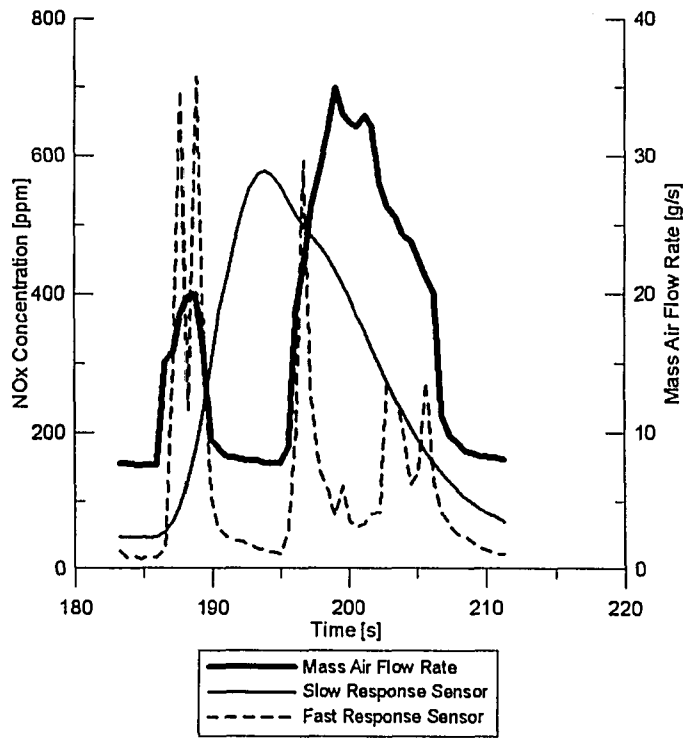
Figure 3-13 Slow Response of NOx Sensor

51
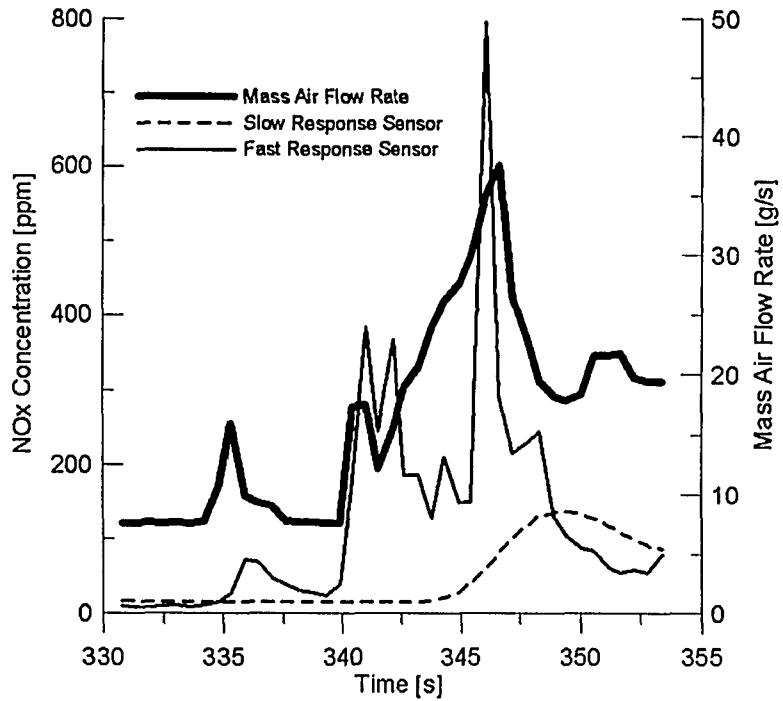
Figure 3-14 Missed NOx Spike
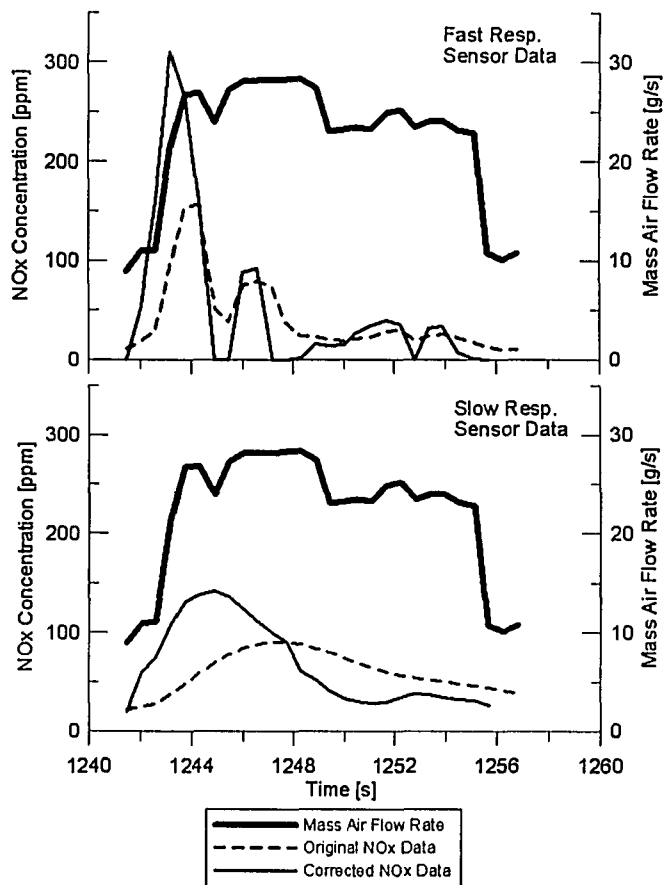
Figure 3-15 Long Transient, Original vs.
Corrected NOx Data (Fast / Slow Response)

52
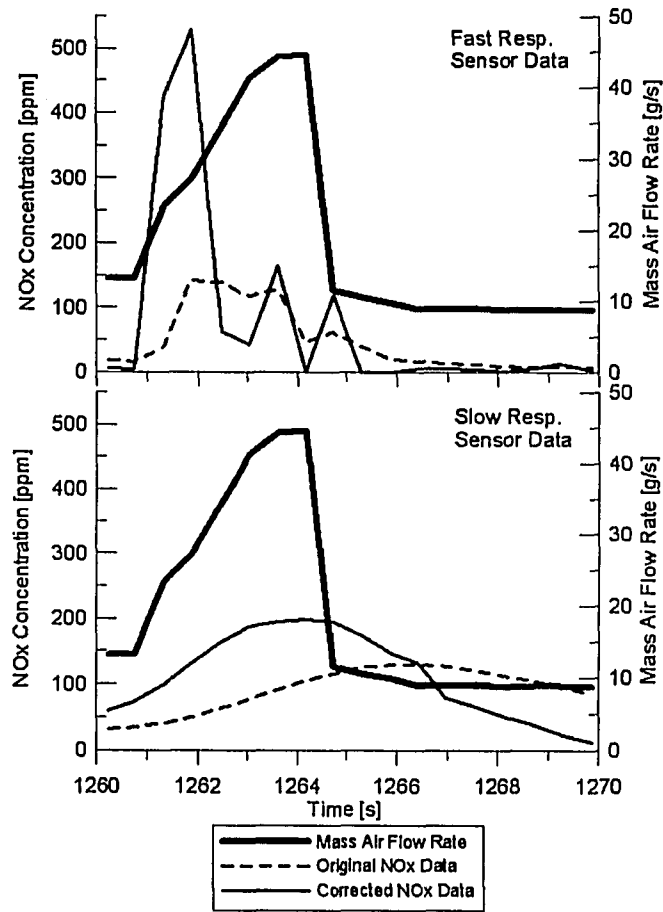
Figure 3-16 Short Transient, Original vs Corrected NOx Data (Fast / Slow Response)

53

REFERENCES

[1] "Canadian Environmental Protection Act, 1999", Canada Gazette, Part II, SOR/2003-1 to 20 and SI/2003-1 to 6, Statutory Instruments 2003, Pg.2 - 499. http://canadagazette.gc.ca/partII/2003/20030101/html/sor2-e.html

[2] United States Environmental Protection Agency, "Federal and California Exhaust and Evaporative Emissions Standards for Light-Duty Vehicles and Light-Duty Trucks," Publication EPA420-B-00-001, Office of Transportation and Air Quality, Feb 2000.

[3] Frey H.C., Rouphail N.M., Unal A., Colyar J.D., "Measurement of On-Road Tailpipe CO, NO, and Hydrocarbon Emissions Using a Portable Instrument," in Proceedings - Annual Meeting of the Air and Waste Management Association, June 24-28, 2001.

[4] Vojtisek-Lom M., Cobb J.T., "Vehicle mass emissions measurements using a portable 5-gas analyzer and engine computer data," in Proceedings - Emissions Inventory, Planning for the Future, Air & Waste Management Association; Pittsburgh, PA, 1997.

[5] Vojtisek-Lom M., Allsop J.E., "Development Of Heavy-Duty Diesel Portable, On-Board Mass Exhaust Emissions Monitoring System With NOx, CO_2, and Qualitative PM Capabilities," SAE Technical Paper 2001-01-3641, Society of Automotive Engineers, 2001.

[6] Truex T.J., Collins J.F., Jetter J.J., Knight B., Hayashi T., Noriyuki K., Suzuki N., "Measurement of Ambient Roadway and Vehicle Exhaust Emissions - An Assessment of Instrument Capability and Initial On-Road Test Results with an Advanced Low Emission Vehicle," SAE Technical Paper, Society of Automotive Engineers, 2000.

[7] Clean Air Technologies International Inc., "Erie County Portable Emissions Monitoring Project Phase 3 and Final Report," Jan 2001, http://www.cleanairt.com/eriecoMAIN.pdf.

[8] Nakamura H., Kihara N., Adachi M., Ishida K., "Development of a wet-based NDIR and Its Application to On-Board Emissions Measurement System," SAE Technical Paper 2002-01-0612, Society of Automotive Engineers, 2002.

[9] Thiel, W., Hornreich C., Morsch O., Seifert G.E., "Problems of Partial Sample Systems for Modal Raw Exhaust Mass Emission Measurement," SAE Technical Paper 2003-01-0779, Society of Automotive Engineers, 2003.

[10] Kihara N., Tsukamoto T., Matsumoto K., Ishida K, Kon.M, Murase T., "Real-time On-board Measurement of Mass Emissions of NOx, Fuel Consumption, Road Load, and Engine Output for Diesel Vehicles," SAE Technical Paper 2000-01-1141, Society of Automotive Engineers, 2000.

[11] Austin, S. and Ross M., "History of Emissions Reduction: Normal Emitters in FTP-type Driving," SAE Technical Paper 2001-01-0229, Society of Automotive Engineers, 2001.

[12] Cadle S.H., et al. "Real-World Vehicle Emissions: A Summary of the Tenth Coordinating Research Council," On-Road Vehicle Emissions Workshop, March 2000.

[13] Weaver C.S., Petty L.E., "Reproducibility and Accuracy of On-Board Emissions Measurements Using the RAVEM^{TM} System," SAE Technical Paper 2004-01-0965, Society of Automotive Engineers, 2004.

[14] Oestergaard K., Porter S., and Nevius T., "Investigation into the Performance of an On-Board Emissions Measurement System Using a Vehicle Exhaust Emissions Simulator," SAE Technical Paper 2003-01-3746E, Society of Automotive Engineers, 2003.

[15] Takada Y., Ueki S., Saito A., "Study on Fuel Economy and NOx Emissions of Medium Duty Hybrid Truck in Real Trafffic Conditions," SAE Technical Paper 2004-01-1086, Society of Automotive Engineers, 2004.

[16] Hawirko J.D., Checkel M.D., "Real-Time, On-Road Measurement of Driving Behavior, Engine Parameters and Exhaust Emissions" SAE Technical Paper 2002-01-1714, Society of Automotive Engineers, 2002.

[17] Hawirko J.D., Checkel M.D., "Quantifying Vehicle Emission Factors for Various Ambient Conditions using an On-Road, Real-Time Emissions System," SAE Technical Paper 2003-01-0301, Society of Automotive Engineers, 2003.

[18] Vojtisek-Lom M., Lambert D.C., Wilson P.J., "Real-world Emissions From 40 Heavy-Duty Diesel Trucks Recruited at Tulare, CA Rest Area," SAE Technical Paper 2002-01-2901, Society of Automotive Engineers, 2002.

[19] U.S. Department of Justice, "Notice of Filing of Consent Decree Under the Clean Air Act," Federal Register, Vol.63, No.212, Nov.3 1998, p.59333 - 59334. http://frwebgate.access.gpo.gov/cgi-bin/multidb.cgi

[20] Jimenez J.L., McRae G.J., Nelson D.D., Zahniser M.S., Kolb C.E., "Remote Sensing of NO and NO_2 Emissions from Heavy Duty Diesel Trucks Using Tunable Diode Lasers," Environmental Science and Technology, Vol.34, No.12, pp.2380-2387, 2000.

[21] Checkel M.D., Brownlee A., Doblanko L., "Optimizing Vehicle Fuel Consumption and Emissions Through Traffic Optimization Using Vehicle and Traffic Forecasting Models," Combustion Canada 99 Technical Paper H 1.4, 1999.

[22] Colorado Department of Public Health and Environment, "Air Quality Data Report - 2002," Publication APCD-TS-B1; CDPHE, Denver, 2003.

[23] Dhaliwal B., Checkel M.D., "Indoor Vehicle Emissions Project," Literature Search for Northwestern Utilities Limited, Jan. 1999.

[24] "Two-Terminal IC Temperature Transducer - AD590," Technical Specifications Data Sheet, Rev.C. Analog Devices, Norwood MA, pg.1-16. http://www.analog.com

[25] Hawley J.G., Brace C.J., Cox A., Ketcher D., Stark R., "Influence of Time-Alignment on the Calculation of Mass Emissions on a Chassis Rolls Dynamometer," SAE Technical Paper 2003-01-0395, Society of Automotive Engineers, 2003.

[26] Bannister C.D. "Further Investigation on Time-Alignment," SAE Technical Paper 2004-01-1441, Society of Automotive Engineers, 2004.

[27] Asano I., Nakamura H., Miyai M., Adachi M., Hosoi K., "Improvement of Modal Mass Analysis with Analyzer Hardware Optimizations and Mathematically Enhanced Response Time," SAE Technical Paper 2004-01-0970, Society of Automotive Engineers, 2004.

CHAPTER 4

Significance of Power Level and Sharpness of Transient Operation on Emissions

The on-board emissions research studies completed for Chapter 4 were developed to identify the impact of vehicle load and acceleration on vehicle emission production. Driving route tests were simulated to represent federal certification cycles of urban and highway driving patterns. A complete US06 test and a partial FTP75 test were chosen as the routes to evaluate due to their ability to cover the majority of vehicle operation conditions. Successful simulations were identified during pre-testing through their ability to represent similar energy usage when compared to full cycle certification tests. The results were analyzed on a full cycle mass emission rate basis due to the importance of these units in calculation of vehicle emission inventories.

57

4.0 Introduction

The use of on-board emissions testing systems cannot currently be used to certify vehicles for emissions compliance due to the lack of precise control which is possible during laboratory dynamometer testing. However, these systems can be used to compliment researchers knowledge of emissions production under a vary different set of ambient conditions, to supplement the pollution control knowledge base. The importance of on-board emissions systems is evidenced by the range and multitude of systems being developed by industry and academics over recent years [1-11] in response to the continual tightening of the U.S. Environmental Protection Agency (EPA) vehicle emission standards.

The effect of acceleration and loading on vehicle emissions performance has been sparsely covered in on-road emissions testing.[10,12] The effect of these two parameters is believed to be of significance to total emission rate figures due to the impact high accelerations and heavy loading have on engine operation. When these parameters are pushed to significantly high levels, the vehicle's engine control module is forced into an open loop control cycle which attempts to meet power demands by running wide open throttle and rich mixtures to deliver maximum power. Since vehicles are only required to meet final weighted average emission rates, the effect of these brief but likely significant emission rates goes unknown.

The goal of this research is to gain a better understanding of the abilities of the current on-road emissions measurement system, and to use the results from testing under various cycles and conditions to evaluate the significance of load and acceleration on full cycle emission rates. The purpose of providing information on real-time and full cycle emission rates for these conditions is to allow designers insight into how to further reduce emission rates during high emitting periods. Future work should include testing of a variety of vehicles since it is known that driving modes generating the highest vehicle emissions differ widely between vehicles.[13]

4.1 Experimental Setup

The development of the current on-board emissions measurement system began in 2001 as a network of independently installed vehicle sensors and an in-cab multi-gas analyzer.[14,15] The evolution of the system to address the issue of nitric oxide (NOx) measurement accuracy, and promote faster installation with less vehicle tampering, have been main priorities in the redesign of the system. The current configuration of the emissions testing system is unchanged from Chapter 3 and will therefore be limited in discussion here.

The on-board emissions system was setup to measure vehicle operation data through a network of individually installed sensors and was supplemented with an On-Board Diagnostics (generation 2) (OBDII) scanner which read engine control

58

module (ECM) data via an OBDII port. Vehicle emissions were measured using a 5-gas emissions analyzer as well as a separate dedicated fast-response NOx sensor. Whereas vehicle operation data was measured real-time as it occurred, remotely locating the portable 5-gas analyzer in the cab produced an exhaust sample transit time delay. The use of a fast-response NOx sensor which was capable of taking measurements of NOx concentration in the exhaust pipe near the source (without the need for sample handling) was therefore seen to be an improvement, as less variability between data synchronization would result. The method for alignment of vehicle and emissions data can be seen in Appendix A and paper [16]. Figure 4-1 illustrates the physical locations of all installed sensors.

The vehicle mounted sensor array measured intake air flow rate, ambient temperature, intake air temperature, coolant temperature, air/fuel ratio, and engine speed. Parameters gathered through the OBDII port included (among others), vehicle speed, intake air flow rate, coolant temperature, intake air temperature, current gear, atmospheric pressure, and engine speed. A portable Vetronix five gas analyzer measured unburnt hydrocarbons (HC), carbon monoxide (CO), carbon dioxide (CO_2), oxygen (O_2), and oxides of nitrogen (NOx). Vetronix was unable to provide a specific list of hydrocarbon species which its analyzer specifically measured. HC species were known to be reported in equivalent units of hexane however, with calibration of the sensor using propane.

The use of a new fast response NOx sensor from Horiba Instruments, provided an improved measurement technology capable of reading NOx concentrations faster and without the problem of sample handling. It also allowed for the possible replacement of a separate air-fuel (A/F) ratio sensor (AFRecorder 2400E) if deemed accurate in comparison to the dedicated A/F sensor. An illustration of the system's sensors and their method of connection to the laptop are shown in Figure 4-2.

4.2 Test Vehicle

A 1999 Chevrolet Silverado C1500, extended cab, four-wheel drive truck was used as the test vehicle for these experiments. The vehicle was equipped with a 5.4 L V8 Vortec gasoline fueled engine, automatic transmission, short-box bed, which operated in two-wheel drive mode for all tests. The dry weight of the vehicle with all sensors and emissions measurement equipment installed measured 2360 kg (~5200 lbs). The gross vehicle weight rating of the Silverado was specified as 2903 kg (~6400 lbs). Vehicle mileage was approximately 112,000 km which was seen as very representative of the type and mileage of vehicles on the road today.[17]

Currently, the C1500 is being used as an emissions research test vehicle, as well as a utility vehicle for engineering student vehicle projects at the University of Alberta. The truck was originally obtained as an experimental vehicle for competition in the 2000 Ethanol Vehicle Challenge sponsored by General Motors and the U.S. and Canadian governments. At the completion of the competition, the

59

vehicle was converted back to the stock gasoline power configuration.

Standard 87 octane fuel was used in the 1999 Silverado, which was purchased from the same Imperial Oil Esso gas station for all tests prior to and during the test period. The effect of gasoline composition on emission rates was not measured in this research but rather eliminated as a variable through use of a consistent fuel composition. Differences in fuel additives, the use of oxygenated fuels, and fuel octane level, was not considered in the scope of this research.

4.3 Driving Route

The creation of simulated driving cycles to represent certification cycles, which identify emissions over numerous operating conditions, was performed and evaluated prior to actual emissions testing. The test routes were designed to simulate the Federal Test Procedure (FTP75) urban cycle and the US06 highway cycle which are two out of the three current certification testing routes.[18] The choice of supplementing the urban drive cycle with the highway cycle was based on the EPAs final conclusions that current vehicle driving patterns are producing speeds and accelerations outside of the urban drive cycle nearly 13% of the time with noticeably different maximum and average speeds obtained.[13]

Tests were conducted on Highway 14 southeast of Edmonton, Alberta on a 4 lane divided highway with fully paved shoulders for the 13 km trip. The test route was a relatively flat section of highway and tests were run in each direction on Highway 14 so as to minimize, as well as evaluate, the effects of grade and wind. Only minor inconveniences to traffic were experienced due to the use of the paved shoulder during high traffic periods and during periods when the vehicle was stopped. To measure the effects of load on vehicle emissions rates, 500 kg of playground sand ballast were added to the test vehicle truck bed box to bring the total weight of the vehicle up to 100% gross vehicle weight rating (GVWR).

The test cycles and simulation cycle durations were also chosen based on recommendations put forth by Battelle under the auspices of the U.S. EPA in a report detailing how to verify on-board emissions measurement systems.[11] It was suggested that the FTP75 and the US06 cycles be used to provide a broad range of real-world driving conditions for which to evaluate on-board emissions systems. Three cycle repeats were suggested to provide repeatability of information, while a minimum time limit per cycle of 15 minutes was suggested. Flag markers placed on the roadside were used to indicate changes in speed and stopping points, in addition to monitoring the vehicle trip odometer.

Figure 4-3 shows the difference in the speed-time trace due to acceleration differences for the US06 cycle with the actual cycle speed-time trace shown in the bottom graph.

60

Simulation cycles were also shown to be quantitatively representative when looking at Table 4-1. Energy differences were found to be within 10% of certification test values and test-to-test repeatability was also very good showing COV values less than 5% for all parameters measured.

The tests conducted took place over a period of two weeks with an initial week of preparation consisting of drive cycle creation, highway selection, flag marker setup, and drive cycle route analysis. Once confidence in producing a repeatable and representative group of test cycles was completed, continuous experiments were conducted so as to minimize temperature effects.

Table 4-1 Driving Cycle Statistics

	Dist. [km]	Time [s]	Avg. Speed [km/h]	Max. Speed [km/h]	Max. Accel. [m/s^2]	Avg. Energy [W-h/km]	Energy Diff. [%]
FTP75 Urban Cycle							
Norm Accel. - No Load	7.89 +/- 0.00	798.4 +/- 9.8	35.5 +/- 0.4	90.2 +/- 0.7	2.1 +/- 0.1	215.4 +/- 2.8	**-3.9**
Norm Accel. - GVWR	7.90 +/- 0.00	811.1 +/- 3.6	35.1 +/- 0.1	89.8 +/- 0.9	2.3 +/- 0.1	245.2 +/- 2.9	**-6.4**
Rapid Accel. - No Load	7.88 +/- 0.00	762.8 +/- 6.4	37.1 +/- 0.3	89.2 +/- 0.7	4.3 +/- 0.2	213.5 +/- 4.0	**-5.0**
Rapid Accel. - GVWR	7.90 +/- 0.01	772.4 +/- 6.7	36.7 +/- 0.3	89.4 +/- 0.7	3.9 +/- 0.1	250.3 +/- 2.7	**-4.6**
US06 Highway Cycle							
Norm Accel. - No Load	12.72 +/- 0.01	610.8 +/- 6.4	75.1 +/- 0.8	126.6 +/- 0.4	2.9 +/- 0.2	310.6 +/- 1.3	**-10.6**
Norm Accel - GVWR	12.74 +/- 0.01	611.4 +/- 5.5	74.9 +/- 0.7	127.5 +/- 0.6	2.5 +/- 0.1	347.0 +/- 3.1	**-10.2**
Rapid Accel. - No Load	12.72 +/- 0.01	598.0 +/- 6.9	76.5 +/- 0.8	128.5 +/- 0.6	4.1 +/- 0.2	318.4 +/- 4.0	**-8.7**
Rapid Accel - GVWR	12.73 +/- 0.00	595.4 +/- 1.0	76.9 +/- 0.1	128.1 +/- 0.8	4.0 +/- 0.3	350.8 +/- 1.2	**-9.3**

4.4 Results

Processing the vehicle operation and emissions data files to yield accurate mass emission rate results based on synchronized data, was done using processing code developed through earlier research.[16] An overview of the code structure and purpose of the individual Matlab files can be seen in Appendix G.

Consideration of data synchronization, the use of fast response NOx sensors, and time response correction issues are also detailed in Chapter 3. Mass emission rate values on a g/km basis were used when comparing emission rates between tests, cycles, and emission types due to their importance in emissions inventory calculations. Total mass emission inventories of on-road vehicles are calculated using an estimate of the mileage of a vehicle and multiplying it by a gram per kilometer emission rate. Appendix D and E provide the equations used in the processing code for evaluating the emissions calculations and vehicle dynamic operation results.

4.4.1 Directional Effects

To minimize the impact of wind and road grade on emission rates, tests were conducted four times consecutively, twice in each direction. Noting that two minor road grades were present in the test section, it was deemed possible that variations in emission rates may occur. After processing the raw data files, it was noticed that in a number of cases, the direction of travel had a significant effect on the fuel consumed and certain species emission rates.

The test-to-test differences are the source of the relatively high standard deviations in overall average reported values of CO_2, NOx, and fuel consumption. Table 4-2 illustrates the percentage change in emissions rate (and fuel consumption) when comparing odd numbered test results with even numbered test averages. NOx emission rates were most affected by direction of travel with changes in rate between 17% and 40%. CO_2 and fuel consumption were closely linked as expected with 6% to 24% differences in values due to travel direction. HC and CO were found to be less effected by the direction of travel as can be seen in Appendix H, Tables H-1 and H-2.

Table 4-2 Percent Change with Direction of Travel

	CO_2		NOx		Fuel Consumed	
Acceleration Rate:	Normal	Rapid	Normal	Rapid	Normal	Rapid
Urban Cycle No Load	6.5	8.9	36.6	28.7	6.3	10.4
Urban Cycle 100% GVWR	16.2	12.9	40.5	25.3	16.8	12.5
Highway Cycle No Load	20.1	24.3	17.3	37.1	14.1	22.7
Highway Cycle 100% GVWR	1.8	0.2	0.4	11.3	1.5	3.9

The effect of the direction of travel is apparent when looking at the results of NOx emission rates on the rapid acceleration US06 highway cycle. It is apparent from

62

Figure 4-4, that aside from slight differences in minimum air-fuel ratios, the majority of the air-fuel ratio response is identical in either direction. However, looking at the NOx concentration indicates a nearly constant offset in concentration which resulted in approximately 30% higher emission rates for test three vs. test four (0.414 g/km vs. 0.317 g/km). Although not shown, the mass air flow rate during this period exhibited a similarly higher offset reading for test three much like the NOx sensor readings.

The reason for these differences was not due to 1 or 2 isolated grade changes. Air-fuel ratio, speed, mass air flow rate, and even concentration profiles appeared similar between tests with offsets rather than dramatic isolated instances as differences. The probable cause of these effects was concluded to be due to longer gentle uphill versus downhill grades or possibly wind effects.

The purpose of this discussion was to illustrate that although attempts were made to negate the effects of grade and wind on final emissions values, the calculated emission rate results indicate that in fact, some directional variation does exist. Therefore, averages should be used to compare results with consideration for the standard deviation of the results.

4.4.2 Effect of Vehicle Load

The design of automobile powertrains is done with the intention of enabling the vehicle to operate at an acceptable performance level when loaded up to 100% GVWR. However, the emissions impact of this acceptable dynamic performance may be increased levels of HC, CO, and/or NOx.

Vehicle emission control systems are intended to produce the lowest possible average emission levels for all three pollutants; HC, CO, and NOx, while operating in a wide range of modes.[19] Under typical normal acceleration conditions, adding a load of 500 kg to a vehicle would have a theoretical impact on emission rates. Vehicle engine operation could be expected to operate in a pre-enrichment mode if the load was considered significant in relation to the test vehicle's capabilities, and emissions production of NOx and CO_2 would be expected to increase similarly. However, normal transient operation and a lack of high loading (to command enrichment levels) would result in little if any change in the measurement of HC and CO.

A qualitative comparison of vehicle operating parameters for a loaded and unloaded urban driving route test is shown in Figure 4-5. In this figure, a portion of an urban driving route showing loaded and unloaded effects on vehicle mass air flow rate and air-fuel ratios, highlights the similarity in measurements which occurred. The urban cycle noticed only one significant and consistent mass air flow rate difference which occurred during the initial brief 90 km/h maximum speed point. Air-fuel ratio readings produced very similar results with unloaded driving conditions showing

63

slightly more enleanments (~ 6 per cycle over the 800 s urban simulation route).

Results from highway drive cycle data showed that very similar MAF and air-fuel ratio readings existed with load. When numerically analyzing the mass air flow rate, the loaded case showed a 10% increase in average g/s results for both MAFs measured. Also, similar fuel shutoff events occurred when comparing loaded versus unloaded operation.

From these results, it is evident that the vehicle was quite capable of performing at 100% GVWR without substantial alteration in engine operation. This finding seems reasonable since other studies by Cicero-Fernandez and Long [12] have found that there exists a load threshold for an open-loop event to occur, which for this test vehicle, may not been reached at the GVWR for the urban driving cycles.

Table 4-3 provides a comparison of the average emission rates of various species between loaded and unloaded modes, for urban and highway driving cycles. The emission rate is followed by a standard deviation resulting from calculations based on four tests at each mode.

The most important parameter in the production and control of exhaust emissions is air-fuel ratio.[20] Since significant air-fuel ratio differences between loaded and unloaded tests have been ruled out (for loads up to GVWR with this vehicle), the expectation that HC and CO emission rates will be unchanged with the addition of load is reasonable.

Table 4-3 Loaded vs. Unloaded Operation (Normal Acceleration)

	On-Board Emissions Measurement					Vehicle Operation	
	HC* [g/km]	CO* [g/km]	CO_2 [g/km]	 [g/g fuel]	NOx [g/km]	Fuel Used [g]	Load (Avg) [kW]
URBAN No Load	0.035 +/- 0.019	1.457 +/- 0.139	371.0 +/- 14.7	3.10 +/- 0.01	0.577 +/- 0.116	946 +/- 36	7.7 +/- 0.2
URBAN 100% GVWR	0.030 +/- 0.024	0.524 +/- 0.061	313.0 +/- 27.4	3.10 +/- 0.01	0.596 +/- 0.117	798 +/- 71	8.6 +/- 0.1
HIGHWAY No Load	0.015 +/- 0.003	0.773 +/- 0.412	279.2 +/- 30.7	3.01 +/- 0.15	0.327 +/- 0.032	1177 +/- 90	23.3 +/- 0.3
HIGHWAY 100% GVWR	0.017 +/- 0.019	1.100 +/- 0.284	302.1 +/- 4.3	3.09 +/- 0.01	0.390 +/- 0.002	1247 +/- 16	26.0 +/- 0.5
Note: * - indicates HC and CO emission rate for the 100% GVWR is the average of three tests (outlier omitted)							

Looking at the hydrocarbon emission rates of Table 4-3, it is apparent that when

64

a load was added to the vehicle, very little change in emission rates occurred within standard deviation limits for both cycles. The expectation that HC would not increase unless significant transients or catalytic converter cool down occurred was therefore confirmed.

Looking at Figure 4-6, it is also apparent that the engine control system basically disregarded the knowledge of engine temperature and ran rich for the first 12 s. of tests 2 (as well as 3 and 4). This is an interesting result which would only be possible with real-time emissions monitoring.

In examining the effect of vehicle load on CO emission rate, it was expected that very little change would be present since no severe power demands were required of the vehicle. High load enrichment and an increase in transient operation are major factors in the creation of high levels of CO and in their absence, the expectation of similar CO results with loading is reasonable.

Urban drive cycle results showed a conclusive decrease of 64% in CO emission rates with increased loading. This may be due to the fact that less severe transients were noticed by the vehicle because loaded tests took approximately 12 s longer to complete on average. Also, the unloaded cycle exhibited a larger fuel consumption which may have contributed to an increase in CO levels for that mode. This was an anomalous event that will be discussed with the analysis of CO_2 emission rates.

The highway test illustrated substantially different results. The CO emission rate increased 42% with vehicle load when comparing average rates, but appeared similar when considering standard deviation. Consideration of the ~10% increase in average mass air flow rate for the loaded case also accounts for part of the unexpected increase in average CO emission rates.

A comparison of CO emissions between cycle types for a loaded application reveals that loaded highway driving produces twice the CO emissions as loaded urban driving. An examination of A/F ratio reveals that the engine ran 0.4 A/F ratio units richer on average when in the highway driving mode with a significantly larger fraction of time spent below the stoichiometric A/F ratio of 14.7. Inspection of the cumulative CO versus time trace found that it was during these excursions below 14.7 (correlated to acceleration rates) in which significant amounts of CO were generated. By comparison, the urban driving cycle maintained close A/F ratio control and had very short in infrequent period where the A/F ratio measured below stoichiometric.

Since a larger power requirement of the engine was experienced in the high load high speed application, the requirement for MAF during the highway cycle was found to be almost 15 g/s higher on average than the urban cycle. The combination of higher concentrations and mass air flow rates therefore resulted in a loaded highway cycle which generated twice the CO mass emission rate as the urban

65

cycle.

The relation between CO_2 emissions and vehicle operation is directly linked to fuel consumption. Increasing fuel consumption leads to an increase in CO_2 emissions. Knowing that an increased power requirement is necessary to accelerate a loaded vehicle, it was assumed that vehicle fuel consumption and hence CO_2 would increase with load. This result was noticed with the US06 highway route with both CO_2 and fuel consumption increasing 8% and 12% respectively with load.

The test vehicle consumed more fuel under the unloaded FTP75 urban simulation test than in the loaded case however. No reasonable explanation for this anomaly could be found. When looking at Table 4-1, all factors indicate the vehicle should have consumed more fuel when loaded since the tests were approximately 12 s longer, average and max speed values were similar, and average energy was approximately 15% higher. Also, Figure 4-7 indicates that similar mass air flow rates and air-fuel ratios resulted between loaded and unloaded tests. Figure 4-8 shows that although the calculated energy consumption on a flat grade is larger for a loaded vehicle, the actual fuel consumed during the test cycle rose faster for the unloaded cycle.

Although no clear explanation for the increased fuel consumption is given, the emission system results relating CO_2 emissions to fuel consumption give confidence in the systems ability to measure not only CO_2 accurately but this anomalous fuel consumption increase. Various manufacturers have suggested that occasional discrepancies in vehicle data or the presence of an unexplained phenomenon could be attributed to poor calibration techniques since not all development engineers have the same expertise.[13]

NOx is formed in the burned combustion gases in the engine cylinder with the majority of the NOx produced by the Thermal (Zeldovich) reaction mechanism.[19] Favorable conditions for nitric oxide production include high temperatures (typical of a spark-ignited engine), with sufficient O_2 and time in the mixture to allow NOx to form. Advanced spark timing, moderate loading, and lean air-fuel ratio operation, all contribute to the production of NOx in an engine.

The focus on NOx is extremely important due to the health implications and difficulty in controlling NOx emissions. For moderate pre-enrichment operating conditions occurring during loaded vehicle operation, it was expected that an increase in NOx emission rates would result. Urban tests have shown that a 3% increase in NOx results due to loading up to the vehicle GVWR, but similar results when considering standard deviation. This unaltered emission rate result was as expected due to vehicle's apparent resistence to operate in the pre-enrichment mode as indicated by the average and range of air-fuel mixtures measured.

When comparing the effect of load on the highway cycle, a conclusive 19% increase in the NOx emission rate can be observed. The higher emission reading with load

66

is as expected and indicates that the vehicle did in fact operate in a pre-enrichment mode. Higher mass air flow rates also contributed to the increase in NOx mass emission rate.

4.4.2.1 Load Effects under Rapid Acceleration

The effects of load on vehicle emission rates can also be examined for rapid acceleration driving cycles. The only species to exhibit a change in emission rate trend with load was HC. Rapid acceleration tests noticed a 50% decrease in rates for both cycles versus unchanged emission rates during normal acceleration testing. Probable causes for this decrease may be due to increased oxidation occurring in the exhaust manifold prior to the catalytic converter due to increased cylinder temperatures with load at high acceleration rates.

The remaining three emissions species (CO, CO_2, and NOx) exhibited similar trends to the normal acceleration trends. Comparing loading effects for rapid acceleration tests showed urban cycle CO emission rates drop 9 g/km with increased loading versus 1 g/km during normal acceleration tests. It should also be noted that conclusive CO emission rate trends were calculated during examination of load at rapid acceleration rates. Examining CO_2 emission rates showed that CO_2 remained well linked to fuel consumption on a g/g fuel basis.

Although NOx exhibited the same increasing trends as the normal acceleration results, the urban cycle proved to be the cycle which showed conclusive increases instead. Urban tests showed a dramatic 56% increase in NOx emission rate versus similar results for the normal acceleration comparison. Highway testing showed an 8% increase, or similar within standard deviation, compared with 19% increase for the normal acceleration.

4.4.3 Effect of Acceleration

It is evident that many drivers on the road today are operating their vehicles in an aggressive manner both on urban and highway driving routes. To an uninformed driver, the magnitude of these pollution effects is not grasped or even a concern. However, knowing aggressive driver behavior exists, emissions control system designers must make attempts to minimize these emission rates, which is the basis for conducting on-board emissions testing of vehicles under rapid acceleration. The tabulated averages with associated standard deviations of the various species emissions are shown in Table 4-4.

Emissions of many species increase as a result of imposing rapid transients on vehicle operation. Unburned hydrocarbon emissions are expected to rise during heavy accelerations due to poor mixture preparation, decreased burning time, and a decrease in the air/fuel ratio.[21-23] As expected, HC emission rates climbed

270% for urban driving routes and 630% for highway driving routes. Table 4-5 provides a summary of the percentage change in emission rates with load and acceleration for all species discussed.

Similar expectations exist for carbon monoxide emissions, noting that high load enrichment occurring during rapid transients prevents sufficient oxygen and time for full conversion of carbon to carbon dioxide. The results for CO were unmistakable with 16 to 36 times more CO emitted for urban and highway drive cycles respectively. It has been previously found that large reductions in HC and CO are possible when the elimination of command enrichment is achieved,[13] and tighter emissions regulations will eventually need to focus on this control improvement to meet standards.

Table 4-4 Normal vs. Rapid Acceleration Operation (No Load)

	Emissions Data					Vehicle Operation	
	HC	CO	CO$_2$		NOx	Fuel Used	Load (Avg)
	[g/km]	[g/km]	[g/km]	[g/g fuel]	[g/km]	[g]	[kW]
URBAN Normal Accel	0.035 +/- 0.019	1.457 +/- 0.139	371.0 +/- 14.7	3.10 +/- 0.01	0.577 +/- 0.116	946 +/- 36	7.7 +/- 0.2
URBAN Rapid Accel	0.129 +/- 0.056	24.18 +/- 5.58	321.9 +/- 17.9	2.81 +/- 0.08	0.303 +/- 0.051	902 +/- 52	7.9 +/- 0.2
HIGHWAY Normal Accel	0.015 +/- 0.003	0.773 +/- 0.412	279.2 +/- 30.7	3.01 +/- 0.15	0.327 +/- 0.032	1177 +/- 90	23.3 +/- 0.3
HIGHWAY Rapid Accel	0.110 +/- 0.043	28.73 +/- 2.90	286.6 +/- 36.1	2.69 +/- 0.03	0.381 +/- 0.072	1356 +/- 160	24.4 +/- 0.6

Maintaining a carbon balance in the exhaust components leads to an uncertainty regarding how CO$_2$ will change with acceleration rate knowing that CO has a tendency to increase during rapid transients. Highway test results shown in Table 4-4 illustrate the measurement of a similar emission rate and the decrease in CO$_2$ proportion to grams of fuel consumed. As a result of the increase CO carbon content, CO$_2$ decreased 10.6%, similar to the urban test results of 9.4%. Although the elevated fuel consumption measured during the normal acceleration has not been explained, the emission rate link with grams of fuel provides confidence in the measurement system.

For high load enrichment occurring during rapid acceleration events, it was expected that the fraction of NOx emitted by the vehicle would decrease. During high load enrichment, air-fuel ratio levels drop substantially, which reduces the amount of oxygen available for formation of NOx. Another factor is reduced in-cylinder temperatures, resulting from the increased richness in fuel mixture, which

68

reduces the temperature driven formation mechanisms of NOx. Also, typically faster engine speeds occurring during rapid transients reduce the available time for NOx formation.

Urban tests showed a noticeable 48% decrease in NOx concentration levels. This result was as expected due to the observed air-fuel ratio and vehicle speed parameters measured and shown in Figure 4-9. It is evident from this figure that rapid acceleration tests are experiencing severe drops in air-fuel ratio whereas normal acceleration tests remain near to stoichiometric conditions. The bottom graph indicates that NOx is higher and remains higher for the bulk of the sampling period with rapid acceleration NOx data decreasing with each rich air-fuel ratio. Each rich air-fuel ratio reading for the rapid transient tests, is a direct result of the increased acceleration rate evidenced by the steeper slope in the speed-time trace.

The use of transient enrichment during rapid acceleration events may be preceded by brief periods of enleanment if calibration optimization for transients is not completed.[13] This enleanment is caused by the fuel control system lag time following throttle opening. This phenomenon appears to be occurring in the first NOx spike of Figure 4-9 for the rapid acceleration. After this event, the vehicle appears to have adapted to acceleration events, thus preventing enleanment but the ECM is unable to prevent subsequent commanded enrichment at rapid accelerations.

The effect of acceleration on NOx emissions during highway tests has shown a 16% increase in emission rate but similar results within standard deviation limits. The expectation of a similar NOx emission rate is a reasonable result due to the fact that there are a limited number of transients relative to cruising periods with which to influence total NOx rates.

4.4.3.1 Loaded Testing, Effect of Acceleration

Comparing loaded versus unloaded acceleration effects has shown that similar trends and quantitative differences exist whether the vehicle is loaded or not. Hydrocarbon emission rates appeared to show less difference due to acceleration when loaded to the vehicle's GVWR with HC increases of 83% and 270% for urban and highway cycles respectively. This change in HC with acceleration is significantly less than the 270% and 630% increase which resulted without a load.

Carbon monoxide emission showed similar results with a 30 fold increase in emission rate for both cycles, and CO_2 was again shown to be well linked to fuel consumption. NOx showed a similar result to the HC species. NOx emission rates were reduced in magnitude when analyzing acceleration effects for loaded vehicles. A 20% decrease in NOx emissions with acceleration rate in the urban cycle results as compared to the 48% decrease experience during normal loaded tests. Highway tests in both cases showed a similar result with no change in NOx measured due

69

to acceleration.

Measurement of similar emission trends with and without a load provides confidence in the on-board emission measurement system's quantitative abilities to generate reliable and accurate results.

4.5 System Evaluation

The calculation of emission rates and anomalous effects was as much a goal of this research study as the evaluation of the system's capabilities in accurately measuring emissions trends. After analyzing the results obtained from post-processing the obtained test data, it can be concluded that the system correctly predicted emissions trends for the majority of the cases which were discussed with HC and NOx showing particularly good results. Also, the effect of acceleration on emission rates, for loaded and unloaded conditions, showed exactly the same trends giving confidence to the emission system repeatability.

For the few instances in which emission rates were different from theoretically predicted values, explanations for the increase were found through examination of vehicle sensor data and application of theory based on those parameter values.

Acknowledging slight test-to-test driving variation, and observing the effect of travel direction on emission rates, the on-board measurement system has been able to show its range of abilities by observing the following vehicle behavior:

1. Vehicle did not reach the load threshold required to enter commanded enrichment during normal acceleration, 100% GVWR tests.

2. The engine control system disregarded the fact that the engine was pre-warmed and simply flooded the engine with fuel (i.e. ran rich) for approximately 12 s during testing, indicating the lack of robust ECM design.

3. Fuel flow was shut off during high deceleration events (off scale lean air-fuel ratio measured)

4. Vehicle was found to be trying to minimize NOx emissions by running tight closed loop fuel system control for controlling NOx emissions during high speed and load operation to improve NOx catalyst conversion efficiency.[13]

70

4.6 Summary Tables

Numerous emission species have been analyzed in Chapter 4 to evaluate the effect acceleration and loading have on mass emission rates. Table 4-5 provides a quantitative summary of the percentage change in emission rate when going to a fully loaded state or to a rapid acceleration state.

Tables 4-6 and 4-7 provide a qualitative summary of the effects of loading and acceleration respectively. These two tables illustrate the expected trends which were predicted prior to emissions testing based on theoretical knowledge. The results show that in the majority of the cases, excellent qualitative results were generated when considering test-to-test standard values. In cases in which the trend differed from the expectation, the cause of this difference was explained using knowledge of vehicle operation data.

Table 4-5 Effect of Loading and Acceleration on Emission Rates

	HC[1]	CO[1]	CO$_2$		NOx	Fuel Consumption	Load[3] (Avg)
	[%]	[%]	[%][4]	[%][5]	[%]	[%]	[%]
URBAN Loading to GVWR	-13.9	-64.0	-15.6	0.0	3.3	-15.7[2]	12.3
HIGHWAY Loading to GVWR	17.5	42.0	8.2	2.7	19.3	5.9	11.7
URBAN Effect of Rapid Accel.	269	1560	-13.2	- 9.4	-47.5	-4.7[2]	3.7
HIGHWAY Effect of Rapid Accel.	633	3620	2.6	-10.6	16.5	15.2	4.6

Note: [1] indicates HC and CO emission rate for the 100% GVWR is the average of three tests (outlier omitted)
[2] fuel consumption decreased with load/acceleration due to unusually high Normal Acceleration tests fuel consumption (% value based on [g/km] rate)
[3] Avg Load does not consider grade effects
[4] Percent based on change in [g/km] rates
[5] Percent based on change in [g/g fuel] rates

71

Table 4-6 Effect of Load Summary - Normal Acceleration Tests

Species	Expected Trend	Result	Explanation
HC	Unchanged - no change in transient nature	Unchanged - within std dev limits	EXPECTED result - HC decline in loaded tests due to catalyst cool down during system warm-up
CO	Unchanged - no change in transient nature - no high load enrichment	URBAN - decrease (64.0%) HIGHWAY - increase (42.0%) (unchanged within std. dev.)	URBAN - decrease due to less severe transients, anomalously high fuel consump. of unloaded test HIGHWAY - EXPECTED result (within std.dev.), increase partially attributed to 10% MAF increase
CO$_2$	Increase - linked to fuel consump.	URBAN - decrease (15.6%) HIGHWAY - increase (8.2%)	URBAN - anomalously high fuel consump. of unloaded test - well linked with fuel consump. HIGHWAY - EXPECTED
NOx	Increase (may be unchanged for URBAN tests due to apparent resistence to operate in pre-enriched mode)	URBAN - increase (3.3%) (unchanged within std. dev.) HIGHWAY - increase (19.3%)	URBAN - EXPECTED - only slight increase noted, noticeable directional effect on results (same rates within std. dev.) - expected due to vehicle avoidance of pre-enrichment mode HIGHWAY - EXPECTED (slight directional effect but no influence on result) - MAF was 10% higher for loaded cases - accounts for part of the increase

Note: "Expected Trend" and "Result" - when increasing from unloaded to fully loaded (GVWR) operation

72

Table 4-7 Effects of Acceleration Summary - Normal Load Tests

Species	Expected Trend	Result	Explanation
HC	Increase - with transient operation	URBAN - increase (269%) HIGHWAY - increase (633%)	EXPECTED
CO	Increase - with high load enrichment - with transient operation	URBAN - increase (1,560%) HIGHWAY - increase (3,620%)	EXPECTED
CO_2	Decrease - on a [g/g fuel] basis - well linked to fuel consump	URBAN - decrease (9.4%) HIGHWAY - decrease (10.6%)	EXPECTED
NOx	Decrease - high load enrichment reduces available O_2 for NO formation	URBAN - decrease (47.5%) HIGHWAY - increase (16.5%) (unchanged within std dev.)	URBAN - EXPECTED HIGHWAY - EXPECTED - predicted increase when comparing avgs, but same within std. dev.

Note: "Expected Trend" and "Result" - when increasing from normal to rapid acceleration operation

4.7 Conclusions

The purpose of this chapter was to evaluate the significance of load and acceleration on full cycle emission rates by analyzing on-board emissions system results under simulated certification cycles of urban and highway routes. An analysis of the driving cycles prior to emissions testing has shown repeatable and representative cycles where conducted.

The presence of a gentle grade in the test route proved to impact emission rates of CO_2 and NOx through manifestation of significant standard deviations. The extent of this test-to-test variability was a 10 - 20% coefficient of variation in NOx rates for 7 of 8 modes tested, with CO_2 impact on the order of 10%. HC and CO were unaffected by the presence of road grade with deviations in values instead resulting from a cooled catalyst prior to testing. Acknowledging the uncertainty in the results still enabled definitive conclusions on acceleration and loading effects.

Loading the test vehicle up to the GVWR resulted in no changes in HC emission rates. CO emissions showed similar unchanged results for the highway cycle but showed a drop in emission rate for the urban cycle. This unexpected drop in urban CO rate with loading, which also affected CO_2 emissions, was likely associated with the anomalously high fuel consumption rate for the unloaded case. CO_2 emissions showed good agreement with fuel consumption and as a result of loaded highway

73

tests, CO_2 emissions rose 8%. NOx emissions exhibited no change in rate on urban routes but a significant 19% increase during highway testing. When loading was compared on a rapid acceleration basis, the numerous transients present in the urban case resulted in an NOx increase of 56% with loading.

Demanding maximum acceleration from the test vehicle has resulted in dramatic increases in HC and CO emission rates. Comparing normal versus rapid acceleration tests, HC emissions rose 270% and 630% for urban and highway tests respectively. CO exhibited even more substantial rises in emission rates with 16 and 36 times the normal acceleration values for urban and highway tests. On a gram per gram fuel basis, CO_2 showed a decrease in emissions of approximately 10% for both urban and highway test routes as a result of the increased CO in the exhaust (due to carbon balancing). NOx emissions decreased 48% for urban routes but remained unchanged within standard deviation limits for the highway route. The limited number of transients in the highway driving route accounted is the probable reason for this avoided decrease in emission rate.

4.8 Future Work

The continuation of on-board emissions measurement studies should focus on examining a wider range of vehicles to compliment the depth of investigation with breadth. Future studies should look at the difference in species cycle emission rates when the vehicle is subjected to various soak times (after being fully warmed up), in a variety of ambient conditions. These tests would simulate vehicles which are used to run errands or other vehicle stopped and start driving patterns. Catalyst warm up time is a critical factor in meeting current and future emissions legislation. The light-off time will be a focus of emissions system improvements due to the significant contribution cold catalysts have on full cycle rates. These types of tests would also ascertain the necessity for using close-coupled catalysts for reducing high emission initial HC and CO events.

The examination of a fleet of varying vehicle types would also enable examination of rich start characteristics. The test vehicle examined in this research was found to disregard knowledge of having a fully warmed engine with rich mixtures dominating the first 12 seconds of operation. With emission regulations becoming increasingly stringent, a comparison of the sophistication of vehicle ECM design to control the early fueling strategy is critical.

A look at the load threshold required to push the vehicle into commanded enrichment for urban and highway driving cycles should also be examined with comparison of threshold values between Tier 1 and Tier 2 vehicles. Heavy load operation is not a consideration of fuel control calibrations and has not been focused on by manufacturers [13], however, Tier 2 emissions standards may have required manufacturers place an increase focus on reducing command enrichment events.

74
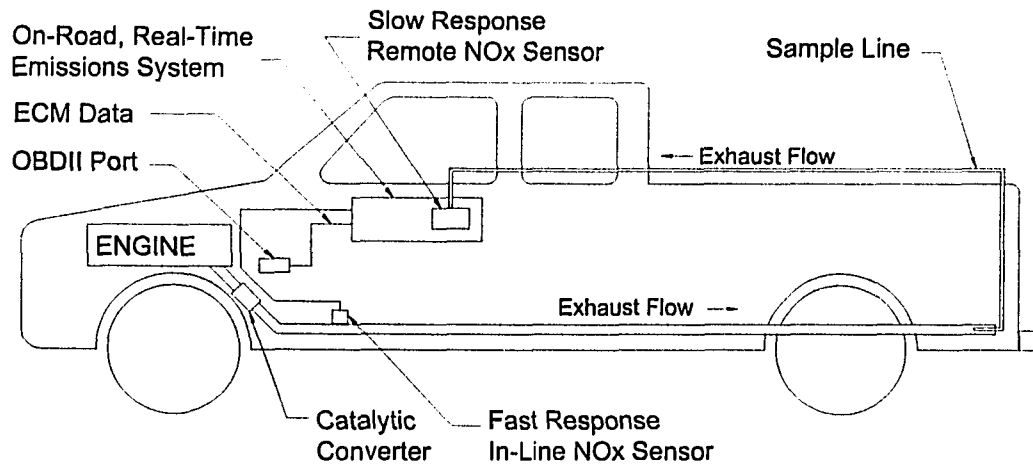
Figure 4-1 Test Vehicle Equipment Setup

On-Road, Real-Time Emissions System

Slow Response Remote NOx Sensor

Sample Line

ECM Data

OBDII Port

Exhaust Flow

ENGINE

Exhaust Flow

Catalytic Converter

Fast Response In-Line NOx Sensor
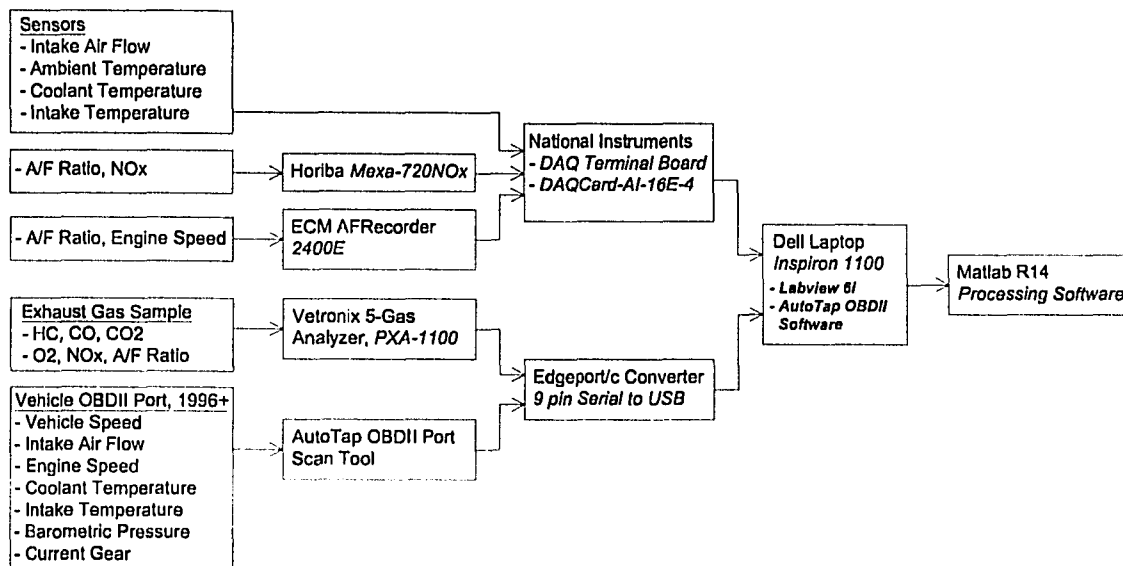
Figure 4-2 Hardware Configuration

Sensors
- Intake Air Flow
- Ambient Temperature
- Coolant Temperature
- Intake Temperature

- A/F Ratio, NOx

- A/F Ratio, Engine Speed

Exhaust Gas Sample
- HC, CO, CO2
- O2, NOx, A/F Ratio

Vehicle OBDII Port, 1996+
- Vehicle Speed
- Intake Air Flow
- Engine Speed
- Coolant Temperature
- Intake Temperature
- Barometric Pressure
- Current Gear

Horiba *Mexa-720NOx*

ECM AFRecorder 2400E

Vetronix 5-Gas Analyzer, *PXA-1100*

AutoTap OBDII Port Scan Tool

National Instruments
- *DAQ Terminal Board*
- *DAQCard-AI-16E-4*

Edgeport/c Converter
9 pin Serial to USB

Dell Laptop
Inspiron 1100
- *Labview 6I*
- *AutoTap OBDII Software*

Matlab R14
Processing Software

75

Figure 4-3 US06 Test Route Comparison

76
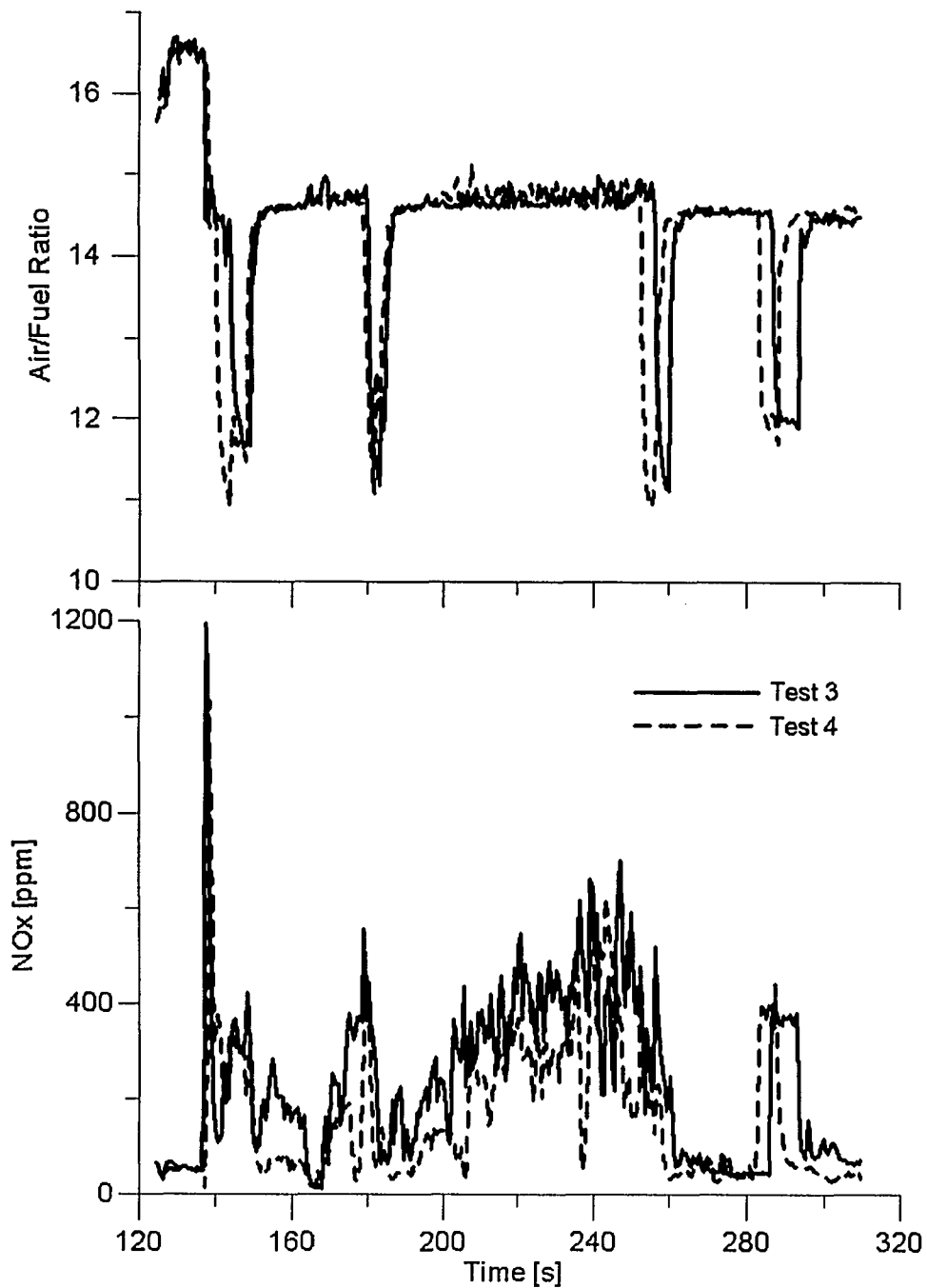
Figure 4-4 Effect of Direction of Travel on NOx Emissions - Highway Cycle, Rapid Acceleration, No Load

77
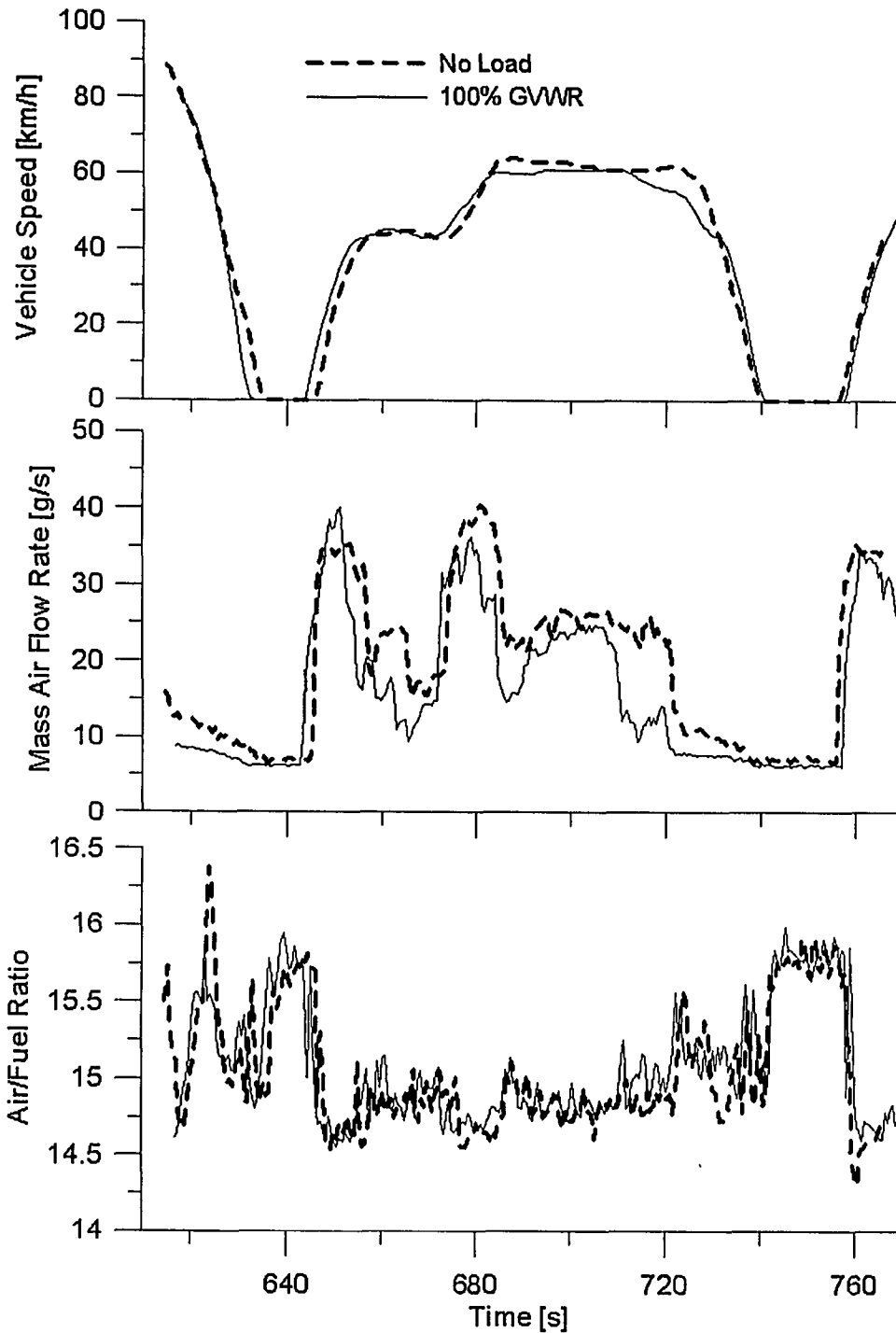
Figure 4-5 Effect of Load - Urban Cycle, Normal Acceleration

78
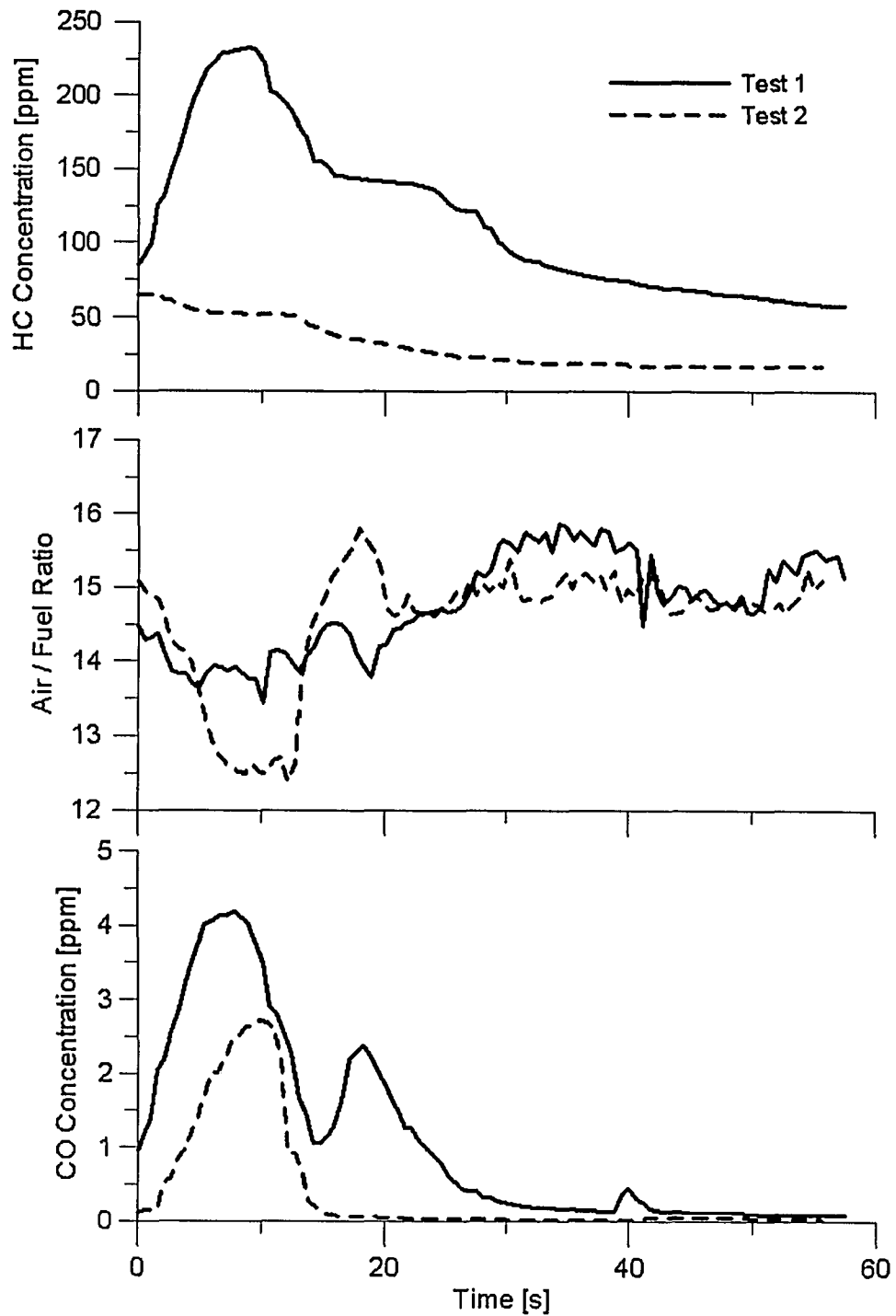
Figure 4-6 Elevated Test 1 Emissions - Urban Cycle, Loaded, Normal Acceleration

79
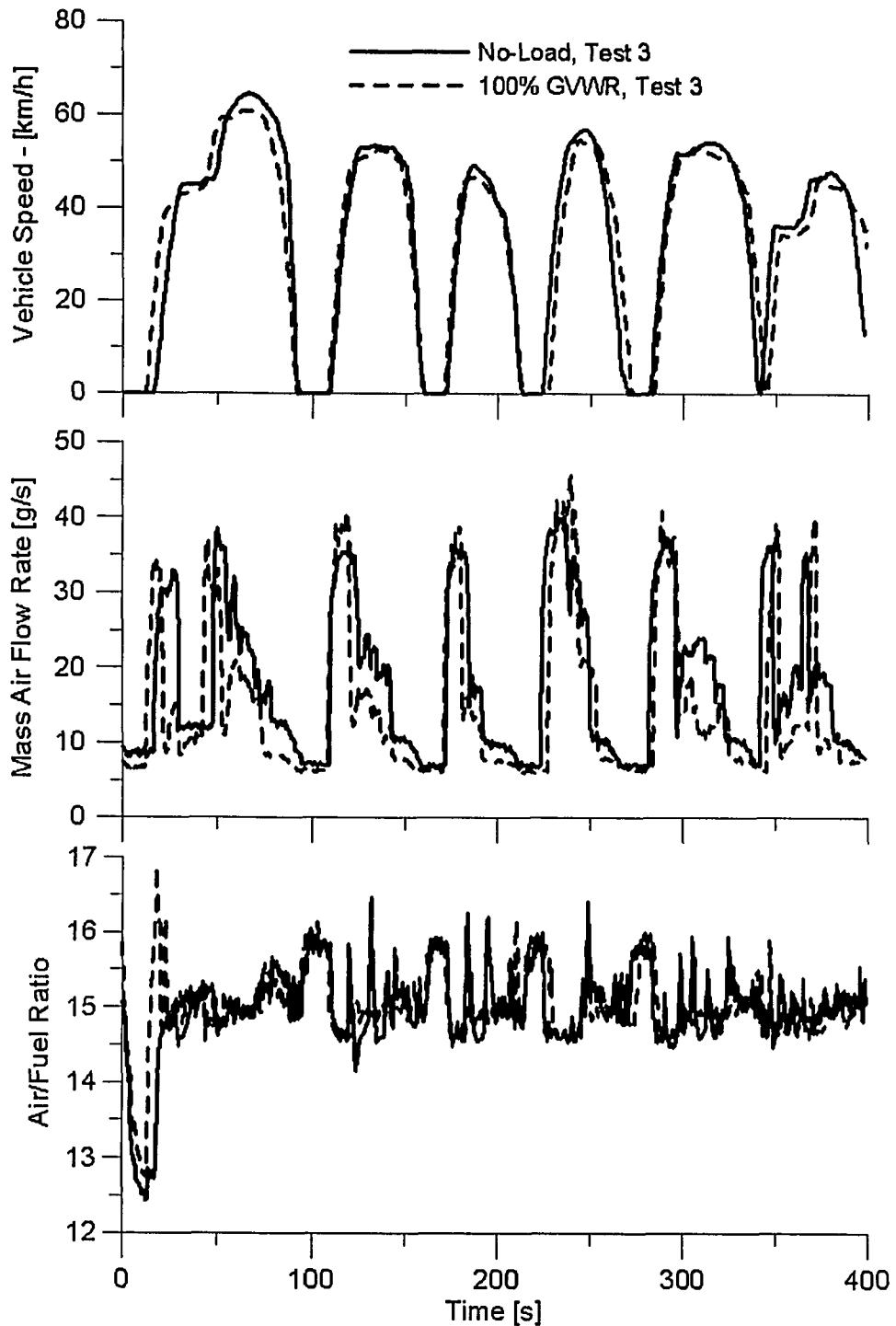
Figure 4-7 Effect of Load - Urban Cycle, Normal Acceleration

80
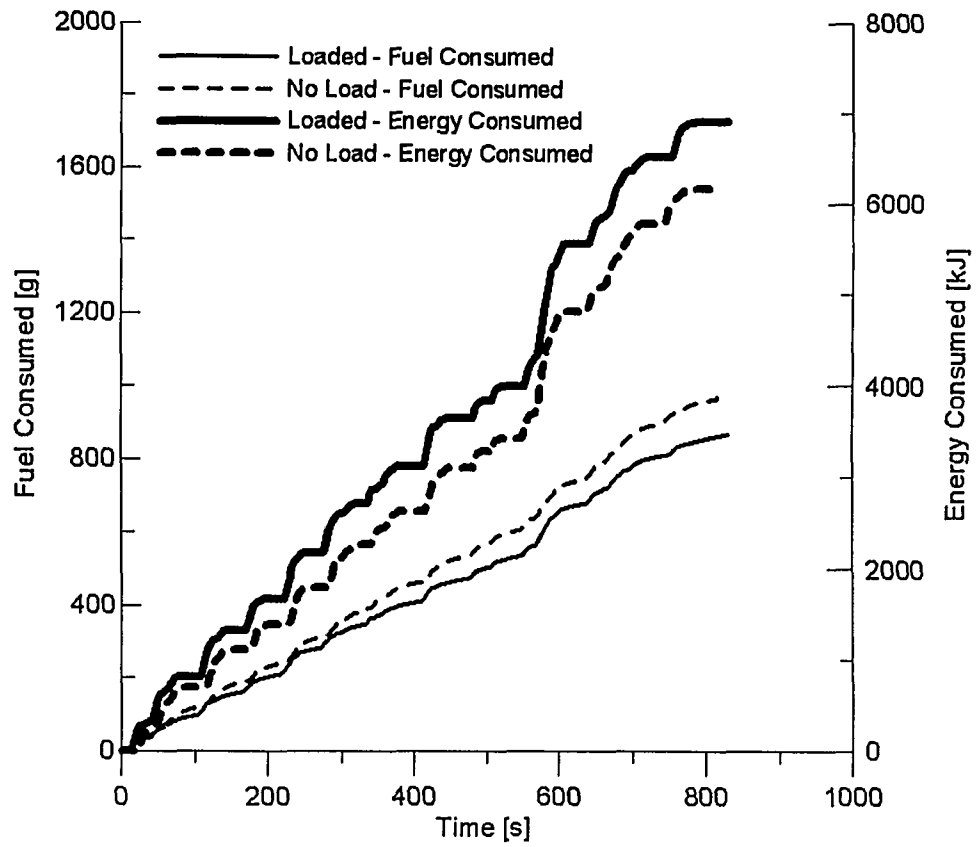
Figure 4-8 Fuel Consumption and Energy Use - Urban Cycle, Normal Acceleration

81
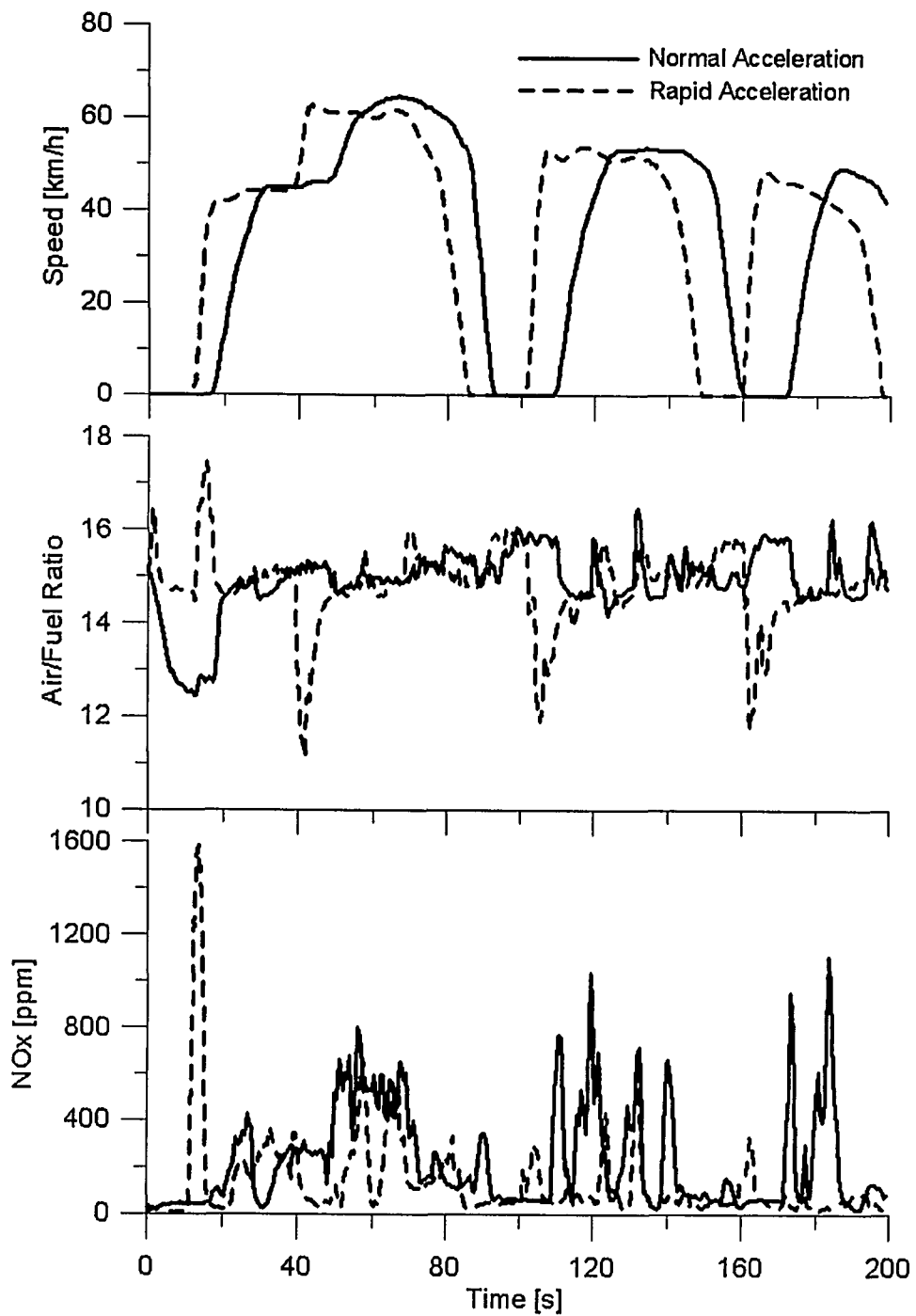
Figure 4-9 Effect of Acceleration on NOx Emission Rate - Urban Cycle, No Load

82

REFERENCES

[1]   Frey H.C., Rouphail N.M., Unal A., Colyar J.D., "Measurement of On-Road Tailpipe CO, NO, and Hydrocarbon Emissions Using a Portable Instrument," in Proceedings - Annual Meeting of the Air and Waste Management Association, June 24-28, 2001.

[2]   Vojtisek-Lom M., Allsop J.E., "Development Of Heavy-Duty Diesel Portable, On-Board Mass Exhaust Emissions Monitoring System With NOx, CO_2, and Qualitative PM Capabilities," SAE Technical Paper 2001-01-3641, Society of Automotive Engineers, 2001.

[3]   Truex T.J., Collins J.F., Jetter J.J., Knight B., Hayashi T., Noriyuki K., Suzuki N., "Measurement of Ambient Roadway and Vehicle Exhaust Emissions - An Assessment of Instrument Capability and Initial On-Road Test Results with an Advanced Low Emission Vehicle," SAE Technical Paper, Society of Automotive Engineers, 2000.

[4]   Nakamura H., Kihara N., Adachi M., Ishida K., "Development of a wet-based NDIR and Its Application to On-Board Emissions Measurement System," SAE Technical Paper 2002-01-0612, Society of Automotive Engineers, 2002.

[5]   Kihara N., Tsukamoto T., Matsumoto K., Ishida K, Kon.M, Murase T., "Real-time On-board Measurement of Mass Emissions of NOx, Fuel Consumption, Road Load, and Engine Output for Diesel Vehicles," SAE Technical Paper 2000-01-1141, Society of Automotive Engineers, 2000.

[6]   Weaver C.S., Petty L.E., "Reproducibility and Accuracy of On-Board Emissions Measurements Using the RAVEM™ System," SAE Technical Paper 2004-01-0965, Society of Automotive Engineers, 2004.

[7]   Oestergaard K., Porter S., and Nevius T., "Investigation into the Performance of an On-Board Emissions Measurement System Using a Vehicle Exhaust Emissions Simulator," SAE Technical Paper 2003-01-3746E, Society of Automotive Engineers, 2003.

[8]   Takada Y., Ueki S., Saito A., "Study on Fuel Economy and NOx Emissions of Medium Duty Hybrid Truck in Real Traffic Conditions," SAE Technical Paper 2004-01-1086, Society of Automotive Engineers, 2004.

[9]   Vojtisek-Lom M., Lambert D.C., Wilson P.J., "Real-world Emissions From 40 Heavy-Duty Diesel Trucks Recruited at Tulare, CA Rest Area," SAE Technical Paper 2002-01-2901, Society of Automotive Engineers, 2002.

[10]   Cicero-Fernandez, P., Long, L.R., "Grades and Other Loads Effects on On-Road Emissions: An On-Board Analyzer Study," California Air Resources Board, Mobile Source Division, Fifth CRC On-Road Vehicle Emissions Workshop, Apr.3-5, 1995.

[11]   Battelle, "Generic Verification Protocol for On-Board Vehicle Emissions Monitors," U.S. Environmental Protection Agency, Environmental Technology Verification program, Aug.2002.

[12]   Cicero-Fernandez, P., Long, J.R., and Winer, A.M., "Effects of Grades and Other Loads on On-Road Emissions of Hydrocarbons and Carbon Monoxide," Journal of Air & Waste Management, ISSN 1047-3289, 47:898-904, 1997.

[13]   U.S. Environmental Protection Agency, Office of Air and Radiation, Office of Mobile Sources, Certification Division, "Final Technical Report on Aggressive Driving Behavior for the Revised Federal Test Procedure Notice of Proposed Rulemaking," Jan.31, 1995. http://www.epa.gov/oms/regs/ld-hwy/ftp-rev/ftp-us06.pdf

[14]   Hawirko J.D., Checkel M.D., "Real-Time, On-Road Measurement of Driving Behavior, Engine Parameters and Exhaust Emissions" SAE Technical Paper 2002-01-1714, Society of Automotive Engineers, 2002.

[15]   Hawirko J.D., Checkel M.D., "Quantifying Vehicle Emission Factors for Various Ambient Conditions using an On-Road, Real-Time Emissions System," SAE Technical Paper 2003-01-0301, Society of Automotive Engineers, 2003.

[16]   Manchur T.B., Checkel M.D., "Time Resolution Effects on Accuracy of Real-Time NOx Emissions Measurements", SAE Technical Paper 2005-01-0674, Society of Automotive Engineers, 2005.

[17]   Canadian Automobile Association, "Autopinion - Presenting the Personal Car Ownership Experiences of More than 20,000 CAA Members," Feb.2003.

[18]   Federal Register, U.S. Environmental Protection Agency, "Motor Vehicle Emissions Federal Test Procedure Revisions; Final Regulations, Part II," 40 CFR Part 86, Oct.22, 1996. http://www.epa.gov/otaq/url-fr/fr22oc96.pdf

[19]   Heywood, J.B., "Internal Combustion Engine Fundamentals," McGraw Hill, New York, 1988.

[20]   Kaspar, J., Fornasiero, P., Hickey, N., "Automotive catalytic converters: current status and some perspectives," Catalysis Today, Elsevier Science, 77 (2003) 419-449.

84

[21]   Ferguson, C.R., Kirkpatrick, A.T., "Internal Combustion Engines - Applied Thermosciences, 2nd Edition," John Wiley & Sons, Inc., New York, 2001.

[22]   Turns, S.R., "An Introduction to Combustion, Concepts and Applications," McGraw Hill, New York, 2000, pp.214,550-594.

[23]   Stone, R., "Introduction to Internal Combustion Engines, 3rd Edition," Society of Automotive Engineers, Inc., Warrendale, PA, 1999.

CHAPTER 5

Accuracy of OBDII Port Data for On-Road Real-Time Emissions Testing

The standardization of an on-board diagnostics port and protocol has allowed researchers to gather real-time data from vehicle sensors through connection of an affordable and robust scan tool. This hardware will permit a reduction in emission system installation time and a reduction in vehicle tampering, which will allow for the testing of a larger fleet of vehicles with improved accuracy. Although vehicle operation tampering is avoided through the use of this method, the uncertainty of vehicle sensor remains unchecked. Chapter 5 will present a comparison of OBD port data information to data gathered from separately installed and calibrated sensor measurements. Data will be compared on a total integral, RMS point-by-point, and linear fit criteria to establish if independent sensors can be removed from future system installations without sacrificing accuracy.

86

5.0 Introduction

The measurement of on-board vehicle emission rates has been evolving for more than ten years as researchers and the automotive industry attempt to improve the quantification of vehicle pollution production under real-world conditions. The impetus for this recent flurry of research is due to increased tightening of certification emission rates for on-road vehicles, as well as society's desire to reduce air pollution.

The development of a standard connector plug and diagnostic test signal by the Society of Automotive Engineers (SAE) in 1988 was seen as the beginning of vehicle sensor network standardization. The eventual expansion of the standard into on-board diagnostics generation two (OBDII) on vehicles produced from Jan.1, 1996 onward, was intended to provide vehicle manufacturers with an improved emission system diagnostic capability. An added benefit was that the OBDII port also enabled emission test engineers the ability to sample a wide variety of vehicle sensors in real-time utilizing an affordable scan tool and laptop.

The number of researchers utilizing OBDII port data has been used infrequently in on-board emissions measurement systems to date,[1-4] with the anticipation that widespread use will be forthcoming due to the resulting benefits. The advantage of using the vehicle's sensors to measure operation characteristics include the availability of data from numerous sensors, reduced installation time, and the elimination of operation tampering. Although OBDII port data is assumed to be accurate by most researchers, the comparison of a test vehicle's sensors versus known calibrated and independently installed sensors would aid in this verification.

The data used for the evaluation of vehicle sensor accuracy came from on-board emission testing experiments conducted in winter/summer 2004 ambient conditions. The testing routes examined urban and highway driving patterns similar to FTP certification tests to enable the examination of a wide variety of vehicle operating modes. The purpose of this chapter is to measure the accuracy and reliability of data gathered through the vehicle's OBDII port, against independently calibrated and installed sensors. The goal of this research was to reduce the time constraint and vehicle operation influence occurring due to the installation of multiple sensors.

5.1 Experimental Setup

Vehicle operation data was gathered as part of a larger emissions measurement system which also measured vehicle pollution concentration levels on-board and in real-time.[5] A list of the vehicle operation parameters measured by the on-board system is shown in Table 5-1. From this table, it is clear that a much greater range of sensor measurements are possible through utilization of OBDII port data.

The vehicle sensors were measured using an AutoTap Scan Tool through

87

connection to an OBDII port on the vehicle, and through serial connection to the on-board laptop. The OBDII port was located above the emergency foot brake pedal on the left side of the driver's footwell. Figure 5-1 shows an overview of the emissions system configuration and the connection of vehicle sensors within this system.

Table 5-1 Vehicle Operation Parameters Measured

ECM - OBDII Port Variables	Installed Sensor Network
Engine Speed [rpm]	Engine Speed [rpm]
Vehicle Speed [km/h]	no
Engine Coolant Temperature [°C]	Engine Coolant Temperature [°C]
Intake Air Temperature [°C]	Intake Air Temperature [°C]
Mass Air Flow Rate [g/s]	Mass Air Flow Rate [g/s]
Barometric Pressure [kPa]	Barometric Pressure [kPa]
Current Gear	no
Calculated Engine Load [%]	Vehicle Load [kW] (calculated)
Ignition Timing Advance [deg]	no
Manifold Absolute Pressure [kPa]	no
Delivered Engine Torque [Nm]	Engine Torque [Nm] (calculated)
Delivered Torque [Nm]	Vehicle Torque [Nm] (calculated)
Desired EGR Position [%]	no
Throttle Position Angle [%]	no
Throttle Position Desired Angle [%]	no

The independently installed sensor network measured: engine speed, engine coolant temperature, intake air temperature, and intake air flow rate. The vehicle's engine speed and one measure of air-fuel ratio were measured using an ECM AFRecorder 2400E. The engine speed measurement was measured through the use of an inductive spark pickup. Coolant temperature was measured by installing an AD590 temperature probe to the coolant line exiting the engine block. Intake air temperature measurements were taken in the vehicle's intake system prior to the intake mass air flow sensors. Intake air flow measurements were made immediately upstream of the factory-installed sensor. Also, barometric pressure was measured at one end of the on-road test using a lab barometer.

The sampling frequency for the independently installed sensors varied between 1.5 and 2.0 Hz while OBDII port data varied between 1.3 and 1.7 Hz depending on the number of parameters being recorded. An increase in the number of recorded

88

parameters from the OBDII port decreased the frequency of individual sensor readings.

5.2 Test Vehicle

A 1999 Chevrolet Silverado C1500, extended cab, four-wheel drive truck was used as the test vehicle for these experiments. The vehicle was equipped with a 5.4 L V8 Vortec gasoline fueled engine, automatic transmission, short-box bed, which operated in two-wheel drive mode for all tests. The dry weight of the vehicle with all sensors and emissions measurement equipment installed measured 2360 kg (~5200 lbs). The gross vehicle weight rating of the Silverado was specified as 2903 kg (~6400 lbs). Vehicle mileage was approximately 112,000 km which was seen as very representative of the type and mileage of vehicles on the road today.[6]

Currently, the C1500 is being used as an emissions research test vehicle, as well as a utility vehicle for engineering student vehicle projects at the University of Alberta. The truck was originally obtained as an experimental vehicle for competition in the 2000 Ethanol Vehicle Challenge sponsored by General Motors and the U.S. and Canadian governments. At the completion of the competition, the vehicle was converted back to the stock gasoline power configuration.

5.3 Results

The validation for removing independently installed sensors from on-board emissions measurement systems must provide assurance that vehicle sensor data is able to provide accurate, timely, and reliable data.

5.3.1 Comparison Criteria

Three criteria were used to judge the suitability of OBD data as a replacement for independently installed sensors. These included the calculation of integral error, root mean square (RMS) error, and a linear agreement test. The purpose of the integral error calculation was to measure how close the total integrated variable versus time profile, came to the result from an independently installed sensor. The equation used to calculate the total integral error is shown in Equation 1.

$$ERROR_{INTEGRAL} = \frac{\left| \int X_{independent}(t)dt - \int X_{OBD}(t)dt \right|}{\int X_{independent}(t)dt} \times 100 \qquad \text{[Equation 1]}$$

The second criteria used for evaluation of OBDII port data accuracy is the

89

calculation of RMS error. The RMS error is a measure of how significant each individual reading differs from the known reading, in this case assumed to be the independently installed sensor. The lower the RMS error, the more accuratethe individual reading each and every time.

$$ERROR_{RMS} = \sqrt{\frac{\sum_i \left[\left(X_{independent,i} - X_{OBD,i} \right)^2 \right]}{n}}$$

[Equation 2]

The last criteria used was a linear agreement test which plotted the known variable on the x-axis and the unknown variable on the y-axis. With each point x,y pair included on this plot, a truly accurate sensor would result in a 1:1 agreement with a known sensor value. The measurement of the coefficient of determination, R^2, will provide a further judgement of the linear agreement between the x and y variables. The calculation of a regression line should be forced through zero as it is assumed both sensors would read zero with a zero reading input. A slope of 1.0263 would indicate that the parameter on the y-axis was producing 2.63% greater average readings than the comparable x-axis parameter.

5.3.2 Parameter Comparison

The error in on-board sensors was evaluated utilizing data gathered from previous emissions measurement studies in both summer conditions and winter conditions. Summer data consisted of 16 independently conducted tests (at various driving modes) and winter calculations were comprised of 11 tests at normal acceleration. These tests were chosen to be relevant to accurately evaluating on-board sensor accuracy due to the wide range of temperatures, operating modes, and driving cycles which were included in the drive cycle development.

Table 5-2 illustrates the average integral error and RMS error for summer and winter testing conditions with focus on the mass air flow rate sensor under normal and rapid acceleration rates. The linear agreement test indicates the percent difference in the average ECM parameter reading and the R^2 coefficient agreement calculation. The linear agreement test was evaluated for summer driving conditions only.

90

Table 5-2 Results of Parameter Comparison Analysis

	Integral Error [% Error / Std.Dev.]		RMS Error [Units Specific to Variable]		Linear Fit [% dif. from known sensor]	
	Summer	Winter	Summer	Winter	Difference [%]	R^2
Mass Air Flow Rate [g/s]						
Normal Accel.	11.1 +/- 3.4	12.6 +/- 1.8	5.3 +/- 1.3	4.7 +/- 0.8	6.7	0.91
Rapid Accel.	3.5 +/- 2.1	-	16.0 +/- 0.8	-	15.7	0.71
Intake Air Temp. [°C]	17.5 +/- 3.3	26.1 +/- 68.8	3.4 +/- 0.9	6.0 +/- 1.6	20.2	0.81
Engine Speed [rpm]	0.2 +/- 0.2	0.11 +/- 0.13	70.0 +/- 29.1	37.3 +/- 13.9	- 1.1	0.98

5.3.2.1 Mass Air Flow Rate

The evaluation of mass air flow rate is one of the most important variables in producing mass emission rate values from on-board emissions systems. As previously discussed in Chapter 3, the accurate and timely measurement of air flow rate and emission concentration data is critical to the emission rate calculation. Replacing the system's independently installed sensor with the on-board sensor therefore requires certainty in the on-board sensor's capabilities over a range of operating conditions and temperatures.

The results presented in Table 5-2 indicate that the integral error, or total error in mass of air measured by each sensor, measured between 3.5 and 12.6% of the actual mass measured by the independently installed sensor. Acknowledging the vast modes of operation under which these sensors were compared, this total mass error is an acceptable difference.

The RMS error provides a better understanding of the individual differences between the sensor readings, which is critical when using real-time data for emission calculations. Mass air flow rate measured during normal acceleration conditions appeared to have a much lower RMS error, 5.3 g/s versus 16.0 g/s during rapid acceleration testing, indicating a possible link between sensor error and acceleration rate. No change in RMS error was noticed with ambient temperature. The link between acceleration rate and the agreement of the air flow sensors is reinforced when the third criteria is considered. The linear agreement test has shown that the percent difference between each measurement rises from 6.7% to 15.7% when driving patterns are changed to include aggressive high transient characteristics.

91

It is important to examine the real-time behavior of the mass air flow sensors to find the source of the sensor error. An examination of Figure 5-2 illustrates some important characteristics regarding ECM mass air flow sensor operation with rapid transients. Looking at a 50 second event involving vehicle transients, the ECM exhibited success in measurement of small changes in flow and engine idle conditions. The figure also indicates that the ECM sensor detected a rise in MAF 3 seconds earlier than the independent sensor, prior to a vehicle acceleration event. This early response detection was a repeatable trend with all normal and rapid accelerations. Possible causes may have been attributed to the installation locations of the two MAF sensors, internal sensor response time, or air flow patterns in the intake system as a result of opening the throttle plate.

Figure 5-2 also shows that in some instances the on-board sensor was unable to measure high (peak) mass air flow rates occurring during rapid acceleration events. However, for the vast majority of the measurements with the exception of peak rapid acceleration events, the on-board mass air flow sensor was able to detect similar peak air flows. The reduced reading may have been due to flow restrictions from the smaller diameter upstream independent sensor, or due to the lower resolution of the ECM sensor.

Figure 5-3 shows a real-time profile of mass air flow rate and vehicle velocity for the majority of a US06 highway driving cycle operating under normal acceleration conditions. This figure indicates that the ECM sensor exhibited a noticeably lower resolution versus the independent sensor which is characteristic of a slower responding sensor. The sensor's inability to resolve mass air flow data to the extent of the faster responding independent sensor, limits its accuracy in measuring flow data but did not inhibit vehicle operation.

The normal acceleration highway test also indicates that the ECM sensor read consistently higher MAF rates during cruising periods. However, during normal acceleration transient events, both sensors showed very good agreement in terms of time of response and magnitude of air flow.

The behavioral differences of the two mass air flow sensors can be seen in Figure 5-4 when looking at the linear agreement test. Table 5-2 indicates that the trendline plotted, produces average mass air flow rates 6.7% above the trendline with an R^2 fit coefficient of 0.93. This figure illustrates the early response of the ECM sensor by noting the numerous points above the 1:1 trendline for air flow rates below 15 g/s. Also, the inability of the ECM sensor to measure similar magnitude peak flow rates appears as data points below the 1:1 line for flow rates over 40 g/s. Additionally, the elevated flow rates at cruising conditions appear as data points slightly above the 1:1 line between 15 and 40 g/s.

Visual inspection of the distribution of points around the MAF trendline suggests a y-axis residual difference, which when plotted in time, would form a sinusoidal pattern with differences in data values from the trendline initially positive for the first

92

half, and negative for the second half. A 1:1 trendline with an equal distribution of (x,y) points above and below the MAF trendline would result in a residual versus time graph which is equally distributed above and below the y-axis zero line. A sinusoidal pattern indicates a lack of correlation between the sensor reading which could be due to calibration, sensor malfunction, or age degradation.

Knowing how the behavior of the ECM sensor compares to a known sensor for varying operation modes has now been established, but the effects of this difference in readings can only be calculated by examining the effect of sensor selection on mass emission rates.

Table 5-3 highlights the difference in NOx mass emission rates for a variety of operating modes when comparing the on-board (ECM) mass air flow sensor to the independent sensor (Indep). Focusing on the change in emission rate indicates that a change of up to 14% exists when utilizing the vehicle air flow sensor. Rapid acceleration tests have illustrated the NOx emission rate values decrease whereas normal acceleration tests tend to result in similar or increased rates. When considering the actual emission rates and the associated standard deviation, the majority of NOx results appear to present similar values which lends confidence to the vehicle sensor.

Table 5-3 Effect of Sensor Selection on NOx Mass Emission Rates

	HIGHWAY			URBAN		
	NOx - Indep [g/km]	NOx - ECM [g/km]	Change [%]	NOX - Indep [g/km]	NOx - ECM [g/km]	Change [%]
No Load, Normal Acceleration						
Average:	0.327	0.358	**9.6**	0.577	0.539	**- 6.5**
Std Dev.:	0.032	0.036	-	0.116	0.121	-
GVWR (Fully Loaded), Normal Acceleration						
Average:	0.390	0.429	**10.0**	0.596	0.668	**12.2**
Std Dev.:	0.002	0.006	-	0.117	0.131	-
No Load, Rapid Acceleration						
Average:	0.381	0.371	**- 2.4**	0.303	0.262	**- 13.5**
Std. Dev.:	0.072	0.080	-	0.051	0.050	-
GVWR (Fully Loaded), Rapid Acceleration						
Average:	0.412	0.402	**- 2.5**	0.472	0.414	**- 12.4**
Std Dev.:	0.049	0.048	-	0.068	0.093	-

93

The results of this analysis can therefore conclude that the ECM intake air flow sensor provides accurate data on engine air flow requirements on the basis of both time and magnitude. The possibility of air leaks occurring after the independent sensor, but before the vehicle sensor, provide a partial explanation for higher mass air flow rates during cruising. Considering the age of the vehicle, the tampering of the intake system due to the installation of a separate sensor, the possible leakage of air into the intake system, and the relatively small 10% change in emission rate values, the use of vehicle ECM air flow data appears acceptable for this test vehicle.

5.3.2.2 Intake Air Temperature

The intake air temperature measurements showed a linear relationship as evidenced in Figure 5-5, but were found to be offset from the actual temperature. Figure 5-5 and Table 5-2 indicate that the ECM temperature measured 20% higher values during summer driving conditions and exhibited noticeable deviation from the linear relationship. The large envelope of temperatures generated an $R^2 = 0.81$ due to the ECM sensor's inability to measure temperature beyond full degree increments. This characteristic is noticeable in Figure 5-5 as numerous 1°C "steps" appear to be characteristic of the relationship.

The results for integral error showed ranges of 18 - 26% and RMS error temperatures of 3-6°C. From these results and a qualitative examination of real-time results from Figure 5-6, the ECM temperature sensor provided adequate relative temperature measurements with an offset from actual temperatures. Figure 5-6 shows that point check tests of temperatures with a third thermocouple type temperature sensor (during real-time measurements), indicate that the actual temperature measured is from the independently installed temperature sensor. Table 5-4 indicates that average error was -1% and 5% for the independent sensor whereas ECM sensor data measured average error of 20% and 34% during two days of data comparisons.

Table 5-4 Intake Temperature Sensor Error

	Error in Indep. Temp Sensor [%]	Error in ECM Temp Sensor [%]
Case 1	-1.5 %	20.3
Case 2	5.3 %	33.6

In both summer and winter conditions, the intake air temperature sensors showed higher values than what actually occurred. This could be due to an inaccurately calibrated temperature sensor from the factory or a sensor which has drifted from calibration over the life of the vehicle. Alternatively, temperature differences were more likely due to the sensor mounting location, since the ECM sensor is closer to

94

the engine which radiates more heat to the surrounding area. Also, intake air passing through two heated film air flow meters may also account for a partial warming of the incoming air. Therefore, knowing relative temperature measurements are accurate, the reliability of thermocouples, and understanding the effect of air warm-up as it enters the engine, it is believed that the vehicles temperature sensor is accurate for emissions measurement studies.

5.3.2.3 Engine Speed

The measurement of engine speed was significant in these emissions studies due to the nature of the measurement system configuration. Recording emissions and vehicle operation data was done through the use of two programs running simultaneously. The originally developed system measured vehicle emissions and operation data through data acquisition hardware and Labview 6.0i software. The modified apparatus supplemented the previous system with data gathered from an OBDII port through an AutoTap scanner and proprietary software combination. The effect of running two separate data gathering software programs necessitated the requirement for data synchronization. The most accurate way to ensure common vehicle operation data was measured and compared simultaneously, was to match engine speed profiles from both data sets. The results of this method proved to be accurate, and the high reliability of the readings from both engine speed sensors ensured minimal data files would be wasted due to improper matching.

The validation for elimination of one the independently installed sensor, given the necessity for engine speed data in each data file, therefore seems unlikely. However, the gas analyzer will not be replaced and knowing it has the capability to measure engine speed, the separate use of the AFRecorder 2400E for measuring engine speed could prove to be redundant and therefore allow for its omission from the system (if accuracy of the OBDII data could be obtained).

Although only preliminary testing of the gas analyzer engine speed sensor measurement was done, similar results and capabilities appear to exist. On-road testing would require comparison of the two sensors before acceptance of a reliable engine speed data stream from the gas analyzer could be obtained.

The current comparison of engine speed with a known, accurate engine speed sensor has shown that both sensors measured nearly identical engine speed profiles as evident by Figure 5-7 and Table 5-2. Figure 5-7 illustrates that for an urban driving route with multiple transients producing rapid changes in engine speed, both the independently installed and on-board engine speed sensor were capable of providing similar transients, profiles, and values. This is confirmed through Table 5-2 where integral error was 0.2% on average and approximately 70 rpm on an RMS error basis. The linear agreement test has also shown acceptable results within a tight envelope ($R^2 = 0.98$) of engine speeds surrounding the 0.989 slope line. The linear agreement test results for the engine speed sensor are shown

95

in Figure 5-8. This test indicates that the vehicle ECM engine speed sensor under predicted the correct value by 1.1% on average.

Based on the quantitative comparison and graphical results, it is clear that the need for the AFRecorder as an engine RPM sensor is not required if similar engine speed measurements could be obtained from the gas analyzer engine speed sensor. The AFRecorder may be completely removed if the Horiba NOx / O_2 sensor can be shown to show similar A/F readings.

5.3.2.4 Engine Coolant Temperature

Measuring engine coolant temperature provides an indication of the relative state of engine warmth. Although it is not directly used in calculating emission rates, vehicle dynamic performance, or other reported data, it can be used to provide information on the engine temperature status relative to steady state operation. Knowing that this measurement may be taken on the engine block or the coolant line to the radiator, a comparison was completed to evaluate how accurate one mounting position would be.

Initial test results taken during winter conditions indicated that measurements of engine coolant temperature showed noticeable differences between the two available sensors. The independently installed sensor was noticeably lower due to its installation position (on the coolant line), but rather served as a relative indication of engine temperature to denote fully warmed steady state operating conditions.

The engine warmup rate and time to initial coolant temperature rise are parameters which could be compared against ECM coolant temperature readings to indicate the importance of the independent sensor mounting location. From an analysis of cold weather testing at -31°C and -8°C, it was noticed that <u>sensor location impacts</u> both <u>delay time to initial coolant temperature reading increase</u> and <u>coolant temperature gradient</u>. Both tests were conducted after an overnight soak of the vehicle under ambient conditions with extreme cold testing conditions utilizing the engine block heater.

The results of Table 5-5 indicate that during cold weather testing, the independently installed temperature probe took approximately 80 seconds longer before measuring an initial temperature increase which is nearly three times longer than the ECM sensor time. Moderate cold temperature testing at -8°C showed a similar trend though not as extreme as expected. In this case, the detection of coolant temperature increase took less than 30 seconds longer or just over twice as long as the ECM sensor.

The coolant temperature gradients also favored the ECM sensor with factors of approximately 3 and 2 for -31°C and -8°C respectively. Standard deviation values are listed to indicate the range of variability in the test results.

96

A real-time emissions measurement test completed under -5°C ambient conditions, showed the difference in coolant temperature measurement characteristics discussed above. From Figure 5-9, the longer time until an initial temperature rise and lower coolant temperature gradient are both evident. The impact is a final warmed up steady-state coolant temperature which occurs noticeably later than the ECM sensor.

Table 5-5 Engine Coolant Temperature Comparison

Test	Avg. Temp [°C]	Time Delay (to Temp Increase) [s]		Coolant Gradient (Temp Increase) [°C / min]	
		Indep.	ECM	Indep.	ECM
Case 1	- 33.5	130	-	2.5	5.5
Case 2	- 30.5	97	44	2.7	6.0
Case 3	- 30.4	157	45	1.9	6.7
Average:	**- 31.4**	**128**	**44.5**	**2.4**	**6.1**
Std.Dev.:	1.8	30	0.7	0.4	0.6
Case 4	- 12.1	44	16	4.8	10.7
Case 5	- 7.4	36	13	5.1	12.4
Case 6	- 5.4	46	20	4.6	9.4
Average:	**- 8.3**	**42**	**16**	**4.8**	**10.8**
Std.Dev.:	3.4	5	4	0.3	1.5

Given the calculated results and figures, it is clear that the location of the coolant temperature sensor is insufficient to judge the accuracy of the engine coolant temperature. However, the precision of the sensor appears to be very good with a reasonable expectation that accuracy may also be very good. For general purposes of measuring engine temperature, warmed up time, and time to an initial coolant temperature rise, the applicability of using ECM data for engine coolant temperature measurements seems reasonable.

5.3.2.5 Barometric Pressure

The measurement of barometric pressure was compared on an average basis rather than an integral or RMS error basis due to the lack of common real-time measurement and the stability of the measurements taken. From a comparison of both summer and winter emissions testing, the results have shown that the vehicle was correctly able to measure the ambient pressure within approximately 2% of the true laboratory measured value.

97

Average Error: 2.2 +/- 0.7 % (Summer Test Conditions)
Average Error: 0.6 +/- 0.5 % (Winter Test Conditions)

Although this finding does lend confidence to the vehicle readings, it does not reduce the number of on-board emissions sensors. It does enable the user to avoid completing manual pressure measurements at the start or end of the test cycle which saves time and reduces redundant measuring. Improved accuracy in the measurement of barometric pressure could have been obtained by using a barometer which was outdoors rather than in the laboratory. Both temperature and building pressure can effect barometric pressure readings.

5.3.2.6 Vehicle Speed

The evaluation of OBDII vehicle speed accuracy data was not compared as the presence of a duplicate measurement sensor was not installed. However, it was believed that the vehicle speed measurement was the most accurate of the sensor readings gathered due to its simple nature of operation and lack of apparent deviation in calibration with time due to its mechanical design.

Should future work desire an independent check of vehicle speed measurements, the use of a fifth wheel measurement sensor may be employed.[7] This sensor consists of a calibrated wheel, axle, and tachometer assembly and operates through the measurement of the rotational speed of the wheel which is in contact with the road or dynamometer rolls. An alternative method of confirmation would use laterally oriented accelerometers to generate a velocity profile.

5.3.2.7 A/F Ratio

The measurement of air-fuel (A/F) ratio is currently done using three sensors. The use of an AFRecorder O_2 sensor was the original sensor used in the development of the emissions system produced by Hawirko [8]. This system also produced a real-time air-fuel ratio from calculation of the exhaust gas concentrations, measured with an on-board five gas analyzer. The improved emissions system has added air-fuel ratio measurement capability through the use of a dual measurement NOx / O_2 sensor. Although originally added to the system for its accurate and responsive NOx sensor, the A/F measurement capability was also seen as a possible replacement for the AFRecorder. Knowing that the AFRecorder has verified OBDII port engine speed data, the verification of the A/F ratio as well, would enable a large and cumbersome instrument to be eliminated from the emission system.

The following comparison will focus on evaluating the accuracy of the Horiba A/F sensor versus the AFRecorder A/F sensor, which is assumed to be known. Table 5-6 shows the results of the Horiba A/F sensor evaluation on the basis of integral error, RMS error, and the linear agreement test criteria. The integral error and RMS

98

error were taken for urban routes only. Fuel shutoff events which occurred during strong decelerations in the highway test, produced lean spiked A/F ratio data which could not be compared due to differences in the span settings. The maximum values of these spikes were left at the default settings of 25 and 50 A/F during software configuration, which would have artificially raised the highway test error results due to this significant lean peak difference.

Table 5-6 Air/Fuel Ratio Sensor Comparison - Horiba vs. AFRecorder

	Integral Error [percent]		RMS Error [ratio]		Linear Fit		
	Summer	Winter	Summer	Winter	Difference [%]	R^2	R^{2*}
Urban Route	2.74+/- 0.76	1.48 +/- 0.18	0.56 +/- 0.15	0.33 +/- 0.06	-2.9	0.66	0.88
Highway Route					-1.0	0.96	0.97
*Note: - R^2 Agreement Coefficient when trendline is NOT forced through the origin - Table shows Horiba A/F sensor error (AFRecorder assumed known)							

Integral error is listed with the average percent error and the associated standard deviation resulting from calculations averaged over a series of 8 tests of differing operating modes. The RMS error is an absolute A/F ratio value with standard deviation results listed as well. From Table 5-6, the integrated air-fuel ratio signal is less than 3% (2.74% and 1.48%) different from the known A/F sensor over the average complete driving cycle. Low standard deviations in both error terms also indicate the repeatability of these findings. RMS error showed average A/F ratio error per point less than 0.6. These two criteria indicate that the sensors are quite capable of measuring very similar air-fuel ratios over a variety of driving types and ambient temperatures.

A closer investigation into the particular source of the integral and RMS error can be done by looking at real-time sensor profiles and results from the linear agreement tests. The real-time profiles of air-fuel ratios shown in Figure 5-10 and 5-11 indicate typical response characteristics associated with both sensors. Urban and highway driving cycles have illustrated that during acceleration events which involve a richening of the A/F mixture, both sensors respond similarly in magnitude and response. This is a good result which generates confidence in the Horiba's A/F sensor since correct measurement of transients is a significant consideration when measuring real-time emissions data.

During cruising and idle modes, the known AFRecorder A/F sensor measured leaner mixtures than the Horiba A/F sensor, as shown in Figure 5-10 for the two transient events highlighted. This test was representative of the recent behavior of the Horiba sensor but is not characteristic of it. Figure 5-11 shows an example of accurate behavior by illustrating correlation between the two A/F ratios measured during tests completed in spring 2004. Knowing this sensor was utilized for both winter 2004 and fall 2004 emissions studies, the possibility exists that the air/fuel

99

ratio measurement capability may have been degrading. Testing with the new Horiba sensor available in inventory in the Engine Laboratory would enable conclusive evaluation of this theory.

An examination of recent tests over numerous cruising speeds, has found that although the two sensors differ in lean A/F measurements at lower urban cruising speeds, the two sensors approached similar values of A/F as speeds increased. Similar results can be conclusively noticed at highway speeds.

The linear fit agreement test has two parameters of comparison, a percent difference value and an agreement correlation coefficient. The difference values of -2.9% and -1.0% in Table 5-6 indicate that the Horiba A/F sensor is producing marginally lower values than the AFRecorder, which is assumed to be known. Urban routes showed higher differences between the sensors due to the AFRecorders tendency to lean the mixture out approximately 0.5 [kg air / kg fuel] more than the Horiba during moderate load cruising conditions. During high speed cruising conditions, A/F ratios remained near stoichiometric conditions for the majority of the mode.

Figure 5-12 indicates the correlation between the A/F [x,y] pairs measured during four different modes on a highway driving cycle. The relatively tight envelope of points near the almost 1:1 trendline indicates good agreement between sensor measurements. The R-squared value in Table 5-6 shows good correlation for highway driving tests with R^2 = 0.96 but less agreement with urban routes. Removing the restriction of forcing the trendline through the origin increases the R^2 value from 0.66 to 0.88. This result indicates that an offset in sensor readings, likely occurring during the idle and lower speed cruising portions, is the likely cause of this diminished correlation. No significant increase in the correlation coefficient is realized when the origin restriction is imposed on the highway test which illustrates the agreement of those results.

A secondary consideration which is of equally valuable importance to measurement accuracy relates to the response rate of the two sensors. A simple qualitative evaluation of the response rates from Figures 5-10 and 5-11 indicates that the two sensors approach their steady state values at nearly the same time with similar resolution. This is a reassuring finding when considering replacement of a known fast responding sensor.

The use of the five gas analyzer to produce A/F readings was insufficient to confirm which of the sensors was accurately reproducing the idle mixture ratio. However, analysis of previous testing from spring 2004 does indicate that the idle A/F readings measured by the AFRecorder are correct. The gas analyzer's capabilities lacked the resolution required to quickly respond to changing air-fuel ratios resulting in a smoothed out profile. The use of the calculated A/F data from the gas analyzer is also not desirable as a source of information due to its sample line delay time which introduces increased error into the synchronization of A/F and vehicle data.

100

5.3.2.8 OBDII Port Information Failure Rate

The replacement of independently installed sensors with on-board vehicle sensors may only be done if the engine control module (ECM) is capable of providing a steady stream of correctly measured data. An analysis of the data gathered through the AutoTap scan unit has shown that there exists instances in the recorded data file in which outliers occur. The frequency of these findings for the most critical parameters measured are shown in Table 5-7. These measurements indicate that erroneous data points occurred for less than 0.5% of the points recorded. The test contained approximately 1300 points. These results are based on an examination of data from 11 tests conducted during the fall 2004 emissions testing experiments. Based on these results, and knowing that typical filtering algorithms would be capable of filtering out the sporadic outliers, it is reasonable to assume that the OBDII port provides very continuous and reliable reporting on vehicle sensor measurements.

Table 5-7 Average Failure Rate of OBDII Parameters

Parameter	Avg Failure Rate		Std. Dev.
	[#]	[%]	[%]
Engine Speed	0	0	0
Vehicle Speed	5.5	0.4	0.2
Coolant Temp	4.4	0.3	0.1
Intake Air Temp	5.9	0.4	0.2
Mass Air Flow Rate	3.2	0.2	0.1
Current Gear	5.2	0.3	0.1
Average Number of Points Examined: 1306			

5.4 Conclusions

The purpose of comparing vehicle operation parameters gathered from an OBDII port scanner and an independent network of sensors, was to illustrate whether the accuracy and reliability of OBD data is sufficient to replace the additional sensors installed in on-board emission measurement systems. From the data gathered over the past year of on-board emission testing, results presented indicate that the majority of sensors produce accurate data over a wide range of operating conditions. The data gathered from the OBDII port was also shown to be nearly free of erroneous data with outliers occurring for less than 0.5% of the points sampled.

The most critical vehicle operation sensor which is used to calculate mass emission rates is the mass air flow rate sensor. Integral error results found that the vehicle's

101

air flow sensor measured 3.5 - 12.6% difference in the total mass of air over a wide range of ambient conditions and driving modes. When the impact on emission rates was considered, a similar result was observed. Emission rates varied between 3% and 13% when using the on-board sensor. Knowing the variety of conditions these sensors were compared at and the importance transients can have on emission rates, the use of on-board air flow rate sensors is known to be valid and accurate.

Intake air temperature was found to be precise but offset from the known sensor values by 3.4°C to 6°C for summer and winter conditions respectively, with sensor position differences accounting for the likely cause. A coolant temperature comparison showed that the vehicle sensor measured shorter initial warmup times and larger gradients in warmup rate. At -31°C the independent sensor measured a warmup rate of 45 seconds versus 128 seconds for the independent sensor. The measured warmup rate was also faster with 6.1°C/min versus 2.4°C/min. Based on these results, it was concluded that ECM data is sufficiently accurate to measure coolant parameters for measuring the warmed up status of a vehicle. The results also illustrate that locating a temperature probe at the coolant outlet of an engine produces added error in measurements.

The sensors which showed the most accurate readings were engine speed, barometric pressure, and vehicle speed. Engine speed and barometric pressure were both accurately read with error of 1% and 2% average error respectively. Vehicle speed was assumed to be the one of the most accurate sensors due to its simple mechanical nature and historically reliable operation.

Using the Horiba A/F ratio sensor to replace the dedicated AFRecorder sensor appears to be valid for the majority of testing conditions and thus enables the removal of the AFRecorder from the emissions system. Integral error less than 3% and RMS error less than 0.6 [A/F units] was found for the urban conditions tested. Recently lean cruising operation at urban speeds has indicated a limitation in the Horiba's measurement capabilities. However, this finding was attributed to sensor age as similar test conditions with a new Horiba sensor proved accurate.

5.5 Future Work

Future work should consider utilizing a new Horiba A/F sensor to evaluate whether a calibration error, sensor age, or other factors can account for this recent lack of lean mixture measurement accuracy. Also, initial testing of the five gas analyzer's engine speed sensor should be completed to verify the sensor's capabilities relative to the proven ECM engine speed readings. Future emissions testing with the current emission system should proceed without the use of the AFRecorder once this verification has been completed. The independent sensor network may also be uninstalled from the current test vehicle with full utilization of the OBD parameters considered accurate. Investigation of alternative vehicles should continue to use the independent MAF sensor for emission rate calculations.

102
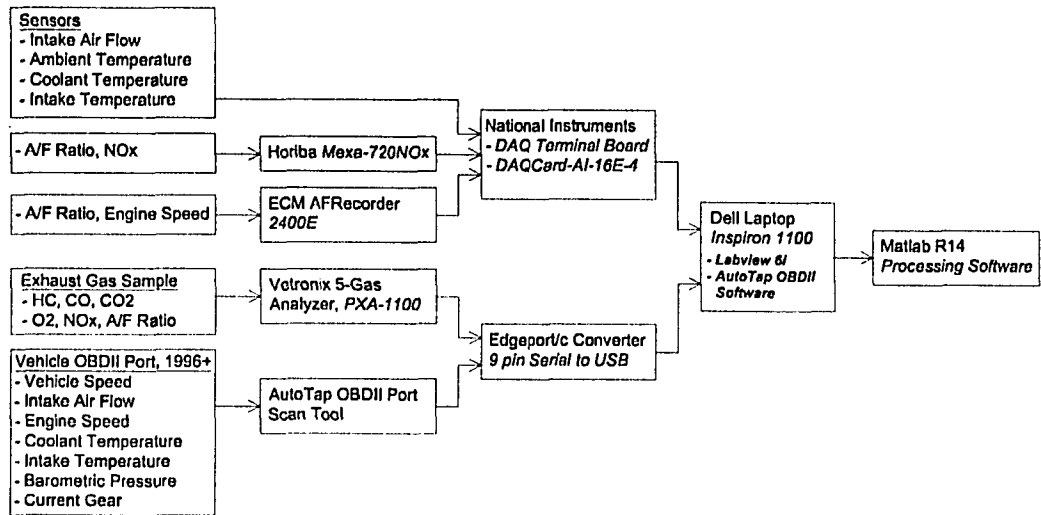
Figure 5-1 Hardware Configuration
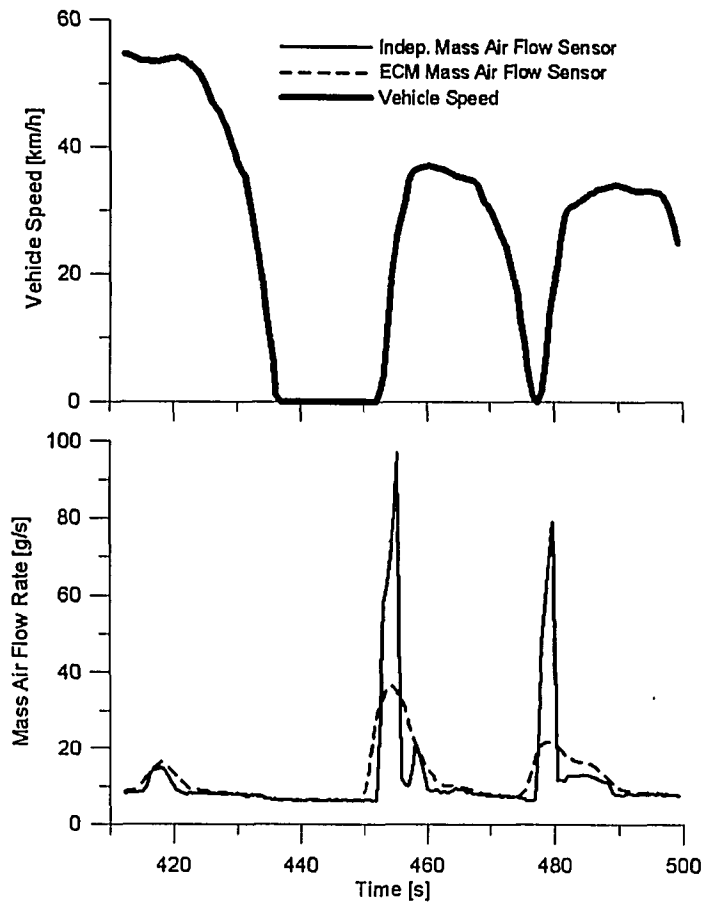
Figure 5-2 Mass Air Flow Sensor Comparison - Rapid Acceleration Test
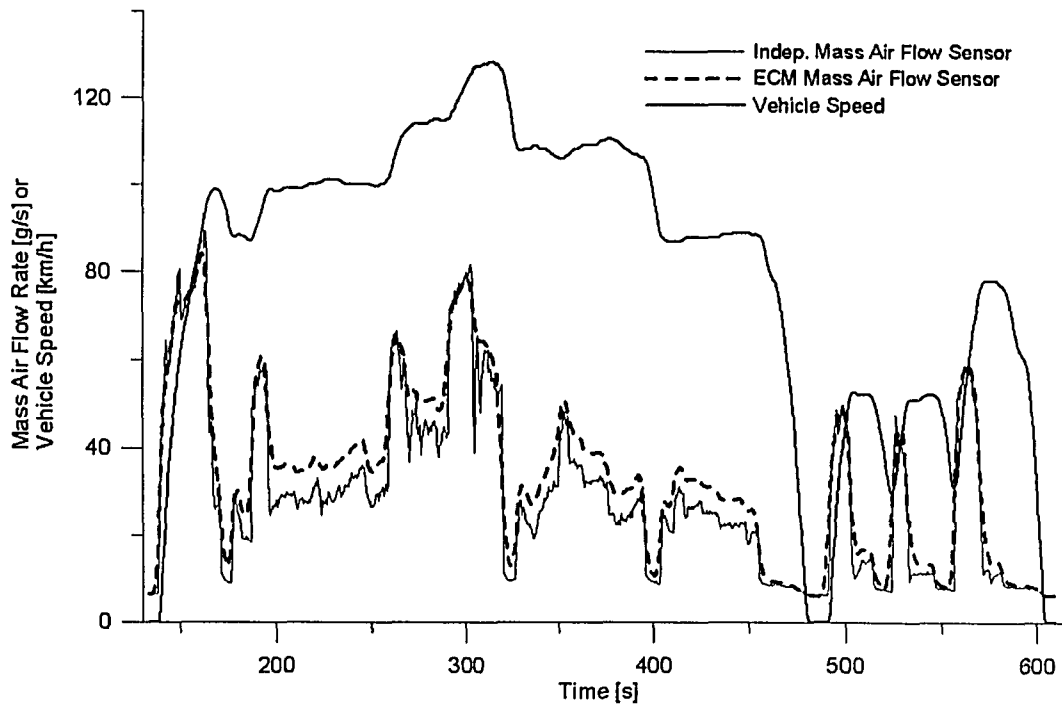
Figure 5-3 Mass Air Flow Sensor Comparison - Normal Acceleration Test
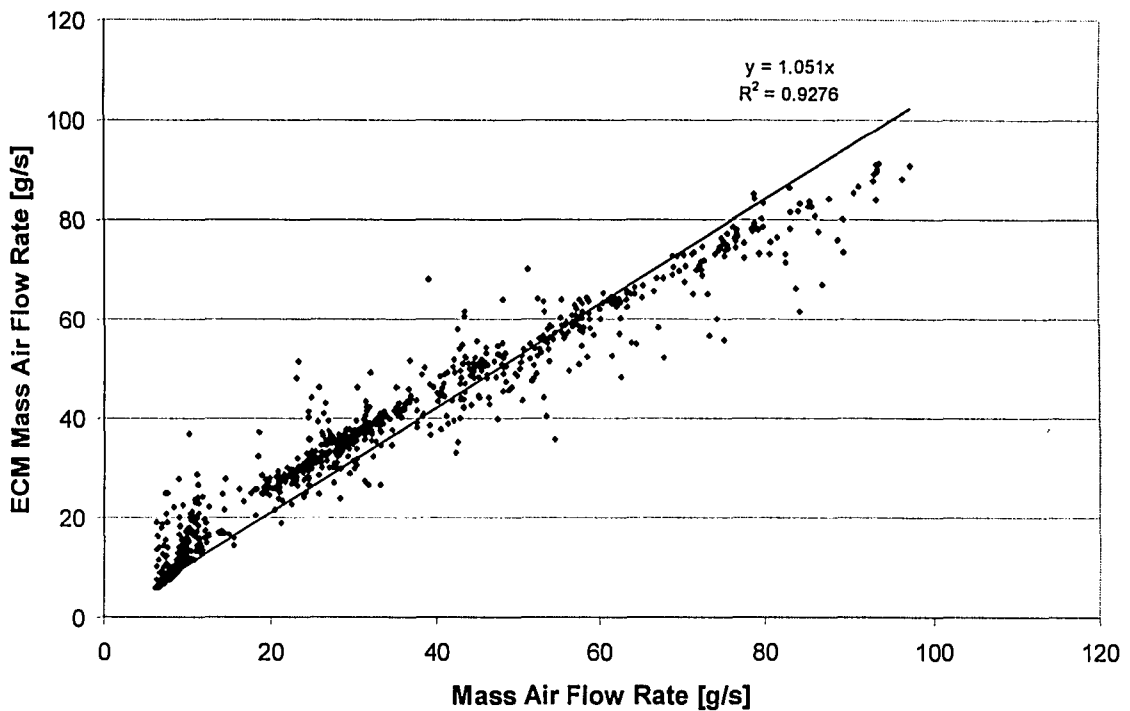
Figure 5-4 Mass Air Flow Sensor Comparison - Highway Cycle, Normal Acceleration, GVWR Loaded

104
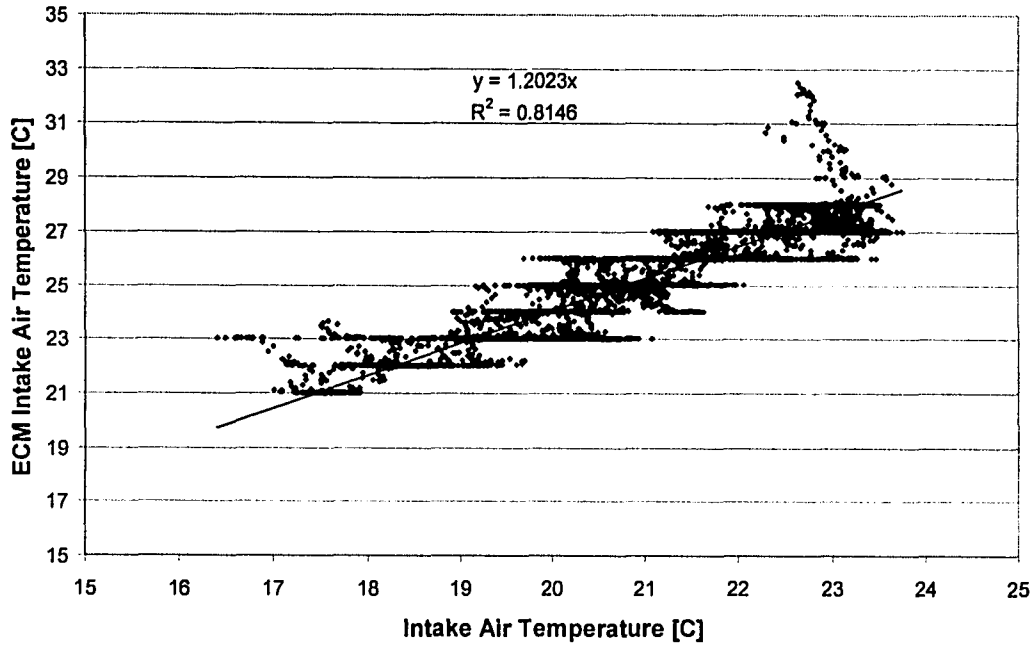
Figure 5-5 Linear Agreement Test - Intake Air Temperature
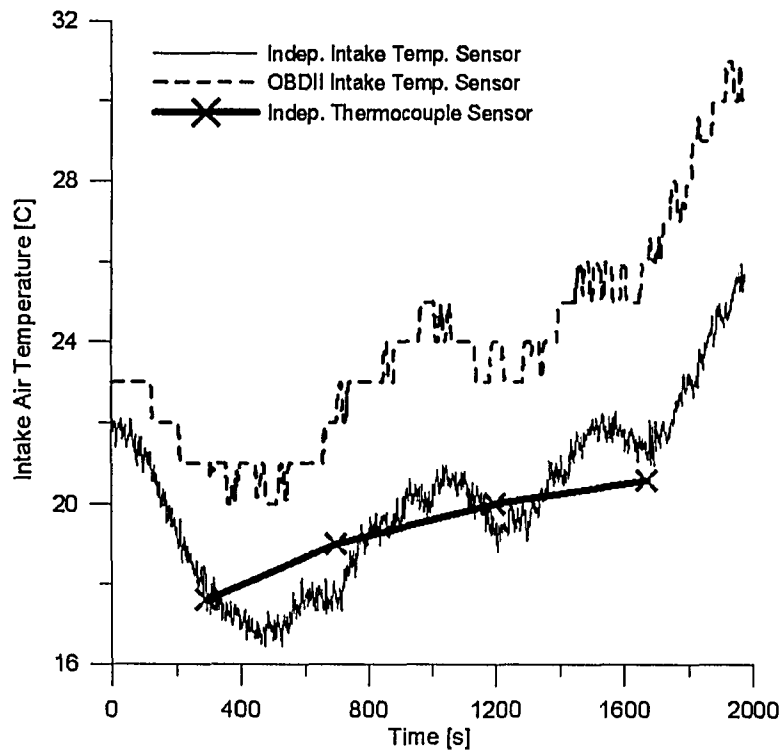
Figure 5-6 Intake Air Temperature Sensor Comparison

105
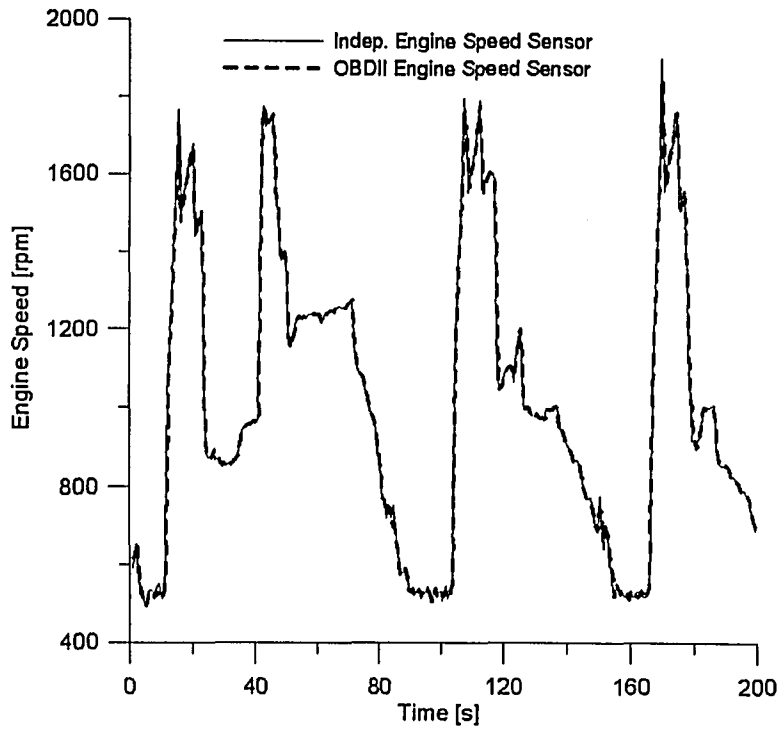
Figure 5-7 Engine Speed Sensor Comparison
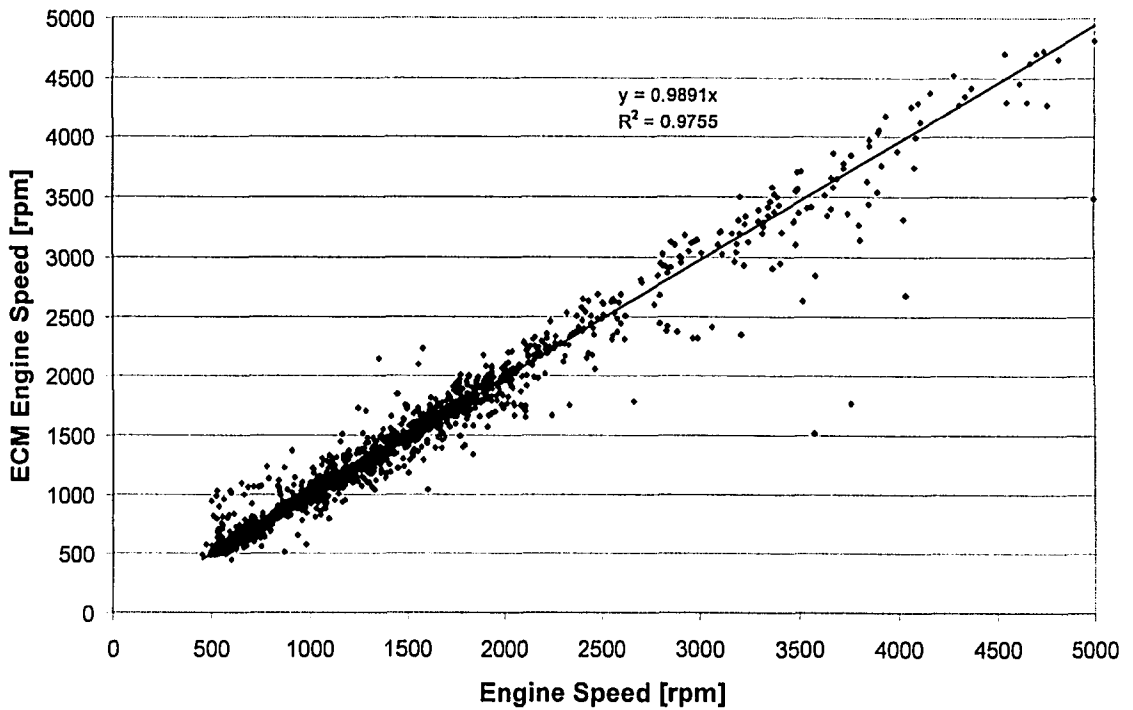
Figure 5-8 Linear Agreement Test - Engine Speed

106
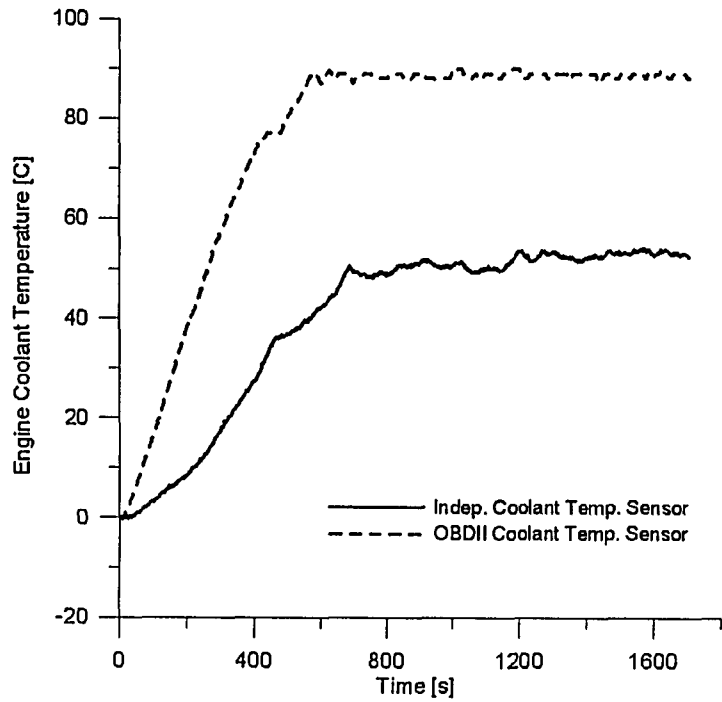
Figure 5-9 Coolant Temperature Sensor
Comparison
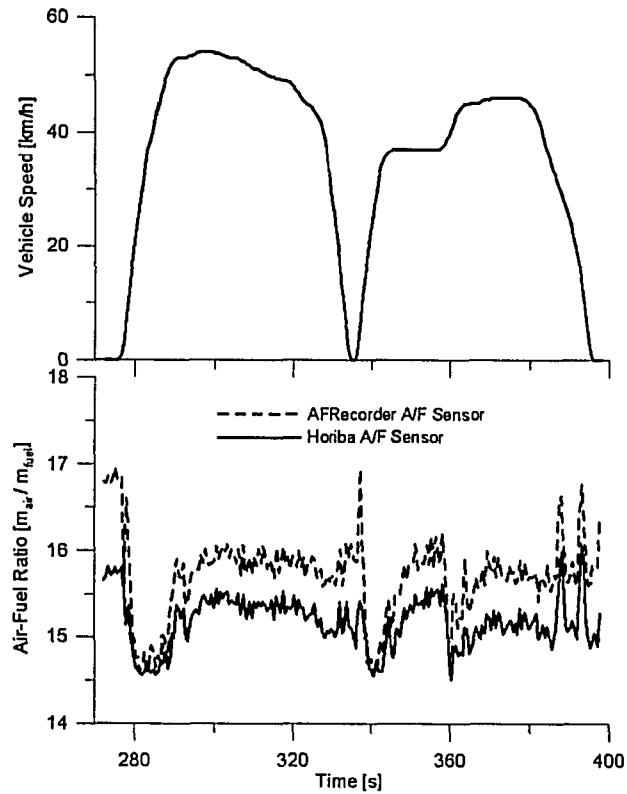
Figure 5-10 Air-Fuel Ratio Sensor
Comparison - Fall 2004 Testing

107
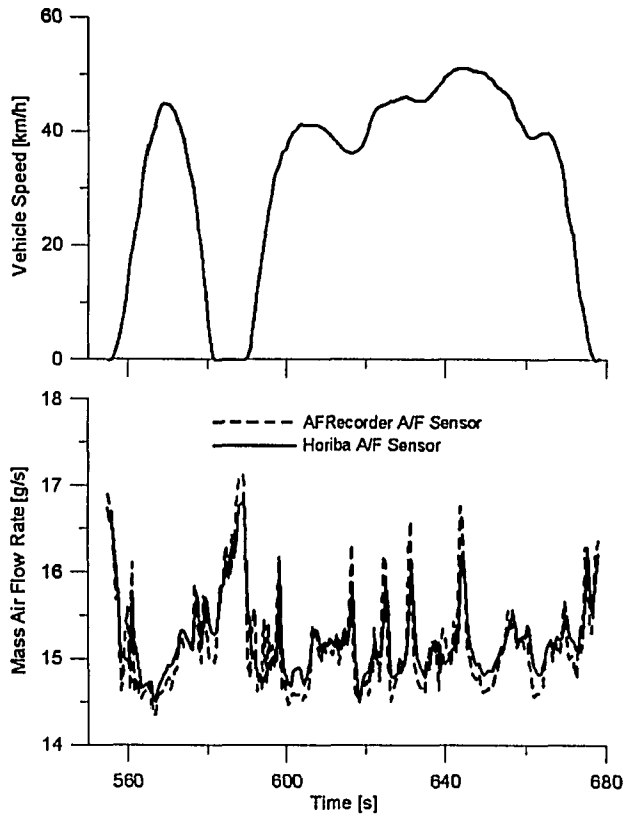
Figure 5-11 Air-Fuel Ratio Sensor Comparison - Spring 2004 Testing
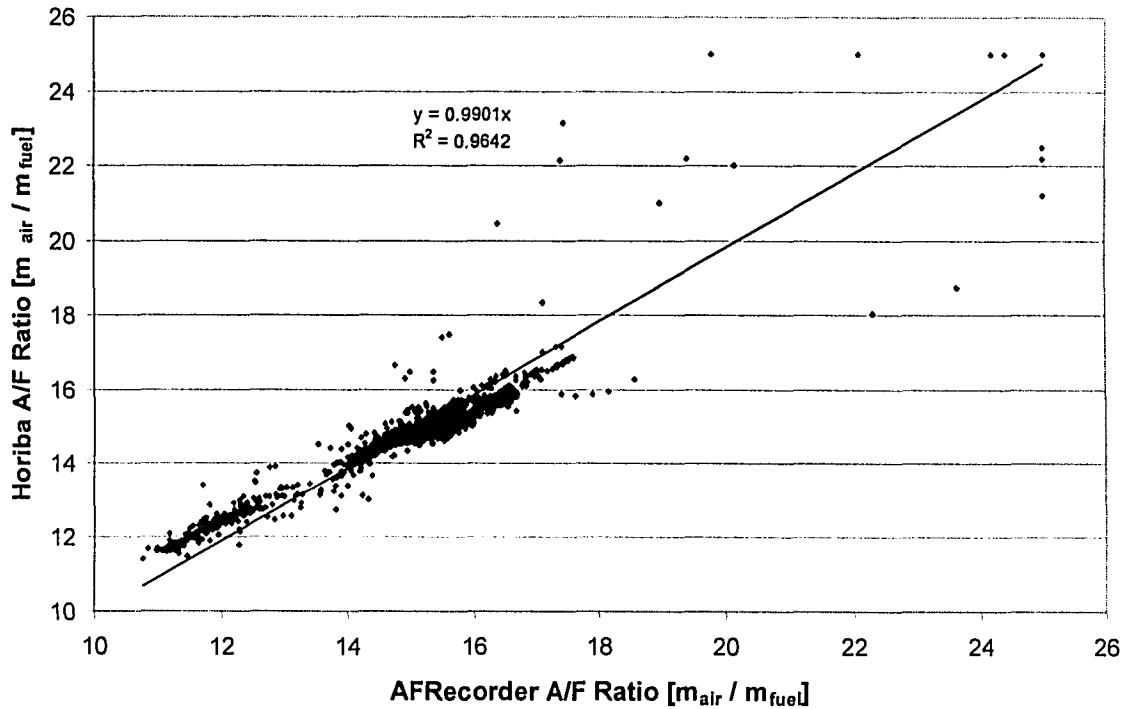
Figure 5-12 Air-Fuel Ratio Comparison - Highway Driving Route

108

REFERENCES

[1]   Frey H.C., Rouphail N.M., Unal A., Colyar J.D., "Measurement of On-Road Tailpipe CO, NO, and Hydrocarbon Emissions Using a Portable Instrument," in Proceedings - Annual Meeting of the Air and Waste Management Association, June 24-28, 2001.

[2]   Vojtisek-Lom M., Cobb J.T., "Vehicle mass emissions measurements using a portable 5-gas analyzer and engine computer data," in Proceedings - Emissions Inventory, Planning for the Future, Air & Waste Management Association; Pittsburgh, PA, 1997.

[3]   Vojtisek-Lom M., Allsop J.E., "Development Of Heavy-Duty Diesel Portable, On-Board Mass Exhaust Emissions Monitoring System With NOx, CO_2, and Qualitative PM Capabilities," SAE Technical Paper 2001-01-3641, Society of Automotive Engineers, 2001.

[4]   Vojtisek-Lom M., Lambert D.C., Wilson P.J., "Real-world Emissions From 40 Heavy-Duty Diesel Trucks Recruited at Tulare, CA Rest Area," SAE Technical Paper 2002-01-2901, Society of Automotive Engineers, 2002.

[5]   Manchur T.B., Checkel M.D., "Time Resolution Effects on Accuracy of Real-Time NOx Emissions Measurements", SAE Technical Paper 2005-01-0674, Society of Automotive Engineers, 2005.

[6]   Canadian Automobile Association, "Autopinion - Presenting the Personal Car Ownership Experiences of More than 20,000 CAA Members", Feb. 2003.

[7]   Cadle S.H., et al. "Real-World Vehicle Emissions: A Summary of the Tenth Coordinating Research Council," On-Road Vehicle Emissions Workshop, March 2000.

[8]   Hawirko J.D., Checkel M.D., "Real-Time, On-Road Measurement of Driving Behavior, Engine Parameters and Exhaust Emissions" SAE Technical Paper 2002-01-1714, Society of Automotive Engineers, 2002.

CHAPTER 6

Conclusions and Future Work

Chapter 6 will summarize the conclusions arrived at through Chapters 3 through 5 with consideration for the goals set in Chapter 1. The goals with which future work should proceed toward solving will also be given, which are based upon experience gained through completion of this project.

The effect of nitric oxide sensor response characteristics was examined for the purpose of evaluating the accuracy of mass emission rate results generated from current slow response sensors. Facilitating this goal required the addition of a HORIBA Mexa-720NOx fast response sensor to a previously developed on-board emissions system. The impact of vehicle load and transient rates was then studied to calculate the change in emission rate resulting from loads up to the maximum vehicle rating and accelerations up to the maximum vehicle capabilities. Engine control module data gathered from the on-board diagnostics port was also assessed to confirm the accuracy of utilization of vehicle sensors in future on-board emissions studies.

Several conclusions can be reached which answer the questions posed in Chapter one, including:

1. In half of the tests conducted, long duration transient vehicle events measured greater emission rates of NOx with the fast response sensor, when compared to a slow response sensor. The other half of cases examined, showed equivalent emission rates between the two sensors. Short temporal transients conclusively showed 20% to several times (100%+) greater emission rates for fast responding sensors. Full cycle certification tests would therefore exhibit higher overall emission rates due to the significant fraction of total emissions produced during acceleration events. On a relative basis to emission production rates, NOx sensor response was found to be a limiting factor in mass emission rate accuracy. Engine operation transients were found to exhibit a time constant less than 1 s, which indicated that both fast and slow response sensors with 2 s and 7 s response times vary from too slow to much-too-slow to accurately resolve concentration and hence mass emission rates.

2. Use of mathematical response correction algorithms has resulted in negligible to 250% increases in mass emission rates for corrected versus uncorrected results. The source of the emission rate increase was a direct result of improved response profile alignment of NOx concentration data and intake air flow profiles, along with greater peak emission concentrations as a result of the correction. When post-processed with the response correction algorithm, slow response sensor data produced emission rate results closer to fast response sensors (versus uncorrected results). However, numerous drawbacks prevent its use as a substitute for fast responding sensors. Impedances include the creation of large emission spikes possibly not occurring, increased noise amplification, and the inability to generate data where no data is present.

3. Increased severity of transient acceleration events found HC emissions which were 270% and 630% greater for urban and highway tests on a gram per kilometer basis. CO emissions showed the greatest species increase due to increased acceleration rates with 16 and 36 times greater emissions produced on urban and highway cycles. Increased CO in the exhaust has resulted in a 10% decrease in CO_2 on a gram per gram fuel basis. Emissions of NOx measured similar expected

111

trends, with a decrease in mass emission rates [g/km] of 48% on urban routes. Comparison of NOx emission rates during highway driving cycles found little change within standard deviation which was likely due to the limited number of transients experienced.

4. Applying a load to the test vehicle, up to its maximum rating, has resulted in no changes to HC emission rates and unchanged CO rates for the highway driving cycle. Mass emissions for CO decreased for the urban drive cycle by 64% which was unexpected but likely attributed to an increased fuel consumption during unloaded tests. CO_2 emissions were found to rise 8% (g/g fuel) when a load was applied during loaded highway driving conditions but remained unchanged during urban routes due to an anomalously high fuel consumption of the unloaded test. NOx emissions showed no change in emission rate with loading during urban test routes but a significant 19% increase during highway testing. Comparing the emission rate effect of load on NOx for rapid acceleration testing resulted in a further increase in emission rates of 56% when loaded up to the vehicle GVWR.

5. On-board diagnostics (OBD) system data has proven to be timely relative to the current measurement system capabilities, as well as reliable with data errors occurring on less that 0.5% of the points recorded. Data gathered over a one year period has shown that the vehicle mass air flow sensor measures emission rates which differ by 3% to 13% versus a results from a known air flow sensor. Intake air temperature was found to be precise but offset from the known sensor values by 3°C to 6°C for summer and winter conditions respectively, with sensor position differences accounting for the likely cause. Engine speed and barometric pressure measured within 1% and 2% average error respectively. The use of OBD port data has been shown to be accurate, reliable, and timely under numerous ambient conditions and operating modes for the vehicle tested which lends confidence to the use of this information in further emission studies.

Future work should continue to research on-board emission studies in numerous areas, including:

1. The use of a faster NOx concentration measurement sensor which could provide response on the same order as engine operation transients and emissions production should be used if commercially available. Additionally, the development of a third generation emissions system at the University of Alberta should focus on improving the frequency at which the data acquisition and ECM systems record measurements. Matching these two parameters to the emission production rate would ensure response lag between emission species production and measurement is eliminated.

2. On-road emissions data generated from this research and the previous research, should be utilized to develop emission models with the goal of producing useful data for the benefit of transportation design, life-cycle analysis, or for use in emission inventory models. A detailed spectral analysis of driving power, MAF, and A/F could

112

also be completed to compliment the model. Finally, a modal analysis which defined emissions production rates by driving mode should be completed to associate significance of mode to emissions species.

3. Examine the initial and full cycle emission rate effects of various length soak times (after being fully warmed up) at various ambient temperatures, to measure the importance of catalyst temperature on emission rates. These tests would simulate vehicles which are used to run errands or other vehicle stopped and start driving patterns.

4. Examine the loading threshold required to push a vehicle into commanded enrichment for urban and highway driving cycles for Tier 1 and Tier 2 vehicles. Heavy load operation is not a consideration of fuel control calibrations and has not been focused on by manufacturers, however, Tier 2 emissions standards may have required manufacturers place an increase focus on reducing command enrichment events. Also, examination of the early post-start operation fuel control strategy would illustrate the development of ECM designs and improvements in startup emissions control.

5. Verification of the Horiba A/F ratio sensor should be completed to ensure that the lean mixture measurement accuracy is simply a result of sensor age. Simultaneous testing should confirm that the Vetronix gas analyzer provides timely and accurate engine speed data when compared to the proven OBD sensor data. An accuracy evaluation of the mass air flow sensor should be undertaken for alternative vehicles to add greater generality to the accuracy results for various types and ages of vehicles.

6. Develop the third generation on-board emissions measurement system with compact size and portability as primary design criteria. This redesign should eliminate the AF Recorder and independent sensor network, after confirmation of the work above is completed for mass air flow sensor data on alternative vehicles.

113

APPENDIX A

Data Alignment and Sensor Response

Appendix A provides supporting work detailing the solution to the time alignment issue as well as the basis for the resolution of temporal response presented in Chapter 3. This appendix details the test procedures and results involved in determining the overall time delays of each emissions species and includes an analysis of variable exhaust flow rates with engine speed. The various data alignment algorithms are discussed and a comparison of sensor response time with sensor age is also included to illustrate the consistency in NOx in-line sensor measurements.

114

The collection of data gathered from emission sensors, the vehicle ECM, and remotely installed sensors does not occur simultaneously and properly matched to vehicle events. Emissions data and remote sensor data are collected using LabView 6.0i at a frequency of approximately 2 Hz. Vehicle ECM data is logged through the proprietary software AutoTap Diagnostic Scanner v.2.04 at a sampling rate of 1.5 Hz (depending on the number of parameters being sampled). From knowledge of the sampling rate, it is immediately evident that a data misalignment is inherently present in the data files gathered. In addition to accounting for a data frequency difference, misalignment between vehicle data and emission data comes in 3 other forms; variable exhaust system delays, sample line transit delay time, and internal analyzer delay time. The variable exhaust system delay time is the only one that applies to Horiba NOx whereas the Vetronix 5-Gas analyzer exhibits all three delays. Chapter 3 has illustrated the various methods used to align data which this appendix will not reiterate.

The purpose of this appendix will be to illustrate how the sources of misalignment were determined and what results were obtained from the completed tests. This appendix will also detail experimental methods and results for determining the sensor response rate to changes in pollutant concentration.

A.1 Internal Delay Time of Vetronix PXA-1100 5-Gas Analyzer

The Vetronix PXA-1100 5-Gas Analyzer is an emissions diagnostic tool which uses separate chambers to analyze exhaust gas composition. It uses Non-Dispersive Infrared (NDIR) technology to analyze CO, CO_2, and HC concentrations, and separate electrochemical cell sensors to measure NOx, and O_2. As a result of using separate cells, the PXA-1100 has different internal delay times for each emissions type sampled due to the transit time required to flow to various chambers.

An experiment was set up to determine the time required for a sample gas to flow from the inlet sample port of the analyzer to each sensor chamber. The internal delay test was conducted by quickly inputting an ambient pressure calibration gas flow into the analyzer input port, while simultaneously pressing a toggle button on the laptop data acquisition software (to denote the start of the flow). The time required to flow to each analyzer chamber was then calculated as the time from flow input to an initial response of each sensor. Figure A-1 shows the response characteristics of the Vetronix gas analyzer due to a step input concentration.

A summary of these results is shown in Table A-1.

115

Table A-1 Internal Delay of Vetronix 5-Gas Analyzer

	Internal Delay [s]	Std. Dev. [s]
HC - NDIR System	3.58	0.28
CO - NDIR System	3.58	0.28
CO_2 - NDIR System	3.58	0.28
O_2 - Chemical Cell	3.80	0.05
NOx - Chemical Cell	6.17	0.05

A.2 Emissions Sample Line Delay Time

The determination of the delay time present in the sample line is important to understand what flow regime is present in the sample line (for sample mixing calculations), and to allow for the calculation of variable exhaust pipe delay times. As a pre-requisite, the calculation of the sample line delay time requires knowledge of the constant internal delay time. Then by measuring the combined transit time through the sample line and the internal delay time of the analyzer, the time through the sample line can be determined.

The experiment conducted to determine the combined delay time was performed by two researchers. After allowing the vehicle to warm up and achieve relatively stable emissions values, the gas analyzer was re-zeroed and allowed to sample exhaust gas from the vehicle. At this point one researcher would remove the sample probe tip from the exhaust pipe (verbally notifying the 2nd researcher) and allow it to sample ambient air. The second researcher present in the vehicle would toggle the start of ambient air sampling on the data logging software which would allow for the determination of the delay time. The combined delay time was then calculated as the time from constant HC values to the point where HC values rapidly declined, due to ambient air entering the sensor chamber. Table A-2 presents the results of these experiments for the various test experiments.

Knowing the internal HC time delay of the gas analyzer then allows for the calculation of the sample line delay time individually. With an HC internal delay time of 3.58 seconds in can be determined mathematically that the transit time in the sample line alone must be a constant 2.62 seconds (approximately 2.5 seconds).

Sample Line + Internal Delay = 6.2 seconds
Sample Line + 3.58 seconds = 6.2 seconds
therefore,
Sample Line = 2.62 seconds

116

Table A-2 Sample Line Delay Time

		Sample Line Tip to Initial Detection	
Test #	Time 1 [s]	Time 2 [s]	Time to Response (time 2 - time 1) [s]
1	5222.24	5228.48	6.2
2	5289.28	5295.56	6.3
3	5319.33	5325.54	6.2
4	5356.18	5362.39	6.2
5	5389.13	5395.33	6.2
6	5424.47	5430.61	6.1
		Average:	6.2
		Std. Dev.:	0.0

Knowledge of the sample line delay time, sample line length, and estimation of flow properties, enables the determination of the Reynolds number for flow in the sample line. Estimating the entrance temperature into the sample line to be 200°C and the exit temperature to be approximately 25°C, with a wet molecular weight of 33.2 kg/kmol under ambient pressure conditions, a density of the flowing fluid can be obtained. The physical size of the sample line is know to be 6.1 m long which results in a velocity through the sample line of 2.33 m/s. The internal diameter of the sample line used to transport the emissions sample is a constant 0.004 m. Finally, the absolute viscosity of the flowing emissions sample is found to be 1.9 x 10^{-5} N-s/m^2 (for a fluid with properties between that of air and carbon dioxide for an average temperature of approximately 100°C). Substituting the above values into the Reynolds equation yields a value of 509, which indicates that the flow is laminar.

$$\text{Re} = \frac{\rho VD}{\mu}$$ [Equation 1]

A.3 Variable Exhaust Pipe Delay Time

The transit time of emissions through the vehicle's exhaust system varies depending on a number of factors including the temperature and pressure of the exhaust, the exhaust flow rate, and the volume of the exhaust system. To quantify this delay time, an experiment was set up so that a spike in HC concentration created at time zero in the engine, would be detected at a later time by the HC sensor in the analyzer. Knowing the sample line transit time and internal delays would then allow the calculation of the exhaust transit time. The HC spike was created by rapidly removing a single spark wire from the driver's side of the engine,

117

thus creating a misfire and therefore an increase in the HC emissions from the engine due to the unburned HC fuel exhausting from the engine.

The test was conducted with two researchers present, one in the vehicle to maintain the desired MAF rate and toggle time zero on the laptop, and a second to remove the spark plug wire and indicate time zero. Sufficient time was initially given for the vehicle emissions system to warm up and thus produce low, stable HC emission values. MAF rates tested ranged from approximately 6.5 g/s (idle) to 45 g/s. Results of these tests are presented below.

Figures A-2 and A-3 summarize the results of the variable exhaust system transit delay time experiments. Plotting the transit time versus exhaust mass flow rate resulted in a near linear fit up to 30 g/s. Exhaust mass flow rates greater than 30 g/s resulted in a fraction of a second transit time and therefore a constant overall time delay due to sample line and internal delays which are unchanged with engine operation. Examining the relationship between delay time and engine speed revealed that a linear trend with engine speed exists, which occurred as expected.

The results of these experiments allowed for the creation of a variable time delay shifting algorithm based on current mass flow rate values. This algorithm provided a robust and theoretically more accurate synchronization of vehicle events and emissions production which was discussed in Chapter 3.

A.4 Conservation of Mass Shifting

The use of a second variable time alignment strategy was also examined which focused on the conservation of mass principle to determine the time delay present in the exhaust pipe. The Conservation of Mass Shifting (or COMS) algorithm, assumes an average temperature and pressure in the exhaust pipe, as well as a molecular weight for exhaust components, to produce an estimated theoretical mass in the exhaust pipe. Referring to Heywood, the use of an average exhaust temperature of 500°C, ambient pressure, and a molecular weight of 33.2 kg/kmol results in a total emissions system mass of 18.6 g.

The transit time in the exhaust pipe was then determined by integrating forward in time (from the current time) to find out how long it would take for the engine to fill the exhaust pipe with the theoretically calculated mass. Then the transit time delay value calculated is used to shift-back the delayed emission reading to align the emissions value to the vehicle event.

A.5 Horiba NOx Sensor Delay Time

The determination of the time shift required to match Horiba NOx sensor data to vehicle data was done using a simplified linear proportion method based on the

118

distance and exhaust transit time of the exhaust system. Knowing that the distance to the Horiba sensor was 53 in. versus the 196 in. length of the exhaust pipe, a fractional amount (53 / 196) of the time taken to reach the end of the exhaust system was used as the Horiba delay time. This resulted in a transit time of 0.71 seconds which was very close to the later <u>optimized value of 0.75 s</u> which confirms the use of this simplified method. It could be argued that these values are essentially the same within known error ranges as well.

A.6 Time Response of Emissions Sensors

A time constant can be defined as the time required for a decaying exponential transient to be reduced to e^{-1} = 0.368 of its final value. Similarly, a time constant can be defined as the time required for a growing exponential transient to reach 1-e^{-1} = 0.632 (63.2%) of its final value. This growing exponential result can be defined in equation form as:

$$C(t) = C_o + \left(C_f - C_o\right)\left(1 - e^{-t/\tau}\right)$$

where: t   - time [s]
         τ - time constant
         C_o - initial concentration
         C_f - final concentration

The determination of the time constant for each species sensor was determined by linearly interpolating between the values bracketing the 63.2% final value. However, a second method for determining the time constant of sensor response data can also be used. Producing a graph of $\ln[(C_f - C) / (C_f - C_o)]$ vs. time, then finding the slope to be $-1/\tau$, will also enable the determination of the time constant. In addition to finding the time constant, the observation of varying slopes from this method, would indicate that a single time constant is not representative of first order simple lag response.

The use of a time constant allows for the quantitative determination of the relative speed of response between sensors. Sensors with a smaller time constant exhibit more rapid response to step changes than sensors with larger time constants. Figures A-4 and A-5, illustrate the relative difference in response between sensors with different time constants for exponential growth and exponential decay functions.

Vetronix 5-Gas Analyzer [PXA-1100]

Evaluating the time response of the internal emissions sensors resulted in time constant values on the order of 1 second for the NDIR measurement system, and

119

of the order of 4 and 7 seconds for the chemical cell O_2 and NOx sensors respectively. Table A-3 illustrates the time constants of each emission measurement sensor.

Table A-3 Vetronix 5-Gas Analyzer Sensor Time Constants

	Measurement System	Time Constant [s]	Std. Dev. [s]
HC	NDIR	1.09	0.77
CO	NDIR	1.04	0.77
CO_2	NDIR	1.69	0.41
O_2	Chemical Cell	4.35	0.29
NOx	Chemical Cell	6.97	0.11

The time response of each sensor can also be seen in Figure A-1, which shows the typical response obtained for each sensor when inputting a step change concentration into the gas analyzer. If the slow response Vetronix NOx sensor is examined more closely, as shown in Figure A-6, it can be seen that the first few seconds of its response do not correlate well with the single time constant first order response curve. The initial response of the NOx sensor, prior to the inflection point, is a result of dispersion in the sample line which was found to persist for all tests for an initial 1-2 second period. The fast response Horiba sensor on the other hand, correlates very well with the first order approximation.

If the previously discussed method of plotting $\ln[(C_f - C) / (C_f - C_o)]$ vs. time, and then finding the slope $- 1/\tau$ is used, it would be possible to determine if a second time constant exists in the sensors behavior. The slope of Figure A-6 is equal to the negative inverse of the time constant, which indicates that the time constant is initially large and changing, before reaching a constant slope for the majority of the remainder of the response.

Looking at the data gathered from the slow response sensor, plotted in Figure A-7, we can determine that there exists more than one time constant present in the NOx sensor measurement behavior. If the first 1 - 2 seconds are removed due to their poor fit, a new curve plotted in Figure A-8 with a time constant of 4.30 seconds can be obtained. The newly fitted simple lag response now appears to accurately reflect the response of the analyzer for the majority of the response. If two linear approximations are used, the resulting time constants for the slow response sensor appear as in Table A-4.

The results of the dual slope time constant show good correlation for the S_2 slope (the main portion of the response) whereas the initial slope S_1 indicates a relatively

120

poor linear approximation. Looking at the single slope approximation, it is evident that the majority of the slope nearly approximates the 4.30 second main slope of the two slope approximation, with very little difference in fit correlation. It should be noted that simple interpolation resulted in time constants of 6.97 +/- 0.11 s. and 7.17 +/- 0.23 s. for two independent sets of experiments.

Table A-4 Slow Response Sensor - Slope Determined Time Constants

	Dual Slope Approx.				Single Slope Approx	
Test	S_1	S_2	R^2_{S1}	R^2_{S2}	S_1	R^2_{S1}
1	19.8	4.70	0.854	0.990	5.18	0.979
2	17.5	4.26	0.865	0.991	4.71	0.980
3	21.4	4.16	0.807	0.994	4.86	0.969
4	15.2	4.20	0.864	0.991	4.73	0.977
5	21.8	4.16	0.800	0.995	4.86	0.969
Avg.	19.1	4.30			4.87	
Std. Dev.	2.78	0.23			0.19	

Horiba NOx Sensor [Mexa-720NOx]

The use of a fast response NOx Sensor is important to understanding NOx emissions generated during short, rapid transients. The speed with which the Horiba ZrO_2 sensor can respond to changes in NOx concentration is therefore of prime importance and therefore required experimental determination of the instruments time constant.

To determine the time constant of the sensor, a step change NOx concentration at the sensor input was required. This step change was achieved through the use of a test rig body and flow control unit. The test rig body provided input and outlet ports and as well as a cavity for installation of the sensor. The input port of the cavity was connected to a 4-way valve with gas supplies of zero/purging gas (N_2 gas) and NOx gas, as well as a port for exhausting the stream not selected by the 4-way valve for input to the test rig.

Gaseous flows sampled by the Horiba ZrO_2 sensor required the presence of O_2 to properly function, which therefore required the addition of a humidification unit to the N_2 stream, and the constant dilution of the NO stream with air by a flow controller. A schematic representation of the experimental setup is shown in Figure A-9.

The experiment was conducted by first allowing the Horiba sensor to sample N_2

121

humidified gas, allowing the sensor to purge all NO from the system in preparation for the step change NO concentration input. The 4-way valve was then quickly switched to allow the sensor to sample NO. This procedure was repeated numerous times at various NO input concentrations to determine if there was any effect on the time constant due to concentration. Also, the effects of aging on the ZrO_2 NOx sensor were also determined through the testing of an aged and new sensor. The results of these tests are summarized in Table A-5 and A-6.

From the data shown above it is evident that the time constant of the NOx sensor is approximately 2.0 seconds and is unaffected by the age of the current sensor (within error limits). Although the Horiba does not monitor the exact age or hours logged by a particular sensor, from monitoring driving cycles performed in fall 2003 and Jan 2004, the sensor can be expected to have sampled exhaust gas for more than 500 km of driving time. Table A-5 and A-6 also illustrate that the time constant of the sensor is not dependent on the concentration of the input NO gas. However, a slight dependence on the flow rate appears to exist with higher flow rates exhibiting smaller time constant values.

Figure A-10 indicates the near identical response of the Horiba NOx sensor when comparing the aged sensor to a new sensor.

Table A-5 Previously Used Horiba Sensor - Time Constant Calculation

	Flow	NOx Input	Time Constant		90% Time Constant	
	[L/min]	[ppm]	Avg [s]	Std.Dev.[s]	Avg [s]	Std.Dev.[s]
01/24/04	4	925	2.19	0.25	5.23	0.41
	4	1950	1.90	0.06	4.92	0.19
	4	2940	2.26	0.17	5.34	0.18
	10	890	1.56	0.21	4.55	0.29
	10	1900	1.76	0.24	4.91	0.27
	10	2880	1.82	0.14	4.78	0.14
02/03/04	4	1800	2.16	0.10	4.61	0.24
	4	2900	2.35	0.07	5.42	0.06
	10	2840	1.96	0.18	4.84	0.22
		Average	2.00	0.26	4.96	0.31

122

Results for the new sensor:

Table A-6 New Horiba Sensor - Time Constant Calculation

	Flow	NOx Input	Time Constant		90% Time Constant	
	[L/min]	[ppm]	Avg [s]	Std.Dev.[s]	Avg [s]	Std.Dev.[s]
02/23/2004	4	1825	2.26	0.17	5.08	0.22
	4	2900	2.39	0.20	5.54	0.20
	10	1725	2.06	0.19	4.39	0.21
	10	2830	2.19	0.15	5.15	0.15
		Average	2.23	0.14	5.04	0.48

If the fast response NOx sensor time constant is examined graphically by plotting $\ln[(C_f - C) / (C_f - C_o)]$ vs. time, an indication of the relative steadiness of the time constant (and correlation to first order response), can be determined. Figure A-11 indicates the repeatability of the tests done to calculate the time constants of the Horiba NOx fast response sensor. From this figure it is evident that the reproducibility of these responses is very consistent over a number of consecutive tests. The x-axis was scaled to a maximum of 6 seconds in which to examine the time constant since it was determined that ~5 seconds was required for 90% response using simple linear interpolation. Therefore, using 6 seconds of data would allow for the majority of response data to be included while simultaneously enabling the graph to focus on the most significant rise time data.

Looking at an individual plot shown in Figure A-12, knowing that it is representative of all tests conducted, the time constant can be found to be a single value, represented by a single sloped best fit line. Table A-7 shows the results of using the single slope method versus use of the simple interpolation method (at the 63.2% of final concentration value) for a particular set of response tests. Good agreement between the single slope and simple interpolation routine exists with both methods predicting approximately 2 seconds as the time constant. When averaging the results of using the simple interpolation method on a number of time constant experiments, an average of 2.00 +/- 0.26 s results which is exactly the result obtained by the single slope method obtained for the test data shown below. Knowing a single time constant exists and from observing the comparison between the Horiba response and an ideal simple lag response in Figure A-8, it can be concluded that this is a first order response instrument.

123

Table A-7 Comparison of Time Constants

Test 1x	Fast Response Sensor - Horiba Time Constant			
	Double Slope		Single Slope	Simple Interpolation
	S_1	S_2	S_1	S_1
A	4.47	2.06	2.06	2.12
B	6.19	2.01	2.03	2.21
C	17.20	1.97	2.00	2.30
D	6.54	1.91	1.93	2.11
E	14.02	1.83	1.87	2.19
Avg.	9.68	1.96	1.98	2.19
Std.Dev.	4.99	0.08	0.08	0.08
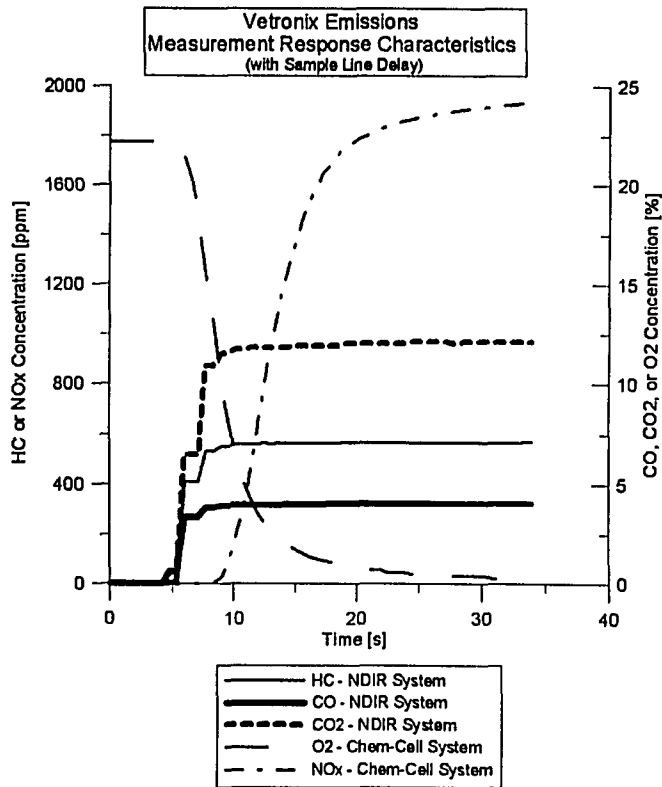
Figure A-1 Vetronix Gas Analyzer Emissions Response Characteristics
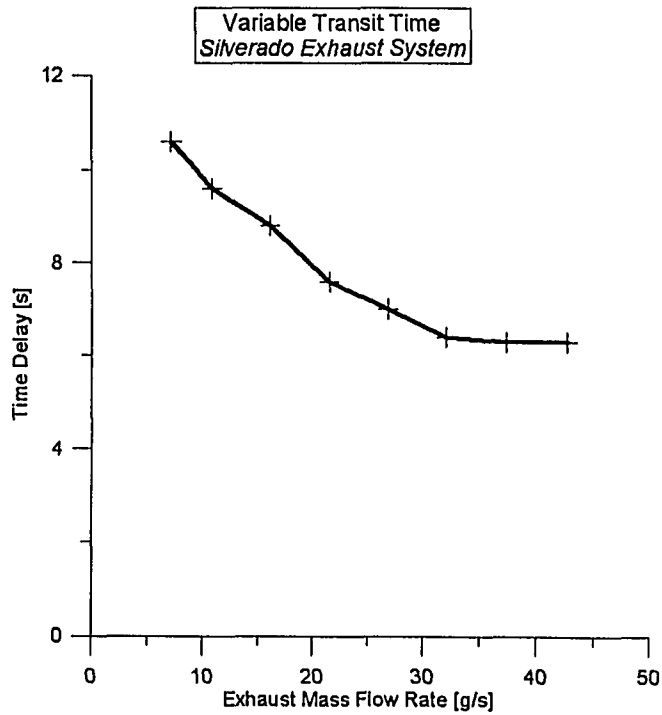
Figure A-2 Variable Exhaust System Transit Delay Time with EMF Rate

125
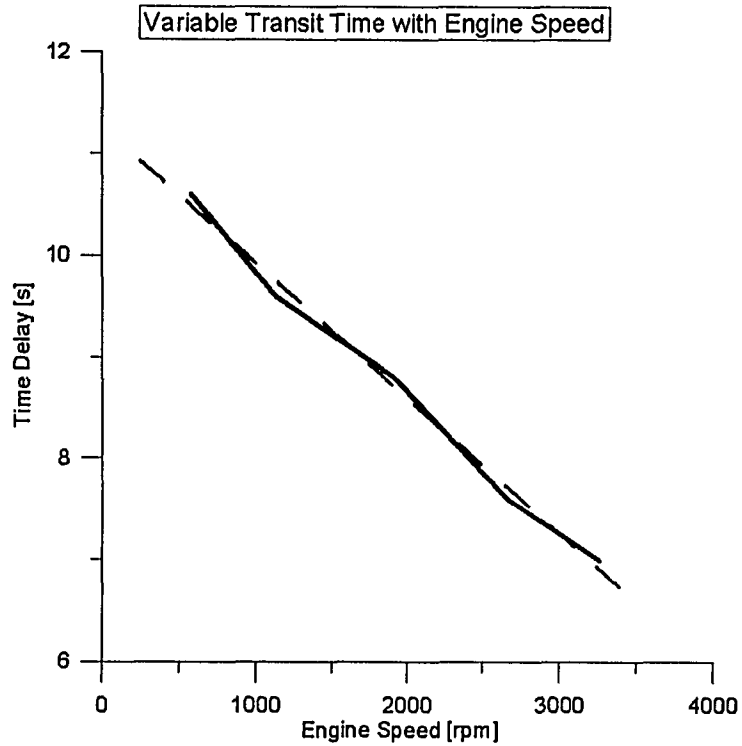
Figure A-3 Variable Exhaust System Transit Delay Time with Engine Speed
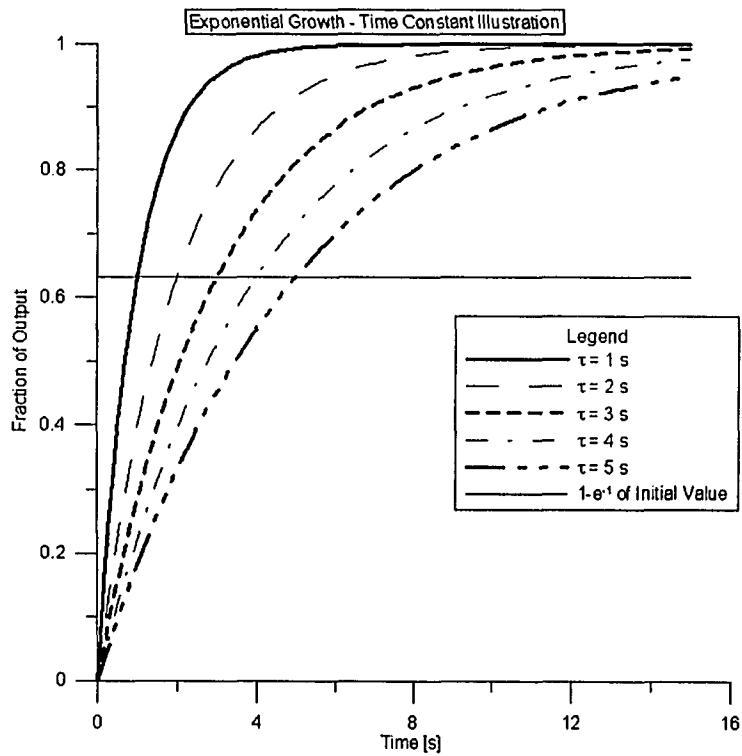
Figure A-4 Relative Time Response Comparison - Exponential Growth

126
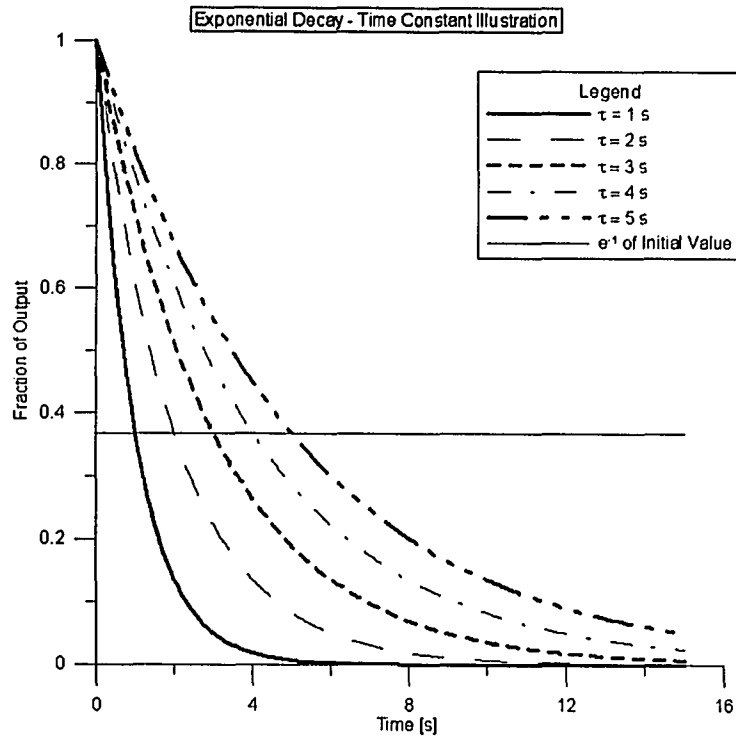
Figure A-5 Relative Time Response Comparison - Exponential Decay
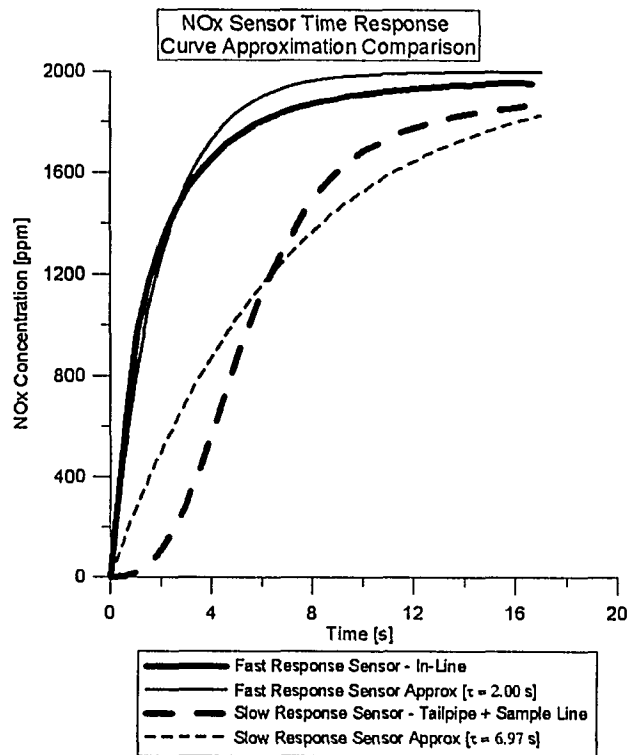
Figure A-6 NOx Sensor Comparison and First Order Correlation

127
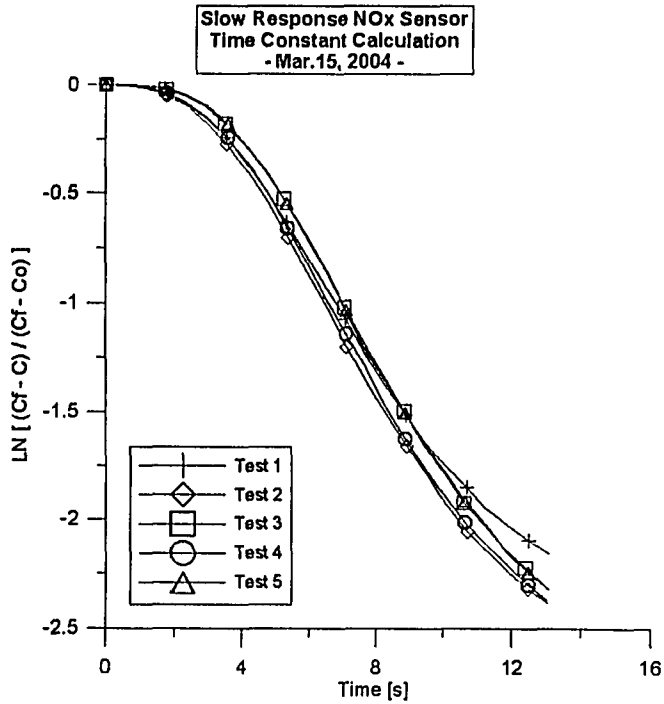
Figure A-7 Slow Resp. Sensor Time Constant Calculation
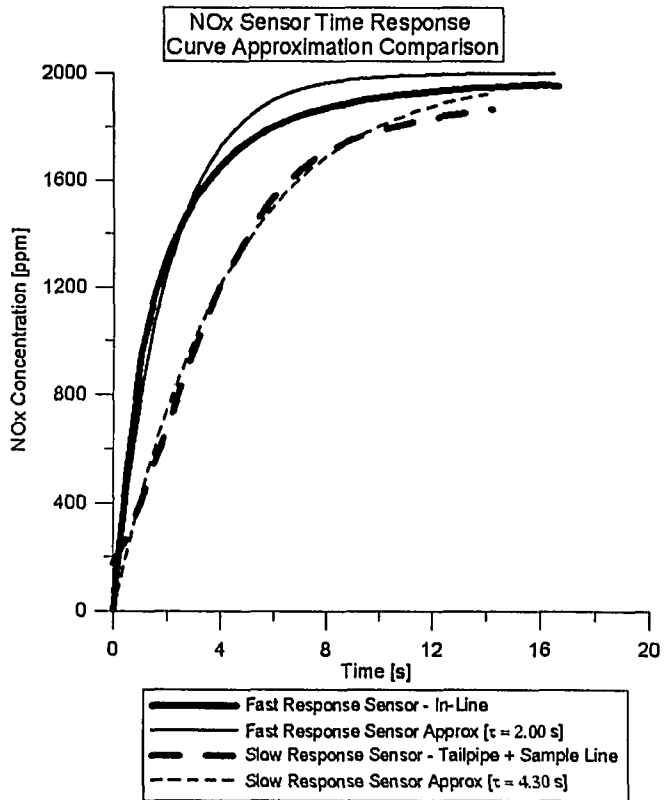
Figure A-8 NOx Sensor Comparison and Adjusted First Order Correlation

128
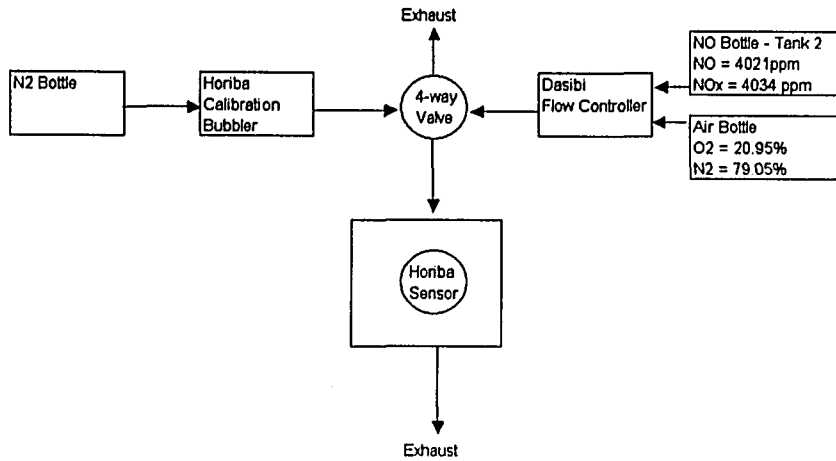
Figure A-9 Horiba Time Constant Experiment - Setup
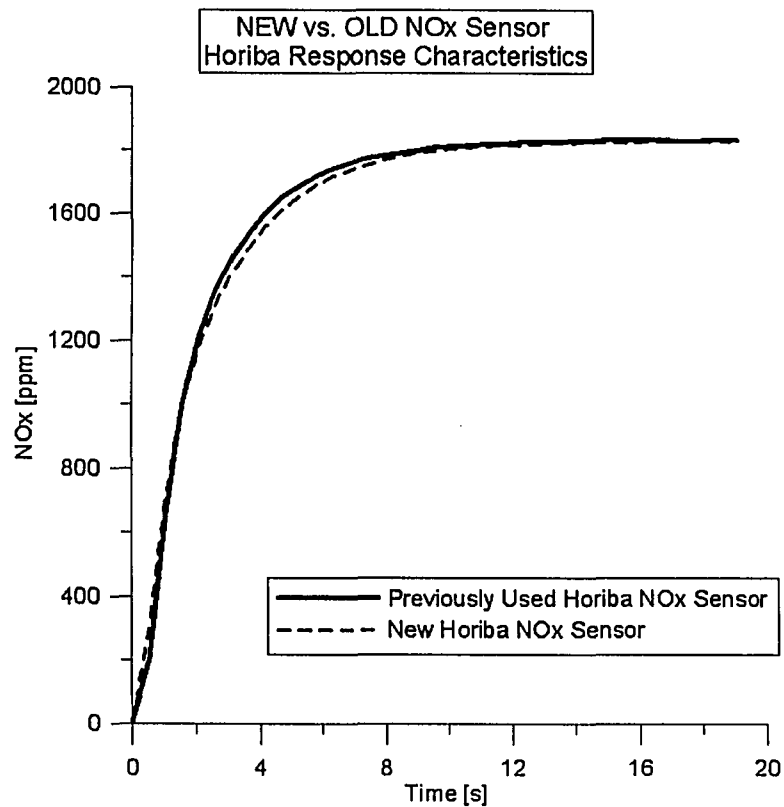
Figure A-10 Effect of Age on Horiba NOx Response
Characteristics

129
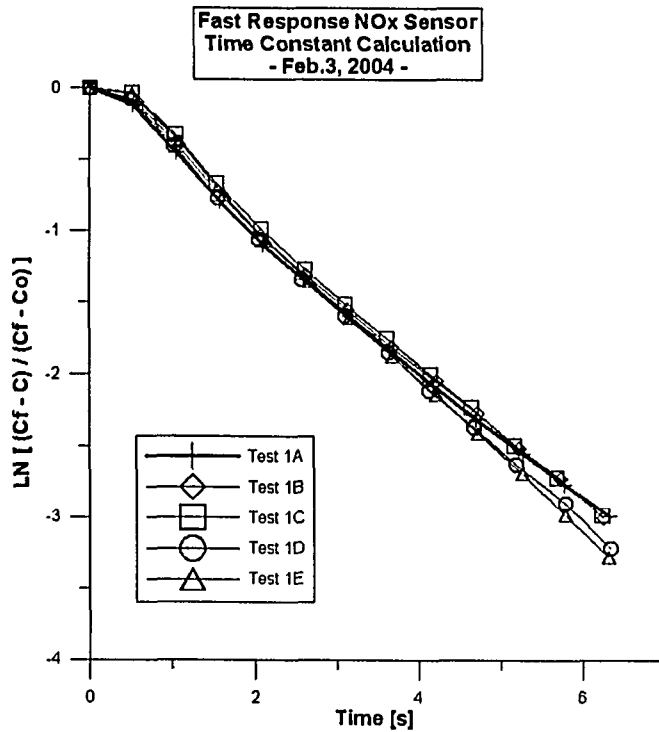
Figure A-11 Horiba Time Constant Determination - Slope Method
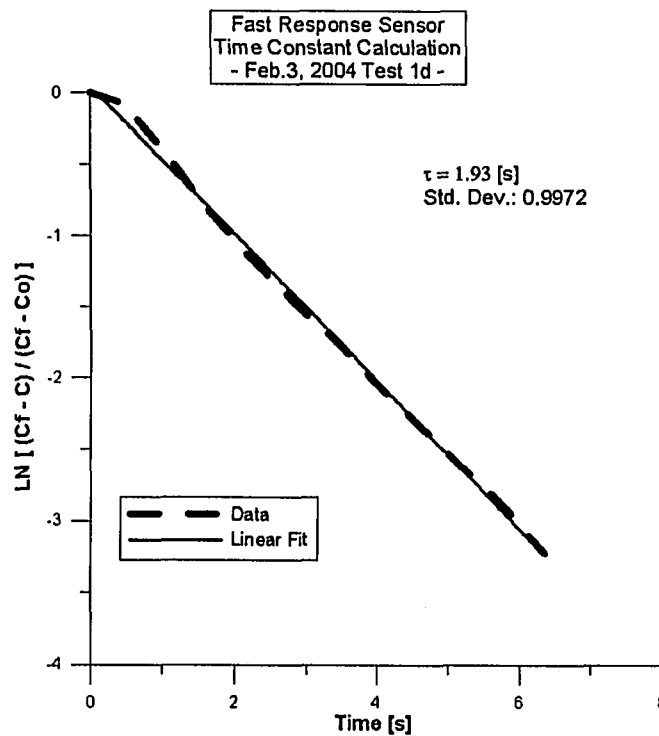
Figure A-12 Horiba Time Constant Slope Approximation

130

APPENDIX B

Response Correction Algorithm

An analytical response correction algorithm was used to improve the response of first order simple lag characteristic measurement equipment in Chapter 3. Appendix B will support this chapter with background and the theory behind this response correction algorithm as well as detail the various options which were considered before selecting a final choice. Options available include the use of single or multiple time constant amplification factors and various numerical differentiating routines which were considered in two and four point variations. Finally, the limitations to using this mathematical correction technique are discussed to ensure users appreciate the extent of the benefits available.

131

The importance of sensor time response has been explained in detail in Chapter 3 of this thesis with supporting information on the experiments conducted shown in Appendix A. The need for a response correcting algorithm to reproduce step changes in concentration due to the sensor response time is essential to improve the accuracy of in-use mass emission measurements. The purpose of this appendix will be to illustrate how the response correcting algorithms function and illustrate the choices available for correcting the real world data.

When inputting a step change concentration to an emission measurement instrument exhibiting simple lag response with a finite time constant, an exponentially growing response is observed. Experiments performed to test the responsiveness of the individual NOx sensors have shown both Vetronix and Horiba NOx sensors exhibit similar although initially different exponential type responses. The results of a typical response to a step change concentration, shown in Figure B-1, illustrate the relative difference in response rate between the fast response Horiba NOx sensor and the slow response Vetronix NOx sensor. The point at which the sensor response reached 63.2% of the final response (defined as the time constant of a simple lag response), was found to be 2.00 s and 6.97 s for the Horiba and Vetronix NOx sensors respectively. The equation for a first order simple lag response is shown below.

$$C(t) = C_o + \left(C_f - C_o\right)\left(1 - e^{-t/\tau}\right)$$ [Equation 1]

B.1 Well-Mixed Flow Model

The use of the well-mixed flow model for correcting the response of first order simple lag response curves has been previously used in emissions measurement analysis [1]. The theory behind the well mixed flow model and response correction in general has been previously discussed in Chapter 3. This appendix will focus on summarizing how the various correction algorithms were designed to support the previously discussed results and theory.

The goal of producing an algorithm to post-process raw emissions data, is to attempt to regain the maximum step change concentration value as quickly as possible while minimizing overshoot of the corrected signal.

$$C_{in} = C + \tau \times \left(\frac{dC}{dt}\right)$$ [Equation 2]

B.2 Algorithm Options

The use of Equation 2 as a means of correcting the first order response of the emissions sensors allows for the variation of τ and concentration gradient in calculating a corrected concentration. Table B-1 illustrates that 3 different time

132

constant (T.C.) function options were available to represent the signal produced by each NOx sensor. The following discussion will illustrate the benefits and limitations of each method and the reasons for choosing the time constants listed in Table B-1.

Table B-1 Response Correcting Algorithm Options

Pt. #	Simple		Enhanced		Optimized	
	Horiba [s]	Vetronix [s]	Horiba [s]	Vetronix [s]	Horiba [s]	Vetronix [s]
1	2.00	4.30	4.50	15.20	3.0	27
2	"	"	2.00	15.20	1.5	27
3	"	"	"	15.20	1.5	15
4	"	"	"	15.20	1.5	10
5	"	"	"	15.20	1.9	7
6	"	"	"	4.30	" "	6
7	"	"	"	"	" "	4
8	"	"	"	"	" "	3
9	"	"	"	"	" "	" "

As shown in Appendix A, both Horiba and Vetronix NOx sensors exhibited response curves very close to first order systems. After calculating the time constant of each sensor, values of 2.00 s and 4.30 s were found to be characteristic of the Horiba and Vetronix NOx sensors respectively. These single values formed the basis for the time constants used in the simple time constant algorithm shown in Table B-1.

Alternatively, plotting the slope of $\ln[(C_f - C) / (C_f - C_o)]$ vs. time would also allow for calculation of the time constant of the sensors, as shown in Appendix A. This method revealed that 2 slopes exist and therefore, a changing time constant with time. This observation prompted the development of the Enhanced time constant algorithm. The values in Table B-1show that the Horiba exhibited a time constant of 4.50 s for the first point but remained relatively constant at 2.00 s for the remaining duration of the response. The Vetronix sensor exhibited two slopes, similar to the Horiba, but responded more slowly up until the 6th point of the response curve, before stabilizing at 4.30 s. The choice of 15.20 s was selected because it was the minimum TC observed, which would therefore prevent excessive overshoot. It was believed that a more effective algorithm could be employed if time constant values were evaluated to this level of detail.

Finally, an Optimized time constant algorithm was explored through backward calculation of multiple response data files. Through knowledge of the gradient,

133

time, and unit step input value, the theoretical time constants required to correct the signal could be calculated. Data was examined and recorded with minimal values at each point utilized as time constants to prevent overshoot in the corrected response signal.

Although the Enhanced and Optimized TC algorithm is not physically accurate for the sensors, it will be explored as an option.

B.3 Numerical Differentiating Routines

Taylor series expansions were employed to derive finite-divided-difference approximations of derivatives, where the error was proportional to the square of the step size. Obtaining higher-accuracy divided-difference formulas is done through retaining more terms of the Taylor series expansion.

For the first two points of the first order simple lag response, a forward finite-divided-difference formula should be used. From [2], this formula takes the form:

$$f'(x_i) = \frac{f(x_{i+1}) - f(x_i)}{h}$$
Eq.[A]   where: $h = t_{i+1} - t_i$

or,

$$f'(x_i) = \frac{-f(x_{i+2}) + 4f(x_{i+1}) - 3f(x_i)}{2h}$$
Eq.[B]   where: $2h = t_{i+2} - t_i$

For the remaining data points in the simple lag response, a centered finite-divided-difference formula was used which considered four points on the curve, two behind the current point and two ahead of the current point. From [2], this formula takes the form:

$$f'(x_i) = \frac{f(x_{i+1}) - f(x_{i-1})}{2h}$$
Eq.[C]   where: $2h = t_{i+1} - t_{i-1}$

or,

$$f'(x_i) = \frac{-f(x_{i+2}) + 8f(x_{i+1}) - 8f(x_{i-1}) + f(x_{i-2})}{12h}$$
Eq.[D]   where: $h = \left(\frac{t_{i+2} - t_{i-2}}{4} \right)$

For maximum and minimum points, a backward differentiating routine was required which is similar in form to the previous forward numerical differentiating routine. From [2], this formula takes the form:

134

$$f'(x_i) = \frac{f(x_i) - f(x_{i-1})}{h}$$

Eq.[E]   where: $h = t_i - t_{i-1}$

or,

$$f'(x_i) = \frac{3f(x_i) - 4f(x_{i-1}) + f(x_{i-2})}{2h}$$

Eq.[F]   where: $2h = t_i - t_{i-2}$

The first (less accurate) numerical differentiating formulas (Eq.[A] and [C]) were used for the points where only the very next point was increasing, whereas for points where more than 1 of the next points was increasing the second (more accurate) formulas (Eq.[B] and [D]) involving more terms was used.

Knowing that two different numerical differentiating routines were available with three possible representative response correcting time constant functions, a total of 6 algorithms therefore became available for exploring. A list of the available algorithms, for each sensor, can be shown below:

1. Single Time Constant, Simple Numerical Differentiation
2. Single Time Constant, Enhanced Numerical Differentiation
3. Enhanced Time Constants, Simple Numerical Differentiation
4. Enhanced Time Constants, Enhanced Numerical Differentiation
5. Optimized Time Constants, Simple Numerical Differentiation
6. Optimized Time Constants, Enhanced Numerical Differentiation

B.3.1 Constant Step Size Assumption Validation

A constant step size assumption was assumed for simplicity and was justified by examining the standard deviation of the step size for a variety of on-road and experimental testing. Table B-2 shows the average and standard deviation step size durations for a variety of tests.

The consideration of unevenly spaced data can be determined by fitting a second-order Lagrange interpolating polynomial to each set of three adjacent points if future work determines this to be necessary. The illustration of this formula and further notes regarding its advantages can be seen in [2] p.533.

135

Table B-2 Average Step Size - Experimental and On-Road Data Result

Test Data	$T_{step,avg}$	Std.Dev.
	[s]	[s]
Lab Data H_Resp	0.524	0.033
Lab Data V_Resp	0.565	0.067
Jan.27, 2004 Test 2	0.570	0.063
Jan.28, 2004 Test 2	0.565	0.042
Jan.29, 2004 Test 1	0.579	0.080
Jan.29, 2004 Test 2	0.568	0.047
Feb.25, 2004 Test 1	0.573	0.079
Feb.27, 2004 Test 3	0.569	0.063
Average:	**0.564**	**0.059**

B.4 Correction Algorithm Limitations

It is important to note at this point some of the failings of the response correction algorithm as they apply to real-world emissions data. First of all, assumed step changes in NOx concentration produced in the engine may not be step change in nature after passing through the catalytic converter (i.e. Smearing due to catalytic processes of trying to reduce NOx to N_2 and O_2). Also, it is being assumed for the duration of each emissions spike, the concentration is being held constant. Due to the complexity and rapid changes in engine operation occurring in the engine and catalytic converter, it can be assumed that all emissions produced are rarely remaining at any steady state value, especially during high power transient events which generate emission spikes. The sampling frequency consideration also plays a role in the accuracy of the differentiating routine used. More discussion regarding this fact will be present in the Appendix C.

136

B.5 Well Mixed Flow Cell Model Derivation

Assume: 1. Qin = Qout   Steady State Steady Flow

M = CQ   Mass of the Cell [kg]
   Where: Q = Constant Volume, and C(t)

Knowing the change in cell mass:

$$\frac{dM}{dt} = \frac{d}{dt}(CQ) = C\frac{dQ}{dt} + Q\frac{dC}{dt} = Q\frac{dC}{dt}$$

is equal to the difference in mass flowing in minus flowing out:

$$\dot{Q}_{in}C_{in} - \dot{Q}_{out}C_{out} = \dot{Q}[C_{in} - C_{out}]$$

Equating the two gives:

$$\frac{Q}{\dot{Q}}\frac{dC}{dt} = C_{in} - C_{out} \qquad \text{Which yields,} \qquad C_{in} = C_{out} + \tau\frac{dC}{dt}$$

On a mass basis which reflects the mole fraction values obtained from the gas analyzer, we can obtain similar results (Refer to Figure B-3):

$$m_{NOx} = Y_{NOx}m_{exh} \qquad \text{Mass of NOx in the Cell [kg]}$$

Knowing the change in cell mass:

$$\frac{dm_{NOx}}{dt} = \frac{d(Y_{NOx}m_{exh})}{dt} = Y_{NOx}\frac{dm_{exh}}{dt} + m_{exh}\frac{dY_{NOx}}{dt} = m_{exh}\frac{dY_{NOx}}{dt}$$

is equal to the difference in mass flowing in minus flowing out:

$$\dot{m}_{exh}[Y_{NOx,in} - Y_{NOx,out}] \qquad \text{Equating the gives:} \qquad \frac{m_{exh}}{\dot{m}_{exh}}\frac{dY_{NOx}}{dt} = Y_{NOx,in} - Y_{NOx,out}$$

on a mole fraction basis,

$$\tau\left(\frac{MW_{NOx}}{MW_{exh}}\right)\frac{d\chi_{NOx}}{dt} = \left(\frac{MW_{NOx}}{MW_{exh}}\right)(\chi_{NOx,in} - \chi_{NOx,out})$$

Which yields, $\chi_{NOx,in} = \chi_{NOx,out} + \tau\dfrac{d\chi_{NOx}}{dt}$

137
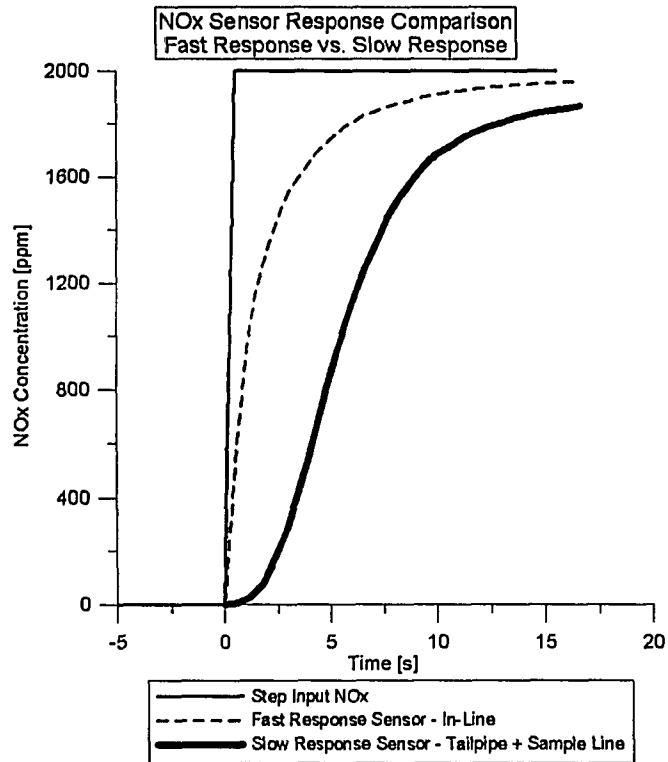
Figure B-1 NOx Sensor Response Comparison (Fast vs Slow Sensor)
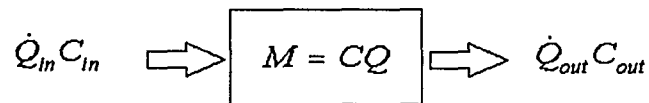
Figure B-2 Well-Mixed Flow Diagram
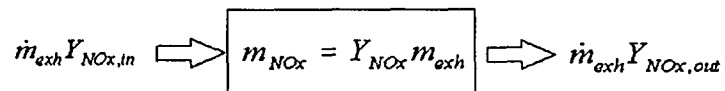
Figure B-3 Well-Mixed Flow Diagram (Mass Basis)

138

REFERENCES

[1]   Truex T.J., Collins J.F., Jetter J.J., Knight B., Hayashi T., Noriyuki K., Suzuki N., "Measurement of Ambient Roadway and Vehicle Exhaust Emissions - An Assessment of Instrument Capability and Initial On-Road Test Results with an Advanced Low Emission Vehicle," SAE Technical Paper, Society of Automotive Engineers, 2000.

[2]   Chapra, S.C., Canale, R.P. "Numerical Methods for Engineers, 2nd Edition," McGraw Hill, New York, 1985, pp.525-535.

139

APPENDIX C

Response Correction Algorithm Accuracy

Appendix C provides justification for the use of the well-mixed flow response correction algorithm and its selected variables. An ideal square wave step input function was first analyzed to ensure the correction algorithm would function under ideal circumstances. Simulation curves for the slow and fast response sensors were then created to supplement the evaluation of the algorithms. Knowing that there existed a degree of noise in the measurement of NOx, an analysis of the noise present in constant concentration NOx readings was performed. A noisy simulation curve was then developed for each NOx sensor. The five simulation curves were analyzed on the basis of integral error, RMS error, and percentage overshoot. Minimizing the error of all three calculations provided the basis for justification of the final algorithm design.

140

A number of algorithms have been developed to correct the simple lag time response of emissions measurement sensors. The use of the well-mixed flow model, described in Appendix B, served as the basis for the development of the algorithms used. The goal of these time response correction algorithms has been to reproduce step change input concentrations by post-processing the gathered on-road emission data. The effectiveness of these algorithms can be visually inspected by qualitatively examining the effect on multiple laboratory step change data files, as well as on-road emissions data. From this subjective viewpoint, the optimization of time constants and numerical differentiation routines can be chosen to most accurately de-filter the gathered data. However, a quantitative and measurable determination of the adequacy of such algorithms is essential before further optimization and confidence can be gained in utilizing the algorithms on a wide-spread scale.

C.1 Response Simulation Curves

To determine the accuracy of the response correcting algorithms, a series of simulated data files were produced which could be analyzed on an individual basis to determine the integral error, RMS error, and percentage overshoot present in each particular algorithm. Integral error is a measure of the percentage difference between the integral of the square input wave and the response corrected NOx curve. RMS error is an indication of how significant each corrected value deviates from the actual step change value. Minimizing this parameter would result in an ideally reproduced step change concentration, which is of greatest significance to the overall mass emission measurement accuracy goal. The final measure of accuracy is percentage overshoot which simply put, indicates the percentage above the step change value to which a maximum concentration was corrected. The overshoot occurring in a response correction algorithm should be minimized in both duration and scale.

The creation of a data file with an arbitrary 2000 ppm step change from a 50 ppm initial/final value, was created as an input file for the Matlab processing software. The step change simulation shown in Figure C-1, was the first simulated response curve which was required to be analyzed and also served as the basis for creating the remaining four simulation curves. The second simulation curve, shown in Figure C-2, took the square wave input and filtered it through a low pass single time constant of 2.00 s, Equation 1, to represent the ideal signal generated by the Horiba NOx analyzer.

$$C(t) = C_o + \left(C_f - C_o\right)\left(1 - e^{-t/\tau}\right) \qquad \text{[Equation 1]}$$

The third simulation curve was developed to represent the Vetronix NOx analyzer and therefore exhibited 2 time response curves of 19.1 and 4.30 seconds for the initial 1.5 s of the curve and the remaining portion respectively. The initial 1.5 s of

141

the curve was estimated as an exponentially rising curve, which fit to the main simple lag curve calculated by Equation 1. The Vetronix NOx simulation response curve can be seen in Figure C-3.

The remaining two simulation curves attempt to more accurately represent the sensor signal by introducing calculated amounts of noise into the signal which are present in on-road emission data files. To determine the amount of noise which is representative of sensor data, an examination of on-road and lab data was conducted. Three separate tests were examined during three separate months of testing.

C.2 Noise Determination

The examination of noise focused on those time periods where both sensors appeared to exhibit stable concentrations, usually during idle or cruising periods. Low concentration values between 0 and 25 ppm were typical of the range examined. Tables C-1, C-2, and C-3 illustrate that the fast response Horiba sensor exhibited standard deviation values of 1.6 to 2.3 ppm whereas the Vetronix NOx sensor exhibited 0.9 to 1.2 ppm for actual on-road data. These results are reasonable and expected. The doubled standard deviation result for the Horiba NOx sensor is to be expected based on the fact that the Horiba NOx sensor has a time constant 2.5 times faster than the Vetronix NOx sensor.

When examining the results obtained by studying laboratory data at elevated and near zero NOx concentrations, it can be seen that at high NOx concentrations, the Horiba instrument exhibited similar standard deviation values to the test values given a constant, known 1840ppm NOx input. However, when purging the sensor, the standard deviation in the signal was reduced below 0.5 ppm indicating very stable readings at low, controlled concentrations. These results indicate that the noise produced in the Horiba NOx sensor can be very low under controlled conditions at both low and high concentrations, however, noise data collected from actual test data should be used to represent the simulated curves.

The standard deviation values used for the creation of the simulated response curves will be 2.4 ppm for the Horiba and 1.3 ppm for the Vetronix as a slight overestimation of the average true noise in the system, based on examination of Tables C-1 through C-3. To encompass a 95% confidence interval for the resulting noise, 2 standard deviations (4.8 ppm and 2.6 ppm) will be used when simulating noise in simulation curves 4 and 5.

It should also be noted that Oestergaard et al. [1] developed an Vehicle Exhaust Emissions System (VEES) which was capable of simulating constant as well as variable exhaust concentration profiles typical of vehicles. The VEES system has the capability of simulating LEV, ULEV, and SULEV emissions levels which was used for testing the On-Board System Emissions bench developed by Horiba.

142

Table C-1 NOx Sensor Noise Comparison - J27_2 Data

	Horiba			Vetronix		
	Average [ppm]	[% error]	Std. Dev. [ppm]	Average [ppm]	[% error]	Std. Dev. [ppm]
J27_2_N-a	10.66	21.43	2.29	10.82	7.01	0.76
J27_2_N-b	9.48	15.98	1.51	9.55	7.91	0.76
J27_2_N-c	11.55	33.11	3.82	12.69	14.48	1.84
J27_2_N-d	5.93	19.59	1.16	11.00	12.66	1.39
J27_2_N-e	7.64	15.83	1.21	10.30	10.45	1.08
J27_2_N-f	11.26	30.40	3.42	10.89	14.71	1.60
Average	9.42	22.72	2.34	10.88	11.20	1.24

Table C-2 NOx Sensor Noise Comparison - F27_3 Data

	Horiba			Vetronix		
	Average [ppm]	[% error]	Std. Dev. [ppm]	Average [ppm]	[% error]	Std. Dev. [ppm]
F27_3_N-a	9.64	18.70	1.80	3.09	42.30	1.31
F27_3_N-b	9.99	26.45	2.64	3.05	66.09	2.01
F27_3_N-c	12.47	14.21	1.77	1.21	70.54	0.85
F27_3_N-d	8.33	13.84	1.15	0.84	77.73	0.66
F27_3_N-e	12.38	12.43	1.54	0.14	249.90	0.35
F27_3_N-f	9.12	13.24	1.21	2.70	27.41	0.74
Average	10.3	16.48	1.69	1.84	89.00	0.99

A study by Oestergaard of steady state ULEV levels of NOx on a Horiba MEXA-720NOx (identical to the fast response Horiba sensor used in this research), found laboratory percent error results of 2 to 6 % for average concentrations in the range of 40 to 10 ppm. This result appears very close to the results obtained from the Horiba Laboratory data collected at approximately zero NO concentration (average of 4 ppm actually measured) which found approximately 12 % error at 4 ppm. It was found from these experiments as well as in [1], that percent error values can rise dramatically at low NO emission levels. Therefore the measured noise for the constant near zero NO concentration laboratory data, appears valid and correct.

143

Table C-3 NOx Sensor Noise Comparison - N18_2 Data

	Horiba			Vetronix		
	Average [ppm]	[% error]	Std. Dev. [ppm]	Average [ppm]	[% error]	Std. Dev. [ppm]
N18_2_N-a	14.82	9.17	1.36	6.32	12.33	0.78
N18_2_N-b	14.00	8.58	1.20	7.50	19.74	1.48
N18_2_N-c	13.81	7.98	1.10	4.75	14.64	0.70
N18_2_N-d	15.12	15.17	2.29	2.21	21.31	0.47
N18_2_N-e	12.57	16.70	2.10	1.82	17.05	0.31
N18_2_N-f	13.15	13.29	1.75	5.95	26.88	1.60
Average	13.91	11.82	1.63	4.76	18.66	0.89

Laboratory Test Data Results

Table C-4 Horiba Noise Calculation - Lab Data

	Constant 1840ppm			Constant 0 ppm		
	Average [ppm]	[% error]	Std. Dev [ppm]	Average [ppm]	[% error]	Std. Dev. [ppm]
R1	1838	0.23	4.27	3.66	17.90	0.66
R2	1842	0.20	3.67	3.87	8.85	0.34
R3	1838	0.16	2.91	3.71	9.33	0.35
R4	1819	0.17	3.04	3.66	13.68	0.50
R5	1806	0.18	3.27	3.93	9.38	0.37
R6	-	-	-	3.83	10.76	0.41
Average	1829	0.19	3.43	3.78	11.67	0.44

The addition of noise to simulations 4 and 5 was introduced using the Box-Muller equation for normal distributions, which generated a "noisy" mean based on a randomly calculated z value, the standard deviation (calculated above), and the current mean value. The two equations which calculate the noise in the signal are shown below:

$$Z = \left(- 2\ln U_1\right)^{1/2} \cos\left(2\pi U_2\right) \qquad \text{[Equation 2]}$$

$$x = Z\sigma + \mu \qquad \text{[Equation 3]}$$

144

Equation 2 generates a random z value from a normal distribution based on two random values U_1 and U_2. This z value is then used to find the new "noisy" mean value using the standard deviation and the actual mean. The result of simulating noise in the signal is shown in Figures C-4 and C-5 for the Horiba NOx and Vetronix NOx sensors respectively.

In order to prove that Equations 2 and 3 are producing normally distributed noise on the data signal, which is reflective of actual sensor noise behavior, the use of matlab programming was undertaken. The program created a constant input signal of 50 ppm, then subjected the signal to Equations 2 and 3 with known mean and standard deviation values for 1000 points of signal data. The results plotted in Figures C-6 and C-7 show that the desired effect of producing a noisy signal with a given standard deviation can be successfully accomplished using Equations 2 and 3. The programing code was run numerous times to gain confidence in repeatability.

C.3 Algorithm Accuracy

The basis for evaluating the accuracy of the correction algorithms was to justify whether the corrections algorithms produced highly accurate, some-what accurate, or extremely noisy de-filtered results of simulated signal responses. Quantified results looked at using the integral error, RMS error, and percentage overshoot, as the basis for determining the effectiveness of the algorithms. These equations are shown below.

$$ERROR_{int} = \frac{\left| \int \chi_{NOx,actual}(t)dt - \int \chi_{NOx,corrected}(t)dt \right|}{\int \chi_{NOx,actual}(t)dt} \times 100 \qquad \text{[Equation 4]}$$

$$ERROR_{RMS} = \sqrt{\frac{\sum_i \left[\left(NOx_{original,i} - NOx_{corrected,i} \right)^2 \right]}{n}} \qquad \text{[Equation 5]}$$

$$P.O. = 100 \times \left(\frac{NOx_{corrected} - NOx_{original}}{NOx_{original}} \right) \qquad \text{[Equation 6]}$$

The results of applying the six correction algorithms, described in Appendix B, are shown in Tables C-5 through C-9. Table C-5 illustrates the error between the simulation curve and the step change input without applying the correction

145

algorithm, to provide a basis for comparing the improvements possible with signal processing.

Table C-5 Error in Simulation Signal (without Response Correction)

	Integral Error [% Diff.]	RMS Error [ppm]	P.O. Error [%]
Simu.Curve 2	0	266	0
Simu.Curve 3	0.05	549	0
Simu.Curve 4	0.05	266	0.56
Simu.Curve 5	0.04	55	0

Tables C-6 and C-7 contrast the effects of the correction algorithm on the accuracy of Horiba NOx data, and Horiba NOx data with noise respectively.

Table C-6 Simulation Curve 2 - Accuracy Analysis

Resp.Corr. Algorithm	Integral Error		RMS Error		Overshoot Error	
	[% Diff.]	Std. Dev.	[ppm]	Std. Dev.	[%]	Std. Dev.
1	0.00	0.00	23	0.00	0.74	0.00
2	0.00	0.00	137	0.00	0.00	0.00
3	1.63	0.00	158	0.00	94.1	0.00
4	1.53	0.00	201	0.00	88.4	0.00
5	0.64	0.00	78	0.00	38.2	0.00
6	0.57	0.00	161	0.00	34.4	0.00

Table C-7 Simulation Curve 4 - Accuracy Analysis

Resp.Corr. Algorithm	Integral Error		RMS Error		Overshoot Error	
	[% Diff.]	Std. Dev.	[ppm]	Std. Dev.	[%]	Std. Dev.
1	0.61	0.75	137	63	2.84	0.77
2	0.66	0.49	206	58	9.19	11.6
3	1.23	0.52	155	46	49.6	48.4
4	2.90	1.08	243	59	90.8	10.1
5	0.24	0.22	117	36	20.7	18.8
6	1.36	0.64	264	74	39.6	15.1

146

Legend:

Simulation Curve
1. Square Wave - both sensors
2. First Order Response - Horiba
3. First Order Response - Vetronix
4. First Order Response with Noise - Horiba
5. First Order Response with Noise - Vetronix

Response Correction Algorithm
1. Single Time Constant - Simple Diff.
2. Single Time Constant - Enhanced Diff.
3. Enhanced Time Constant - Simple Diff.
4. Enhanced Time Constant - Enhanced Diff.
5. Optimized Time Constants - Simple Diff.
6. Optimized Time Constants - Enhanced Diff.

Tables C-8 and C-9 contrast the effects of the correction algorithm on the accuracy of Vetronix NOx data, and Vetronix NOx data with noise respectively. The above legend applied to Table C-6 and C-7, as well as Table C-8 and C-9.

Table C-8 Simulation Curve 3 - Accuracy Analysis

Resp.Corr. Algorithm	Integral Error		RMS Error		Overshoot Error	
	[% Diff.]	Std. Dev.	[ppm]	Std. Dev.	[%]	Std. Dev.
1	0.03	0.00	268	0.00	0.23	0.00
2	0.23	0.00	422	0.00	10.6	0.00
3	4.32	0.00	396	0.00	209	0.00
4	7.15	0.00	655	0.00	306	0.00
5	7.11	0.00	384	0.00	145	0.00
6	1.25	0.00	412	0.00	68.1	0.00

Table C-9 Simulation Curve 5 - Accuracy Analysis

Resp.Corr. Algorithm	Integral Error		RMS Error		Overshoot Error	
	[% Diff.]	Std. Dev.	[ppm]	Std. Dev.	[%]	Std. Dev.
1	0.14	0.10	271	3	2.89	0.96
2	0.96	0.56	420	12	8.49	2.77
3	3.06	2.18	339	88	130	101
4	5.52	4.66	573	134	201	133
5	6.23	4.41	357	150	123	89.5
6	1.54	0.70	391	30	38.0	28.3

Although it was not tabulated, all response correction algorithms were able to reproduce the step change concentration profile of Figure C-1 with no difficulty as indicated by zero error in all error types. This observation indicates that the correction algorithms were able to properly distinguish a step change algorithm and

147

avoid unnecessarily amplifying the signal which gives confidence in the algorithms. The following section will discuss the error results of Tables C-5 through C-9.

C.3.1 Integral Error

Integral error was calculated by measuring the area under the concentration versus time curve, and finding the percent difference between the results generated for the step change input signal versus the corrected signal. This error type is significant because it is an indication of the total ppm reading measured during the response. Any reduction in this total ppm value would therefore result in lower mass emission results.

Figure C-8 indicates the integral error for the various response correction algorithms and the simulation curve corrected. An important finding of the accuracy analysis was that the simplified single time constant Horiba and Vetronix NOx correction algorithms, showed better accuracy than either of the variable time constant algorithms on an integral error basis. This result was as expected as the simulation curves were ideal simulated signals (and signals with noise) which would be more accurately corrected by an exact single time constant algorithm from which it was derived.

However, in all cases, integral error was made worse through use of a correction algorithm, as integral error for the uncorrected simulations was essentially zero as shown in Table C-5. This was because simulation curve 2 was to slow to respond to a rise in concentration but also to slow to return to zero value. It should be noted that a large standard deviation exists between integral error values for some of the variable time constant algorithms (response correction algorithms 3 - 6) with individual values ranging from approximately 0.5 - 1.0% integral error to upwards up 10% error. Single time constant integral error values were much better with individual error values ranging from 0 - 2 % through numerous noise iteration trials. This result indicates that the single time constant algorithms were most appropriate for use as a correction algorithm due to the minimized integral error. The use of the optimized time constant algorithm would also be a consideration (algorithm 5) if it was not for the 20%+ overshoot present in the signal which is not present with the single time constant algorithms.

If a comparison is made between NOx sensors with differing responses, the result is a lower integral error for the Horiba NOx simulation compared to the Vetronix NOx simulation (when noise is disregarded). This result indicates the decreased difficulty associated with correcting a single time constant fast response signal.

The effect of noise on integral error was different between response correction algorithms. For the single time constant algorithms, it can be conclusively noted that noise resulted in an increase in integral error. However, looking at the variable time constant algorithms, it was shown that in the majority of cases (for average

148

integral error), the addition of noise would be detrimental to the enhanced differential algorithms, but beneficial to the simple differentiation algorithms. It should be noted that the presence of large standard deviations in integral error values prevents definitive determination of the effect of noisy data.

Figures C-9 and C-10 indicate the difference in response obtained during iterative data processing of a variable time constant algorithm processing a noisy Vetronix NOx data signal. These results indicate the <u>wide range in initial response possible due to the randomly generated noise</u>. Figure C-9 indicates corrected data overshoot on the order of 6% versus overshoot greater than 200% for Figure C-10 with the only difference in input signal being the generation of random normally distributed noise. In these two figures, the enhanced time constant simple differentiation routine was used to correct the data, though similar results were observed for all variable time shifting algorithms.

C.3.2 Percent Overshoot Error

The percent overshoot criteria was examined as a means of evaluating accuracy due to the strong impact large concentrations have on mass emission rates. Producing large overshoots as shown in Figure C-10 introduces further error to the corrected signal because maximum levels are only achieved through large amplification of small concentration gradients. Replacing a <u>small measured value</u> with a <u>large processed value</u> (with somewhat uncertain maximum values) is not beneficial to the end result. Therefore, the <u>minimal overshoot criteria</u> will be used to judge the goodness of the algorithm.

When examining the percentage overshoot data shown in Tables C-5 through C-9, it is immediately evident that the <u>single time constant algorithms (1 and 2), exhibit substantially less pronounced overshoot</u> relative to the variable time shifting algorithms. Percentage overshoot on the order of 0 to 10% was observed whereas variable time constant algorithms exhibited near zero to 300% overshoot depending on the noise present in the signal. The dependence of percent overshoot on noise is due to the fact that the variable time shift algorithms use large initial time constants for the first few data points (based on laboratory data analysis) which would cause significant overshoot in a simulated signal but muted and responsive correction in a signal where the first few points are noise. On an average reading basis from a limited scope of iterations, the percent overshoot appears to be <u>reduced</u> with noise although this cannot be stated conclusively. Percent overshoot was less for the optimized time constants (a seven point time constant varying scheme) versus the enhanced time constants (a two point time constant varying scheme).

149

C.3.3 RMS Error

The final error measurement type calculated was the RMS error. Low RMS error is the ultimate benefit of the response correction algorithm because it is an indication of the goodness of step change response reproduction by data post-processing. The nature of the mass emissions rate calculation which multiplies instantaneous NOx concentrations and mass air flow rate (among other variables), requires the lowest possible RMS error for accuracy. Table C-5 above illustrates the RMS Error present in the simulated signals before correction and therefore any reduction in those error values for the particular simulation curve should produce more accurate and representative mass emission rate results. This should be done without substantially effecting the total integral error present in the post-processed signal.

Having examined the RMS error data it can be seen that the first few points of the rise and subsequent fall (of the concentration level), dominated the final error value reported. This observation was the basis for the development of optimized time constants which would quickly amplify the first few slow response data points thereby attempting to reduce the magnitude of RMS error. It has been shown however that the drawback to this method introduces the possibility of large overshoot for ideal first order signals, and variable overshoot results for noisy simulated data.

Figure C-12 shows the results of RMS error for the various response correction algorithms and simulated signals. From the average readings plotted in Figure C-12 and also shown in Tables C-5 through C-9, the RMS error was minimized when using the single time, constant simple differentiation routine (algorithm 1). It should be noted that large standard deviation occurred between readings of the RMS error for the iterated noisy data but regardless, still show algorithm 1 with the lowest RMS error. Horiba NOx corrected data found RMS error tended to increase when noise was added, whereas Vetronix RMS error tended to stay constant when noise was added.

C.4 Differentiation Routine Comparison

The enhanced differentiation algorithm does not appear to exhibit a trend (more or less accurate than simple differentiation) when it comes to integral error. However, a number of spikes labeled "tail spikes" were seen when using the enhanced differentiation routine. "Tail spikes" were designated as such due to the fact that they occur at the trailing edge of the step change input just prior to the step change value returning to its steady zero value (50ppm in these simulations). The three point (forward) and five point (centered) enhanced differentiation routine was found to be the cause of these spikes as the routine generated large inaccurate (sign reversals) slopes due to the multi-point nature of the routine. It should be noted that the tail spike in Figure C-13 was created by the optimized time constant algorithm

150

with enhanced differentiation on a non-noisy vetronix simulated response signal. Because the signal is non-noisy in nature, it is evident that at no point in the response should a positive slope occur on a decreasing NOx concentration signal.

The enhanced differentiation routine did show a trend toward increasing the error in the RMS error category however. This is a negative impact on the corrected signal as RMS error is an indication of how well each individual point aligns with the input (square wave) signal. The use of the simple differentiation routine (two points) appears to therefore produce more reliable results. It should be noted however that the simulated and actual sampling frequency of the emission system was approximately 2 Hz which may be insufficient for advanced differentiation routines. The time response of NOx production is on the order of a fraction of a second, whereas the slow response sensor is on the order of 7 seconds. When observing transient NOx data results with time, it is evident that large "jumps" in concentration, due to slow sampling rates, may be resulting in erroneous differentiating results. A more frequent sampling rate would smooth out the response and be more conducive to enhanced differentiation. Therefore, sampling rate limitations are also a supporting factor in choosing simple differentiation over an enhanced version.

C.5 Algorithm Sensitivity to Simulation Time Constants

The investigation of error on simulated signals with time constants other than the average value is also of interest due to the fact that error in the calculation of the actual time constants exists. Looking at Appendix A, we can see that the Horiba NOx sensor response time calculated over a number of tests range between 1.56 and 2.35 s with an overall average of 2.00 +/- 0.26 s. When comparing the previously used sensor to the new sensor time constant of 2.23 +/- 0.14 s, we notice a slight difference as well (although well within the 95% confidence interval). Therefore, looking at the impact of the response correcting algorithms at 80%, 90%, 110%, and 120% of the average time constant value will allow for the determination of the algorithm accuracy (within the 95% confidence interval of the time constant) when the time constant differs from the average value of 2.00 s.

Looking at tests conducted on the Vetronix NOx sensor, time constant values of 6.97 +/- 0.11 s and 7.17 +/- 0.23 s were measured from the simple linear interpolation routine. This is not representative of the true response of the signal however (as shown in Appendix A), due to the fact that the first 2 seconds respond in a non-simple lag routine. Looking at the time constant determined by the slope method, it is evident from Appendix A that the majority of the slope responds at 4.30 +/- 0.23 s. Examining 80%, 90%, 110%, and 120% of the 4.30 s time constant would therefore encompass greater than 95% of all time constant values expected.

Table C-10 below indicates the range of time constants examined which encompass the 95% (and greater) confidence interval for the Horiba and Vetronix NOx sensors.

151

Table C-10 95% Confidence Interval - Time Constant Range

	80% T.C.	90% T.C.	110% T.C.	120% T.C.
Horiba NOx	1.60 s	1.80 s	2.20 s	2.40 s
Vetronix NOx	3.44 s	3.87 s	4.73 s	5.16 s

Tables C-11 through C-16 illustrate the effect of the sensor time constant on the accuracy of the various response correction algorithms. Non-noisy simulated signals of the Horiba and Vetronix sensors were examined to prevent noise variations from effecting accuracy comparisons. Although less accurate than a noisy signal comparison, the results will be used as a first approximation to determine the general effect of the simulated time constant value on response accuracy.

152

Table C-11 Simulation Curve 2 - Integral Error

	Integral Error [%]				
Resp. Corr. Algorithm	Tau = 80%	Tau = 90%	Tau = 100%	Tau = 110%	Tau = 120%
1	0.46	0.14	0.00	0.00	0.00
2	0.21	0.06	0.00	0.00	0.00
3	2.68	2.05	1.63	1.39	1.18
4	2.06	1.78	1.53	1.31	1.12
5	1.09	0.84	0.64	0.46	0.31
6	0.95	0.75	0.57	0.41	0.27

Table C-12 Simulation Curve 2 - RMS Error

	RMS Error [ppm]				
Resp. Corr. Algorithm	Tau = 80%	Tau = 90%	Tau = 100%	Tau = 110%	Tau = 120%
1	34	21	23	40	60
2	100	117	137	157	176
3	218	185	158	137	122
4	221	208	201	201	206
5	106	87	78	78	86
6	146	151	161	175	189

Table C-13 Simulation Curve 2 - Percent Overshoot Error

	Percent Overshoot Error [%]				
Resp. Corr. Algorithm	Tau = 80%	Tau = 90%	Tau = 100%	Tau = 110%	Tau = 120%
1	13.30	6.74	0.74	0.00	0.00
2	14.39	5.86	0.00	0.00	0.00
3	128.24	109.84	94.13	80.58	68.78
4	118.04	102.27	88.36	76.08	65.21
5	62.65	49.47	38.24	28.57	20.16
6	55.85	44.42	34.39	25.57	17.78

153

Table C-14 Simulation Curve 3 - Integral Error

	Integral Error [%]				
Resp. Corr. Algorithm	Tau = 80%	Tau = 90%	Tau = 100%	Tau = 110%	Tau = 120%
1	1.47	0.48	**0.03**	0.04	0.13
2	**0.21**	0.22	0.23	0.24	0.88
3	6.49	5.09	4.32	4.07	**3.95**
4	8.14	7.57	7.15	6.82	**4.62**
5	9.22	8.02	7.11	6.36	**5.78**
6	**1.23**	1.24	1.25	1.26	2.02

Table C-15 Simulation Curve 3 - RMS Error

	RMS Error [ppm]				
Resp. Corr. Algorithm	Tau = 80%	Tau = 90%	Tau = 100%	Tau = 110%	Tau = 120%
1	272	268	**268**	272	278
2	**394**	408	422	437	432
3	464	425	396	375	**375**
4	766	700	655	625	**572**
5	462	417	384	**363**	366
6	380	395	412	431	**371**

Table C-16 Simulation Curve 3 - Percent Overshoot Error

	Percent Overshoot Error [%]				
Resp. Corr. Algorithm	Tau = 80%	Tau = 90%	Tau = 100%	Tau = 110%	Tau = 120%
1	19.4	8.89	0.23	**0.00**	0.26
2	10.62	10.62	10.62	10.62	**0.78**
3	251.51	227.89	208.68	192.76	**179.34**
4	403.04	349.02	305.63	270.03	**240.3**
5	178.33	159.78	144.70	132.19	**121.65**
6	68.11	68.11	68.11	68.11	**0.46**

154

C.5.1 Integral Error - Sensitivity Analysis

Looking at Table C-11, it is evident that as the time constant of the Horiba NOx simulated response increases (%Tau), the integral error decreases, approaching the uncorrected error values shown in Table C-5. This indicates that as the Horiba response correction algorithms become less influential on the simulated signal, the integral error approaches uncorrected error levels near zero. This is as expected, however, values in Table C-14, which show the integral values for the Vetronix simulation curve with varying time constants, show varying increase/decrease trends with time constant changes.

The exception to this is the single time constant simple differentiation algorithm which behaves as expected with the lowest integral error occurring at the 100% Tau value with increasing error at any other time constant. These results are shown in Figure C-14, but it should be noted that even though the minimum error occurs at 100% Tau, no significant impact on integral error occurs. A maximum of 2% error resulting near the max possible Vetronix time constant range of the 95% confidence interval, would not be expected to substantially effect overall results.

C.5.2 RMS Error - Sensitivity Analysis

Figures C-14 and C-15 illustrate the sensitivity of the best correction algorithms to changes in the simulation curve time constants. Figure C-15 shows that both the single time constant and optimized time constant algorithms (with simple differentiation), produce their minimum RMS error when the time constant of the simulation curve has the same time constant as the algorithm used. Figure C-14 has been shown to have the lowest integral error at 100% Tau, but also exhibits the lowest RMS error at 100% as well. These result lend confidence to the fact that the most appropriate algorithm to use for correcting the first-order response is a single time constant, simple differentiation algorithm.

C.5.3 Percent Overshoot Error - Sensitivity Analysis

A clear observation regarding the percent overshoot error can easily be seen from Table C-13 and C-16, and Figure C-16. As the simulated signals became more responsive it was observed that the effect of the correction algorithm was to reduce the overshoot of the corrected signal. This is an obvious result but repeats the reassurance that the correction algorithms and sensitivity analysis programming code are generating accurate results.

155

C.6 Algorithm Conclusions

The choice of which algorithm to utilize in the correction and subsequent analysis of real world transient emission data, can now be done with confidence through quantified comparison of the choices available. The goal of the response correction algorithm chosen should be to produce near zero integral error, with minimal overshoot, and the lowest possible RMS error. The RMS error criteria is the most influential criteria to be evaluated because it represents the accuracy with which individual points can be reproduced to the theoretical actual emission value. Since mass emission rates require the point-by-point (in time) multiplication of mass flow rate, concentration, and a constant, accurate individual concentrations at each time stamp are of prime importance.

From all accounts, the choice of using the single time constant simple differentiation algorithm appears best. For the Vetronix NOx data, this algorithm produced the lowest integral error, percent overshoot, and RMS error when compared to all other correction algorithms. The Horiba NOx data could use either of two possible correction algorithms including the single time constant simple differentiation algorithm or the optimized time constant simple differentiation algorithm. Both corrections generated similar integral and RMS error results with the optimized time constant algorithm results becoming more favorable with noise. Significant overshoot and variation using the optimized time constant is a drawback of the algorithm however, and therefore suggests the increased complexity may not produce added benefit.

The choice of which differential algorithm to use appears clear for a few reasons. In the majority of cases, error (all types) appeared to be raised through the use of the enhanced differential algorithm. Also, the previously discussed issue of producing tail spikes near the end of a step change concentration, favors the use of simple differentiation. It is also more representative to assume the sensors are behaving as single time constant devices due to the physical nature of their design.

For these reasons, the use of the single time constant, simple differentiation algorithm has been chosen to post-process Vetronix and Horiba NOx data.

156
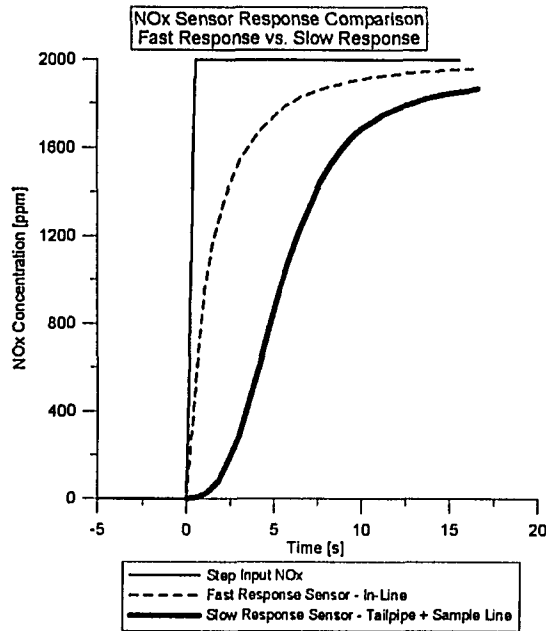
Figure C-1 Square Wave, Step
Change Input - Simulation 1
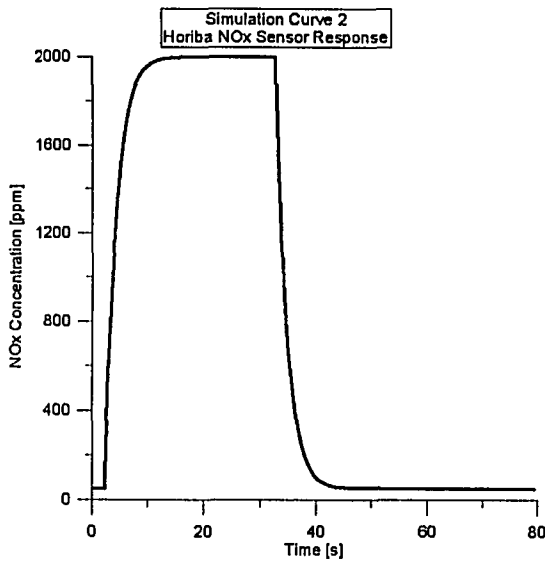
Figure C-2 Horiba NOx Sensor
Response - Simulation 2
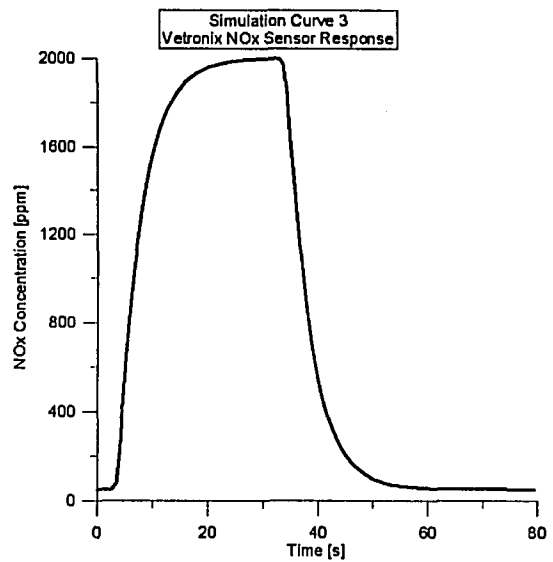
Figure C-3 Vetronix NOx Sensor
Response - Simulation 3

157
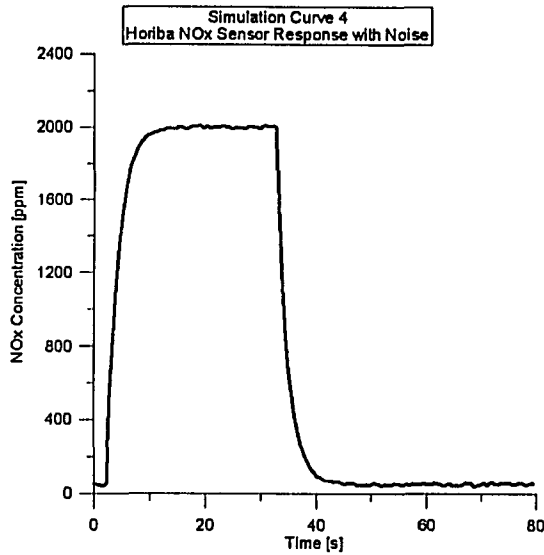
Figure C-4 Horiba NOx Sensor Response with Noise - Simulation 4
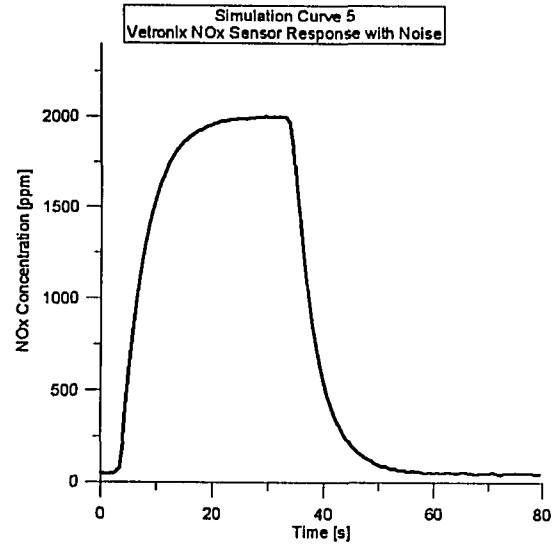
Figure C-5 Vetronix NOx Sensor Response with Noise - Simulation 5
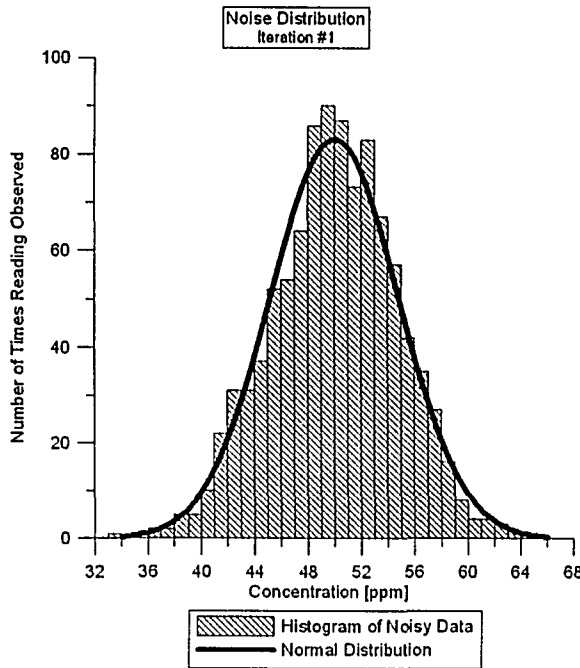
Figure C-6 Noise Profile - Normal Distribution Iteration 1
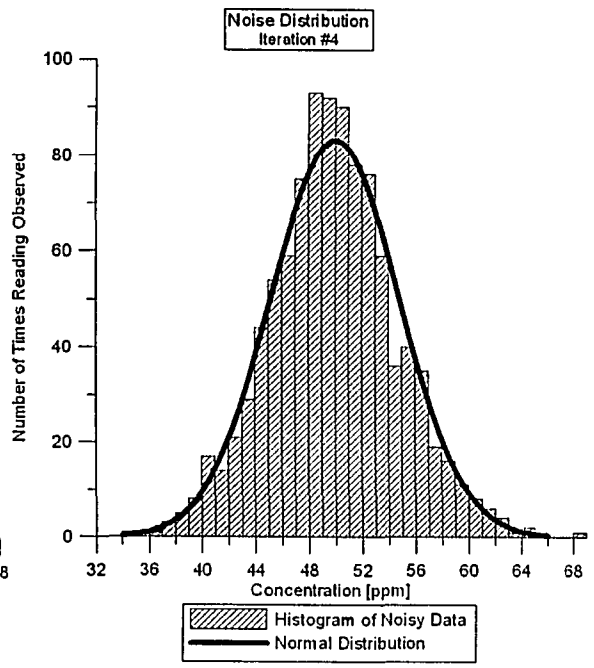
Figure C-7 Noise Profile - Normal Distribution Iteration 2

158
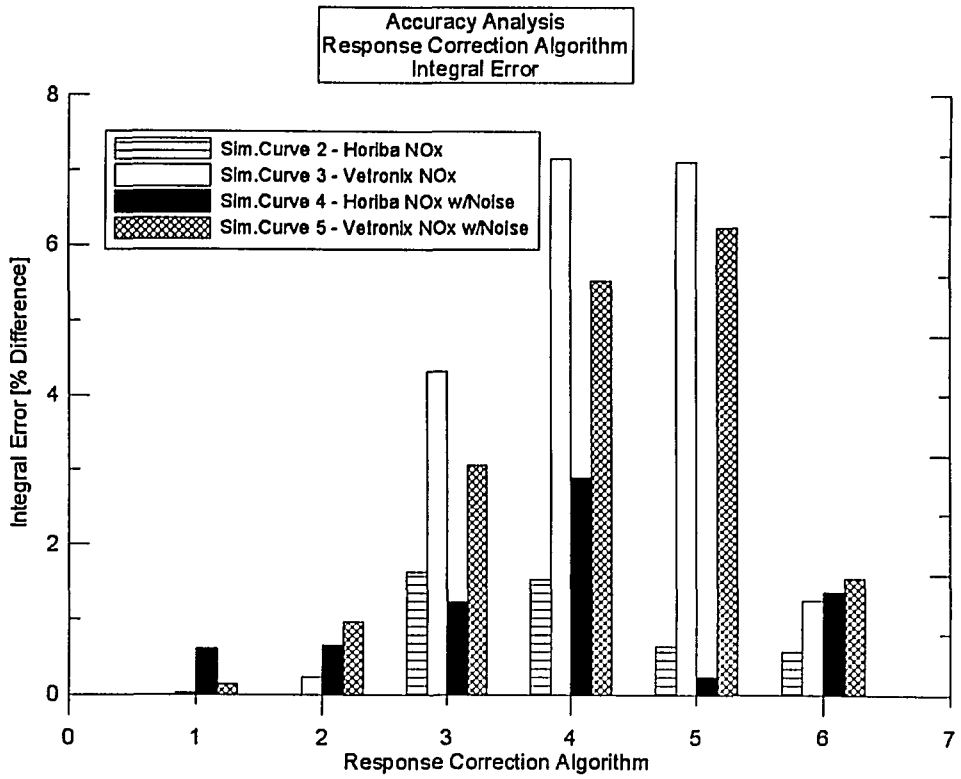
Figure C-8 Average Integral Error Results
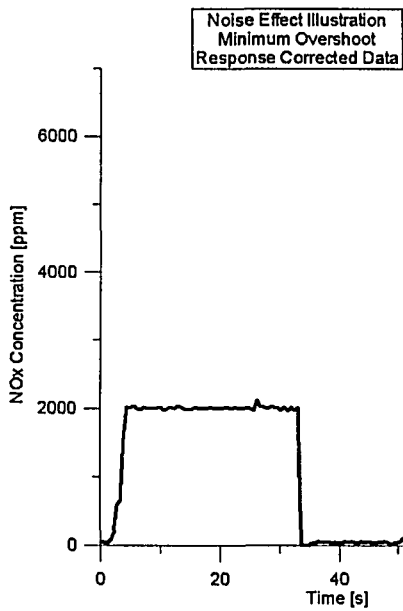
Figure C-9 Noisy Signal Preventing Overshoot
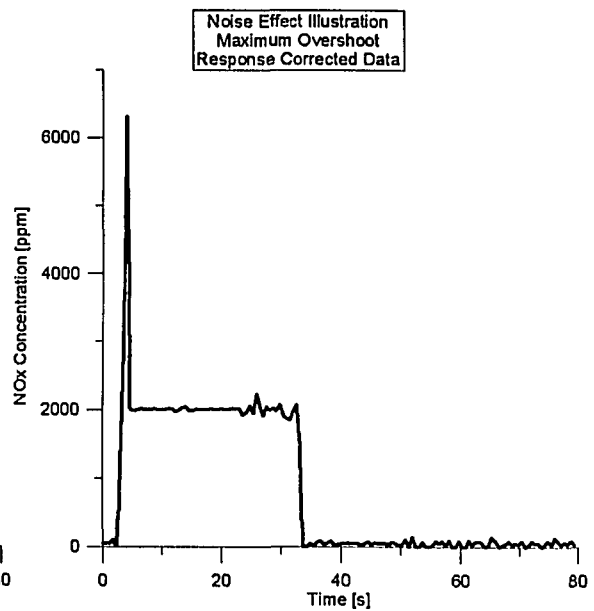
Figure C-10 Noisy Signal Exhibiting Overshoot

159
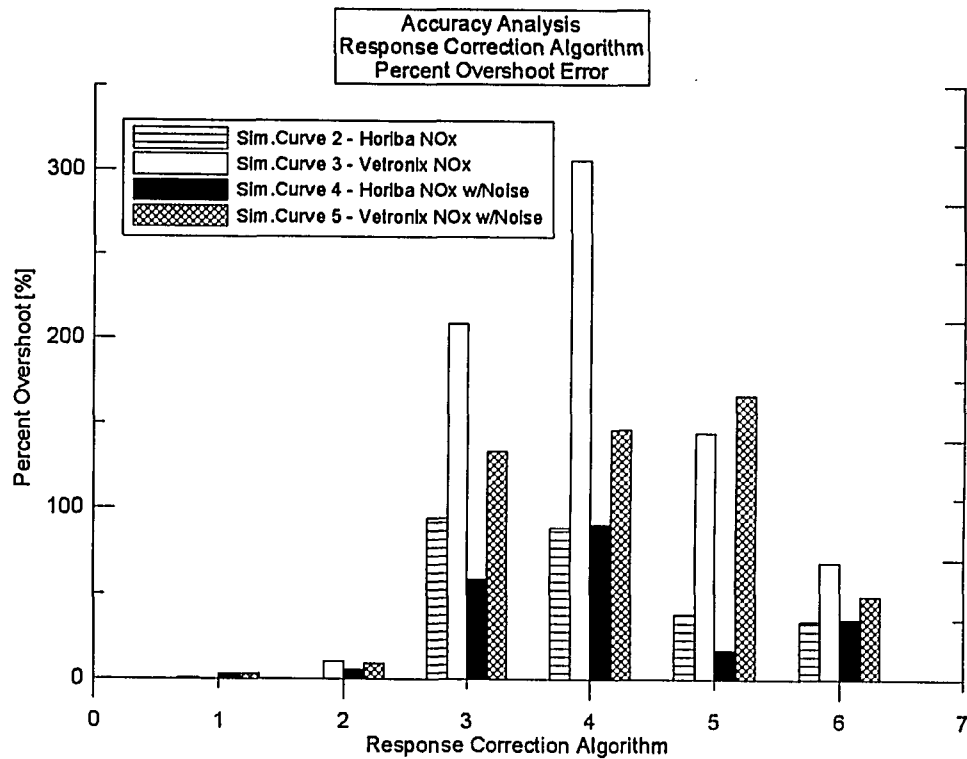
Figure C-11 Average Percent Overshoot Error Results
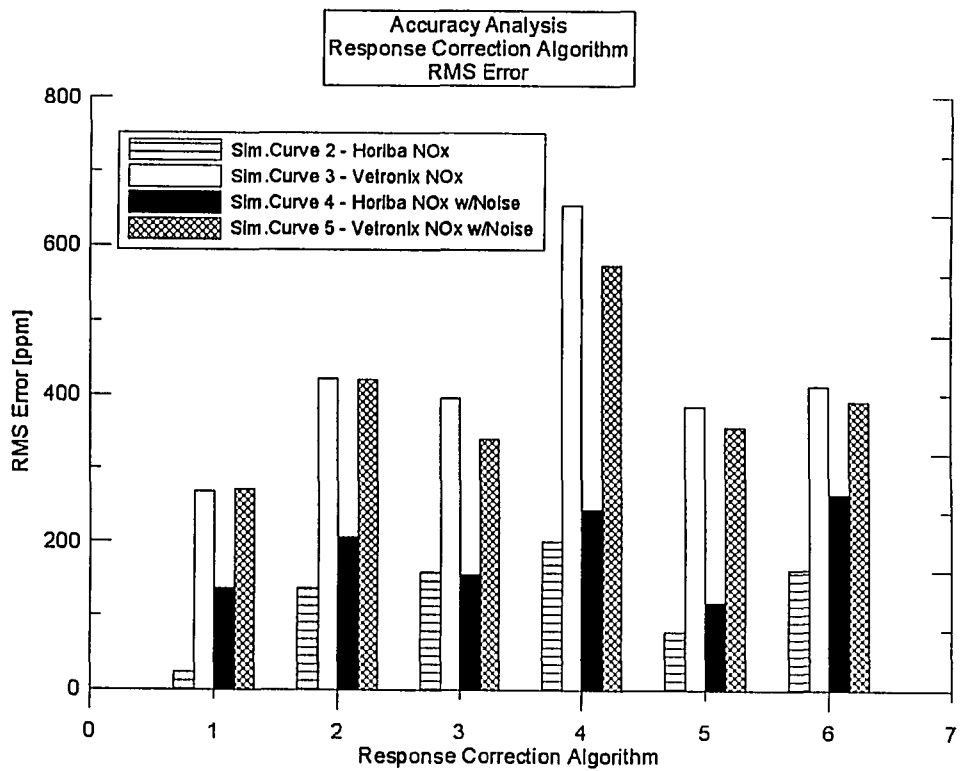
Figure C-12 Average RMS Error Results

160
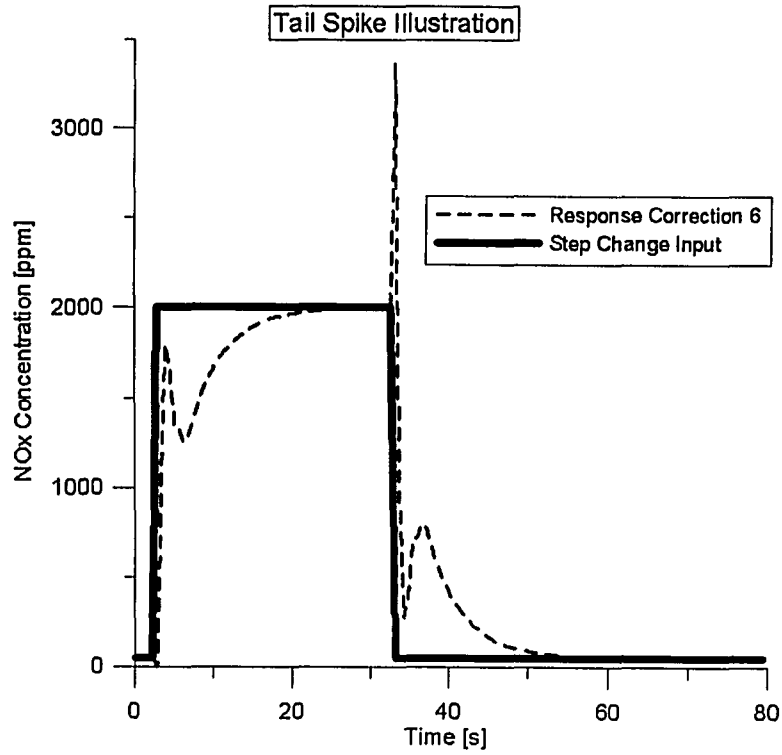
Figure C-13 Tail Spike Illustration
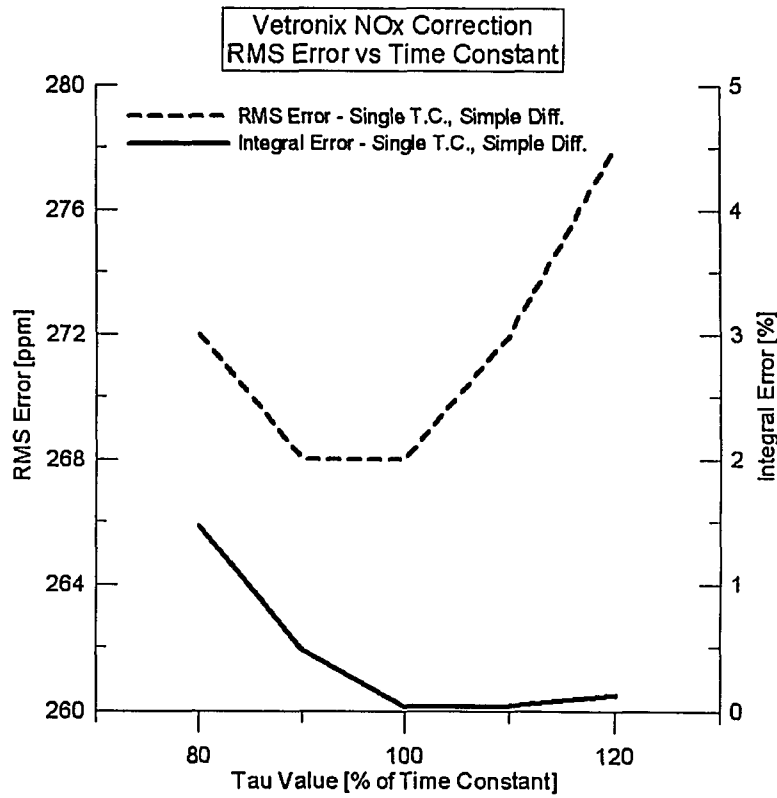
Figure C-14 Vetronix NOx Error Sensitivity to Time Constant

161
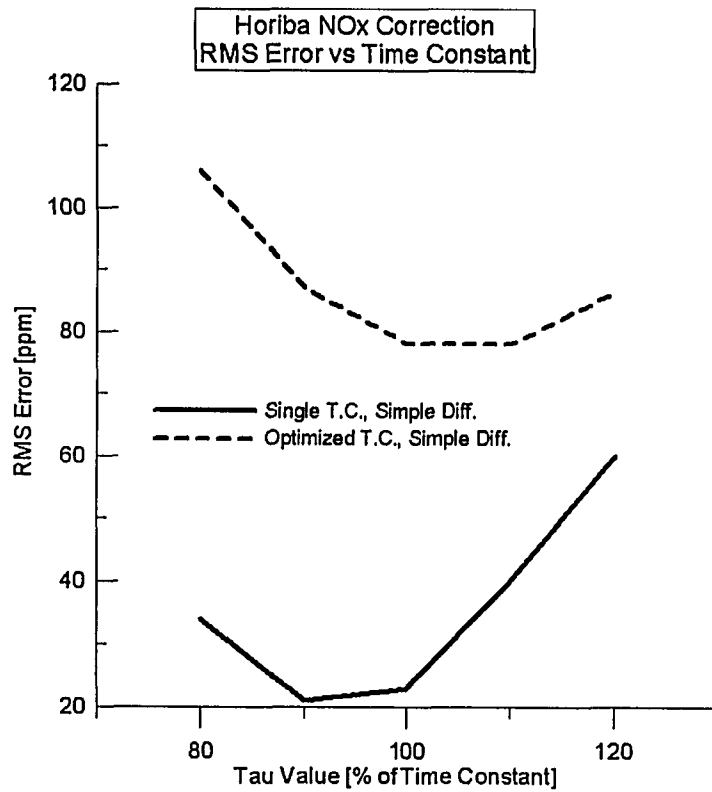
Figure C-15 Horiba NOx RMS Error Sensitivity to Time Constant
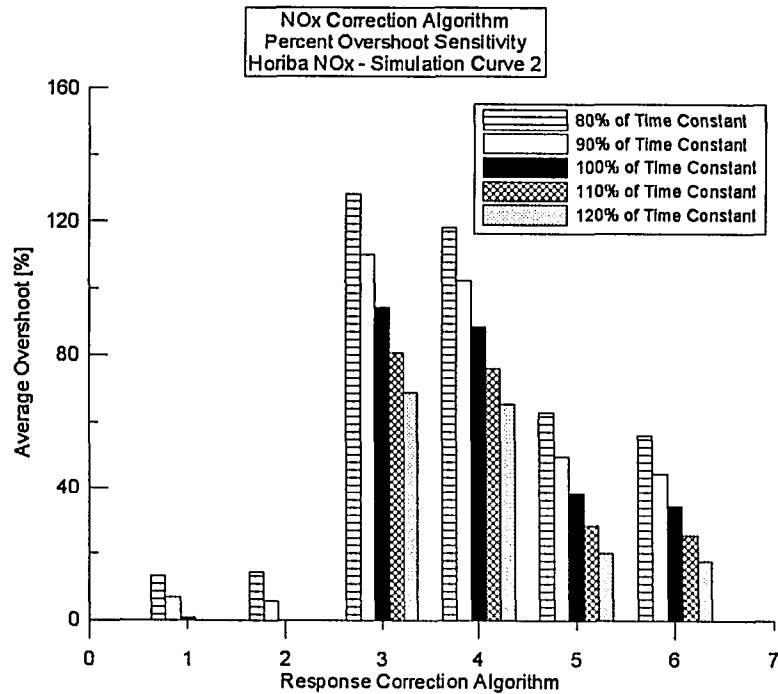
Figure C-16 Horiba NOx Percent Overshoot Sensitivity to Time Constant

162

REFERENCES

[1]   Oestergaard K., Porter S., and Nevius T., "Investigation into the Performance of an On-Board Emissions Measurement System Using a Vehicle Exhaust Emissions Simulator," SAE Technical Paper 2003-01-3746E, Society of Automotive Engineers, 2003.

APPENDIX D

Emissions Calculations & Uncertainty Analysis

The equations used to calculate emission rates in various formats and the uncertainty of the associated result are listed in Appendix D and utilized in the post-processing Matlab code. Tables illustrating the specifications of the sensors used in the on-board emissions measurement system are also given in terms of range, resolution, and accuracy.

164

D.1 Accuracy of Emissions Measurement Equipment

Table D-1 Vetronix PXA-1100 5-Gas Analyzer Specifications

GAS	RANGE	RESOLUTION	ACCURACY
HC	0 - 20,000 ppm	1 ppm	5 % of reading
CO	0 - 10%	0.01%	5 % of reading
CO2	0 - 20%	0.1%	5 % of reading
O2	0 - 25%	0.01%	5 % of reading
NOx	0 - 4000 ppm	1 ppm	32 ppm at 0 - 1000 ppm 60 ppm at 1001 - 2000 ppm 120 ppm at 2001 - 4000 ppm

Table D-2 Horiba MEXA-720NOx Specifications

GAS	RANGE	RESOLUTION	ACCURACY
NOx	0 - 3000 ppm	1 ppm	+/- 30 ppm at 0 - 1000 ppm +/- 3 % at 1001 - 2000 ppm +/- 5 % at 2001 - 3000 ppm
A/F	3.99 - 500.00	0.01 A/F	+/- 0.35 A/F at 9.5 - stoich. +/- 0.15 A/F at stoich +/- 0.40 A/F at stoich - 20.00 +/- 0.90 A/F at 20.01 - 30.00 A/F +/- 1.70 A/F at 30.01 - 40.00 A/F +/- 2.60 A/F at 40.01 - 50.00 A/F +/- 3.70 A/F at 50.01 - 60.00 A/F +/- 0.5 vol% O2 at > = 60.01 A/F

Siemens HFM 62B - Mass Air Flow Meter

Range: 2-135 g/s
Resolution: 0.01 g/s
Accuracy: 1.0 g/s (assumed over all MAF rates)
- Accuracy   +/- 3 %
- Temperature Influence +/- 2 %
- Long term Stability   +/- 2 %

165

Table D-3 ECM AFRecorder Specifications

ITEM	RANGE	RESOLUTION	ACCURACY
A/F	10.0 - 20.0 A/F (for gasoline)	0.1 A/F	+/- 0.5 A/F at 10.0 - 12.0 A/F +/- 0.3 A/F at 12.0 - stoich +/- 0.1 A/F at stoich +/- 0.3 A/F at stoich - 18.0 A/F +/- 0.5 A/F at 18.0 - 20.0 A/F
Engine Speed	100 - 9,999 rpm	1 rpm	+/- 0.1 %

Table D-4 AD590 Temperature Sensors Specifications

TEMP SENSOR	RANGE	RESOLUTION	ACCURACY
- Coolant - Intake Air - Ambient	-55.0 to 150.0°C	0.1°C	+/- 0.5°C (at -55°C worst case) or 1.0%

The uncertainty, ε_R, in the variable of interest R, can be calculated as,

$$\varepsilon_R{}^2 = \sum_{i=1}^{n} \left(\frac{\partial R}{\partial x_i} \varepsilon_{xi} \right)^2$$

where

$R = R(x_1, x_2, x_3, ..., x_i)$ - resultant of interest

x_i - variable in equation R

ε_{xi} - absolute error in variable x

Therefore, the partial derivative of R must be calculated for each x_i variable and the uncertainty in each variable ε_{xi} must also be calculated to produce the uncertainty ε_{Ri}, in R.

D.2 Emission Equations and Uncertainty Analysis

The general balanced chemical equation for the burning of a hydrocarbon fuel is:

C_xH_y + A (O_2 + 3.76 N_2) --> B C_6H_{14} + D CO + E CO_2 + F O_2 + G NO + I N_2 + J H_2O

where A, B, D, E, F, G, I, J are the mole fractions of the associated species. Mole fractions B, D, E, F, and G are converted to mole fractions from the original absolute values determined by the Vetronix PXA-1100 5-Gas Analyzer.

166

Species Balance - Mole Fraction   units: [mol]

Hydrocarbons: $B = \chi_{HC} = \dfrac{[HC]}{1,000,000}$ where [HC] units = ppm

Carbon Monoxide: $D = \chi_{CO} = \dfrac{[CO]}{100}$ where [CO] units = per

Carbon Dioxide: $E = \chi_{CO2} = \dfrac{[CO_2]}{100}$ where [CO$_2$] units = per

Oxygen Balance: $F = \chi_{O2} = \dfrac{[O_2]}{100}$ where [O$_2$] units = per

Oxides of Nitrogen: $G = \chi_{NOx} = \dfrac{[NO_x]}{1,000,000}$ where [NOx] units = ppm

Error in Species Mole Fractions (absolute):   units: [mol]

$\varepsilon_{[B]} = \varepsilon_{[HC]} = 0.05 * B$

$\varepsilon_{[D]} = \varepsilon_{[CO]} = 0.05 * D$

$\varepsilon_{[E]} = \varepsilon_{[CO2]} = 0.05 * E$

$\varepsilon_{[F]} = \varepsilon_{[O2]} = 0.05 * F$

$\varepsilon_{[G]} = \varepsilon_{[NOx]} = 32 \times 10^{-6}$ for 0-1000ppm

60×10^{-6} for 1001 - 2000ppm

120×10^{-6} for 0-1000ppm

The mole fraction of nitrogen present in the exhaust sample is calculated by assuming 1 kilomole of dry based products enters the 5-Gas analyzer. By subtracting the mole fractions of the other species measured by the analyzer, the fraction of N$_2$ present can be determined.

Nitrogen [mol]: $I = 1 - B - D - E - F - G$

Error in Nitrogen Calculation [mol]:

$$\varepsilon_I = \left[\left(\frac{\partial I}{\partial B} \times \varepsilon_B \right)^2 + \left(\frac{\partial I}{\partial D} \times \varepsilon_D \right)^2 + \left(\frac{\partial I}{\partial E} \times \varepsilon_E \right)^2 + \left(\frac{\partial I}{\partial F} \times \varepsilon_F \right)^2 + \left(\frac{\partial I}{\partial G} \times \varepsilon_G \right)^2 \right]^{1/2}$$

which yields,

$$\varepsilon_I = \left[\varepsilon_{[B]}^2 + \varepsilon_{[D]}^2 + \varepsilon_{[E]}^2 + \varepsilon_{[F]}^2 + \varepsilon_{[G]}^2 \right]^{1/2}$$

167

The amount of air present in the reactants can be calculated by performing a nitrogen balance. G, and I are mole fractions of NOx and N_2 respectively.

Air [mol]:

$$A = \frac{G + 2I}{2 \times 3.76}$$

Error in Air Calculation [mol]:

$$\varepsilon_A = \left[\left(\frac{\partial A}{\partial G} \times \varepsilon_G\right)^2 + \left(\frac{\partial A}{\partial I} \times \varepsilon_I\right)^2\right]^{1/2} = \left[\left(\frac{1}{2 \times 3.76} \times \varepsilon_G\right)^2 + \left(\frac{1}{3.76} \times \varepsilon_I\right)^2\right]^{1/2}$$

The amount of water present in the exhaust is determined from an oxygen balance.

Water [mol]: $J = 2A - D - 2E - 2F - G$

Error in Water Calculation [mol]:

$$\varepsilon_J = \left[\left(\frac{\partial J}{\partial A} \times \varepsilon_A\right)^2 + \left(\frac{\partial J}{\partial D} \times \varepsilon_D\right)^2 + \left(\frac{\partial J}{\partial E} \times \varepsilon_E\right)^2 + \left(\frac{\partial J}{\partial F} \times \varepsilon_F\right)^2 + \left(\frac{\partial J}{\partial G} \times \varepsilon_G\right)^2\right]^{1/2}$$

$$\varepsilon_J = \left[\left(2 \times \varepsilon_A\right)^2 + \left(-1 \times \varepsilon_D\right)^2 + \left(-2 \times \varepsilon_E\right)^2 + \left(-2 \times \varepsilon_F\right)^2 + \left(-1 \times \varepsilon_G\right)^2\right]^{1/2}$$

which yields,

$$\varepsilon_J = \left[\left(2 \times \varepsilon_A\right)^2 + \left(\varepsilon_D\right)^2 + \left(2 \times \varepsilon_E\right)^2 + \left(2 \times \varepsilon_F\right)^2 + \left(\varepsilon_G\right)^2\right]^{1/2}$$

Calculation of the air/fuel ratio requires finding the ratio of the molar mass of the air to the molar mass of the fuel.

Air/Fuel Ratio [m_{air}/m_{fuel}]:

$$\frac{A}{F} = \frac{A \times 4.76 \times 28.97}{(x \times 12.01) + (y \times 1.01)}$$

Error in Air/Fuel Ratio Calculation (for Vetronix Data) [m_{air}/m_{fuel}]:
- assume 'x' and 'y' are known (i.e. $\varepsilon_x = \varepsilon_y = 0$)

168

$$\varepsilon_{AIF} = \left[\left(\frac{\partial A/F}{\partial A} \times \varepsilon_A \right)^2 + \left(\frac{\partial A/F}{\partial x} \times \varepsilon_x \right)^2 + \left(\frac{\partial A/F}{\partial y} \times \varepsilon_y \right)^2 \right]^{1/2} = \frac{\partial A/F}{\partial A} \times \varepsilon_A$$

which yields,

$$\varepsilon_{AIF} = \frac{4.76 \times 28.97}{(x \times 12.01) + (y \times 1.01)} \times \varepsilon_A$$

(A/F equation and its associated error equation are computed to find the error in the Vetronix PXA-1100 A/F Reading)

Exhaust Molecular Weight [g/mol]:

$$MW_{exh} = B \times MW_{HC} + D \times MW_{CO} + E \times MW_{CO2}$$
$$F \times MW_{O2} + G \times MW_{NOx} + I \times MW_{N2} + J \times MW_{H2O}$$

where: $MW_{HC} = 86.18$ [g/mol]; $\qquad MW_{CO} = 28.01$ [g/mol];
$\qquad MW_{CO2} = 44.01$ [g/mol]; $\qquad MW_{O2} = 32.00$ [g/mol];
$\qquad MW_{NOx} = 30.01$ [g/mol]; $\qquad MW_{N2} = 28.01$ [g/mol];
$\qquad MW_{H2O} = 18.02$ [g/mol];

Error in Exhaust Molecular Weight Calculation [g/mol]:

$$\varepsilon_{MWexh} = \left[\left(\frac{\partial MWexh}{\partial B} \times \varepsilon_B \right)^2 + \left(\frac{\partial MWexh}{\partial D} \times \varepsilon_D \right)^2 + \left(\frac{\partial MWexh}{\partial E} \times \varepsilon_E \right)^2 + \left(\frac{\partial MWexh}{\partial F} \times \varepsilon_F \right)^2 \right.$$
$$\left. + \left(\frac{\partial MWexh}{\partial G} \times \varepsilon_G \right)^2 + \left(\frac{\partial MWexh}{\partial I} \times \varepsilon_I \right)^2 + \left(\frac{\partial MWexh}{\partial J} \times \varepsilon_J \right)^2 \right]^{1/2}$$

which yields,

$$\varepsilon_{MWexh} = \left[\left(MW_{HC} \times \varepsilon_B \right)^2 + \left(MW_{CO} \times \varepsilon_D \right)^2 + \left(MW_{CO2} \times \varepsilon_E \right)^2 + \left(MW_{O2} \times \varepsilon_F \right)^2 \right.$$
$$\left. + \left(MW_{NOx} \times \varepsilon_G \right)^2 + \left(MW_{N2} \times \varepsilon_I \right)^2 + \left(MW_{H2O} \times \varepsilon_J \right)^2 \right]^{1/2}$$

Mass Fuel Flow Rate [g fuel/s]: $\qquad MFF = \dfrac{MAF}{A/F}$

Error in Mass Fuel Flow Rate Calculation [g fuel/s]:

$$\varepsilon_{MFF} = \left[\left(\frac{\partial MFF}{\partial MAF} \times \varepsilon_{MAF}\right)^2 + \left(\frac{\partial MFF}{\partial A/F} \times \varepsilon_{A/F}\right)^2\right]^{1/2} = \left[\left(\frac{1}{A/F} \times \varepsilon_{MAF}\right)^2 + \left(\frac{-MAF}{(A/F)^2} \times \varepsilon_{A/F}\right)^2\right]^{1/2}$$

which yields,

$$\varepsilon_{MFF} = MFF \times \left[\left(\frac{\varepsilon_{MAF}}{MAF}\right)^2 + \left(\frac{\varepsilon_{A/F}}{A/F}\right)^2\right]^{1/2}$$

Fuel Economy Calculation [km/L]:

Fuel Density [g/L] or [kg/m³]:

$$\rho_{fuel} = \rho_{water} \times SG_{fuel} = 740$$

where:

SG_{fuel}	Specific Gravity of Fuel (0.740) [43]
ρ_{fuel}	Density of Fuel [kg/m³]
ρ_{water}	Density of Water [= 1000 kg/m³]

Weight Fraction of Carbon in Fuel:

$$Y_{CH1.85} = \frac{12.011}{12.011 + (1.85 * 1.008)} = 0.866$$

Carbon Fuel Density [g C / L]:

$$\rho_{fuel,C} = \rho_{fuel} \times Y_{CH1.85} = 740 \times 0.866 = 641$$

Mass of Carbon in Exhaust [g]:

Mass C in HC $= 0.866 \times \overline{ER}_{dist,HC}$

Mass of C in CO $= 0.429 \times \overline{ER}_{dist,CO}$

Mass of C in $CO_2 = 0.273 \times \overline{ER}_{dist,CO2}$

and finally fuel economy [km/L],

170

$$FE = \frac{641}{0.866\overline{ER}_{dist,HC} + 0.429\overline{ER}_{dist,CO} + 0.273\overline{ER}_{dist,CO2}}$$

Mass Emission Rate (Instantaneous) [g/s]:

$$ER_{time,i} = \frac{MW_i}{MW_{exh}} \times \chi_i \times (MAF + MFF)$$

Error in <u>Instantaneous</u> Mass Emission Rate Calculation [g/s]:
- assume ε_{MWi} (the error in molecular weight of each species) = 0

$$\varepsilon_{ERtime,i} = \left[\left(\frac{\partial ER_{time,i}}{\partial MW_i} \times \varepsilon_{MWi} \right)^2 + \left(\frac{\partial ER_{time,i}}{\partial MW_{exh}} \times \varepsilon_{MWexh} \right)^2 + \left(\frac{\partial ER_{time,i}}{\partial \chi_i} \times \varepsilon_{\chi i} \right)^2 \right.$$
$$\left. + \left(\frac{\partial ER_{time,i}}{\partial MAF} \times \varepsilon_{MAF} \right)^2 + \left(\frac{\partial ER_{time,i}}{\partial MFF} \times \varepsilon_{MFF} \right)^2 \right]^{1/2}$$

which yields:

$$\varepsilon_{ERtime,i} = ER_{time,i} \times \left[\left(\frac{\varepsilon_{MWexh}}{MW_{exh}} \right)^2 + \left(\frac{\varepsilon_{\chi i}}{\chi i} \right)^2 + \left(\frac{\varepsilon_{MAF}}{MAF + MFF} \right)^2 + \left(\frac{\varepsilon_{MFF}}{MAF + MFF} \right)^2 \right]^{1/2}$$

When reporting final calculated emissions results, cumulative error of the integrated mass emission rate requires that the total mass error be computed, then divided by the total time to yield a mass emission rate [g/s].

Total Mass Emission Calculation [g]:
(calculate the total mass emission at each time stamp)

$$M_i = ER_{time,i} \times \Delta t$$

Error in Total Mass Emission Calculation [g]:
(calculate the mass emission error at each time stamp)

$$\varepsilon_{Mi} = \varepsilon_{ERtime,i} \times \Delta t$$

171

(calculate the total mass emission error)

$$\varepsilon_{Mi,total} = \sqrt{\sum_{1}^{n} \left(\varepsilon_{Mi}\right)^2}$$

Total Mass Emission Rate Calculation [g/s]:

$$\overline{ER}_{time,i} = \frac{M_{i,total}}{t}$$

Error in Total Mass Emission Rate Calculation [g/s]:

$$\varepsilon_{\overline{ER}time,i} = \frac{\varepsilon_{Mi,total}}{t}$$

Total Mass Emission Rate Calculation [g/km]:

$$\overline{ER}_{dist,i} = \frac{M_{i,total}}{D_{total}}$$

Error in Total Mass Emission Rate Calculation [g/km]:
- This equation involves error in the distance component which increases complexity relative to the g/s error equation in which no error in the time variable was assumed.

$$\varepsilon_{\overline{ER}dist,i} = \left|\overline{ER}_{dist,i}\right| \times \left[\left(\frac{\varepsilon_{Mi,total}}{M_{i,total}}\right)^2 + \left(\frac{\varepsilon_{D,total}}{D_{total}}\right)^2\right]^{1/2}$$

$\varepsilon_{D,total}$ - shown in Appendix E (vehicle calculation equations and uncertainty analysis)

Mass Emissions Rate (Instantaneous) [g/kWh]:

$$ER_{pow,i} = \frac{ER_{time,i} \times 3600}{P}$$

172

Error in Instantaneous Mass Emission Rate Calculation [g/kWh]:

$$\varepsilon_{ERpow,i} = \left[\left(\frac{\partial ER_{pow,i}}{\partial ER_{time,i}} \times \varepsilon_{ERtime,i}\right)^2 + \left(\frac{\partial ER_{pow,i}}{\partial P} \times \varepsilon_P\right)^2\right]^{1/2}$$

which yields,

$$\varepsilon_{ERpow,i} = \left|ER_{pow,i}\right| \times \left[\left(\frac{\varepsilon_{ERtime,i}}{ER_{time,i}}\right)^2 + \left(\frac{\varepsilon_P}{P}\right)^2\right]^{1/2}$$

where: P   - Instantaneous Power of the Vehicle (calculated in Appendix E)

ε_P - Error in Instantaneous Power (calculated in Appendix E)

Total Mass Emissions Rate [g/kWh]:

$$\overline{ER}_{pow,i} = \frac{M_{i,total}}{W_{total}}$$

Error in Total Mass Emission Rate Calculation [g/kWh]:

    - This equation involves error in the power component which increases complexity relative to the g/s error equation in which no error in the time variable was assumed.

$$\varepsilon_{\overline{ERpow,i}} = \left|\overline{ER}_{pow,i}\right| \times \left[\left(\frac{\varepsilon_{M,total}}{M_{i,total}}\right)^2 + \left(\frac{\varepsilon_{Wtotal}}{W_{total}}\right)^2\right]^{1/2}$$

where: W_{total} - Total Work of the Vehicle (calculated in Appendix E)

ε_{Wtotal} - Error in Total Work (calculated in Appendix E)

Mass Emissions Rate (Instantaneous) [g/g fuel]:

$$ER_{fuel,i} = \frac{ER_{time,i}}{MFF}$$

Error in Instantaneous Mass Emission Rate Calculation:

$$\varepsilon_{Epowi} = \left[\left(\frac{\partial ER_{pow,i}}{\partial ER_{time,i}} \times \varepsilon_{ERtime,i}\right)^2 + \left(\frac{\partial ER_{pow,i}}{\partial MFF} \times \varepsilon_{MFF}\right)^2\right]^{1/2}$$

173

which yields,

$$\varepsilon_{ERfuel,i} = \left| ER_{fuel,i} \right| \times \left[\left(\frac{\varepsilon_{ERtime,i}}{ER_{time,i}} \right)^2 + \left(\frac{\varepsilon_{MFF}}{MFF} \right)^2 \right]^{1/2}$$

where MFF   - Mass Fuel Flow Rate [g/s] (calculated above)
     ε_{MFF} - Error in Mass Fuel Flow Rate [g/s] (calculated above)

Total Fuel Consumed [g fuel]:
    (calculate the fuel consumed at each point in the trip)

$$M_{fuel} = ER_{fuel,i} \times \Delta t$$

(calculate the total amount of fuel)

$$M_{fuel,total} = \sum_1^n M_{fuel}$$

Error in Total Fuel Consumed [g fuel]:
    (calculate the mass of fuel error at each time stamp)

$$\varepsilon_{Mfuel} = \left| \varepsilon_{MFF} \times \Delta t \right|$$

(calculate the total mass of fuel error)

$$\varepsilon_{Mfuel,total} = \sqrt{\sum_1^n \left(\varepsilon_{Mfuel} \right)^2}$$

Total Mass Emission Rate [g / g fuel]:

$$\overline{ER}_{fuel,i} = \frac{M_{i,total}}{M_{fuel,total}}$$

Error in Total Mass Emission Rate [g / g fuel]:

$$\varepsilon_{\overline{ER}fuel,i} = \left| \overline{ER}_{fuel,i} \right| \times \left[\left(\frac{\varepsilon_{Mi,total}}{M_{i,total}} \right)^2 + \left(\frac{\varepsilon_{Mfuel,total}}{M_{fuel,total}} \right)^2 \right]^{1/2}$$

174

REFERENCES

[1]   Hawirko, J.D. "Modeling Vehicle Emission Factors Determined with an In-Use & Real-Time Emissions Measurement System," Master of Science Thesis, Department of Mechanical Engineering, University of Alberta, 2003.

[2]   Turns, S.R. "An Introduction to Combustion, Concepts and Applications," McGraw Hill, New York, 2000.

[3]   Stone, R. "Introduction to Internal Combustion Engines, 3rd Edition," Society of Automotive Engineers Inc., Warrendale, PA, 1999.

[4]   2000 SAE Handbook, Vol.1, "Constant Volume Sampler System For Exhaust Emissions Measurement", SAE J1094 JUN92, p.13.140.

APPENDIX E

Vehicle Dynamics Calculations & Uncertainty Analysis

Appendix E illustrates the vehicle model and equations which were developed to represent the physical resistences to dynamic behavior. A vehicle dynamic model was implemented to determine the instantaneous amount of energy used by the vehicle to relate emissions results with vehicle tractive power requirements over transient and full cycle analysis periods. The method for calculation of uncertainty is also shown to allow integration into future programming for improved analysis functionality. Appendix E also describes the Coast Down Test methodology and equations used to calculate the drag coefficient Cd and the rolling resistence coefficient Cr.

176

E.1 Accuracy of Measured Vehicle Data

Table E-1 Accuracy of Vehicle Parameters

Parameter	Symbol	Data Source	Accuracy
Coefficient of Drag	Cd	Calculated	10%
Coefficient of Rolling Resistance	Cr	Calculated	10%
Height of Vehicle	H	Measured	5% - assumed
Mass of Vehicle	m	Measured	100 kg - assumed
Molecular Weight of Air	MW_{air}	Known	0% - assumed known
Pressure	P	Wind Tunnel Manometer	+/- 0.1 mmHg or +/- 0.013 kPa
Time	t	Vehicle ECM	0 % - assumed known
Universal Gas Constant	R_u	Known	0% - assumed known
Velocity	V	Vehicle ECM	+/- 0.25 km/h or +/- 0.069 m/s
Width of Vehicle	W	Measured	5% - assumed

Typical values for the two resistence coefficients are as follow:

Coefficient of Drag: $C_d = 0.3 - 0.9$

Coefficient of Rolling Resistence: $C_r = 0.01 - 0.08$

E.2 General Vehicle Equations

The vehicle dynamic model calculates the amount of power transmitted to the road by the vehicle. Dynamic vehicle models are well-developed and understood [4]. They consider aerodynamic, rolling, and inertial resistence in accounting for all forces on the vehicle. These forces are shown graphically in Figure E-1.

Inertial Resistence

Aerodynamic Resistence

Rolling Resistence
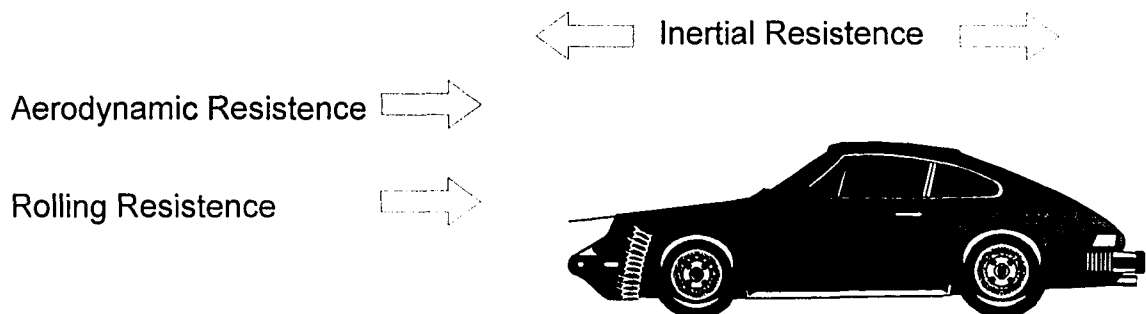
Figure E-1 Vehicle Dynamic Model

177

The tractive power calculation shown below is a combination of aerodynamic, rolling, and inertial resistence operating on the vehicle. Tractive power was calculated at each time step in the data analysis, which allowed the calculation of instantaneous energy consumption, and total energy used for the driving cycle.

Total Power:
$$P = \frac{V \times \left(F_{aero} + F_{rolling} + F_{inertial} + F_{climb}\right)}{1000}$$

where units are: V [m/s], F_x [N], P [kW]

In addition to vehicle velocity, Yates [1] illustrates that wind velocity also plays a factor in the aerodynamic drag on the vehicle. Instantaneous wind speeds were not considered in these calculations, i.e. $V_{wind}(t)$ was set equal to zero.

The aerodynamic resistence or drag on the vehicle, is due air pressure forces on the vehicle created as the vehicle travels.

Aerodynamic Resistance (Drag):
$$F_{aero}(t) = \frac{1}{2}\rho_{air} \times C_d \times FA \times \left(V(t) + V_{wind}(t)\right)^2$$

Rolling Resistance:
$$F_{rolling} = m \times g \times C_r$$

Inertial Resistence:
$$F_{inertial}(t) = m \times a(i)$$

Before finding the error in the aerodynamic, rolling, and inertial resistance, a number of other variables need to be calculated and their associated error equations determined. The first parameter required to calculate the aerodynamic resistence on the vehicle is air density.

Air Density [kg/m³]:
$$\rho_{air} = \frac{p_{amb} \times MW_{air}}{R_u \times T_{amb}(t)}$$

Error in Air Density Calculation [kg/m³]:

$$\varepsilon_{pair} = \rho_{air} \times \left[\left(\frac{\varepsilon_{Pamb}}{P_{amb}}\right)^2 + \left(\frac{\varepsilon_{Tamb}}{T_{amb}}\right)^2\right]^{1/2}$$

The drag coefficient Cd and the frontal area can be determined from an analysis of the data from a coast down test, as described below. The associated error in Cd x FA is given by:

178

$$\varepsilon_{Cd \times FA} = (Cd \times FA) \times \left[\left(\frac{\varepsilon_{Cd}}{Cd} \right)^2 + \left(\frac{\varepsilon_{FA}}{FA} \right)^2 \right]^{1/2}$$

This equation has one unknown ε_{FA} in it which must be solved for; knowing the equation required to find the frontal area. Vehicle frontal area was calculated as 80% of the product of the height and the width of the vehicle (minus the side mirrors). The currently accepted method of measuring frontal area uses the 80% term to account for the open area under the vehicle and the side mirrors [4].

Frontal Area [m^2]: $\qquad FA = 0.8 \times W \times H$

Error in Frontal Area Calculation [m^2]:

$$\varepsilon_{FA} = FA \times \left[\left(\frac{\varepsilon_W}{W} \right)^2 + \left(\frac{\varepsilon_H}{H} \right)^2 \right]^{1/2}$$

Sufficient information to calculate the error in the aerodynamic resistence calculation is now available knowing the error in vehicle velocity is +/- 0.25 km/h (or +/- 0.069 m/s).

Error in Aerodynamic Resistence Calculation [N]:

$$\varepsilon_{Faero} = F_{aero} \times \left[\left(\frac{\varepsilon_{Cd}}{Cd} \right)^2 + \left(\frac{\varepsilon_W}{W} \right)^2 + \left(\frac{\varepsilon_H}{H} \right)^2 + \left(\frac{\varepsilon_{pair}}{\rho_{air}} \right)^2 + \left(2 \times \frac{\varepsilon_V}{V} \right)^2 \right]^{1/2}$$

With the appropriate substitutions this error equation can be rewritten as:

$$\varepsilon_{Faero} = F_{aero} \times \left[\left(\frac{\varepsilon_{Cd \times FA}}{Cd \times FA} \right)^2 + \left(\frac{\varepsilon_{pair}}{\rho_{air}} \right)^2 + \left(2 \times \frac{\varepsilon_V}{V} \right)^2 \right]^{1/2}$$

The error in the rolling resistance equation can immediately be calculated as:

Error in Rolling Resistence Calculation [N]:

$$\varepsilon_{Frolling} = F_{rolling} \times \left[\left(\frac{\varepsilon_m}{m} \right)^2 + \left(\frac{\varepsilon_{Cr}}{Cr} \right)^2 \right]^{1/2}$$

Knowing that the error in the gravitational constant ε_g, is zero.

179

The last vehicle resistence calculation equation to determine the error for, is the inertial resistence equation. Before the error in this equation can be calculated the error associated with the acceleration term must be determined.

Instantaneous vehicle acceleration is calculated by differentiating the speed-time trace gathered by the vehicle ECM. The acceleration term uses the velocity and time of the next and the previous time steps to determine the current acceleration.

Acceleration [m/s^2]:
$$a(i) = \frac{V_{i+1} - V_{i-1}}{t_{i+1} - t_{i-1}}$$

Error in Acceleration Calculation [m/s^2]:

$$\varepsilon_{ai} = \left[\left(\frac{\partial a_i}{\partial V_{i+1}} \times \varepsilon_{Vi+1}\right)^2 + \left(\frac{\partial a_i}{\partial V_{i-1}} \times \varepsilon_{Vi-1}\right)^2 + \left(\frac{\partial a_i}{\partial t_{i+1}} \times \varepsilon_{ti+1}\right)^2 + \left(\frac{\partial a_i}{\partial t_{i-1}} \times \varepsilon_{ti-1}\right)^2\right]^{1/2}$$

Assuming there is no error in the time stamp value (i.e. $\varepsilon_t = 0$), we can rewrite this equation as:

$$\varepsilon_{ai} = a_i \times \left[\left(\frac{\varepsilon_{Vi+1}}{V_{i+1} - V_{i-1}}\right)^2 + \left(\frac{\varepsilon_{Vi-1}}{V_{i+1} - V_{i-1}}\right)^2\right]^{1/2}$$

which can be rewritten in a simple form knowing the error in V_{i+1} is the same as V_{i-1}:

$$\varepsilon_{ai} = \frac{\sqrt{2} \times a_i \times \varepsilon_V}{V_{i+1} - V_{i-1}}$$

Now that all variable errors have been determined, the final vehicle resistence error calculation can be found.

Error in Inertial Resistence Calculation [N]:

$$\varepsilon_{Finertial} = F_{inertial} \times \left[\left(\frac{\varepsilon_m}{m}\right)^2 + \left(\frac{\varepsilon_a}{a}\right)^2\right]^{1/2}$$

Once all the resistence equation errors are determined, the uncertainty in vehicle power can then be determined.

Error in Vehicle Power Calculation [kW]:

180

$$\varepsilon_P = P \times \left[\left(\frac{\varepsilon_V}{V} \right)^2 + \left(\frac{\varepsilon_{Faero}}{\sum F} \right)^2 + \left(\frac{\varepsilon_{Frolling}}{\sum F} \right)^2 + \left(\frac{\varepsilon_{Finertial}}{\sum F} \right)^2 \right]^{1/2}$$

Error in Total Vehicle Power Calculation [kW]:

$$\varepsilon_{P,total} = \sqrt{\sum_1^n P^2}$$

Also, the speed-time trace is used to determine the instantaneous distance traveled, D [m], at each time step. Knowing the velocity and the time we find the total distance traveled at any point in time t [s] is:

Distance: $$D(t) = V \times t$$

If we continue to assume that the time stamp recorded has no error in it, $\varepsilon_t = 0$, then the error in the distance calculation becomes:

Error in Distance Calculation (Instantaneous) [m]:

$$\varepsilon_D = \left| D \times \frac{\varepsilon_V}{V} \right|$$

Error in Distance Calculation (Total) [m]:

$$\varepsilon_{D,total} = \sqrt{\sum_1^n \left(\varepsilon_D \right)^2}$$

The total work done by the vehicle can be calculated by integrating the total positive power vs. time curve. Positive power is considered only since the negative values of power do not add work back into the system.

Total Work Done / Energy Consumed (Instantaneous) [kJ]:

$$W = P \times t \ [kJ] \qquad \text{or} \qquad W = \frac{P \times t}{3600} \ [kWh]$$

where: P   - Power of Vehicle [kW]
       t   - time [s]

181

Error in Instantaneous Work Done Calculation [kWh]:

$$\varepsilon_W = \left| W \times \frac{\varepsilon_P}{P} \right|$$

where: W - Work Done [kWh]
       P - Power of Vehicle [kW]

Total Error in Work Done Calculation [kWh]:

$$\varepsilon_{Wtotal} = \sqrt{\sum_1^n \left(\varepsilon_W \right)^2}$$

The total torque required to drive the wheels of the vehicle can be defined as the sum of the torque due to aerodynamic, rolling, and inertial forces.

Aerodynamic Torque: $T_{aero} = F_{aero} \times r_{tire}$
Rolling Torque: $T_{rolling} = F_{rolling} \times r_{tire}$

The torque required to accelerate a vehicle can be defined using Newton's 2nd Law. Knowing the acceleration, tire radius, and mass of the vehicle, the inertial torque of the vehicle can be calculated. The mass of the vehicle should include not only the vehicle mass (translational mass) but an additional mass factor (to account for driveline rotary inertias) as well [3]. The mass factor typically used for a range of vehicles are shown in the table below.

Table E-2 Mass Factor for Various Vehicles

	Mass Factor		
	High Gear	Second Gear	Low Gear
Small Car	1.11	1.20	1.50
Large Car	1.09	1.14	1.30
Truck	1.09	1.20	1.60

In equation form the definition of mass factor can be determined knowing the product of the final drive ratio and transmission ratio.

$$m_f = \frac{m + m_r}{m} = 1 + 0.04 + 0.0025 \times N_{tf}^2$$

where $N_{tf} = N_t \times N_f$

182

Although the equation for calculation of the mass factor was published in 1957, it is useful as a first approximation. [3] The inertial torque can now be written as:

Inertial Torque:

$$T_{inertial} = m \times m_f \times a \times r_{tire}$$

Finally, summing up the torque required to be produced by the vehicle under the given conditions:

Torque at the Wheels:

$$T_{wheels} = T_{aero} + T_{inertial} + T_{rolling}$$

Knowing the torque produced at the wheels enables the calculation of torque produced at the engine.

Torque at the Engine: $T_{engine} = \dfrac{T_{wheels}}{N_{tf}}$

E.3 Coast Down Testing

Before calculations of aerodynamic and rolling resistence can be completed, the coefficient of drag (C_d) and coefficient of rolling resistence (C_r) must be determined. The calculation of C_d and C_r is accomplished through coast down testing of the vehicle. The simplified dynamic model used here, allows separation of the aerodynamic and rolling resistence forces.

The coast down test procedure begins through selection of a flat roadway in which to complete the test, typically rural highways allow for sufficient space and time to conduct the tests. Selection of a road with a slight road grade does not hinder the results however due to the consideration of road grade in the coefficient's equation. The experiment begins by accelerating the vehicle up to a speed of 100 to 120 km/h, shifting into neutral, and then saving vehicle speed data as the vehicle coasts to a stop. The effects of wind are accounted for by repeating the test in each direction and averaging the coefficients. Ambient temperature, pressure, and vehicle mass at the time of the test are recorded in order to determine C_d and C_r.

In the absence of a propulsive force, rolling resistance and aerodynamic drag account for the dissipation of kinetic energy (both translational and rotating). The derivation of the equation used to calculated the C_d and C_r of the vehicle is shown below.

183

From Newton's 2nd Law, $\sum F = ma$

$$F_{inertial} - F_{aero} - F_{rolling} - m \times g \times Sin\theta = m \times a(t)$$

Inertial Force is related to Engine Torque as;

$$F_{inertial} = \frac{2 \times T_e \times \eta_t}{D \times N_t} - \frac{4I_{eg}}{D^2}$$

Substituting the inertial force component into Newton's 2nd Law yields:

$$T_e = \frac{DN_t}{2\eta_t}\left\{\left(m + \frac{4I_{eq}}{D^2}\right) \times a + \frac{1}{2} \times A \times C_D \times \rho \times \left(V + V_{wind}\right)^2 + m \times g \times \left(C_r + Sin\theta\right)\right\}$$

Assume [1]:

$I_{eg} = 0$ Inertia of rotating components (engine and gearbox) is negligibly small

$T_e = 0$ At "free-wheeling" / coasting conditions, engine torque is zero

Having completed the derivation of the equation to calculate the rolling and drag coefficients, and including assumptions from [1] it can be shown that:

$$\left(-\frac{a(t)}{g} - \sin\theta\right) = A_{front} \times C_D \times \left(\frac{\rho_{air} \times V(t)^2}{2 \times m \times g}\right) + C_r$$

This equation is now in the form of y = mx + b, and therefore can be used to plot a curve such that $A_{front}C_D$ is the slope and Cr is the y-intercept of the plot. Results of coast down tests completed on the 1999 Chevrolet Silverado Test vehicle are shown below.

Table E-3 Coast Down Test Results - Loaded vs Unloaded

1999 Chevrolet Silverado		
	Jul.22, 2003	Aug.31, 2004
Temperature [C]	29	20
Ambient Pressure [mmHg]	703.0	703.6
Road Grade [degrees]	0	0
Total Vehicle Mass	2360* Typical Load	2900** GVWR Load
Tire Pressure	52/50/52/44	52/50/47/50
Cd (average)	0.627	0.632
Cd (std. dev.)	0.062	0.029
Cr (average)	0.008	0.009
Cr (std. dev.)	0.002	0.003

* - with vehicle and driver
** - with vehicle, driver, and sand ballast (in truck box) - at GVWR

The results on the next page show the test to test variation between trips made. The data shown below was generated from a Matlab program created to determine the Cd and Cr coefficients for a given set of coast down data produced from OBDII port data.

185

Truck Loaded with 500kg Additional Load (to GVWR)

Test Results for a 1999 Chevrolet Silverado - E85 UofA
Test Conducted at - TEMPERATURE: 20.00 [C] and PRESSURE: 93.8 [kPa]

SUMMARY TABLE OF COAST DOWN FILE ANALYSIS

Cd	Cr
0.629	0.013
0.627	0.013
0.590	0.006
0.667	0.006
0.649	0.006

Average Cd	Std Dev. Cd	Average Cr	Std Dev. Cr
0.632	0.029	0.009	0.003

Truck without 500kg Additional Load:

Test Results for a 1999 Chevrolet Silverado - E85 UofA
Test Conducted at - TEMPERATURE: 29.00 [C] and PRESSURE: 93.7 [kPa]

SUMMARY TABLE OF COAST DOWN FILE ANALYSIS

Cd	Cr
0.685	0.006
0.656	0.006
0.687	0.005
0.623	0.008
0.533	0.011
0.577	0.009

Average Cd	Std Dev. Cd	Average Cr	Std Dev. Cr
0.627	0.062	0.008	0.002

NOTES:
Drag Coefficient, Cd [unitless] - Expected Value: 0.3 to 0.9
Rolling Resistance Coefficient. Cr [unitless] - Expected Value: 0.01 to 0.08 (or $0.006 < Cr < .02$)

186

REFERENCES

[1]   Yates, A.D.B., Mkwanazi, S. "Methodology for Determining Octane Response at Different Altitudes for Vehicles Equipped with Knock Sensors," SAE Technical paper 2002-01-1663, Society of Automotive Engineers, 2002.

[2]   White, R.A., Korst, H.H. "The Determination of Vehicle Drag Contributions from Coast -Down Tests," SAE Technical Paper 720099, Society of Automotive Engineers, 1972.

[3]   Metz, G.L., Metz, D.L. "Deriving Wheel HP and Torque from Accelerometer Data," SAE Technical paper 2000-01-3544, Society of Automotive Engineers, 2000.

[4]   Gillespie, T.D. "Fundamentals of Vehicle Dynamics," Society of Automotive Engineers, USA, 1992.

[5]   Holman, J.P. "Experimental Methods for Engineers," McGraw Hill, Inc., 6th Edition, New York, 1994. P.51-55.

[6]   Incropera, F.P., DeWitt, D.P. "Introduction to Heat Transfer," John Wiley & Sons, New York, 1996. p. 388-427.

[7]   Vegte, J.V. "Feedback Control Systems," Prentice Hall, Englewood Cliffs, 1994, p.11-25.

[8]   Hawirko, J.D. "Modeling Vehicle Emission Factors Determined with an In-Use & Real-Time Emissions Measurement System," Master of Science Thesis, Department of Mechanical Engineering, University of Alberta, 2003.

APPENDIX F

Sensor Calibrations

A number of sensors were used in measuring the emission rates from the test vehicle. Before gathering any data from the vehicle, calibration of all sensors was completed to provide accurate results and in some sensors, to determine the sensor reading from an analog voltage output. Appendix F details the experiments conducted in calibrating the sensors, and the results obtained.

F.1 Vetronix PXA-1100 5-Gas Analyzer

The Vetronix PXA-1000 5-Gas Analyzer was calibrated by performing a single point calibration using a quad-blend calibration gas. A second point used by the analyzer sampled ambient air to set the analyzer zero point. The calibration gas used, calibrated to the following concentrations; CO - 4.0%, CO_2 - 12.0%, HC (as propane) - 1200ppm, and NOx - 2000ppm.

F.2 AD590 Temperature Sensors

Three temperature sensors were equipped on the vehicle to determine intake air temperature, ambient temperature, and coolant temperature. The use of an AD590 type temperature sensor was chosen because of its accuracy, linearity of output, and wide range of temperatures measurable. Calibration of these three sensors was done using a three point calibration method. Each sensor was immersed in three operating conditions; an ice bath, ambient air, and near-boiling water. The sensors were isolated from the water during the hot and cold tests by heat shrink, which kept the sensor dry and allowed the sensor little thermal resistence so that it could accurately measure the temperature. The results of the temperature sensor calibrations are shown in Figures F-1, F-2, and F-3.

Examination of the coefficient of determination shows that all three sensors have R^2 values above 0.999 indicating good linear fit over the range of temperatures tested. The following calibration curves were used to convert the analog voltage output to a temperature:

Intake Temperature Sensor:	$y = 1041.3x - 286.68$
Ambient Temperature Sensor:	$y = 1031.2x - 283.19$
Coolant Temperature Sensor:	$y = 1008.0x - 277.00$

F.3 Mass Air Flow Meter

The mass air flow meter used for these experiments was a Siemens HFM 62B automotive mass air flow sensor. Alternative Fuel Systems employs the use of the Siemens HFM 62B in their fuel systems and therefore has explored the calibration curve of this particular sensor. Also, calibration of the 62B sensor by Hawirko has confirmed these results and its stability over time. However, an experiment was conducted to confirm previous calibration tests and to ensure the tested mass air flow sensor tested would perform similarly.

An experiment was set up to measure the pressure drop through a nozzle while simultaneously measuring the output voltage of the sensor. The results would then allow for the calculation of a mass flow rate versus output voltage knowing equipment specification and ambient conditions. A schematic of the test is shown in Figures F-4.

189

Experimental results illustrated in Figure F-5 show that the calibration curve previously obtained from Alternative Fuel Systems and Hawirko was valid for a significant portion of the full range of flow rates. The differences between the two curves indicate that minor over prediction of mass air flow rate is experienced during low flow rates. High flow rates show the opposite effect with slight to large under predictions of flow rate with increasing flow.

F.4 Horiba MEXA-720NOx Sensor

The MEXA-720NOx sensor is calibrated using a four point calibration procedure for NO and a three point calibration procedure for A/F ratio. The sensor was calibrated in a Horiba calibration unit which provides the sensor with a humidified gas flow to enable the presence of O_2 in the flow for proper sensor operation. Humidification of the gas flow changes the concentrations of the gas species, due to the presence of water vapor in the new flow, which is compensated for in the calibration test sheets created.

Zero, span, mid-range, and high-range NO concentrations are sent to the sensor which produces the appropriate NO calibration curve for the 0-5 Volt analog output signal the unit sends.

A/F ratio is accomplished similarly through the exposure of the sensor to zero, span, and rich-point calibration gases. The presence of a rich-point calibration point allows the sensor to more accurately measure the A/F ratios in oxygen deficient flows.

F.5 AFRecorder Air/Fuel Ratio Sensor

The A/F ratio sensor of the AFRecorder 2400E was calibrated using a single-point calibration method whereby the instrument was exposed to ambient air with an O_2 concentration of 20.9% for a period of approximately 10 seconds. The sensor only requires calibration when the ambient air concentration reading is not 20.9%.

190

AD590 Intake Temperature Calibration Curve

Fit Results
Fit 1: Linear
Equation Y = 1041.278738 * X - 286.6847805
Number of data points used = 3
Average X = 0.311333
Average Y = 37.5
Residual sum of squares = 0.188129
Regression sum of squares = 3804.31
Coef of determination, R-squared = 0.999951
Residual mean square, sigma-hat-sq'd = 0.188129
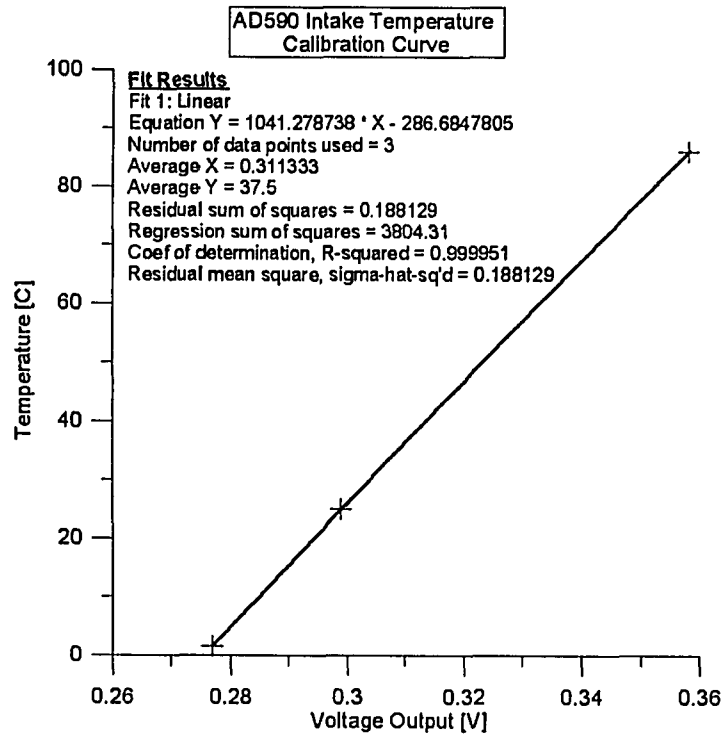
Figure F-1 AD590 Intake Temperature - Calibration Curve

AD590 Ambient Temperature Calibration Curve

Fit Results
Fit 1: Linear
Equation Y = 1031.162661 * X - 283.1915875
Number of data points used = 3
Average X = 0.311, Average Y = 37.5
Residual sum of squares = 0.0253633
Regression sum of squares = 3804.47
Coef of determination, R-squared = 0.999993
Residual mean square, sigma-hat-sq'd = 0.0253633
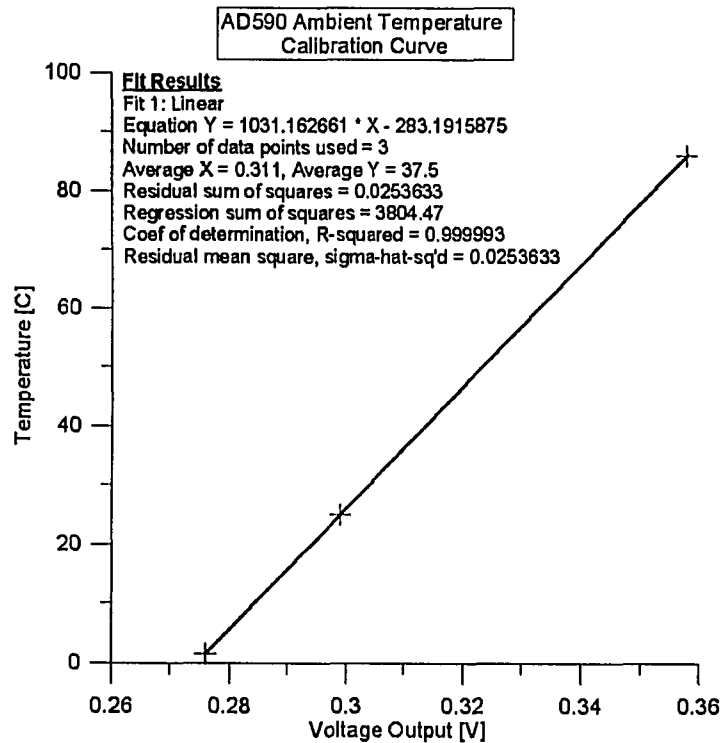
Figure F-2 AD590 Ambient Temperature - Calibration Curve

191

AD590 Coolant Temperature Calibration Curve

Fit Results
Fit 1: Linear
Equation Y = 1008.012821 * X - 277
Number of data points used = 3
Average X = 0.312, Average Y = 37.5
Residual sum of squares = 0.259615
Regression sum of squares = 3804.24
Coef of determination, R-squared = 0.999932
Residual mean square, sigma-hat-sq'd = 0.259615
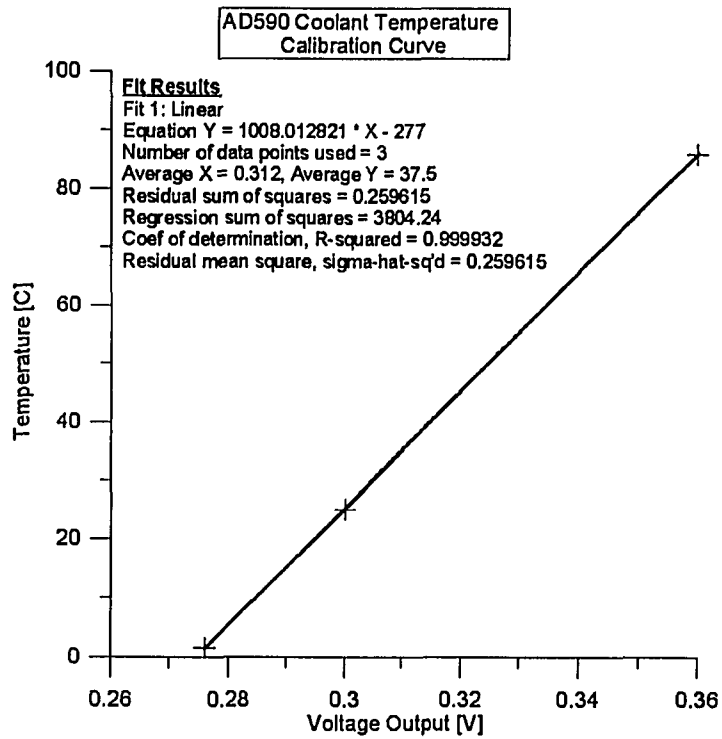
Figure F-3 AD590 Coolant Temperature - Calibration Curve
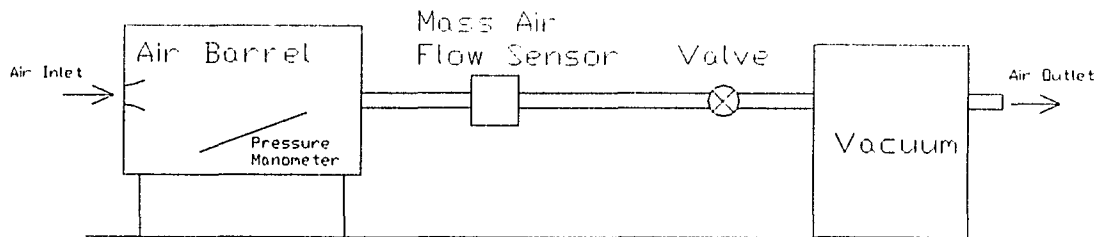
Figure F-4 Mass Air Flow Sensor Calibration Test Setup

192
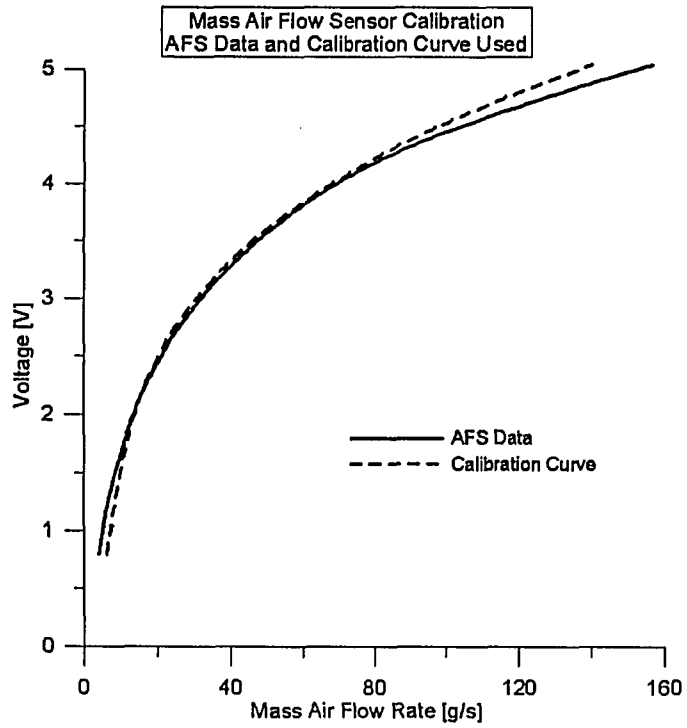
Figure F-5 MAF Sensor Calibration Curve vs. AFS Calibration Data

APPENDIX G

Matlab Processing Code

The creation of Matlab programming code which could read in raw sensor data, manipulate and calculate desired parameters, then output results to data files, was developed in order to process the vast quantity of data gathered from on-road tests. Matlab processing code was written in stages and based on earlier work completed by Hawirko. Knowledge of the previous hierarchical outline allowed for the creation of an efficient programming code which was capable of being extended easily to other areas of investigation. All programming code written was original to this research. Appendix G outlines the hierarchy of this programming code, a description of each ".m" file used, and an identification of the relationship between each program. Each program contains extensive comments with a nearly complete list of parameter definitions given in "Emissions2.m" for further clarity.

194

G.1 Program Hierarchical Format

Emissions2.m
- *The MAIN Emissions Processing / Analysis Software*
      Setup.m
      SetupVehicle.m
      GrossData.m
      NetData.m
      FilterData.m
      CombineData.m
      TimeAlignData1.m
      CompareData.m
      CalcData.m
            Histogram.m
      Uncertainty.m
      SaveData.m
      Accuracy.m
            RespCorrection.m
      RespCorrection.m
      Graph.m
            Truncate.m
            Export.m
      OBDaccuracy.m

SteadyState.m
- *Calculates Emission Averages from Steady State Data*

CoastDown.m
- *Calculates the Cd,Cr constants for a vehicle based on a Coast Down Test*
      CDTfilter.m

NoiseChecker.m
- *APPENDIX Supporting Program - Adds Noise to a Signal*

195

G.2 Version Specific Notes

- Two different data file formats exist for ECM data. The removal of data parameters effects Data files produced after Aug.31, 2004. For data files analyzed BEFORE Aug.31, 2004, simply answer the first question when prompted by Emissions2.m and program will continue as normal.

- Different Time Alignment Algorithms exist. TimeAlignData1.m was determined to be the correct version and should be used. Other alignment algorithms TimeAlignData#.m consider variable time shifting routines. See the description at the top of these files for more info on their function.

G.3 Program Descriptions

Emissions2.m
　　　　LEVEL 1,　　written by: Travis Manchur　-　May 8, 2003

Purpose:　　To provide all the calculations and processing required to analyze on-road emissions (this is the MAIN/CENTRAL program)
Used in:　　(nothing, top level m file)
Uses:　　Setup.m, SetupVehicle.m, GrossData.m, NetData.m, FilterData.m, CombineData.m, TimeAlignData.m, CompareData.m, CalcData.m, Error.m, Graph.m

Setup.m
　　　　LEVEL 2,　　written by: Travis Manchur　-　May 8, 2003

Purpose:　　To give data parameters a column number based on where they are stored in the original data matrix and to set the emission data time delay constants
Used in:　　Emissions#.m, CoastDown.m
Uses:　　(nothing)

SetupVehicle.m
　　　　LEVEL 2,　　written by: Travis Manchur　-　May 13, 2003

Purpose:　　To store vehicle specific data required to calculate tractive power, etc.
Used in:　　Emissions#.m, CoastDown.m
Uses:　　(nothing)

196

GrossData.m
LEVEL 2,   written by: Travis Manchur   -   May 9, 2003

Purpose: Gets all the data from the raw .csv data files (gathered during
             testing) and converts them to matrices oMgas and oMecm
Used in: Emissions#.m
Uses: (nothing)

NetData.m
LEVEL 2,   written by: Travis Manchur   -   May 9, 2003

Purpose: Create new data matrix which starts when vehicle starts (eliminates
             initially non-running time) and fix time stamp
Used in: Emissions#.m
Uses: (nothing)

FilterData.m
LEVEL 2,   written by: Travis Manchur   -   May 9, 2003

Purpose: To filter out erroneous data readings ("spikes" and "dips") and
             smooth out the data values collected. FILTERING IS DONE FOR:
             Coolant Temp, Intake Temp, Ambient Temp, ECM Speed, ECM
             Intake Temp, ECM Mass Air Flow, ECM Coolant Temp, and ECM
             Current Gear
Used in: Emissions#.m
Uses: (nothing)

CombineData.m
LEVEL 2,   written by: Travis Manchur   -   May 11, 2003

Purpose: Combine Filtered Data Matrices into 1 Matrix using Gas Analyzer
             Time as the Base Time
Used in: Emissions#.m
Uses: (nothing)

TimeAlignData1.m
LEVEL 2,   written by: Travis Manchur   -   May 20, 2003

Purpose: Constant Time Delay - The emissions data (ONLY) gathered by the
             gas analyzer will be shifted to line up with the vehicle data
             (accounts for time delay due to transport time from the engine
             through the exhaust pipe through the sample hose and into the
             analyzer)
Used in: Emissions#.m
Uses: (nothing)

197

CompareData.m
      LEVEL 2,   written by: Travis Manchur - July 24, 2003

Purpose:	To compare the difference in readings for MAF (g/s), Coolant Temp (C), Intake Air Temp (C), Engine Speed (RPM), Barometric Pressure (kPa), and possibly later Calculated Engine Load
Used in:	Emissions#.m
Uses:	(nothing)

CalcData.m
      LEVEL 2,   written by: Travis Manchur - May 11, 2003

Purpose:	To calculate the remaining vehicle variables of interest from the gathered data
Used in:	Emissions#.m
Uses:	(nothing)

Uncertainty.m
      LEVEL 2,   written by: Travis Manchur - May 17, 2004

Purpose:	Lists equipment measurement accuracy/error & then calculates the quantitative error AT EACH TIME STAMP for all calculations/readings/etc.
Used in:	Emissions#.m, Truncate.m
Uses:	(nothing)

SaveData.m
      LEVEL 2,   written by: Travis Manchur - February 25, 2004

Purpose:	To save calculated matrices into excel programs for later use in graphing/plotting
Used in:	Emissions#.m
Uses:	(nothing)

Accuracy.m
      LEVEL 2,   written by: Travis Manchur - July 20, 2004

Purpose:	Calculates the accuracy of the response correction algorithms available by evaluating simple lag responses, data response with more than 1 time constant, and the effect of noisy sample data.
Used in:	Emissions#.m
Uses:	RespCorrection.m

Graph.m
LEVEL 2,   written by: Travis Manchur   -   May 26, 2003

Purpose: To produce Graphs/Charts/Trends/Summary Tables/Export
            Options, etc. which may be useful to the user to analyze the
            processing which has been done on the collected data.
Used in: Emissions#.m
Uses: Truncate.m

RespCorrection.m
LEVEL 2 & 3,   written by: Travis Manchur   -   Jun 7, 2004

Purpose: A dynamic response compensation algorithm used to correct the
            simple first order lag response of the vetronix & horiba NOx
            sensors
Used in: Accuracy.m, Emissions#.m
Uses: (nothing)

Truncate.m
LEVEL 3,   written by: Travis Manchur   -   May 27, 2003

Purpose: Allow User to Select an Analysis Range of Interest (Truncate Data)
            (and subsequently view the graphical results in Graph.m)
Used in: Graph.m
Uses: Uncertainty.m

Export.m
LEVEL 3,   written by: Travis Manchur   -   December 23, 2003

Purpose: To allow the user to export the data summary to a text file
Used in: Graph.m
Uses: (nothing)

OBDaccuracy.m
LEVEL 1,   written by: Travis Manchur   -   December 2, 2004

Purpose: Determines the accuracy of ECM data
Used in: Emissions#.m
Uses: (nothing)

Histogram.m
LEVEL 3,   written by: Travis Manchur   -   January 22, 2004

Purpose: To Produce Various Histograms Showing Various Items of Interest
Used in: CalcData.m
Uses: (nothing)

199

SteadyState.m
        LEVEL 1,   written by: Travis Manchur - July 23, 2003

Steady State Emissions Calculator for Steady State Emission Testing

Purpose: To find the average and standard deviation of the various
                emissions recorded at steady state conditions
Used in: (nothing)
Uses: (nothing)

CoastDown.m
        LEVEL 1,   written by: Travis Manchur - July 14, 2003

Coast Down Test Program - a supplement to the On-Road In-Use Emissions
Analysis Program

Purpose: To calculate the vehicle specific drag and rolling coefficients
                through calculations performed on data during a Coast Down Test -
                only uses data collected from the AutoTap Unit
Used in: (nothing)
Uses: CDTFilter.m, SetupVehicle.m, Setup.m

CDTfilter.m
        LEVEL 2,   written by: Travis Manchur - July 23, 2003

Purpose: To filter out erroneous data readings ("spikes" and "dips") and
                smooth out the data values collected. FILTERING IS DONE FOR:
                ECM Speed (obtained during a Coast Down Test)
Used in: CoastDown.m
Uses: (nothing)

NoiseChecker.m
        LEVEL 1,   written by: Travis Manchur - July 30, 2004

Purpose: Adds noise to a constant concentration signal for copying and
pasting to excel to   ensure noise generated is fitting a normal distribution
with the same standard   deviation as intended.
Used in: (nothing)
Uses: (nothing)

200

APPENDIX H

Supplemental Data Tables

A complete tabulated record of the calculated emissions and operational test results obtained from the analysis of experiments conducted for Chapter 4 is listed in Appendix H. These tables provide the individual test readings with the associated coefficient of variation for each mode and emissions species. An explanation for the large deviation in hydrocarbon and carbon monoxide values is also discussed.

201

Chapter 4 discussed the effect of vehicle transients and load on mass emission rates of various emission species. Appendix H provides a complete tabulated record of the individual test results in addition to an explanation for elevated HC and CO readings measured during some initial tests.

The average vehicle load values presented in Table H-1 and H-2 do not consider road grade, wind, or other external vehicular influences in its determination, which is why average vehicle load does not appear to be changing with direction. However, the presence of a sizeable standard deviation in both urban and highway loaded tests is concerning and requires explanation.

The cause of this large standard deviation in the average was due to dramatic reductions in HC emission rates from test one through four as shown in Tables H-1 and H-2. The initial high HC emission rate was assumed to be caused by a cooling of the catalytic converter, to temperatures which were likely below light off temperatures. Although the vehicle was driven 21 km in highway and urban traffic to produce a fully warmed vehicle prior to testing, the first test of the day did not begin until a 10 minute emissions analyzer warm up period was completed. This soak time is the likely source of the catalytic converter cool off. Rapid acceleration tests were completed immediately after the normal transient tests, which explains why these modes did not exhibit a changing HC emission rate.

The HC concentration trace of Figure 4-6 shows that the first test of the loaded highway cycle mode, produced noticeably higher HC emissions than the following tests, even though the air-fuel ratio comparison supports lower HC emissions for test 1. Kaspar [1] showed that air-fuel ratio has a significant effect on catalyst conversion efficiency when utilized off of stoichiometric conditions. With vehicle load, transients, and air-fuel ratio causes rules out, the probability is high that catalyst cool down was the cause of the initial HC emission rate spike.

Examining the CO emission rate, has shown a number of interesting results. Primarily, the presence of a large initial CO emission rate for test one of both loaded driving cycles, which was 2 to 4 times the average of the remaining three tests (Table H-1). Examining Figure 4-6 for the urban drive cycle and noting the above justification for the theory of a cooled catalyst, accounts for the source of the first test CO emission rate outlier. It is also known that catalytic converter efficiency of CO is even more dramatically effected by air-fuel ratio than HC, indicating that test 1 should have had a much lower CO emission rate due to tighter A/F control. This implies once more the theory that the vehicle's catalytic converter experienced a noticeable cool down.

202

Table H-1 US06 Highway Driving Cycle Simulation Test Results

Test	Emissions Results					Operation Characteristics			
	HC	CO	CO$_2$		NOx	Duration	Fuel Consumed		Load
	[g/km]	[g/km]	[g/km]	[g/g fuel]	[g/km]	[s]	[g fuel]	[g fuel/km]	[kW]
No Load, Normal Acceleration									
1	0.017	0.365	242	2.78	0.290	604	1108	87.1	23.7
2	0.018	1.139	303	3.09	0.357	608	1247	98.0	23.3
3	0.011	0.473	266	3.09	0.311	617	1091	85.9	23.0
4	0.013	1.116	306	3.08	0.349	616	1263	99.2	23.1
Average:	0.015	0.773	279	3.01	0.327	611	1177	92.6	23.3
Std Dev.:	0.003	0.412	30.7	0.15	0.032	6	90.4	7.0	0.32
GVWR (Fully Loaded), Normal Acceleration									
1	0.105	2.126	300	3.09	0.388	611	1239	97.2	26.1
2	0.039	1.358	301	3.08	0.393	617	1243	97.7	25.6
3	0.007	1.146	298	3.08	0.391	606	1236	97.0	26.6
4	0.006	0.796	308	3.09	0.389	615	1270	99.7	25.7
Average:	0.017	1.100	302	3.09	0.390	612	1247	97.9	26.0
Std Dev.:	0.019	0.284	4.4	0.01	0.002	5	15.6	1.2	0.45
No Load, Rapid Acceleration									
1	0.173	32.8	314	2.70	0.466	605	1484	116.6	23.9
2	0.099	26.0	257	2.68	0.325	594	1220	96.0	24.8
3	0.089	27.9	321	2.72	0.414	605	1504	118.1	23.9
4	0.080	28.2	254	2.65	0.317	593	1215	95.6	24.8
Average:	0.110	28.7	287	2.69	0.381	599	1356	106.6	24.4
Std. Dev.:	0.043	2.90	36.1	0.03	0.072	7	160	12.5	0.55
GVWR (Fully Loaded), Rapid Acceleration									
1	0.071	31.2	290	2.65	0.462	597	1392	109.4	26.9
2	0.059	32.7	301	2.64	0.433	596	1450	113.9	27.1
3	0.053	31.3	288	2.65	0.406	596	1386	108.8	27.1
4	0.068	33.3	298	2.63	0.347	596	1440	113.2	26.9
Average:	0.063	32.1	294	2.64	0.412	596	1417	111.3	27.0
Std Dev.:	0.008	1.03	6.2	0.01	0.049	1	32.7	2.6	0.11

Note: * - indicates HC and CO emission rate for the 100% GVWR (Normal Acceleration Test) is the average of three tests (outlier omitted)

203

Table H-2 FTP75 Urban Driving Cycle Simulation Test Results

Test	Emissions Results					Operation Characteristics			Load
	HC*	CO*	CO_2	CO_2	NOx	Duration	Fuel Consumed		Load
	[g/km]	[g/km]	[g/km]	[g/g fuel]	[g/km]	[s]	[g fuel]	[g fuel/km]	[kW]
No Load, Normal Acceleration									
1	0.063	1.32	376	3.10	0.718	797	957	121	7.73
2	0.028	1.60	362	3.10	0.447	792	921	117	7.83
3	0.019	1.36	390	3.09	0.613	813	993	126	7.48
4	0.031	1.55	357	3.08	0.528	795	914	116	7.58
Average:	0.035	1.46	371	3.09	0.577	799	946	120	7.66
Std. Dev.:	0.019	0.139	14.7	0.01	0.116	9	36.4	4.6	0.16
GVWR (Fully Loaded), Normal Acceleration									
1	0.144	2.150	338	3.11	0.686	812	860	109	8.50
2	0.054	0.533	288	3.11	0.507	808	731	92.6	8.68
3	0.031	0.579	335	3.09	0.706	816	859	109	8.48
4	0.006	0.459	291	3.10	0.484	810	741	93.8	8.73
Average:	0.030	0.524	313	3.10	0.596	812	798	101	8.60
Std. Dev.:	0.024	0.061	27.4	0.01	0.117	3	71.0	9.0	0.13
No Load, Rapid Acceleration									
1	0.175	21.5	340	2.86	0.368	761	936	119	8.01
2	0.074	18.7	317	2.89	0.280	756	865	110	8.20
3	0.179	31.7	331	2.73	0.313	770	957	122	7.73
4	0.088	24.9	299	2.77	0.249	767	850	108	7.81
Average:	0.129	24.2	322	2.81	0.303	764	902	115	7.94
Std. Dev.:	0.056	5.58	17.9	0.08	0.051	6	52.4	6.7	0.21
GVWR (Fully Loaded), Rapid Acceleration									
1	0.060	15.3	358	2.93	0.490	781	968	123	9.00
2	0.056	15.7	315	2.92	0.422	772	853	108	9.19
3	0.058	18.5	358	2.89	0.560	775	979	124	9.19
4	0.046	13.9	323	2.91	0.416	765	877	111	9.42
Average:	0.055	15.8	339	2.91	0.472	773	919	116	9.20
Std. Dev.:	0.006	1.96	22.7	0.02	0.068	7	63.3	7.9	0.17

Note: * - indicates HC and CO emission rate for the 100% GVWR (Normal Acceleration Test) is the average of three tests (outlier omitted)

204

Table H-3 Coefficient of Variation in Emission Rates

Test	HC [%]	CO [%]	CO_2 [%]	NOx [%]
URBAN				
Normal Accel No Load	54.3	9.5	4.0	20.1
Normal Accel 100% GVWR	80.0	11.6	8.8	19.6
Rapid Accel No Load	43.4	23.1	5.6	16.8
Rapid Accel 100% GVWR	10.9	12.3	6.7	14.4
HIGHWAY				
Normal Accel No Load	20.0	53.3	11.0	9.8
Normal Accel 100% GVWR	118.0	25.8	1.5	0.5
Rapid Accel No Load	39.1	10.1	12.6	18.9
Rapid Accel 100% GVWR	12.7	3.2	2.1	11.9

REFERENCES

[1]   Kaspar, J., Fornasiero, P., Hickey, N., "Automotive catalytic converters: current status and some perspectives," Catalysis Today, Elsevier Science, 77 (2003) 419-449.